Hochauflösende Spurenstoffmessungen an polaren Eisbohrkernen: Glazio-chemische und klimatische Prozessstudien

Inauguraldissertation

der Philosophisch-naturwissenschaftlichen Fakultät
der Universität Bern

vorgelegt von

Matthias Bigler

von Oberthal

Leiter der Arbeit:
Prof. Dr. T. F. Stocker

Abteilung für Klima- und Umweltphysik
Physikalisches Institut der Universität Bern

Hochauflösende Spurenstoffmessungen an polaren Eisbohrkernen: Glazio-chemische und klimatische Prozessstudien

Inauguraldissertation

der Philosophisch-naturwissenschaftlichen Fakultät
der Universität Bern

vorgelegt von

Matthias Bigler

von Oberthal

Leiter der Arbeit:
Prof. Dr. T. F. Stocker

Abteilung für Klima- und Umweltphysik
Physikalisches Institut der Universität Bern

Von der Philosophisch-naturwissenschaftlichen Fakultät angenommen.

Bern, den 17. Juni 2004

Der Dekan:
Prof. Dr. G. Jäger

Inhaltsverzeichnis

Kapitel 1

Einleitung

1.1 Polare Eisschilder als Klimaarchiv

Der antarktische und der grönländische Eisschild speichern den grössten Teil des auf der Erde vorhandenen Süsswassers. Aufgrund der vorherrschenden extremen klimatischen Bedingungen wurden im Laufe der Jahrtausende die Niederschläge schichtweise abgelagert und erhalten. Ein Teil dieses Schnees wird vom Wind verfrachtet oder zurück in die Atmosphäre sublimiert. In den zentralen, hochgelegenen Gebieten der polaren Eisschilde sind diese Prozesse jedoch vernachlässigbar und es kann von einer stetigen Akkumulation ausgegangen werden (Abbildung 1.1). Frische Niederschläge überdecken die früheren, Schnee verdichtet sich zu porösem Firn und unter der zunehmenden Last der neu gefallenen Niederschläge bildet sich schliesslich Eis. In diesem Eis eingeschlossen finden sich Luftblasen, welche mit zunehmender Tiefe im Eisgefüge gelöst werden. Trotzdem wachsen Eisschilder nicht beliebig an. Mit der stetigen Massenzufuhr in den zentralen Gebieten ist ein ebenso stetiger Massenverlust an den Rändern der Eisschilder verbunden (Abbildung 1.1), so dass ein einigermassen stabiles Gleichgewicht aufrecht erhalten wird und die Höhe der Eisschilder, bei gleichbleibenden klimatischen Bedingungen, nicht nennenswert variiert.

Sucht man im Innern dieser Kältewüsten Regionen auf, die sich durch eine ebenförmige Topographie des Felsbettes unter dem Eis auszeichnen, findet man in den bis über drei Kilometer mächtigen Eismassen ein regelmässig geschichtetes, lückenloses und hochaufgelöstes Archiv der vergangenen Niederschläge und in den Blasen die Zusammensetzung der früheren

Abbildung 1.1: Antarktischer Eisschild bei Dome C und antarktische Küste bei Dumont d'Urville.

Atmosphärenluft. Mit Tiefenbohrungen durch das Eis bis zum Felsbett kann anhand der gewonnenen Eisbohrkernen dieses Archiv, zurückgehend in der Zeit, erschlossen werden.

Durch verschiedenste Prozesse wird die Zusammensetzung der Niederschläge und der Atmosphäre bestimmt und verändert. Viele dieser Prozesse sind Schwankungen unterworfen, die sich tageszeitlich, jahreszeitlich oder bedingt durch die Erdbahnelemente im Verlaufe von Jahrtausenden verändern. Andere haben einen episodischeren Charakter. Vielen dieser Prozesse ist gemeinsam, dass sie in einem komplexen Wechselspiel eng mit dem Klima verknüpft sind, dieses beeinflussen und/oder von ihm beeinflusst werden. Die Eisbohrkerne sind somit nicht nur ein Archiv für vergangene Niederschläge und Atmosphärenzusammensetzungen, sondern enthalten komplexe Signale, die eng mit der Dynamik des Klimasystems der Erde verknüpft sind.

Für vor allem in polfernen Breiten lebende Menschen scheint das vergangene Klima der polaren Gebiete irrelevant zu sein. Das ist jedoch nicht der Fall, da das Klimasystem der Erde über die Dynamik der Atmosphäre und der Ozeane global gekoppelt ist und gerade die polaren Gebiete empfindlich auf Veränderungen reagieren oder ebensolche verstärken. Die polaren Gebiete spielen eine wichtige Rolle innerhalb des globalen Klimasystems.

Eisbohrkerne und die darin enthaltenen Informationen des vergangenen Klimas helfen das Verständnis über dieses komplexe System zu verbessern und relevante Mechanismen zu erkennen. Die Fragen sind aber zu komplex, als dass sie durch Untersuchungen der polaren Eisbohrkerne alleine beantwortet werden können. Erst unter Einbezug verschiedener, weiträumig verteilter Klimaarchive sind signifikante Fortschritte innerhalb der Paläoklimatologie möglich. Diese wiederum trägt nur einen Teil zum gesamten Verständnis bei. Das langfristige Betreiben

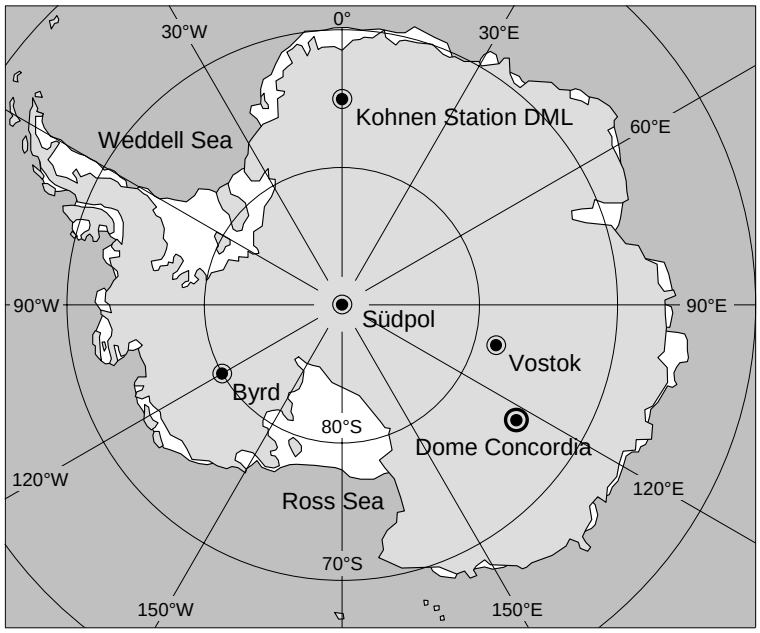

Abbildung 1.2: Antarktiskarte mit den im Text erwähnten Tiefbohrungen.

von engmaschigen Messnetzen rund um den ganzen Globus, experimentelle Grundlagenforschung und das Erstellen und Untersuchen von einfachen wie umfassenden Klimamodellen bilden weitere Eckpfeiler in der Erforschung des Klimas. Ein dritter, aktueller und umfassender Überblick über den Stand der Klimaforschung und insbesondere über die Klimaveränderungen erschien im Jahre 2001 im Rahmen des Intergovernmental Panel on Climate Change IPPC [*IPCC*, 2001].

1.2 Eisbohrkerne von Dome C und NorthGRIP

Nach den grossen Erfolgen mehrerer Tiefbohrungen in Grönland (unter anderen GRIP und GISP2) und der Antarktis (unter anderen Byrd und Vostok) wurde in den Neunzigerjahren das European Project for Ice Coring in Antarctica (EPICA) gestartet. Im Rahmen dieses Projektes sollen zwei neue Tiefbohrungen durchgeführt werden, eine in Dome Concordia (Dome C) und eine in Dronning Maud Land (Abbildung 1.2). Dome C ist einer der unwirtlichsten Orte der Erde, auf 3233 m ü. M. in der Ostantarktis gelegen (75°06' Süd, 123°21' Ost) und gut 1000 km von der Küste entfernt (Abbildung 1.3). Die Jahresmitteltemperatur liegt bei -54.5°C und der jährliche Schneefall beträgt knapp 3 cm in Wasseräquivalent. Der Eisschild ist an dieser Stelle etwa 3310 m mächtig. Aufgrund der geringen Niederschlagsrate bietet sich dieser Ort für eine Bohrung an, welche Eisbohrkerne für einen zeitlich möglichst weit zurückreichenden Datensatz liefern soll. Obwohl die Bohrung (Abbildung 1.4) das Felsbett noch nicht ganz erreicht hat, wurden an den gewonnenen Eisbohrkernen bereits Analysen durchgeführt, die vielversprechende Resultate zeigen [*EPICA community members*, 2004]. Das Alter der tiefsten Schichten reicht 740 Tausend Jahre vor heute (ka BP) zurück, somit erstrecken sich die gewonnenen Klimainformationen über acht glazial-interglaziale Zyklen und übertreffen den bisher längsten Eiskerndatensatz aus Vostok um gut 300'000 Jahre. Im überlappenden Bereich stimmen die Daten sehr gut überein. Die neuen Daten von Dome C (Abbildung 1.5) zeigen zwischen 430 und 740 ka BP weniger ausgeprägte, im Verhältnis zu den Kaltphasen jedoch länger dauernde Warmzeiten (Marine Isotope Stage MIS 11, 15, 17), als die nachfolgenden Warmzeiten (MIS 5, 7, 9). Falls das verbleibende Eis bis zum Felsbett noch gebohrt werden kann, was wegen der erhöhten Eistemperatur eine grosse Herausforderung ist, wird der Datensatz schliesslich bis fast eine Million Jahre vor heute zurückreichen.

Abbildung 1.3: Die Stationen von Dome C in der Antarktis und NorthGRIP in Grönland (Foto links J. Flückiger, rechts Universität Kopenhagen).

Abbildung 1.4: Bohrzelt mit Bohrturm in Dome C; Bohrkopf mit Eisbohrkern (Foto rechts J. Flückiger).

Der zweite Bohrort im Rahmen von EPICA liegt auf der entgegengesetzten Seite der Antarktis, in Dronning Maud Land (DML) bei Kohnen Station (Abbildung 1.2). In dieser Region, die an den Südatlantik grenzt, möchte man einen detailreichen Eisbohrkern gewinnen, der möglicherweise Bezüge zum Klima im nordatlantischen Raum aufweist.

Im nordatlantischen Raum kann man unter anderem Eisbohrkerne aus Grönland untersuchen. Diese reichen aufgrund der viel höheren Niederschlagsraten weniger weit zurück, aber weisen eine bessere zeitliche Auflösung auf. Das ist sehr nützlich, denn in den Eisbohrkernen von Grönland zeigen sich während der Eiszeit und im Übergang zwischen Eiszeit und Warmzeit abruptere Schwankungen, als in den Klimadaten aus der Antarktis. Diese Schwankungen, die sogenannten Dansgaard-Oeschger-Events (D/O) detaillierter zu untersuchen, war eines der Ziele, weshalb zeitgleich zu EPICA ein kleineres Projekt unter der Führung von dänischen

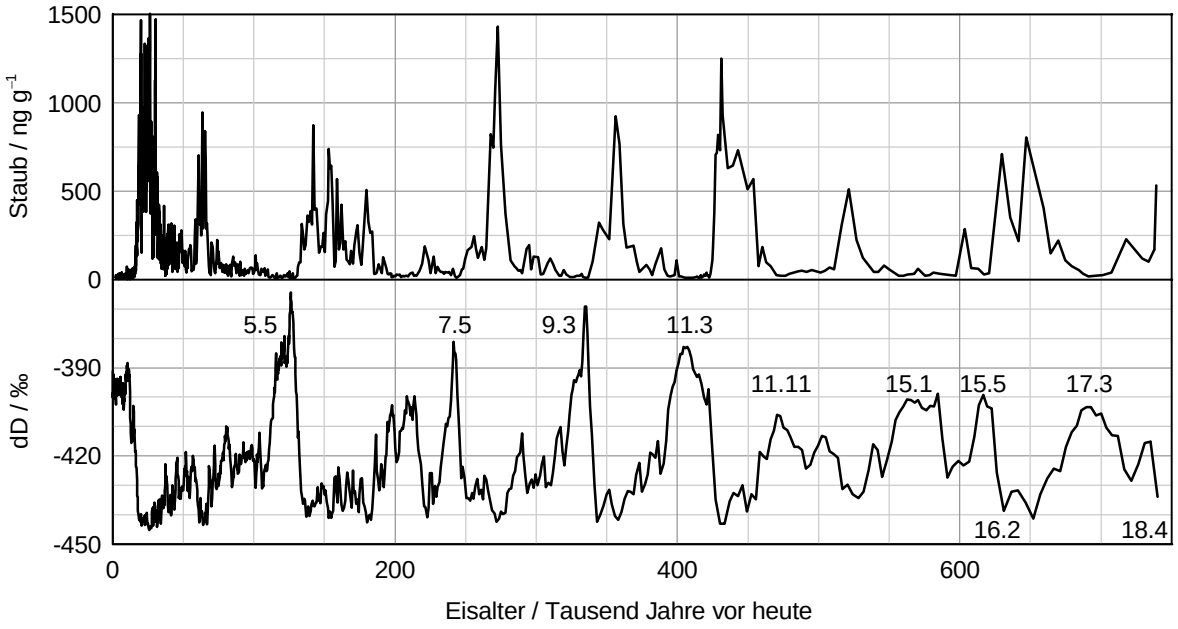

Abbildung 1.5: Staubmessungen und δD (ein Proxy für die lokale Temperatur) vom EPICA Dome C Eisbohrkern [*EPICA community members*, 2004].

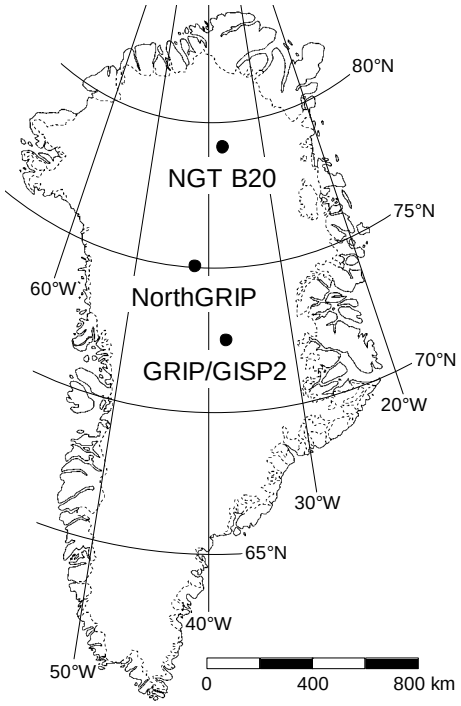

Abbildung 1.6: Grönlandkarte mit den im Text erwähnten Bohrorten.

Forschern, mit breiter internationaler Beteiligung, in Nordgrönland (NorthGRIP) in Angriff genommen wurde. In NorthGRIP (75°06' Nord, 42°19' West, 2917 m ü. M. – Abbildung 1.3 und 1.6) wurde das Hauptziel verfolgt, bis ins Eis der letzten Warmzeit (Eem) zu bohren. Die Stabilität der Eem-Warmzeit und die Übergänge in die vorangehende und nachfolgende Eiszeit sind für die Klimaforschung von grossem Interesse. Im Sommer 2003 konnte die Bohrung erfolgreich bis auf das Felsbett in einer Tiefe von 3085 m vorgetrieben werden. Gemessen an der ursprünglichen Zielsetzung resultiert nicht in allen Punkten ein Erfolg. Wegen hoher geothermischer Wärme schmolz der Eisschild von unten her stärker ab als erwartet, so dass das älteste Eis nur bis etwa in die Mitte der Eem-Warmzeit zurückreicht. Dafür ist die Schichtung bis auf den Felsgrund erhalten und wegen der geringeren Ausdünnung der einzelnen Schichten ist die Auflösung besser als erwartet. Mit diesen neuen grönländischen Klimadaten kann nun schlüssig gezeigt werden, dass die beiden Datensätze der früher gebohrten Kerne GRIP und GISP2 im untersten Teil (älter als 105 ka BP) vom Felsbett her gestört wurden und klimatisch nicht interpretierbar sind [*North Greenland Ice-Core Project (NorthGRIP) Members*, 2004].

1.3 Spurenstoffe in polaren Eisbohrkernen

Die vorliegende Arbeit befasst sich mit der Messung und Interpretation von Spurenstoffen an den beiden Eisbohrkernen von Dome C und NorthGRIP. Was sind Spurenstoffe, was ist ihre klimatische Bedeutung, welchen Prozessen sind sie unterworfen?

Eine Vielzahl von Stoffen aus verschiedenen Quellen gelangen auf unterschiedlichen Wegen in die Atmosphäre und bilden dort das Aerosol [*Warneck*, 1999]. Dieses ist Bestandteil der

Abbildung 1.7: Frisches Meereis zwischen McMurdo und Terra Nova Bay im November 2001; Frostblumen auf neuem und altem Meereis, im Hintergrund die Endurance (Foto rechts F. Hurley, um 1915).

Luft, wird transportiert, modifiziert und unter anderem mit dem Niederschlag wieder aus der Atmosphäre entfernt. Wichtige Aerosolquellen sind das Meer (Seesalz), Wüstengebiete (Mineralstaub), Vulkane, die Biomasse und die anthropogenen Emissionen.

Der Niederschlag in den zentralen Gebieten der Eisschilder und die polaren Luftmassen sind im Vergleich zu Luft und Niederschlag aus niedrigeren Breiten in der Regel kaum verunreinigt. Die auf den ersten Blick vernachlässigbar kleine Menge an Spurenstoffen in den polaren Eisbohrkernen, zeigen jedoch bei genauerem Hinsehen einen immensen Informationsgehalt über die Atmosphärenzusammensetzung und die klimatischen Bedingungen vergangener Zeiten, aber auch über glazio-chemische Prozesse im Zusammenhang mit der Deposition. Die Massenkonzentration der beobachteten Spurenstoffe kann um mehrere Grössenordnungen schwanken (Abbildungen 1.9, 1.10 und 1.11).

Neben der Nassdeposition von Spurenstoffen mit dem Niederschlag in Form von Schnee, spielt vor allem in der Zentralantarktis, wo die Niederschlagsraten sehr klein sind, die Trockendeposition eine wichtige Rolle. Darunter versteht man die gravitations- oder windbedingte Ablagerung von Aerosolen auf der Schneeoberfläche zwischen einzelnen Niederschlagsereignissen. Einige der Spurenstoffe werden irreversibel deponiert. Von reversibler Deposition spricht man, wenn Spurenstoffe, abhängig beispielsweise von Temperatur und Akkumulationsrate, wieder in die Atmosphäre entweichen. Es kann auch später noch zu post-depositionalen Effekten kommen, wenn sich Spurenstoffe zum Beispiel innerhalb der Eismatrix bewegen. All diese Prozesse müssen entweder hinreichend bekannt oder vernachlässigbar sein, wenn man von der Messung von Spurenstoffen an Eisbohrkernen auf deren atmosphärische Konzentration vor der Deposition schliessen will.

Die atmosphärische Konzentration gewisser Aerosole wiederum beeinflusst den Strahlungshaushalt der Erde und damit das Klima direkt, oder als Kondensationskeime bei der Wolkenbildung indirekt. Viele dieser Aerosoleffekte sind noch ungenügend erforscht und ergeben deshalb Unsicherheiten bei der Modellierung des Klimasystems [*Anderson et al.*, 2003]. Einen Überblick über die wichtigsten Aerosolklassen und deren klimatische Effekte findet sich unter anderem in der Dissertation von *Röthlisberger* [2000].

Speziell mit Spurenstoffmessungen an Eisbohrkernen befasst sich der Übersichtsartikel von *Legrand und Mayewski* [1997]. Drei neuere Arbeiten, die ebenfalls Spurenstoffmessungen an Eisbohrkernen als Grundlage haben, seien hier kurz vorgestellt. *Adams et al.* [2003] fanden eine statistische Korrelation zwischen explosiven Vulkanausbrüchen, aufgezeichnet in Eisbohrkernen, und anschliessenden El Niño Klimaereignissen im pazifischen Raum. *Curran et al.* [2003] konnten zeigen, dass zwischen Methansulfonsäure in einem antarktischen Eisbohrkern und satellitengestützen Beobachtungen der Meereisbedeckung im ostantarktischen Sektor ein Zusammenhang besteht. Die Auswertung der so kalibrierten, weiter zurückreichenden Methansulfonsäuremessungen wiesen auf eine Abnahme der Meereisbedeckung um 20% im untersuchten Gebiet seit 1950 hin. Die Oberfläche des frisch gebildeten Meereises (Abbildung 1.7) in polaren Gebieten ist die bedeutendere Quelle für das Seesalzaerosol [*Wagenbach et al.*, 1998; *Rankin et al.*, 2002], als brechende Wellenkämme, die in niedrigeren Breiten für die Produktion verantwortlich sind. Dieser Sachverhalt wurde von *Wolff et al.* [2003] dahingehend interpretiert, dass Seesalzaerosolmessungen in antarktischen Eisbohrkernen eher Aussagen über die Meereisbildungsrate zulassen und nicht wie bisher üblich als Indikatoren für einen verstärkten meridionalen Transport gedeutet werden dürfen.

1.4 Beitrag dieser Arbeit

1.4.1 Feldarbeiten

Die Beteiligung an den zwei grossen Eiskernbohrungen in Dome C und in NorthGRIP bilden die Basis der vorliegenden Dissertation. Die Hauptarbeit in der ersten Phase bestand darin, im Rahmen dieser internationalen Projekte zwei Messkampagnen vorzubereiten und durchzuführen. Diejenige in NorthGRIP im Sommer 2000 und diejenige in der Antarktis auf Dome C im Südsommer 2001/2002 [*EPICA Dome C 2001–02 science and drilling teams*, 2002; *Flückiger und Bigler*, 2003]. In beiden Fällen wurde die an der Abteilung für Klima- und Umweltphysik entwickelte und gebaute Continuous Flow Analysis (CFA) Messanlage eingesetzt (Abbildung 1.8), die in den Publikationen *Sigg et al.* [1994], *Röthlisberger et al.* [2000] *(Publikation im Unterkapitel 2.10)* sowie im Kapitel 3 beschrieben ist. Vor den jeweiligen Feldarbeiten wurde das Messsystem in Bern gründlich revidiert, optimiert, teilweise erweitert und anschliessend nach Grönland, respektive in die Antarktis versandt (etwa 1000 kg Material). Die wesentlichen methodischen Neuerungen, die im Rahmen der experimentellen Arbeiten realisiert wurden sind (1) Verbesserungen des Sulfatnachweissystems (Unterkapitel 3.3), (2) die Neukonstruktion eines Schmelzkopfes inklusive kleinerer Verbesserungen an der CFA-Schmelzanlage (Abbildung 1.8, Unterkapitel 3.2), sowie (3) die Einführung eines Partikelmessgerätes (Unterkapitel 3.4).

Während den mehrmonatigen Messkampagnen wurde die CFA-Anlage jeweils während sechs Tagen pro Woche rund um die Uhr betrieben, mit dem Ziel, möglichst umfassende und detailreiche Spurenstoffdatensätze aufzuzeichnen. Konkret wurden die wasserlöslichen Massenkonzentrationen von Kalzium Ca^{2+}, Natrium Na^{+}, Ammonium $NH_4{}^{+}$, Sulfat $SO_4{}^{2-}$ (nur in NorthGRIP), Nitrat $NO_3{}^{-}$, Wasserstoffperoxyd H_2O_2 und Formaldehyd HCHO am Schmelzwasser kontinuierlich geschmolzener Eiskernproben gemessen (in $\mathrm{ng\,g^{-1}}$ oder gleichbedeutend ppbw). In gleicher Weise wurde auch die elektrolytische Gesamtleitfähigkeit des Schmelzwassers erfasst (in $\mu\mathrm{S\,cm^{-1}}$), sowie die Gesamtkonzentration und Grössenverteilung der wasserunlöslichen Partikel (in Anzahl Partikel $\mathrm{ml^{-1}}$ oder $\mathrm{ng\,g^{-1}}$). Im Anschluss an die

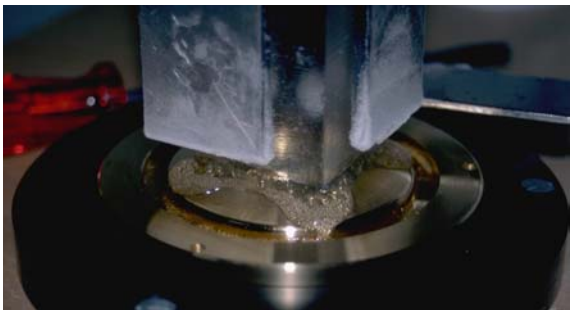
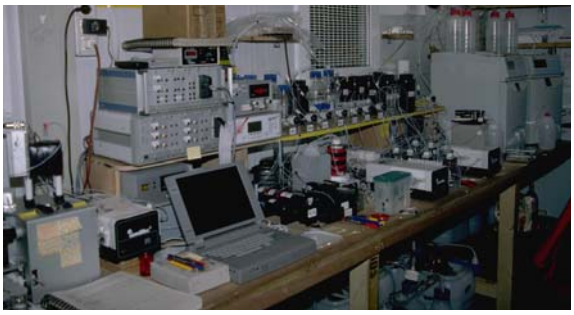

Abbildung 1.8: CFA-Schmelzkopf und CFA-Messanlage in Dome C 2001/2002 (Foto rechts J. Flückiger).

Feldarbeiten erfolgte die zeitaufwendige Auswertung der hochaufgelösten Daten. Diese Arbeiten konnten für den im Jahr 2000 gemessenen Teil des NorthGRIP Eisbohrkerns abgeschlossen werden. Beim 2001/2002 gemessenen Abschnitt des Dome C Kerns liegen mehr als zwei Drittel der Daten fertig ausgewertet vor. Damit konnten im Rahmen dieser Dissertation die verfügbaren CFA-Spurenstoffdaten vervielfacht werden. Zusammen mit einem nordgrönländischen Firnkern (NGT B20, Diplomarbeit [*Bigler*, 2000]), der zu Beginn der Dissertation fertig ausgewertet wurde, liegen nun drei umfassende, hochaufgelöste Spurenstoffdatensätze vor, die in der Folge kurz vorgestellt werden.

1.4.2 Spurenstoffdaten von Dome C

Der erste Teil der antarktischen Dome C Spurenstoffmessungen bis zu einer Tiefe von 585 m wurde in der Dissertation von *Röthlisberger* [2000] veröffentlicht. Mit den neuen Daten kommt das Tiefenintervall von 585 bis 2162 m dazu. Der grösste Teil dieser Erweiterung (769 bis 2162 m) wurde während der Feldsaison 2001/2002 in Dome C am Kern EDC99 gemessen. Die knapp 200 m dazwischen stammen vom Kern EDC96 und wurden in einer kleineren Messkampagne im Herbst 2000 am Alfred-Wegener-Institut (AWI) in Bremerhaven verarbeitet. Bis jetzt ausgewertet sind alle Messdaten bis in eine Tiefe von 1165 m und das Tiefenintervall von 1433 bis 1855 m. Dies entspricht den Zeitintervallen von der Gegenwart bis 78 ka BP und von 103 bis 151 ka BP. Abbildung 1.9 gibt einen Überblick über alle bisher ausgewerteten CFA-Daten von Dome C, es sind dies: Ca^{2+}, Na^{+}, $NH_4{}^{+}$, $NO_3{}^{-}$, H_2O_2, HCHO, elektrolytische Gesamtleitfähigkeit, Partikelgesamtkonzentration und -grössenverteilung. In der Figur nicht dargestellt sind die Resultate von H_2O_2 und HCHO, die abschnittsweise noch einen Offset aufweisen, weil die Blankmessungen nicht korrigiert wurden. Beide Komponenten zeigen jedoch mit Ausnahme der obersten Firnabschnitte praktisch keine detektierbaren Massenkonzentrationen. In Dome C wurde das $SO_4{}^{2-}$ nicht mit der CFA-Nachweismethode gemessen, sondern zusammen mit Chlorid mittels quasi-kontinuierlicher Ionenchromatographie (FIC) durch eine Gruppe der Universität Florenz. Wasser der CFA-Schmelzanlage wurde nicht nur vom FIC-System verwendet, sondern auch zur Speisung eines neugebauten Autosamplers, der diskrete Proben in einer Tiefenauflösung von ungefähr 10 cm für weitere Ionenchromatographie-Messungen sammelte. Diese wurden oder werden noch von den verschieden an EPICA beteiligten europäischen Labors analysiert. Neue CFA-Daten von Dome C wurden in den folgenden Publikationen verwendet: *Röthlisberger et al.*, 2002; *Röthlisberger et al.*, 2003; *Bigler et al.*, 2004; *Bigler et al.*, 2004; *Durand et al.*, 2004; *Röthlisberger et al.*, 2004.

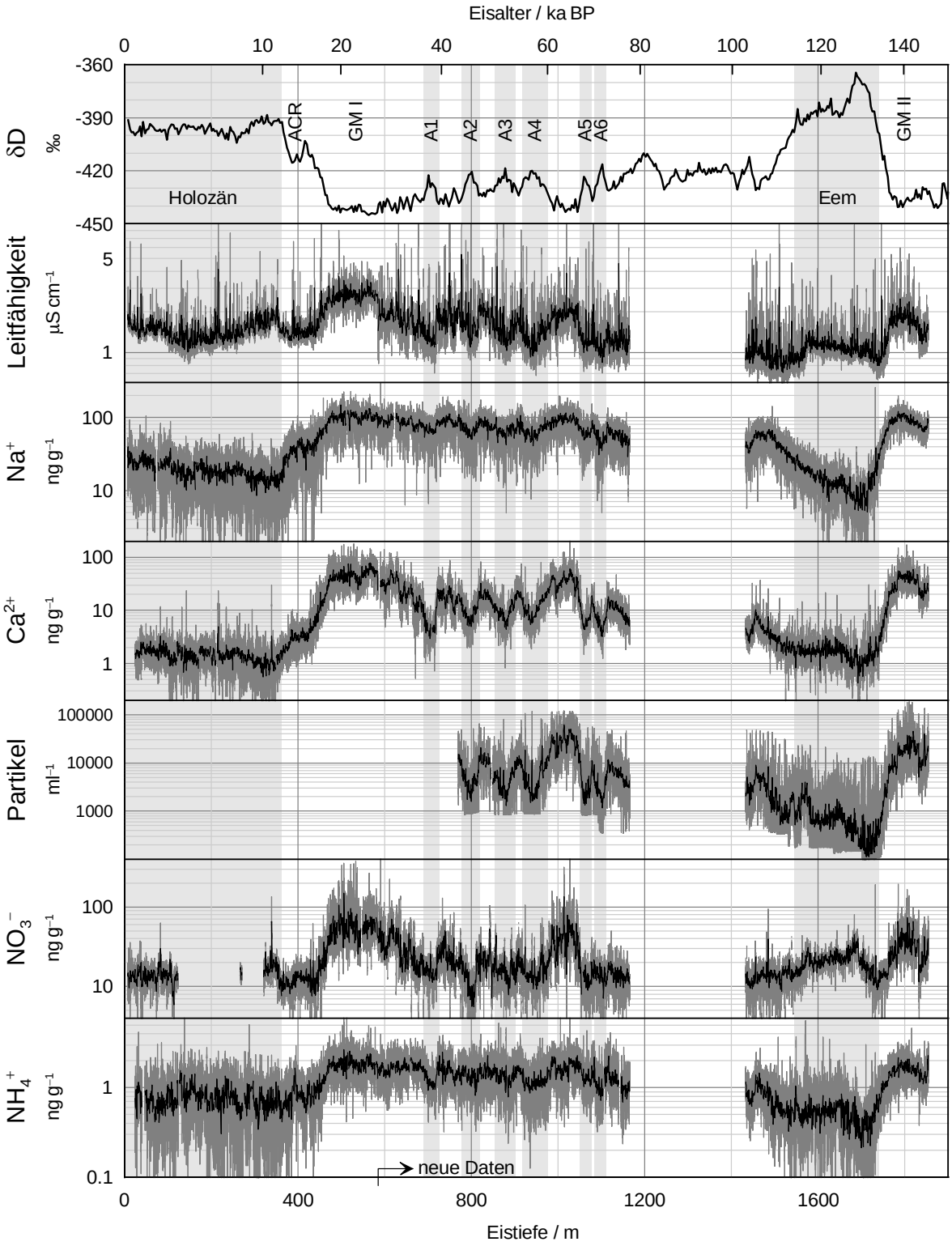

Abbildung 1.9: CFA-Daten von Dome C zusammen mit δD [*EPICA community members*, 2004]; grau 0.5 cm- und schwarz 55 cm-Mittelwerte; das Partikelmessgerät wurde erst ab Saison 2001/2002 eingesetzt; die im Rahmen dieser Arbeit neu gewonnenen Daten sind mit einem Pfeil gekennzeichnet; Daten um 1200 bis 1400 m Tiefe sind noch nicht ausgewertet; speziell bezeichnete Abschnitte neben dem Holozän und dem Eem sind das 'Antarctic Cold Reversal' (ACR), die beiden letzten glazialen Maxima (GMI und GMII) und sechs antarktische Warmereignisse (A1 bis A6).

1.4.3 Spurenstoffdaten von NorthGRIP

Die neuen grönländischen NorthGRIP Daten decken das Tiefenintervall von 1405 bis 2930 m ab und umfassen damit den gesamten Übergang in das letzte Glazial und den grössten Teil dieser Kaltzeit, etwas weiter zurück als D/O-Event 23. Das entsprechende Zeitintervall reicht von ziemlich genau 110 bis 10 ka BP. In NorthGRIP wurden alle CFA-Komponenten gemessen: Ca^{2+}, Na^{+}, $NH_4{}^{+}$, $SO_4{}^{2-}$, $NO_3{}^{-}$, H_2O_2, HCHO, elektrolytische Gesamtleitfähigkeit, Partikelgesamtkonzentration und -grössenverteilung. Im Vergleich zur Pionierarbeit von *Fuhrer* [1995], die am GRIP-Eisbohrkern Messungen von Ca^{2+}, $NH_4{}^{+}$, H_2O_2 und HCHO durchführte, konnte die Zahl der Komponenten und die Datenauflösung beträchtlich erhöht werden. Zudem weist der neue NorthGRIP Datensatz bei $NH_4{}^{+}$ und H_2O_2 weniger Lücken auf, deckt hingegen das Holozän nicht ab. Abbildung 1.10 gibt einen Überblick über die vollständig ausgewerteten CFA-Daten. Wie schon in Unterkapitel 1.4.2 sind die Resultate von H_2O_2 und HCHO nicht abgebildet, welche abgesehen vom Übergang in die letzte Eiszeit praktisch keine detektierbaren Massenkonzentrationen zeigen. Auch in NorthGRIP wurde ein Teil des Schmelzwassers abgezweigt und von Hand und teilweise mit Hilfe eines Autosamplers für spätere Ionenchromatographie-Messungen in Kopenhagen, Stockholm und Heidelberg gesammelt. Die Auflösung dieser diskreten Proben beträgt normalerweise 55 cm. Teile der neuen CFA-Daten von NorthGRIP wurden in den folgenden Publikationen verwendet: *Ruth et al.*, 2002; *Mortensen et al.*, 2004; *Svensson et al.*, 2004. Es ist geplant, die verbleibenden untersten Eisbohrkerne in nächster Zeit zu analysieren und den Datensatz bis in die Eem-Warmzeit zu vervollständigen.

1.4.4 Spurenstoffdaten von NGT B20

Die CFA-Daten von NorthGRIP decken im wesentlichen den glazialen Teil des Eisbohrkerns und nur einen kleinen Teil des frühen Holozäns ab. Hochaufgelöste Holozän-Daten gibt es jedoch vom Firnkern NGT B20, der im Rahmen der AWI-Nordgrönlandtraverse (NGT) gebohrt und 1999 in Bern analysiert wurde (Diplomarbeit *Bigler*, 2000). Dieser 148 m lange Firnkern stammt aus Nordostgrönland (78°50' Nord, 36°30' West, 2147 m ü. M.), einem Gebiet, das sich für grönländische Verhältnisse durch eine kleine mittlere Jahresschichtdicke von nur 10 cm auszeichnet. Jahresschichten sind jedoch über den ganzen Kern erhalten und können zwischen eindeutig identifizierbaren und genau datierten Vulkanhorizonten abgezählt werden. Die Datierung des Firnkerns ist daher auf ±5 Jahre genau. Folgende CFA-Komponenten wurden gemessen: Ca^{2+}, Na^{+}, $NH_4{}^{+}$, $SO_4{}^{2-}$, $NO_3{}^{-}$, H_2O_2, und die elektrolytische Gesamtleitfähigkeit. Die hochaufgelösten Daten sind in Abbildung 1.11 dargestellt. Sie fanden Eingang in folgenden Veröffentlichungen: *Bigler*, 2000; *Bigler et al.*, 2002; *Röthlisberger et al.*, 2002.

1.4.5 Untersuchung klimatischer Mechanismen in der Südhemisphäre

Das südliche Südamerika ist die dominante Quelle des nach Dome C verfrachteten kontinentalen Aerosols [*Delmonte et al.*, 2004]. Das wasserlösliche Ca^{2+} gemessen am Dome C Eisbohrkern kann jedoch nicht direkt als Indikator für das kontinentale Aerosol verwenden werden, da insbesondere in Warmzeiten ein nicht unwesentlicher Teil vom Ca^{2+} aus dem Meer stammt. Umgekehrt ist das Meer nicht die einzige Quelle von Na^{+}, das in Dome C deponiert wird. Vor allem in den Kaltzeiten wird ein unbekannter Na^{+}-Anteil mit dem kontinentalen Aerosol eingetragen. Basierend auf den hochaufgelösten Daten und speziell auf ganz hohen Peakwerten, wird in *Bigler et al.* [2004] *(Publikation im Unterkapitel 2.1)* ein Verhältnis von

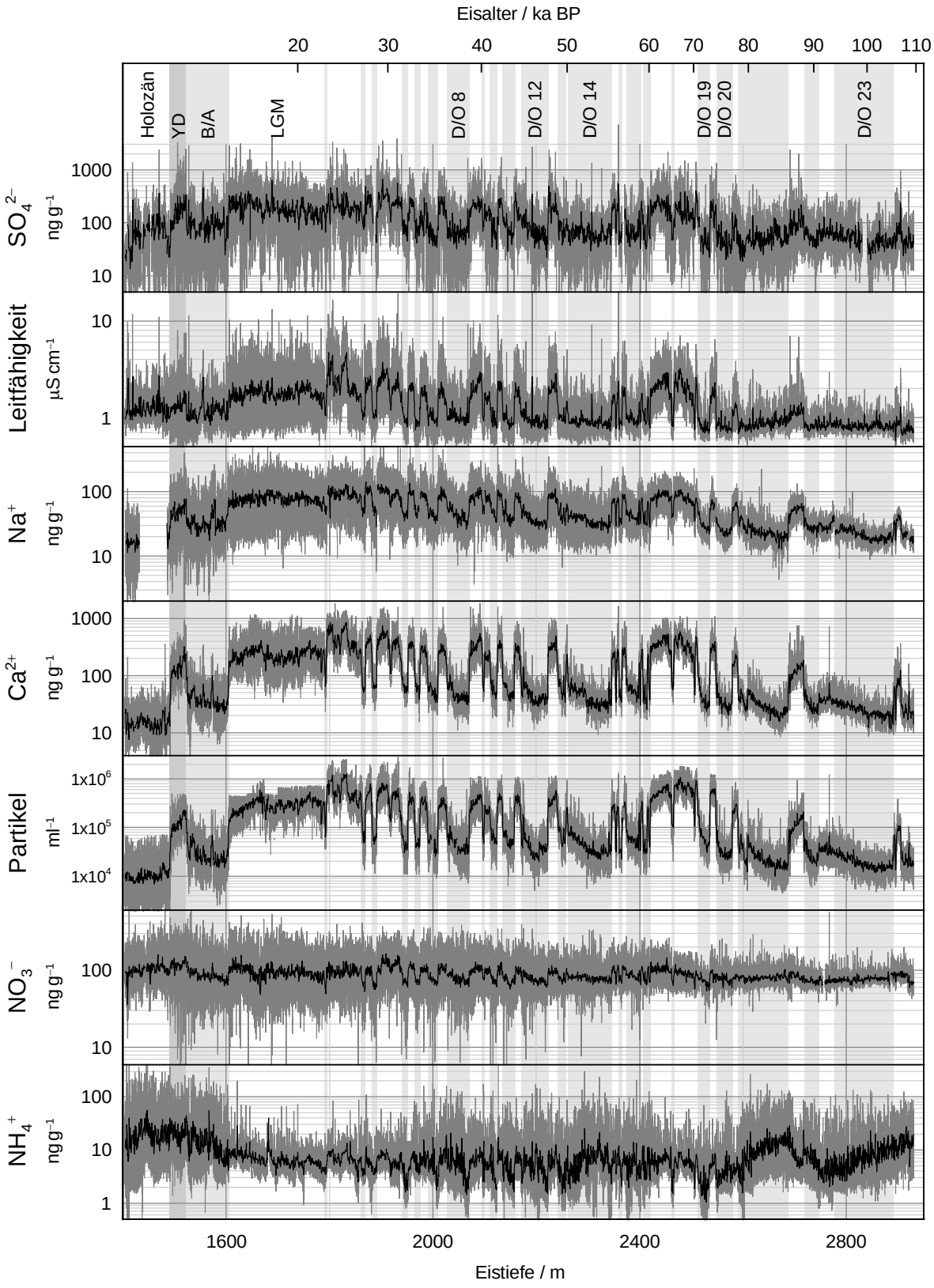

Abbildung 1.10: CFA-Daten von NorthGRIP; grau 0.5 cm- und schwarz 55 cm-Mittelwerte; speziell bezeichnete Abschnitte neben dem Holozän sind die Jüngere Dryas (YD), das Bølling-Allerød (B/A), das letzte glaziale Maximum (LGM) und einige der Dansgaard/Oeschger-Events (D/O).

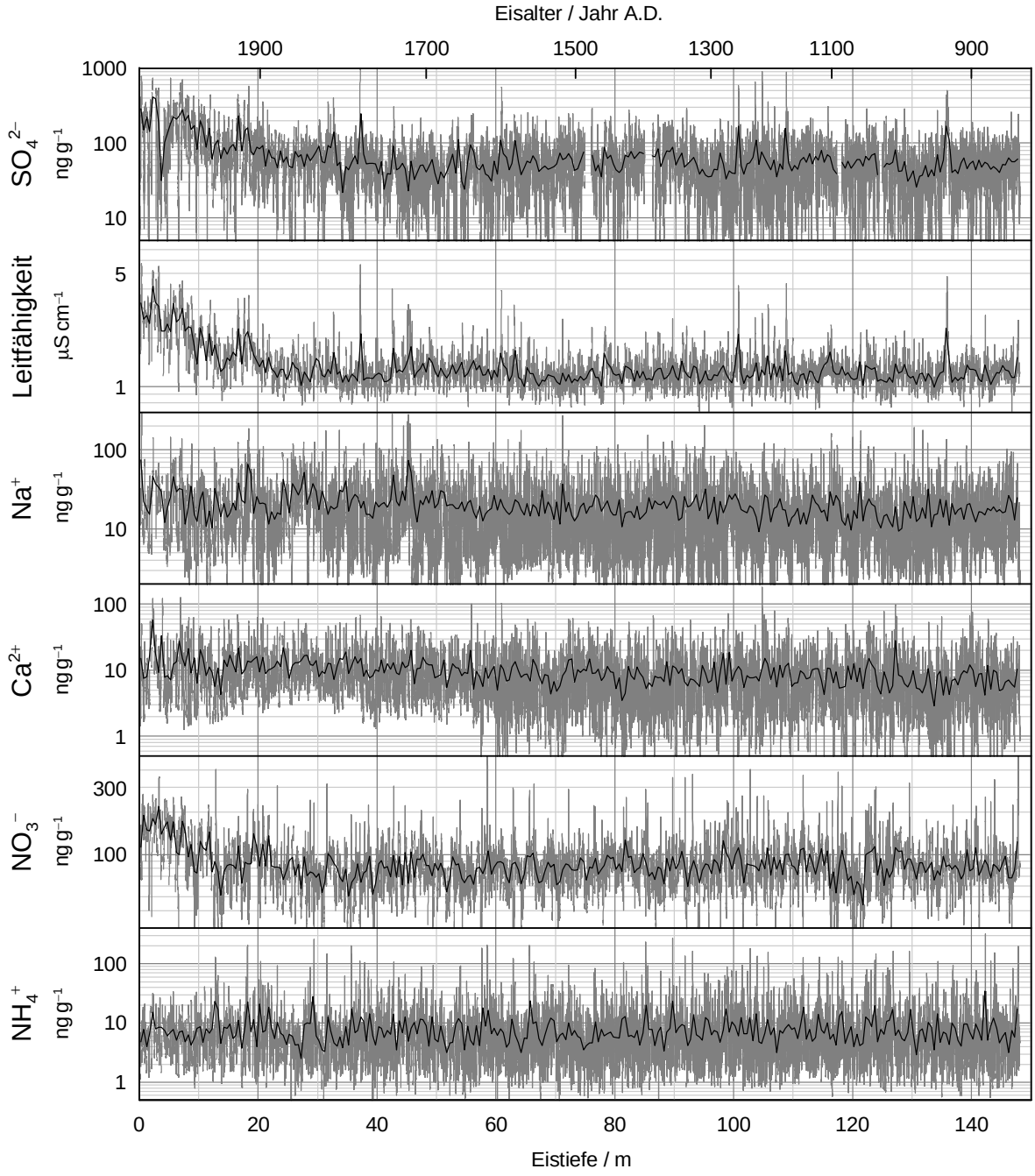

Abbildung 1.11: CFA-Daten von NGT B20; grau 0.2 cm- und schwarz 50 cm-Mittelwerte; die Zeitreihen überdecken ungefähr die letzten 1200 Jahre; deutlich zu sehen ist der anthropogene Anstieg von $SO_4{}^{2-}$ und $NO_3{}^-$ über die letzten 150 Jahre, der sich auch in der elektrolytischen Leitfähigkeit zeigt.

kontinentalem (Na^+/Ca^{2+}) abgeleitet, das die Trennung der beiden Quellenbeiträge zum gesamten Na^+ und Ca^{2+} ermöglicht. Das datenbasierte Verhältnis passt gut zu Messungen, die am heutigen Aerosol direkt in Patagonien durchgeführt wurden. Die Untersuchung ergibt einen kleineren relativen Anteil des Seesalzaerosols am Gesamtaerosol als bisher angenommen. Das bedeutet, dass vor allem unter glazialen Bedingungen die kontinentalen Quellen von Na^+, aber auch von Cl^-, wesentlich zum Aerosol beigetragen haben. Daher dürfen Na^+-Messungen nicht als rein marines Signal interpretiert werden.

Wenn die beiden Quellenbeiträge zu Na^+ und Ca^{2+} entkoppelt sind, man also das Seesalz-Natrium (ss-Na^+) und das Nicht-Seesalz-Kalzium (nss-Ca^{2+}) kennt, kann teilweise auf die klimatischen Bedingungen in der jeweiligen Quellenregion geschlossen werden. Höhere Werte eines irreversibel deponierten Spurenstoffes können aber nicht ausschliesslich mit einer grösseren Quellenstärke erklärt werden, sondern auch durch eine Intensivierung des Transports von der Quelle in die Antarktis. Viele Beobachtungen wurden bis anhin mit einer bedeutenden Verstärkung des meridionalen Transportes während glazialer Perioden erklärt [*Petit et al.*, 1999]. Interpretationen von Modellresultaten weisen jedoch in letzter Zeit darauf hin, dass sich der Transport nicht stark verändert hat [*Krinner und Genthon*, 2003; *Lunt und Valdes*, 2001] und dass sich glazial-interglaziale Veränderungen in der Spurenstoffdeposition durch Modifikationen der Quelle erklären lassen, wie im Fall von ss-Na^+ [*Wolff et al.*, 2003]. Die folgenden zwei Publikationen gehen in dieselbe Richtung.

Die zweite Hälfte der letzten Eiszeit und der Übergang von der letzen Eiszeit in die heutige Warmzeit (Termination I) werden anhand von Dome C Daten der letzten 45 ka in der Veröffentlichung von *Röthlisberger et al.* [2002] *(Publikation im Unterkapitel 2.2)* untersucht. Die Termination I wiederspiegelt zuerst vor allem eine klimatisch bedingte Abschwächung der kontinentalen Aerosolquellen im südlichen Südamerika. Erst gegen Ende des Übergangs hat allenfalls eine Anpassung der atmosphärischen Zirkulationsmuster stattgefunden. Die wärmeren Abschnitte innerhalb der letzten Kaltzeit weisen so tiefe Ca^{2+}-Messwerte auf, dass das Klima im südlichen Südamerika zu der Zeit vermutlich feuchter war, als üblicherweise in der Eiszeit.

Dank den neuen Daten von Dome C in *Bigler et al.* [2004] *(Publikation im Unterkapitel 2.3)* kann der Untersuchungszeitraum nun bis zurück in die vorletzte Eiszeit ausgedehnt werden. Damit lässt sich auch die letzte Warmzeit, das Eem, samt den beiden Übergängen am Anfang und am Ende (Termination II, Inception I) im Detail untersuchen. Das Eem erweist sich als stabile Klimaperiode und ähnelt im grossen und ganzen der heutigen Warmzeit, war aber etwas wärmer [*EPICA community members*, 2004; *Petit et al.*, 1999]. Vermutlich gab es im frühen Eem weniger Meereis rund um die Antarktis, als im Holozän, was sich in sehr tiefen Na^+-Messwerten äussert. Ca^{2+} ist hingegen im ersten Teil des Eem höher als im Holozän, was auf ein feuchteres Klima im südlichen Südamerika schliessen lässt. Erst am Ende der Eem-Warmzeit und in der Inception I werden Holozän-ähnliche Werte erreicht. Da sich die beiden Spurenstoffmessungen gerade entgegengesetzt verhalten, kann eine Veränderung der Transportmechanismen kaum für diese Beobachtungen verantwortlich gemacht werden. Weiter wurde gefunden, dass die Meereisbildungsrate und die antarktische Temperatur in Warmzeiten stärker gekoppelt sind, als in Kaltzeiten. Es scheint, als ob sich die Meereisbildung unter einer gewissen Schwellentemperatur im Glazial nicht mehr stark verändern würde, obwohl die Temperatur gewissen Schwankungen ausgesetzt ist. Der Eintrag von kontinenta-

lem Aerosol aus dem südlichen Südamerika, der in Warmzeiten unabhängig scheint von der antarktischen Temperatur und Meereisbildungsrate, reagiert hingegen empfindlich auf glaziale Temperaturschwankungen.

Deshalb werden Ca^{2+}-Messungen in *Röthlisberger et al.* [2004] *(Publikation im Unterkapitel 2.4)* beigezogen, um den Einfluss des atmosphärischen Staubeintrags auf die Eisendüngung des südlichen Ozeans abzuschätzen und damit die Veränderungen der atmosphärischen CO_2-Volumenkonzentration zu quantifizieren. Es kann gezeigt werden, dass Änderungen der biologischen Produktivität im südlichen Ozean, als Antwort auf den veränderten Staubeintrag, nur einen Viertel des CO_2-Anstiegs während der Termination I erklären können. Der restliche Anstieg muss durch andere Prozesse erklärt werden. Einer davon ist der Staubeintrag in den Nordpazifik, der zusätzlich maximal einen Zehntel des CO_2-Anstiegs erklären kann. Dies führt über auf die Nordhemisphäre, die jedoch über die Ozeanzirkulation und atmosphärische Prozesse eng mit der Südhemisphäre gekoppelt ist.

1.4.6 Untersuchung klimatischer Mechanismen in der Nordhemnisphäre

Der NorthGRIP Eisbohrkern reicht zurück bis in die Mitte der Eem-Warmzeit, welche wie in der Antarktis etwas wärmer war, als die heutige Warmzeit [*North Greenland Ice-Core Project (NorthGRIP) Members*, 2004]. Bis jetzt liegt noch keine Publikation über die Messungen der wasserlöslichen Spurenstoffe des glazialen Teils des neuen Eisbohrkerns vor. Einzig die Partikeldaten wurden interpretiert und in *Ruth et al.* [2003] *(Publikation im Unterkapitel 2.5)* veröffentlicht. Änderungen im glazialen atmosphärischen Partikeltransport werden anhand von Variationen der Partikelgrössenverteilungen und unter Einbezug eines einfachen Modells abgeschätzt. Durch Transportveränderungen allein können die Messresultate nicht erklärt werden. Auch in der Nordhemisphäre spielen Quellenänderungen eine wichtige Rolle. Ferner wird gezeigt, dass Quellenänderungen und Transportänderungen zwei unabhängige Prozesse sind, die durch externe Mechanismen angetrieben werden.

Fallstudien in *Ruth et al.* [2002] *(Publikation im Unterkapitel 2.6)* weisen darauf hin, dass die Partikelgesamtkonzentration und das wasserlösliche Ca^{2+} durchaus gut korrelieren, aber sowohl in verschiedenen Klimaperioden (basierend auf Mittelwerten), wie auch in verschiedenen Jahreszeiten (basierend auf den hochaufgelösten Daten) ein unterschiedliches Massenverhältnis aufweisen. Bei hohen Massenkonzentrationen ist das Verhältnis von Ca^{2+} zu Staub jeweils tief. Ist im Eis vulkanische Säure vorhanden, verändert sich das Verhältnis ebenfalls, weil mehr Ca^{2+} gelöst wird. Das bedeutet, dass Ca^{2+}-Messungen nicht uneingeschränkt als Indikator für die Partikelkonzentration verwendet werden dürfen.

Die während der Diplomarbeit [*Bigler*, 2000] gewonnenen $SO_4{}^{2-}$-Daten wurden zusammen mit weiteren CFA-Spurenstoffmessungen des nordostgrönländischen Firnkerns NGT B20 in der Publikation *Bigler et al.* [2002] *(Publikation im Unterkapitel 2.7)* verwertet. Über die gesamte Länge des Kerns, der die letzten 1200 Jahre abdeckt, kann ein jahreszeitlich schwankendes $SO_4{}^{2-}$-Signal nachgewiesen und zum Zählen der Jahresschichten mit verwendet werden. Die mittlere saisonale Maximalkonzentration hat sich während dem deutlich sichtbaren anthropogenen Anstieg im Vergleich zur vorindustriellen Zeit etwas mehr vom Frühsommer in den Frühling verschoben. Sieht man von $SO_4{}^{2-}$-Spitzen vulkanischen Ursprungs ab, können

vor 1850 keine signifikanten langfristigen Veränderungen des SO_4^{2-}-Hintergrundbeitrags festgestellt werden. Der vulkanische Beitrag scheint jedoch um 1200 n. Chr. etwas höher gewesen zu sein als üblich, denn in dieser Zeit lässt sich eine Häufung überdurchschnittlicher SO_4^{2-}-Peaks beobachten. Solche Peaks werden auch in *Mortensen et al.* [2004] verwendet, um im NorthGRIP-Eisbohrkern mögliche Vulkanereignisse zu identifizieren, die nicht nur lösliche Säure, sondern auch vulkanische Gläser, sogenanntes Tephra, enthalten. Die Identifikation von charakteristischen Tephra-Zusammensetzungen ermöglicht die genaue Zuordnung zu einzelnen Vulkanausbrüchen und damit die Synchronisation mit anderen Eisbohrkernen, aber auch mit marinen Sedimentkernen aus dem ganzen nordatlantischen Raum.

1.4.7 Untersuchung glazio-chemischer Prozesse

Die Untersuchung von glazio-chemischen Prozessen scheint auf den ersten Blick spezialisierte Grundlagenforschung zu sein. Rückschlüsse von Eisbohrkernmessungen auf die atmosphärische Zusammensetzung und schliesslich die klimatische Interpretation sind jedoch nur dann verlässlich möglich, wenn die Prozesse, die bei der Deposition und kurz- oder längerfristig danach stattfinden, bekannt und quantifiziert sind. Dies gilt nicht nur für Spurenstoffe im Eis, sondern auch für Gase in den Luftblasen und Klathraten [*Flückiger*, 2003; *Monnin*, 2004; *Tschumi*, 1999]. Die nachfolgenden Publikationen beziehen sich aber ausschliesslich auf glaziochemische Prozesse im Zusammenhang mit Spurenstoffmessungen im Eis.

In der Publikation von *Röthlisberger et al.* [2003] *(Publikation im Unterkapitel 2.8)* wird die reversible Deposition von Chlorid Cl^- in Dome C untersucht. Weil Cl^- und Na^+ in Warmzeiten vor allem aus dem Meer stammen, dürfte man eigentlich erwarten, dass deren Meerwasserverhältnis auch im Eis erhalten bleibt. Man beobachtet jedoch an der Oberfläche einen Cl^--Überschuss und weiter unten einen Cl^--Mangel. Dies kann damit erklärt werden, dass das Seesalzaerosol in der Atmosphäre mit Salpeter- und Schwefelsäure reagiert, wobei HCl gebildet wird. Dieses hat eine etwas längere Lebensdauer und wird vermutlich unabhängig vom restlichen Seesalzaerosol nach Dome C transportiert, was an der Oberfläche zu einem Überschuss führt. Vor allem wegen der geringen Akkumulationsrate ist dieser Depositionsvorgang reversibel, HCl kann wieder in die Atmosphäre entweichen, was schliesslich netto zu einem Verlust führt. Unter glazialen Bedingungen scheint dieser Prozess nicht stattzufinden, obwohl die Akkumulation noch viel kleiner ist. Es scheint, dass die hohe Verfügbarkeit von basischem Mineralstaub zu einer Neutralisierung der atmosphärischen Salpeter- und Schwefelsäure führt, so dass die HCl-Bildung beim Seesalzaerosol nicht stattfinden kann und das Cl^- nicht vom Na^+ entkoppelt wird, was wiederum post-depositionale Verluste verhindert. In glazialen Zeiten beobachtet man daher ein erhaltenes Seewasserverhältnis im Dome C Eisbohrkern. Weil aber in diesen Perioden der kontinentale Staubeintrag dominierend ist, der auch kontinentales Na^+ und Cl^- nach Dome C bringt, muss das kontinentale Verhältnis einen ähnlichen Wert haben wie das marine [*Bigler et al.*, 2004].

Neben Cl^- ist gemäss *Röthlisberger et al.* [2002] *(Publikation im Unterkapitel 2.9)* auch NO_3^- post-depositionalen Effekten ausgesetzt. Anhand zahlreicher Daten von ganz Grönland und aus der ganzen Antarktis konnte die Abhängigkeit der rezenten NO_3^--Deposition von Temperatur und Akkumulationsrate demonstriert werden. Ob die Temperatur oder die Akkumulationsrate ursächlich ist, kann nicht beantwortet werden, weil beide stark korreliert sind. In Gebieten mit hoher Akkumulationsrate beobachtet man tiefe NO_3^--Massenkonzentrationen,

wenn die Temperatur hoch ist. In Niedrigakkumulationsgebieten werden NO_3^--Verluste hauptsächlich durch Fotodegradation verursacht.

Glazio-chemische Fragestellungen werden unter Beizug von CFA-Spurenstoffmessungen auch in den Publikationen von *Durand et al.* [2004] und *Svensson et al.* [2004] angesprochen. In der ersten wird der Einfluss von Verunreinigungen auf das Kornwachstum im Dome C Eis untersucht, welches mit zunehmender Tiefe einen Trend zu immer grösseren Kristallkörnern aufweist. In der zweiten Publikation wird unter anderem die hohe Korrelation zwischen hochaufgelösten Spurenstoffmessungen und der optisch sichtbaren Schichtung im NorthGRIP-Eisbohrkern diskutiert.

1.5 Ausblick

Nach dem Verlust des meisten CFA-Materials beim Rücktransport aus der Antarktis im Frühjahr 2003, muss die Messanlage vollständig neu aufgebaut werden. Diese Arbeiten sind im Rahmen einer Dissertation in Angriff genommen worden und bereits weit fortgeschritten. Dabei wird angestrebt, aus der Not eine Tugend zu machen, und das Equipment nicht einfach nachzubauen, sondern wo immer möglich zu aktualisieren und optimieren, mit dem Ziel, möglichst rasch ein noch verlässlicheres, und jeweils schneller auf- und abgebautes CFA-System zu erhalten. Experimentelle Anpassungen und neue Software sollen zudem auch eine schnellere Datenauswertung ermöglichen und die Datenqualität weiter erhöhen. Eine Vereinfachung des gesamtem CFA-Systems wird es erleichtern, weitere Komponenten hinzuzufügen. Im Vordergrund stehen dabei Cl^-- und TOC-Messungen. Zudem wäre eine Optimierung bestehender Komponenten, zum Beispiel $SO_4{}^{2-}$, durchaus wünschenswert.

Die Transferfunktionen der reversibel deponierten Spurenstoffe NO_3^- und Cl^- sind quantitativ nach wie vor nicht bekannt. Daher fehlt die notwendige Grundlage, NO_3^- und Cl^- klimatisch interpretieren zu können und als unabhängige Indikatoren zur Rekonstruktion der Akkumulationsrate zu nutzen. Um diese Lücke zu schliessen, braucht es Modellierungsarbeiten, sowie weitere Feld- und Labormessungen von Oberflächenschnee und der Atmosphäre.

Ein grosser Teil der Dome C Daten ist noch nicht ausgewertet. Der Abschluss dieser zeitintensiven Arbeiten, die im Rahmen einer weiteren Dissertation durchgeführt werden, wird die Interpretation von Spurenstoffmessungen über mindestens acht glazial-interglaziale Zyklen oder bis mindestens 800 ka BP ermöglichen. Eine solch lange Zeitspanne konnte anhand von Eisbohrkernen noch nie untersucht werden. Haben die Mechanismen, die für die letzten 150 ka diskutiert wurden, über die gesamte Zeitspanne Gültigkeit? Sind hochaufgelöste Spurenstoffmessungen in derart altem Eis noch interpretierbar oder haben post-depositionale, diffusive Prozesse die Signalcharakteristik zerstört? Es ist bereits jetzt absehbar, dass der Dome C Datensatz zukünftige Referenz für Eisbohrkernresultate wird. Aber auch der zweite EPICA Eisbohrkern von DML dürfte aufgrund der hohen Auflösung neue Massstäbe setzen und Aussagen ermöglichen, die mit den Dome C Daten nicht möglich sind.

Es ist geplant, die NorthGRIP-Spurenstoffdaten anlässlich eines Post Doc Stipendiums (finanziert vom Schweizerischen Nationalfonds) in Kopenhagen vertieft zu interpretieren. Dazu

sollen vor allem klimawirksame Prozesse untersucht werden, die auf jährlichen oder jahreszeitlichen Zeitskalen stattfinden und eine hohe Datenauflösung erfordern. Dazu gehört zum Beispiel das Erstellen einer Vulkanchronologie über die letzte Eiszeit anhand der hochaufgelösten $SO_4{}^{2-}$-Messungen. Weiter soll durch den Vergleich der beiden hochaufgelösten $NH_4{}^{+}$-Datensätze von GRIP und NorthGRIP die räumliche Variabilität der Signale untersucht und bestenfalls auf Veränderungen der Waldbrandaktivität auf dem nordamerikanischen Kontinent geschlossen werden. Bei beiden Untersuchungen geht es um die Charakterisierung des nordhemisphärischen Klimas während der letzten Eiszeit.

Basierend auf den umfassenden CFA-Datensätzen, die in den letzten Jahren gewonnen werden konnten, und die erst teilweise interpretiert worden sind, kann also in Zukunft noch mit zahlreichen weiteren Erkenntnissen gerechnet werden.

Kapitel 2

Publikationen

2.1 The continental contribution to the water-soluble aerosol deposited on the East Antarctic plateau (EPICA Dome C)

Matthias Bigler, Regine Röthlisberger, Fabrice Lambert, Thomas F. Stocker, Geneviève C. Littot, Eric W. Wolff, Dietmar Wagenbach

Journal of Geophysical Research
2004, in preparation

The continental contribution to the water-soluble aerosol deposited on the East Antarctic plateau (EPICA Dome C)

Matthias Bigler[1], Regine Röthlisberger[1], Fabrice Lambert[1], Bernhard Stauffer[1], Thomas F. Stocker[1], Genevieve C. Littot[2], Eric W. Wolff[2], Dietmar Wagenbach[3]

[1] Climate and Environmental Physics, Physics Institute, University of Bern, Switzerland
[2] British Antarctic Survey, Cambridge, United Kingdom
[3] Institute of Environmental Physics, University of Heidelberg, Germany

Abstract

Water-soluble ions like sodium Na^+, calcium Ca^{2+}, and chloride Cl^- preserved in ice cores, originating from both marine and continental sources are important proxies to reconstruct past climatic processes. However, it is difficult to quantify the contribution from the continental sources, particularly during glacial periods. Based on high-resolution data from an East Antarctic ice core (EPICA Dome C), continental aerosol ratios of Na^+, Ca^{2+} and Cl^- are deduced and compared to the water-soluble fraction of aerosols from Patagonia and the southern Pampas, the most likely source region. By using the derived ratios it turned out that during glacial maxima approximately 40-50% of Na^+, and 30-40% of Cl^- originate from continental sources, in contrast to previously estimated smaller quantities based on mean crust values. Furthermore, the inferred continental Cl^- to Na^+ ratio is similar to the marine one, allowing for the preservation of the bulk seawater ratio of Cl^- and Na^+ during glacial maxima, despite the substantial contribution from continental sources.

1. Introduction

Impurities in ice cores bear information regarding past changes in their sources, transport patterns and deposition mechanisms [*Legrand and Mayewski*, 1997]. However, many substances routinely analysed in ice cores represent a mixture of several different sources, complicating the interpretation of the observed variations in terms of climatic conditions in the different source regions and the large-scale transport from the various sources to the ice sheets.

Calcium Ca^{2+}, an important water-soluble inorganic ion in polar snow and ice, is commonly used as a proxy for the continental aerosol, however, at a remote site such as Dome C in East Antarctica its present-day contribution is of the same order as the Ca^{2+} originating from the marine source [*Röthlisberger et al.*, 2002]. Sodium Na^+ and chloride Cl^- on the other hand are generally considered as marine proxies [*Röthlisberger et al.*, 2003; *Wolff et al.*, 2003], although some Na^+ and Cl^- is presumably brought in by continental aerosols, especially during glacial periods when the input was large.

Given the mean continental aerosol mass ratio $(Na^+/Ca^{2+})_{cont}$ and the mean marine mass ratio $(Ca^{2+}/Na^+)_{mar}$ the measured concentrations (in ng g^{-1}) can be separated reasonably well into a sea-salt (e.g. ss-Na^+) and a non-sea-salt part (nss-Ca^{2+}):

$$[\text{ss-Na}^+] = [\text{Na}^+] - [\text{nss-Ca}^{2+}] \cdot \left(\frac{\text{Na}^+}{\text{Ca}^{2+}}\right)_{\text{cont}} \quad (1)$$

$$\wedge \quad [\text{nss-Ca}^{2+}] = [\text{Ca}^{2+}] - [\text{ss-Na}^+] \cdot \left(\frac{\text{Ca}^{2+}}{\text{Na}^+}\right)_{\text{mar}} \quad (2)$$

$$\Longleftrightarrow \quad [\text{ss-Na}^+] = \frac{[\text{Na}^+] - [\text{Ca}^{2+}] \cdot \left(\frac{\text{Na}^+}{\text{Ca}^{2+}}\right)_{\text{cont}}}{1 - \left(\frac{\text{Na}^+}{\text{Ca}^{2+}}\right)_{\text{cont}} \cdot \left(\frac{\text{Ca}^{2+}}{\text{Na}^+}\right)_{\text{mar}}} \quad (3)$$

$$\wedge \quad [\text{nss-Ca}^{2+}] = \frac{[\text{Ca}^{2+}] - [\text{Na}^+] \cdot \left(\frac{\text{Ca}^{2+}}{\text{Na}^+}\right)_{\text{mar}}}{1 - \left(\frac{\text{Na}^+}{\text{Ca}^{2+}}\right)_{\text{cont}} \cdot \left(\frac{\text{Ca}^{2+}}{\text{Na}^+}\right)_{\text{mar}}} \quad (4)$$

Marine ratios are strongly related to the well-determined bulk seawater ratios, and changes over glacial-interglacial periods are assumed to be negligible. In addition $(Ca^{2+}/Na^+)_{mar} = 0.038$ [*Bowen*, 1979] is numerically small, therefore the calculation of nss-Ca^{2+} is not particularly critical. On the other hand the composition of the continental aerosol is fairly uncertain and depends strongly on the exact source material [*Warneck*, 1999], with $(Na^+/Ca^{2+})_{cont}$ ranging from 0.086 for mean sediment, 0.33 for mean soils (with a range over several orders of magnitude) to 0.56 for mean crust [*Bowen*, 1979]. Therefore the calculation of ss-Na^+ is associated with large uncertainties when the continental aerosol input is dominant, especially under glacial conditions.

Source separation has so far been based on literature values for the mean crust [*de Angelis et al.*, 1987; *Legrand et al.*, 1988; *Röthlisberger et al.*, 2002], although the true ratios could differ significantly from these assumed values, causing considerable uncertainty in the resulting ss-Na^+ and nss-Ca^{2+} records.

In this study, we derive continental ratios of Na^+, Ca^{2+} and Cl^- from the aerosol deposited at Dome Concordia based on high-resolution data from the European Project for Ice Coring in Antarctica (EPICA) Dome C ice core. By comparing the Ca^{2+}/Na^+ ratios of single peaks, we obtain the range of possible observed ratios. Events dominated by marine input will reflect the seawater ratio, whereas major continental events will approach the continental aerosol ratio. As other sources of Ca^{2+} and Na^+ are negligible, the data has to lie within the boundaries set by the marine and the continental ratios. Based on these ratios, we then calculate ss-Na^+ and nss-Ca^{2+} and compare the marine and the continental contribution over the last two glacial interglacial transitions.

2. Analytical Methods and Data

Water-soluble Na^+ and Ca^{2+} have been measured during four measuring campaigns between 1997 and 2002 using a Continuous Flow Analysis system (CFA) as described in *Röthlisberger et al.* [2000]. The chronology and the accumulation rate estimates are according to *Schwander et al.* [2001] and *EPICA community members* [2004]. The East Antarctic Dome C drill site (75°06'S; 123°21'E; 3233 m about sea level) is characterised by a mean annual surface temperature of –54.5°C and a mean accumulation rate today of 25 kg m^{-2} a^{-1}. The records presented in *Röthlisberger et al.* [2004; 2002] are extended back to 78 ka before present (BP) and from 103 to 151 ka BP, respectively (Figure 1). The older part covers the entire last interglacial period, the Eemian, as well as the glacial maximum of the penultimate glacial, thus allowing us to compare data from two interglacial periods (Holocene, Eemian) and two glacial periods including their glacial maximum (GM I, II).

In this study we use high-resolution data (0.5 cm values), which represent sub-annual to annual resolution, except for GM II, during which the resolution is reduced towards biennial values. Considering the very low accumulation rate at Dome C, predominant dry deposition of impurities [*Legrand*, 1987], wind driven mixing of the surface snow and fractionation processes due to frost formation [*Iizuka et al.*, 2004] the analytical resolution is sufficient to trace the preserved deposition of Na^+ and Ca^{2+}. The detection limits of the measurements were of the order of 4 ng g^{-1} for Na^+ and 0.4 ng g^{-1} for Ca^{2+}, and all our results are in good agreement with ion-chromatography (IC) measurements [*Littot et al.*, 2002].

Mean measurement errors of Na^+ and Ca^{2+} are less than 10% [*Röthlisberger et al.*, 2000]. Supplementary IC measurements on discrete samples from GM II were done in the clean room at the British Antarctic Survey in Cambridge.

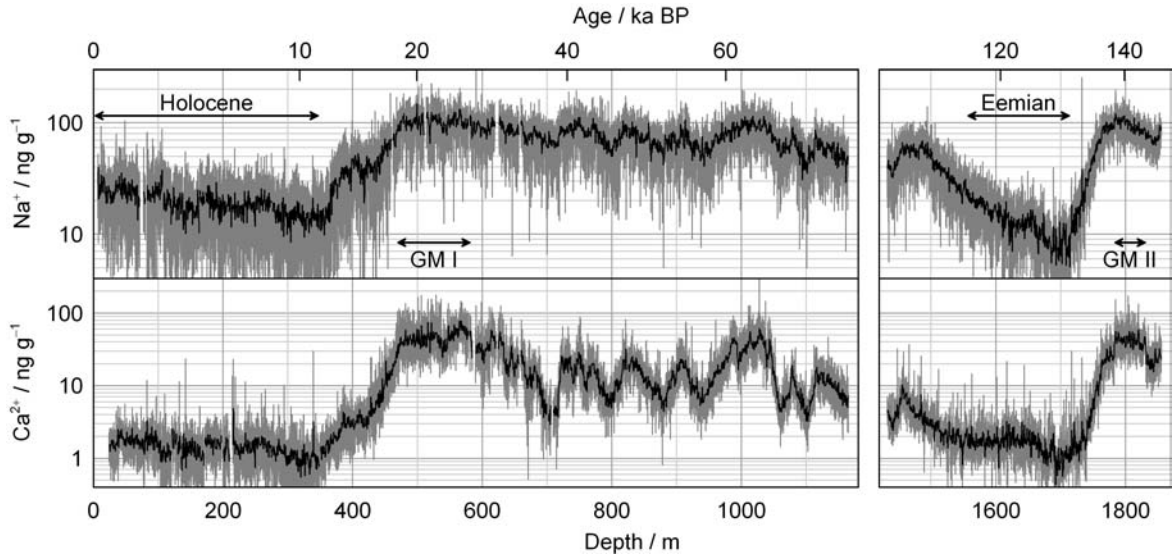

Figure 1. Na^+ and Ca^{2+} measurements (concentration in ng g^{-1}) from the EPICA Dome C deep ice core (EDC96 and EDC99) in 0.5 cm (grey lines) and 55 cm (black lines) resolution covering two interglacial periods (Holocene, Eemian) and partly two glacial periods including their glacial maxima (GM I, II).

3. Data-based estimate of continental aerosol ratios

In Figure 2a, we examine the relationship between the high-resolution Na^+ and Ca^{2+} measurements as proposed by *Warneck* [1999]. For a single aerosol source for both Na^+ and Ca^{2+}, all data should be aligned along a proportional line with the slope of the (Na^+/Ca^{2+}) ratio of the source material. However, such a simple relationship cannot be expected due to the contribution of material from a marine and a continental source showing different ratios. Given the extraordinary high depth resolution of the records, we assume to record both, events of only marine aerosol input and, under glacial conditions, events of predominantly continental aerosol input. This then results in an upper and lower proportional line (lying parallel to each other in a double logarithmic plot) representing the marine and continental aerosol ratios.

Holocene and Eemian data in Figure 2a are indeed limited by the bulk seawater ratio. The same holds true for data from the previous two glacial maxima, where the continental ratio is limiting, under the assumption, that it is reasonably constant. If not, the limitation represents at least the lower bound of the continental aerosol ratio. Apart from the predominantly marine or continental peaks, most events represent a mixture of the two sources, resulting in values somewhere in between the two boundaries given. The same applies to any averaged data, where possible unambiguous continental or marine events are blurred.

Another striking limitation of data points appears as an upper envelope (dashed line in Figure 2a), which is a mixing line giving the maximum contribution of marine to the total aerosol. If the continental aerosol contained almost no Na^+ and thus $(Na^+/Ca^{2+})_{cont}$ were very small or zero, such a mixing line would be horizontal. This is obviously not the case, indicating a substantial Na^+ contribution from the continental source.

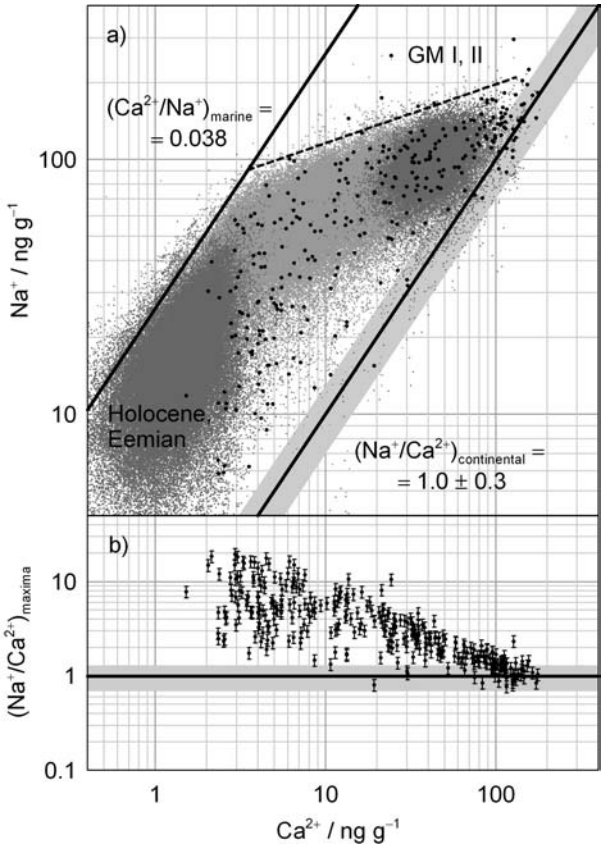

Figure 2. (a) Scatter plot of all Na^+ and Ca^{2+} measurements in 0.5 cm resolution (light grey) as shown in Figure 1; the minima of both axes are set to the detection limits. Dark grey represents the interglacial data (Holocene, Eemian) at the bottom left, and the glacial maxima data (GM I, II) at the top right. Black dots are extraordinarily high Ca^{2+} peaks with reference to the background level and corresponding Na^+ values. Black lines indicate the marine and continental aerosol ratios, the latter with an estimated error band. The dashed line at the top indicates a mixing line giving the maximum contribution of marine to the total aerosol. (b) Ratio (Na^+/Ca^{2+}) of the extraordinarily high Ca^{2+} peaks versus the Ca^{2+} value (black dots) with error bars accounting for measurement uncertainty, and the data-deduced continental aerosol ratio (black line) with estimated error band.

The proportional line of the limiting continental ratio based on all data points is not very well defined. So, to deduce $(Na^+/Ca^{2+})_{cont}$ from water-soluble Na^+ and Ca^{2+} we selected extraordinary Ca^{2+} peaks and corresponding Na^+ peaks within ± 0.5 cm (black dots in Figure 2a and 2b) which are likely to represent mainly continental aerosol input. As a restrictive and robust peak criterion, we used the running median of a 2.5 m wide window plus four times the mean absolute deviation on the same window based on the logarithmic 0.5 cm data. This resulted in 305 peaks, approximately one per mil out of $3{\cdot}10^5$ data points. Only a few of these extraordinary peaks are lying on the proportional line representing the continental ratio, most of them comprise a marine contribution as well. In Figure 2b the (Na^+/Ca^{2+}) ratios of these peaks are plotted versus the Ca^{2+} concentrations, showing a convergence to the lower envelope of $(Na^+/Ca^{2+})_{cont} = 1.0 \pm 0.3$. The error is estimated based on the analytical uncertainty and the possibility of a remaining marine contribution. The conservative estimate of –30% for the lower error is justified by the fact that if there is just a small remaining marine contribution to Ca^{2+} quite high amounts of ss-Na^+ are resulting due to the numerically low $(Ca^{2+}/Na^+)_{mar}$ ratio. However, +30% is probably an overestimation of the upper error. In Figure 2a a good agreement of the peak value-based continental aerosol with the limitation of all high-resolution measurements can be seen.

The data-derived continental ratio can now be used together with the bulk seawater ratio to calculate the ss-Na^+ and the nss-Ca^{2+} contributions (Equations 1 and 2) of the Dome C data shown in Figure 1. Results are given in Figure 3 smoothed with a Gaussian filter (cut off length 50m) to track the general

features. For comparison our results are shown along with the temperature proxy δD [*EPICA community members*, 2004]. Conspicuous are the low ss-Na^+ fractions of 50-60% during glacial maxima (GM I, II), which increase to 60-90% during the last glacial period. On the other hand, ss-Na^+ contribution during the last interglacial period, the Eemian, is lower than during the Holocene, whereas the situation for nss-Ca^{2+} is opposite. The reason is, that the Na^+ levels during the Eemian are significantly lower than Holocene values, while Ca^{2+} was increased.

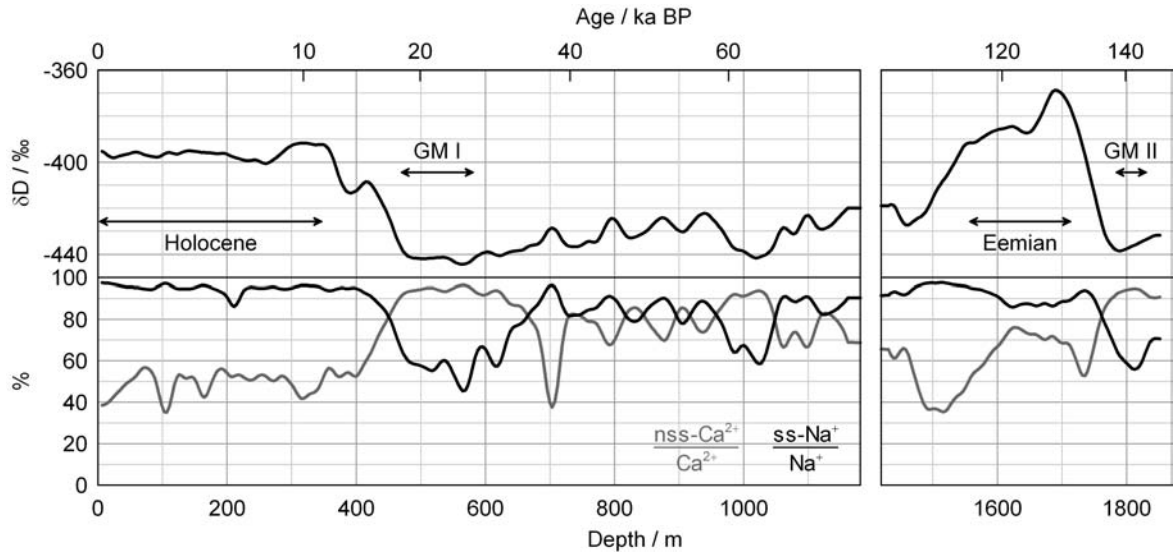

Figure 3. Percentages of ss-Na^+ to the total Na^+ (black lines) and nss-Ca^{2+} to the total Ca^{2+} (grey lines) during different climatic periods from the EPICA Dome C deep ice core along with the temperature proxy δD [*EPICA community members*, 2004]; All data are smoothed with a Gaussian filter (cut off length 50 m).

Analogous to ss-Na^+ (Equation 1), ss-Cl^- can be calculated based on Cl^- and $(Cl^-/Ca^{2+})_{cont}$, whereas nss-Ca^{2+} (Equation 2) can be expressed based on Ca^{2+}, ss-Cl^- and $(Ca^{2+}/\ Cl^-)_{mar}$. We therefore have four equations altogether. With IC measurements of Ca^{2+}, Na^+ and Cl^- on 10 cm mean samples and the $(Na^+/Ca^{2+})_{cont}$ ratio as derived above, we can calculate the remaining unknown, $(Cl^-/Ca^{2+})_{cont}$, although even at a coarser resolution. Due to post-depositional effects affecting Cl^- preservation at Dome C, only samples with a concurrent Ca^{2+} concentration ≥ 20 ng g^{-1} are considered. In these cases post-depositional effects are minor and additionally, volcanic contribution to Cl^- can be neglected [*Röthlisberger et al.*, 2003]. The resulting databased average value of $(Cl^-/Ca^{2+})_{cont}$ is 1.7 and hence $(Cl^-/Na^+)_{cont}$ is 1.7, which is close to the bulk seawater ratio. We estimate errors at about 30%.

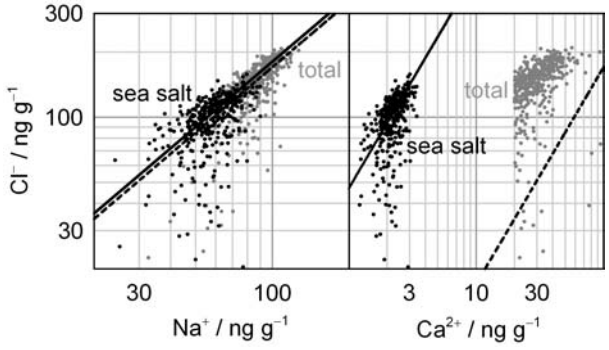

Figure 4. Scatter plot of Na^+, Ca^{2+} and Cl^- measurements by IC from dusty glacial periods (Ca^{2+} ≥ 20 ng g^{-1}) within the EPICA Dome C deep ice core (EDC99) in 10 cm resolution (light grey). In black the calculated ss-Na^+, ss-Ca^{2+} and ss-Cl^- values based on high-resolution-data-derived continental aerosol ratios (broken black lines) and the marine ratios (black lines). The ratios $(Cl^-/Na^+)_{mar}$ and $(Cl^-/Na^+)_{cont}$ are very similar.

Using this set of continental aerosol ratios to calculate the ss-Cl^-, ss-Na^+ and ss-Ca^{2+} during dusty glacial periods ($Ca^{2+} \geq 20$ ng g^{-1}) leads to the results shown in Figure 4. The few outliers of the chloride measurements are related to post-depositional effects occurring even in dusty glacial periods. It is also obvious from Figure 4, that due to the coarser resolution (10 cm means), and therefore stronger mixing of both source contributions, the data points show up clearly above the lower proportional line representing the mean continental aerosol ratios. To conclude, we suggest to use $(Na^+/Ca^{2+})_{cont} = 1.0$, $(Cl^-/Ca^{2+})_{cont} = 1.7$ and $(Cl^-/Na^+)_{cont} = 1.7$ for sea-salt and non-sea-salt calculations at the Dome C site instead of mean crust values, especially for glacial periods, where the resulting fractions are heavily influenced by these ratios.

4. Comparison with aerosol properties of the potential source region

Based on isotopic ratios measured on water-insoluble dust, the mainly southern South American continental origin was confirmed [*Grousset et al.*, 1992] and declared to remain unchanged over different glacial stages, despite the observed huge dust concentration variations [*Basile et al.*, 1997]. Additional evidence for a strong influence of this single dominant source for high southern latitudes comes from a quite similar overall composition of the aerosol deposited on the Antarctic continent, despite the different meteorological conditions at different sites [*Delmas and Petit*, 1994]. Recently, the glacial continental aerosol source was even more restricted to regions south of 37°S, thus the southern Pampas and Patagonia [*Smith et al.*, 2003], which is the only land mass in the Southern hemisphere of significant size located inside the belt of Westerlies. They control the climate by discharging most of their water content in the Andes, continuing as dry winds to the east, producing an orographic desert, picking up large volumes of dust, and hence moving to the east-southeast crossing the latitude of 80°S [*Iriondo*, 2000].

Delmas and Petit [1994] postulated that the frequently exposed continental shelf during glacial periods was the dominant aerosol source, providing a mixture of carbonate marine sediments, continental material and sea salt. Furthermore they reported a similarity of the present Antarctic aerosol to the one found in ice cores from glacial periods and speculated that the present Antarctic aerosol originates mainly from ice age Aeolian deposits in southern South America. In contrast, significant contributions of the continental shelf were ruled out based on isotope measurements [*Basile et al.*, 1997], which was explained by a probably humid environment on the exposed shelf and, the presence of vegetation. Again, *Zárate* [2003] doubted about this argumentation based on only a few isotopic ratio measurements, regarding the complexity of the region consisting of glacial, glaciofluvial, and volcanic sediments derived from the Andes, being modified by aeolian and fluvial processes; he alludes to outwash plains from the fluvial system probably formed on the emerged continental shelf with high sediment availability. Therefore, the role of the exposed continental shelf during glacial sea level decrease seems to be unresolved.

The relative content of Na^+ and Cl^- in the continental aerosol deposited in Dome C is higher than expected based on mean crust values [*Bowen*, 1979]. Assuming that the composition has remained more or less constant over time and that modifications during transport are negligible or remain the same, we compare our results from the glacial Dome C ice core to present-day properties of the aerosol and soils in the southern Pampas and Patagonia, the dominant source regions. *Bowen* [1979] suggested that the highly mobile ions Cl^- and Na^+ are expected to be depleted at the surface of soils where rainfall is abundant but enriched at the surface of aridisols as they appear in source region. *Ramsperger et al.* [1998a; 1998b] examined wind blown dust at different sites around 38°S over several years. The mineralogical composition of soils and dust at these sites were similar and homogenous over time, suggesting the common source of the dust. Dust and soils show distinctly higher salt concentrations compared to average West African dust, for example. Additionally, salts originating from saline soils of the Pampas and the neighbouring arid zone may contribute. Marine aerosol influence is only significant for one site proximate to the coast [*Ramsperger et al.*, 1998a; 1998b], which we exclude here. They found the following ratios of water-soluble ions of the windblown dust, averaged over all sites and data: $(Na^+/Ca^{2+})_{Patagonian\ dust} = 0.85$ and $(Cl^-/Na^+)_{Patagonian\ dust} = 2.0$, which are in very good agree-

ment with our results. When looking at soluble ion ratios in soil instead of dust then even higher enrichments of Na^+ and Cl^- are found [see also *Bouza et al.*, 1993]. *Prospero et al.* [2002] pointed to the fact that this arid and sub-arid area contains great saline areas and brackish streams. Therefore the composition of the water-soluble aerosol contributions can be explained with the contribution of dust from Patagonia or the southern Pampas, solely, although we cannot exclude a contribution from the exposed continental shelf based on our analysis.

5. Conclusion

We showed evidence that for the very limited source area of continental glacial aerosols transported to the East Antarctic ice sheet the contribution of water-soluble Na^+ and Cl^- was higher than previously assumed. Mean crust values that were up to now used for source contribution estimates turn out to be unsuitable for this restricted source area. Therefore, previous studies underestimated the continental contribution to Na^+ and Cl^- and overestimated the marine contribution during glacial times, as indicated in *Delmas and Petit* [1994]. Referred to the entire water-soluble Na^+ deposition, ss-Na^+ contributes only about 50-60% during the glacial maxima. Hence, records of total Na^+ [e.g. *Petit et al.*, 1999] do not represent a purely marine signal during glacial times. For Ca^{2+}, corrections are small, and previous studies are not significantly affected.

Under the condition that post-depositional effects are negligible during glacial maxima, the same as for Na^+ holds true for Cl^- records, with a sea-salt-fraction of 60-70% referred to the total Cl^-. Until now it was assumed that Cl^- has no significant continental source [*Röthlisberger et al.*, 2003]. Because we observed a ratio of $(Cl^-/Na^+)_{cont}$ corresponding to $(Cl^-/Na^+)_{mar}$, the (Cl^-/Na^+) during glacial maxima corresponds to the bulk seawater ratio as well, although the continental aerosol contributes strongly. A different explanation for this behaviour could be that the total Na^+ content of the ice from the last glacial maximum consists of ss-Na^+ only, thus the contribution of Na^+ and Cl^- from the continental aerosol and their ratio relative to Ca^{2+} would be negligible. However, based on our high-resolution data this hypothesis can be ruled out.

Similar estimates should be done on other ice core sections from the East Antarctic plateau and from other Antarctic sites in order to corroborate our findings. This approach might also allow characterizing differences in dust source regions for different Antarctic sites. However, such an analysis requires a network of high-resolution data that is not yet available from other ice cores.

Acknowledgments

This work is contribution XX to the “European Project for Ice Coring in Antarctica” (EPICA), a joint ESF (European Science Foundation) / EC scientific programme, funded by the European Commission and by national contributions from Belgium, Denmark, France, Germany, Italy, Netherlands, Norway, Sweden, Switzerland and the United Kingdom. We thank all the scientist involved in the fieldwork to obtain this comprehensive data set.

References

Basile, I., F.E. Grousset, M. Revel, J.R. Petit, P.E. Biscaye, and N.I. Barkov, Patagonian origin of glacial dust deposited in East Antarctica (Vostok and Dome C) during glacial stages 2, 4 and 6, *Earth and Planetary Science Letters*, *146* (3-4), 573-589, 1997.

Bouza, P., H.F. Delvalle, and P.A. Imbellone, Micromorphological, physical, and chemical characteristics of soil crust types of the central Patagonia region, Argentina, *Arid Soil Research and Rehabilitation*, *7* (4), 355-368, 1993.

Bowen, H.J.M., *Environmental Chemistry of the Elements*, Academic Press, London, 1979.

de Angelis, M., N.I. Barkov, and V.N. Petrov, Aerosol concentrations over the last climatic cycle (160 kyr) from an Antarctic ice core, *Nature*, *325* (6102), 318-321, 1987.

Delmas, R.J., and J.R. Petit, Present Antarctic aerosol composition: A memory of ice age atmospheric dust?, *Geophysical Research Letters*, *21* (10), 879-882, 1994.

EPICA community members, Eight glacial cycles from an Antarctic ice core, *Nature*, 2004.

Grousset, F.E., P.E. Biscaye, M. Revel, J.R. Petit, K. Pye, S. Joussaume, and J. Jouzel, Antarctic (Dome C) ice-core dust at 18 ky BP - isotopic constraints on origins, *Earth and Planetary Science Letters*, *111* (1), 175-182, 1992.

Iizuka, Y., Y. Fujii, N. Hirasawa, T. Suzuki, H. Motoyama, T. Furukawa, and T. Hondoh, SO_4^{2-} minimum in summer snow layer at Dome Fuji, Antarctica, and the probable mechanism, *Journal of Geophysical Research - Atmospheres*, *109* (D4), 2004.

Iriondo, M., Patagonian dust in Antarctica, *Quaternary International*, *68*, 83-86, 2000.

Legrand, M., Chemistry of Antarctic snow and ice, *Journal de Physique*, *48* (C-1), 77-86, 1987.

Legrand, M., and P. Mayewski, Glaciochemistry of polar ice cores: A review, *Reviews of Geophysics*, *35* (3), 219-243, 1997.

Legrand, M.R., C. Lorius, N.I. Barkov, and V.N. Petrov, Vostok (Antarctica) ice core: Atmospheric chemistry changes over the last climatic cycle (160,000 years), *Atmospheric Environment*, *22* (2), 317-331, 1988.

Littot, G.C., R. Mulvaney, R. Röthlisberger, R. Udisti, E.W. Wolff, E. Castellano, M. de Angelis, M.E. Hansson, S. Sommer, and J.P. Steffenssen, Comparison of analytical methods used for measuring major ions in the EPICA Dome C (Antarctica) ice core, *Annals of Glaciology*, *35*, 299-305, 2002.

Petit, J.R., J. Jouzel, D. Raynaud, N.I. Barkov, J.-M. Barnola, I. Basile, M. Bender, J. Chappellaz, M. Davis, G. Delaygue, M. Delmotte, V.M. Kotlyakov, M. Legrand, V.Y. Lipenkov, C. Lorius, L. Pépin, C. Ritz, E. Saltzman, and M. Stievenard, Climate and atmospheric history of the past 420,000 years from the Vostok ice core, Antarctica, *Nature*, *399*, 429-436, 1999.

Prospero, J.M., P. Ginoux, O. Torres, S.E. Nicholson, and T.E. Gill, Environmental characterization of global sources of atmospheric soil dust identified with the Nimbus 7 Total Ozone Mapping Spectrometer (TOMS) absorbing aerosol product, *Reviews of Geophysics*, *40* (1), 2002.

Ramsperger, B., L. Herrmann, and K. Stahr, Dust characteristics and source-sink relations in eastern west Africa (SW-Niger and Benin) and South America (Argentinean pampas), *Zeitschrift für Pflanzenernährung und Bodenkunde*, *161* (4), 357-363, 1998a.

Ramsperger, B., N. Peinemann, and K. Stahr, Deposition rates and characteristics of aeolian dust in the semi-arid and sub-humid regions of the Argentinean Pampa, *Journal of Arid Environments*, *39* (3), 467-476, 1998b.

Röthlisberger, R., M. Bigler, M. Hutterli, S. Sommer, B. Stauffer, H.G. Junghans, and D. Wagenbach, Technique for continuous high-resolution analysis of trace substances in firn and ice cores, *Environmental Science & Technology*, *34* (2), 338-342, 2000.

Röthlisberger, R., M. Bigler, E.W. Wolff, F. Joos, E. Monnin, and M.A. Hutterli, Ice core evidence for the extent of past atmospheric CO_2 change due to iron fertilisation, *Geophysical Research Letters*, 2004.

Röthlisberger, R., R. Mulvaney, E.W. Wolff, M.A. Hutterli, M. Bigler, M. de Angelis, M.E. Hansson, J.P. Steffensen, and R. Udisti, Limited dechlorination of sea-salt aerosols during the last glacial period: Evidence from the European Project for Ice Coring in Antarctica (EPICA) Dome C ice core, *Journal of Geophysical Research - Atmospheres*, *108* (D16), 2003.

Röthlisberger, R., R. Mulvaney, E.W. Wolff, M.A. Hutterli, M. Bigler, S. Sommer, and J. Jouzel, Dust and sea salt variability in central East Antarctica (Dome C) over the last 45 kyrs and its implications for southern high-latitude climate, *Geophysical Research Letters*, *29* (20), 2002.

Schwander, J., J. Jouzel, C.U. Hammer, J.R. Petit, R. Udisti, and E. Wolff, A tentative chronology for the EPICA Dome Concordia ice core, *Geophysical Research Letters*, *28* (22), 4243-4246, 2001.

Smith, J., D. Vance, R.A. Kemp, C. Archer, P. Toms, M. King, and M. Zárate, Isotopic constraints on the source of Argentinian loess - with implications for atmospheric circulation and the provenance of Antarctic dust during recent glacial maxima, *Earth and Planetary Science Letters*, *212* (1-2), 181-196, 2003.

Warneck, P., *Chemistry of the Natural Atmosphere*, 927 pp., Academic Press, San Diego, 1999.

Wolff, E.W., A.M. Rankin, and R. Röthlisberger, An ice core indicator of Antarctic sea ice production?, *Geophysical Research Letters*, *30* (22), 2003.

Zárate, M.A., Loess of southern South America, *Quaternary Science Reviews*, *22* (18-19), 1987-2006, 2003.

2.2 Dust and sea salt variability in central East Antarctica (Dome C) over the last 45 kyrs and its implications for southern high-latitude climate

Regine Röthlisberger, Rob Mulvaney, Eric W. Wolff, Manuel A. Hutterli, Matthias Bigler, Stefan Sommer, Jean Jouzel

Geophysical Research Letters
29(20), 1963, 2002 and *30*(5), 1216, 2003 (correction)

GEOPHYSICAL RESEARCH LETTERS, VOL. 29, NO. 20, 1963, doi:10.1029/2002GL015186, 2002

Dust and sea salt variability in central East Antarctica (Dome C) over the last 45 kyrs and its implications for southern high-latitude climate

Regine Röthlisberger,[1,2] Robert Mulvaney,[1] Eric W. Wolff[1] Manuel A. Hutterli[3] Matthias Bigler,[2] Stefan Sommer,[2] and Jean Jouzel[4]

Received 21 March 2002; accepted 24 June 2002; published 22 October 2002.

[1] A detailed record of non-sea-salt calcium, a proxy for dust, and sea-salt sodium, a proxy for sea salt, covering the last 45 kyr is presented. It shows that in the first part of the transition from the last glacial period to the Holocene (18–15 kyr BP), the changes in dust flux mainly reflect changes at the dust source, namely vegetation cover and local climate. The changes in the later part of the transition (12–11 kyr BP) are similar in extent to the changes seen in sea salt and most likely reflect a reorganization of the atmospheric circulation. During the last glacial period, considerable variation of dust but not of sea salt is observed, pointing to climatic changes in Patagonia, the main dust source for Dome C. A comparison of the glacial records from Dome C and Taylor Dome suggests that similar influences controlled aerosol input at both sites during this period. *INDEX TERMS:* 3344 Meteorology and Atmospheric Dynamics: Paleoclimatology; 1620 Global Change: Climate dynamics (3309); 9310 Information Related to Geographic Region: Antarctica; 0368 Atmospheric Composition and Structure: Troposphere—constituent transport and chemistry. **Citation:** Röthlisberger, R., R. Mulvaney, E. W. Wolff, M. A. Hutterli, M. Bigler, S. Sommer, and J. Jouzel, Dust and sea salt variability in central East Antarctica (Dome C) over the last 45 kyrs and its implications for southern high-latitude climate, *Geophys. Res. Lett.*, *29*(20), 1963, doi:10.1029/2002GL015186, 2002.

1. Introduction

[2] Dust and sea salt records from polar ice cores have been widely used to infer past changes in atmospheric circulation and climatic conditions in the source region as well as in the Antarctic (e.g., [*Legrand et al.*, 1988; *Steig et al.*, 2000]) and have served as a control for atmospheric general circulation model (AGCM) simulations of atmospheric dust distribution in the past [*Reader et al.*, 1999; *Mahowald et al.*, 1999]. Generally, higher levels of impurities have been observed during the last glacial period in all Antarctic ice cores. The large increase in dust is assumed to be caused by increased production in the dust source region and more vigorous transport. Sea salt concentrations are thought to be influenced by the sea ice position and wind speed in the potential source region as well as the transport from there to the ice core site.

[3] Compared to Greenland ice core records, the Antarctic dust and sea salt records showed much smaller variations during the last glacial period [*Legrand et al.*, 1988; *Legrand and Delmas*, 1988], which may at least partially be attributed to limited resolution. The only Antarctic record showing marked variation of dust and sea salt during the last glacial period was from Taylor Dome, a site next to the Ross ice shelf, thus relatively close to the coast and possibly susceptible to regional climate changes [*Steig et al.*, 2000].

[4] Here we present the first high-resolution record of calcium (Ca^{2+}, a proxy for dust [*Fuhrer et al.*, 1999]) and sodium (Na^{+}, a proxy for sea salt) together with deuterium (δD) from an inland Antarctic site. The drilling in the frame of the European Project for Ice Coring in Antarctica (EPICA) at Dome C (75° 06′S, 123° 24′E, 3233 m a.s.l., approximately 1100 km from the nearest coast) reached a depth of 780 m by the end of the 1998/99 field season, corresponding to an age of approximately 45 kyrs [*Schwander et al.*, 2001]. The detailed records are discussed in terms of changes in aerosol source and transport and compared to the near-coastal records from Taylor Dome.

2. Methods

[5] Ca^{2+} and Na^{+} were analysed using a continuous flow analysis system (CFA) [*Röthlisberger et al.*, 2000]. Generally, the detection limit was of the order of less than 1 ppb for Ca^{2+} and a few ppb for Na^{+}. There may be some intervals with larger uncertainty due to unstable conditions of the analytical system, but a comparison with ion-chromatographic methods has shown a good overall agreement [*Littot et al.*, 2002]. Apart from 200 m that have been analysed with the same setup at the Alfred Wegener Institute in Bremerhaven, Germany in 2000, all analyses were made at Dome C during the 1997/98 and 1998/99 field seasons. δD measurements were carried out in Saclay, France using the uranium reduction technique and an automatic sample injection device [*Vaughn et al.*, 1998].

3. Results and Discussion

[6] As some of the Ca^{2+} found in the ice at Dome C is of marine origin, the Ca^{2+} concentrations reflect changes in dust and in sea salt levels. Similarly, some Na^{+} derives from continental dust. Assuming a Ca^{2+}/Na^{+} ratio of 0.038 for marine aerosols (R_m) and 1.78 for average crust (R_t) [*Bowen*, 1979], we calculated the sea-salt-Na^{+} (ss-Na^{+}= Na^{+} - $\frac{nss-Ca^{2+}}{R_t}$) and the non-sea-salt-Ca^{2+} (nss-Ca^{2+} = Ca^{2+}

[1]British Antarctic Survey, Cambridge, England, UK.
[2]Climate and Environmental Physics, University of Bern, Bern, Switzerland.
[3]Department of Hydrology and Water Resources, University of Arizona, Tucson, Arizona, USA.
[4]Laboratoire des Sciences du Climat et de l'Environnement, Gif-sur-Yvette, France.

0094-8276/02/2002GL015186$05.00

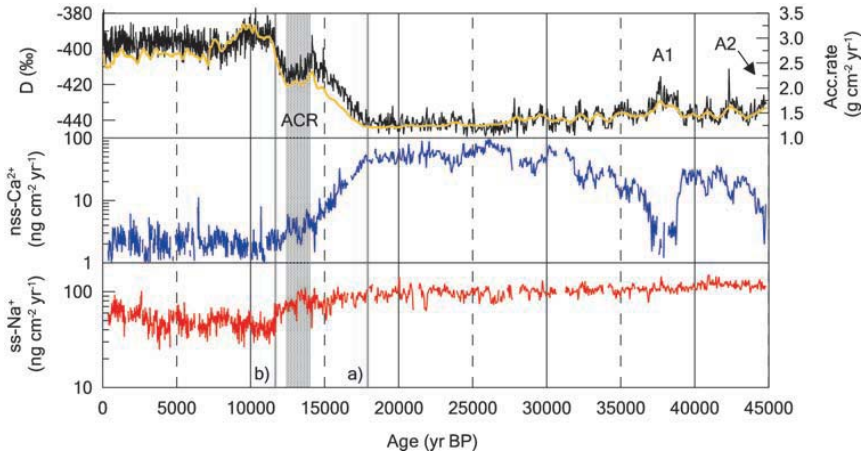

Figure 1. Fluxes of ss-Na^+ and nss-Ca^{2+}, as well as the δD and the accumulation rate (yellow line, [*Schwander et al.*, 2001]) from the top 780 m of the EPICA Dome C deep ice core at 55 cm resolution. The vertical grey lines refer to the beginning (a) and the end (b) of the Transition, the shaded area corresponds to the Antarctic Cold Reversal (ACR).

$- R_m \cdot$ ss-Na^+). In the Holocene, the terrestrial input at Dome C is extremely low, the marine contribution to Ca^{2+} is around 50% and the terrestrial Na^+ is of the order of 2%. During the last glacial maximum (LGM, 18–24 kyr B.P.), only 7% of Ca^{2+} came from sea salt, whereas 24% of Na^+ came from terrestrial dust. However, the Ca^{2+}/Na^+ ratio varies for different types of terrestrial material. We did the above calculation also for average soil and average sediment Ca^{2+}/Na^+ ratios. This led to similar percentages for Holocene and glacial ss-Ca^{2+} and Holocene nss-Na^+, while the glacial nss-Na^+ ranged from 3% to 24% depending on the Ca^{2+}/Na^+ ratio used. However, based on aluminium measurements [*Legrand and Delmas*, 1988], the ratio for the average crust seems to be the most suitable value and was thus used to calculate nss-Ca^{2+} and ss-Na^+.

[7] In agreement with previous results obtained from Antarctic ice cores (e.g., [*Steig et al.*, 2000; *Legrand et al.*, 1988; *Legrand and Delmas*, 1988; *Watanabe et al.*, 1999]), nss-Ca^{2+} and ss-Na^+ concentrations in the Dome C record were higher during the last glacial period. At the LGM, nss-Ca^{2+} concentrations were approximately 50 times higher than during the Holocene, and ss-Na^+ approximately 5 times. During the transition, nss-Ca^{2+} and ss-Na^+ concentrations decreased steadily from glacial levels to a relatively stable level during the Antarctic Cold Reversal (ACR, 14–12.5 kyr B.P.), and then further to Holocene levels. Concentrations of nss-Ca^{2+} changed by a factor of 23 from LGM to ACR levels, while ss-Na^+ concentrations decreased only by a factor of 2. Both nss-Ca^{2+} and ss-Na^+ concentrations dropped further by a factor of 2.3 from the ACR to the early Holocene. The changes seen in nss-Ca^{2+} concentrations agree with insoluble dust measurements [*Delmonte et al.*, 2001], with particle number and mass concentration changing by a factor of 50 from the LGM to the Holocene and a factor of 2 from the ACR to the Holocene.

[8] At Dome C, the accumulation rate is very low (2.7 g cm^{-2} yr^{-1}, [*Schwander et al.*, 2001]) and was reduced by a factor of approximately 2 during the last glacial period. Since there is so little precipitation, dry deposition is the dominating process for sea salt and dust deposition [*Legrand*, 1987]. In order to compensate as well as possible for the dilution effect of changes in the accumulation rate, we consider the changes in nss-Ca^{2+} and ss-Na^+ flux calculated with the accumulation rates of *Schwander et al.*, 2001 in the following discussion.

3.1. Transition

[9] The ss-Na^+ flux was almost constant during the last glacial period and changed only by a factor of 2 from the LGM to the early Holocene (Figure 1). Most of the changes during the transition happened after the ACR [*Stenni et al.*, 2001]. nss-Ca^{2+} flux on the other hand changed dramatically in the early phase of the transition, and the change from the ACR to the Holocene was of similar extent as for ss-Na^+. According to a recent study of dust transport to Dome C based on back trajectory calculations [*Lunt and Valdes*, 2001], the dust transport was reduced during the LGM. These results are supported by dust particle measurements [*Delmonte et al.*, 2001], which showed a slightly smaller particle mode and a smaller geometric standard deviation of the particle size distribution in the glacial than in the Holocene, indicative of a tendency to longer transport paths and less meridional transport. On the other hand, based on GCM simulations *Krinner and Genthon* [2002] concluded that the dust transport from Patagonia to Dome C was faster during the LGM, in contrast to the studies by *Lunt and Valdes* [2001] and *Delmonte et al.* [2001]. But at any rate, based on these studies the changes in dust transport to Antarctica were small and cannot account for the large changes seen in dust. Therefore, substantial changes at the dust source, which is believed to be mainly located in Patagonia [*Basile et al.*, 1997], must have occurred in order to explain the high dust input during the LGM and the different behaviour of nss-Ca^{2+} and ss-Na^+ during the transition.

[10] The potential dust source area decreased with rising sea level, but the period of rapid sea level rise (around 14 kyr BP [*Guilderson et al.*, 2000]) coincides with a period of almost no changes in dust, suggesting that the contribution

from continental shelves to the total dust transported to Dome C is not dominant. This is in agreement with a study comparing the isotopic composition of dust from the Argentine continental shelf and the dust from Dome C and Vostok [*Basile et al.*, 1997]. Based on various palaeoenvironmental proxies, Patagonia experienced a warming and a concomitant glacier retreat around 17,330 yr BP (e.g., *McCulloch and Davis*, [2001] and references therein). The warmer climate promoted vegetation growth, which was supported by an increase in effective moisture around 16,910 yr BP [*McCulloch and Davis*, 2001]. Therefore, dust entrainment was hindered by soil moisture and vegetation cover, which led to a decrease in aeolian dust as observed in the Dome C record. Changes in local wind speed might have had an influence on dust uplift as well, with lower wind speeds leading to less dust. From 15,330 yr BP to approximately 12,200 yr BP, *McCulloch and Davis* [2001] report a relatively dry phase, accompanied by glacier advances. During this period (ACR), the nss-Ca^{2+} fluxes at Dome C remained more or less constant. Around 12,200 yr BP, trees and shrubs started to spread, indicating a second warming step in southern South America. However, this second warming was not paralleled by an increase in precipitation, but a relatively dry climate prevailed for several millennia. Nonetheless the nss-Ca^{2+} flux at Dome C decreased further between the ACR and the Holocene by almost a factor of 2. As the change is similar to the changes seen in ss-Na^{+}, we suggest that a reorganization of the atmospheric circulation led either to changes in transport or source fluxes at both the dust and sea salt source.

3.2. 25 to 45 kyr B.P.

[11] In the earlier part of the last glacial period, from 45 to approximately 25 kyr B.P., the δD record showed a few distinct oscillations. These variation in stable isotopes have been observed in other Antarctic ice cores [*Blunier et al.*, 1998] and have been referred to as A1 and A2 (Figure 1). The nss-Ca^{2+} flux changed considerably during these two major events, but even on a shorter timescale, it parallels the minor variations seen in δD (Figure 1). The ss-Na^{+} flux on the other hand seems unaffected by these changes.

[12] As seen in Figure 2, the lowest nss-Ca^{2+} fluxes during the oscillations in the glacial period were as low as during the Holocene. At 39 kyr B.P., nss-Ca^{2+} flux dropped

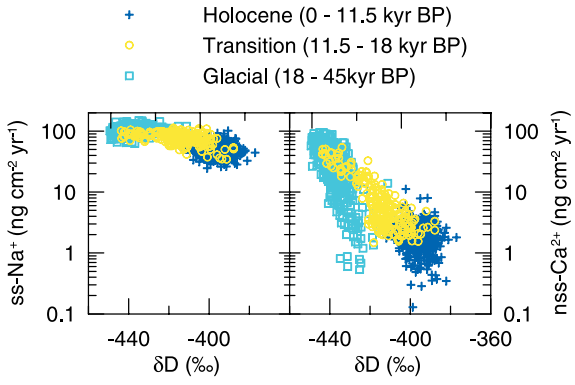

Figure 2. Fluxes of ss-Na^{+} and nss-Ca^{2+} versus δD, 55 cm averages.

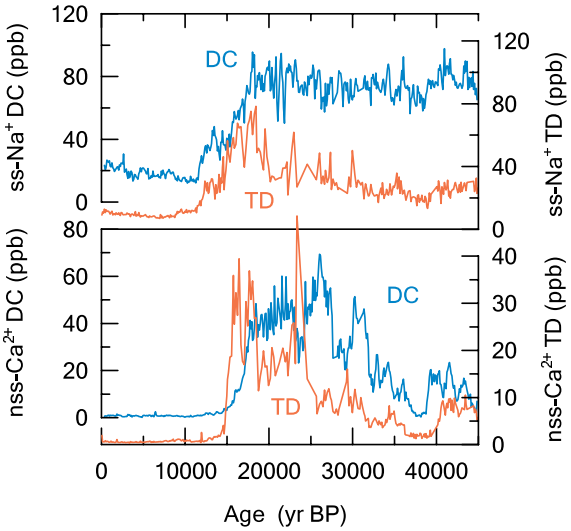

Figure 3. Concentrations of ss-Na^{+} and nss-Ca^{2+} (100-yr averages) from Dome C and Taylor Dome [*Steig et al.*, 2000].

from 30 to 3 ng cm^{-2} yr^{-1} within approximately 400 years. In contrast to nss-Ca^{2+}, the variation in the ss-Na^{+} flux during the glacial period was small compared to the change from glacial to Holocene ice. The fact that sea salt fluxes were doubled during the last glacial period compared to the Holocene despite the expansion of sea ice indicates that atmospheric circulation and the hydrological cycle are most likely the factors dominating sea salt aerosol flux at Dome C. Major changes in these two factors should therefore be reflected in ss-Na^{+} as well as nss-Ca^{2+}. Thus, the cause of the glacial flux changes only seen in nss-Ca^{2+} must lie instead in Patagonia, analogous to the above discussion of the transition. This implies drastic changes in southern Patagonian climate during the last glacial period, most likely in temperature and precipitation, that were coeval with changes in temperature at Dome C.

[13] In Figure 3, we compare the nss-Ca^{2+} and ss-Na^{+} concentrations of Dome C with the ones measured at Taylor Dome [*Steig et al.*, 2000]. The data are shown as 100-yr averages based on the st9810 timescale. However, *Mulvaney et al.* [2000] have shown that this timescale needs to be revised around the transition from the LGM to the Holocene. We therefore only refer to the general shape of the nss-Ca^{2+} and ss-Na^{+} records but not to the timing of the changes. Sea salt and dust concentrations were higher at Dome C than at Taylor Dome by about a factor of 2, which reflects most likely the dilution effect of higher accumulation rates at Taylor Dome than at Dome C. While one would expect that large changes in dust input would manifest at Dome C and Taylor Dome in a similar way [*Mulvaney et al.*, 2000], it is rather surprising that also the general shape of the sea salt records of both sites are similar, as the sea salt source is so much closer to Taylor Dome than to Dome C. However, empirical orthogonal function (EOF) analysis of the chemical records from Taylor Dome has shown that the dominant EOF, which is thought to reflect

atmospheric circulation systems, explains more than 90% of the variability of sodium and calcium [*Steig et al.*, 2000] The similarity of the sea salt as well as the dust records of the two sites during the last glacial period suggests that not only sea salt and dust aerosol were closely linked through large-scale circulation patterns, but that this influenced primary aerosol input to central and near coastal Antarctica in a similar way.

4. Conclusions

[14] The dust record of the EPICA ice core from Dome C is closely linked with palaeoclimatic records from southern Patagonia during the transition from the last glacial period to the Holocene. The vast changes by a factor of 24 in nss-Ca^{2+} flux observed in the early part of the transition reflect changes in vegetation cover and soil moisture in Patagonia that prevented dust uplift. During the last glacial period, considerable changes in the nss-Ca^{2+} flux are observed, but no changes in ss-Na^{+}. It is unlikely that the massive changes in atmospheric transport that would be necessary to cause the changes in dust flux would not be reflected in ss-Na^{+}. Therefore, the nss-Ca^{2+} record from Dome C documents relatively rapid climatic changes in southern South America, coeval with temperature variations at Dome C. The nss-Ca^{2+} as well as the ss-Na^{+} records from Dome C and Taylor Dome are very similar in form during the last glacial period, with little variation in the sea salt concentration in contrast to huge changes in dust, indicating similar influences controlling aerosol input in near coastal and central Antarctica.

[15] **Acknowledgments.** This work is contribution No. 491 to the "European Project for Ice Coring in Antarctica" (EPICA), a joint ESF (European Science Foundation)/EC scientific programme, funded by the European Commission and national contributions from Belgium, Denmark, France, Germany, Italy, the Netherlands, Norway, Sweden, Switzerland, and the United Kingdom. R. R. thanks the SNF for financial support and J. Schwander for valuable discussion and providing data.

References

Basile, I., F. E. Grousset, M. Revel, J. R. Petit, P. E. Biscaye, and N. I. Barkov, Patagonian origin of glacial dust deposited in East Antarctica (Vostok and Dome C) during glacial stages 2, 4, and 6, *Earth Planet. Sci. Lett.*, *146*, 573–589, 1997.

Blunier, T., J. Chappellaz, J. Schwander, A. Dällenbach, B. Stauffer, T. F. Stocker, D. Raynaud, J. Jouzel, H. B. Clausen, C. U. Hammer, and S. J. Johnsen, Asynchrony of Antarctic and Greenland climate change during the last glacial period, *Nature*, *394*, 739–743, 1998.

Bowen, H. J. M., *Environmental chemistry of the Elements*, Academic Press, London, 1979.

Delmonte, B., J. R. Petit, and V. Maggi, Glacial to Holocene implications of the new 27,000-year dust record from the EPICA Dome C (East Antarctica) ice core, *Clim. Dyn.*, in press, 2001.

Fuhrer, K., E. W. Wolff, and S. J. Johnsen, Timescales for dust variability in the Greenland Ice Core Project (GRIP) ice core in the last 100,000 years, *J. Geophys. Res.*, *104*, 31,043–31,052, 1999.

Guilderson, T. P., L. Burckle, S. Hemming, and W. R. Peltier, Late Pleistocene sea level variations derived from the Argentine Shelf, *G3 (Geochemistry, Geophysics, Geosystems)*, 1, 2000.

Krinner, G., and C. Genthon, Tropospheric transport of continental tracers towards Antarctica under varying climatic conditions, *Tellus*, submitted, 2002.

Legrand, M., Chemistry of Antarctic snow and ice, *Journal de Physique*, *C1*, 77–86, 1987.

Legrand, M., and R. J. Delmas, Soluble impurities in four Antarctic ice cores over the last 30,000 years, *Ann. Glaciol.*, *10*, 116–120, 1988.

Legrand, M., C. Lorius, N. I. Barkov, and V. N. Petrov, Vostok (Antarctica) ice core: atmospheric chemistry changes over the last climatic cycle (160,000 years), *Atm. Env.*, *22*, 317–331, 1988.

Littot, G. C., R. Mulvaney, R. Röthlisberger, R. Udisti, E. W. Wolff, E. Castellano, M. de Angelis, M. Hansson, S. Sommer, and J. P. Steffensen, Comparison of analytical methods used for measuring major ions in the EPICA Dome C (Antarctica) ice core, *Ann. Glaciol.*,in press, 2002.

Lunt, D. J., and P. J. Valdes, Dust transport to Dome C, Antarctica at the Last Glacial Maximum and present day, *Geophys. Res. Let.*, *28*, 295–298, 2001.

Mahowald, N., K. Kohfeld, M. Hansson, Y. Balkanski, S. P. Harrison, I. Prentice, M. Schulz, and H. Rodhe, Dust sources and deposition during the last glacial maximum and current climate: A comparison of model results with paleodata from ice cores and marine sediments, *J. Geophys. Res.*, *104*, 15,895–15,916, 1999.

McCulloch, R. D., and S. J. Davis, Late-glacial and Holocene palaeoenvironmental change in the central Strait of Magellan, southern Patagonia, *Palaeogeogr. Palaeoclim. Palaeoecol.*, *173*, 143–173, 2001.

Mulvaney, R., R. Röthlisberger, E. W. Wolff, S. Sommer, J. Schwander, M. A. Hutterli, and J. Jouzel, The transition from the last glacial period in inland and near-coastal Antarctica, *Geophys. Res. Let.*, *27*, 2673–2676, 2000.

Reader, M. C., I. Fung, and N. McFarlane, The mineral dust aerosol cycle during the Last Glacial Maximum, *J. Geophys. Res.*, *104*, 9381–9398, 1999.

Röthlisberger, R., M. Bigler, M. Hutterli, S. Sommer, B. Stauffer, H. G. Junghans, and D. Wagenbach, Technique for continuous high-resolution analysis of trace substances in firn and ice cores, *Environ. Sci. Techn.*, *34*, 338–342, 2000.

Schwander, J., J. Jouzel, C. U. Hammer, J. R. Petit, R. Udisti, and E. Wolff, A tentative chronology for the EPICA Dome Concordia ice core, *Geophys. Res. Let.*, *28*, 4243–4246, 2001.

Steig, E. J., D. L. Morse, E. D. Waddington, M. Stuiver, P. M. Grootes, P. A. Mayewski, M. S. Twickler, and S. I. Whitlow, Wisconsinan and Holocene climate history from an ice core at Taylor Dome, western Ross Embayment, Antarctica, *Geografiska Annaler*, *82A*, 213–235, 2000.

Stenni, B., V. Masson-Delmotte, S. Johnsen, J. Jouzel, A. Longinelli, E. Monnin, R. Röthlisberger, and E. Selmo, An Oceanic Cold Reversal during the last deglaciation, *Science*, *293*, 2074–2077, 2001.

Vaughn, B., J. W. C. White, M. Delmotte, M. Trolier, O. Cattani, and M. Stievenard, An automated system for the uranium reduction method of hydrogen isotope analysis of water, *Chem. Geol.*, *152*, 309–319, 1998.

Watanabe, O., K. Kamiyama, H. Motoyama, Y. Fujii, H. Shoji, and K. Satow, The palaeoclimate record in the ice core at Dome Fuji station, East Antarctica, *Ann. Glaciol.*, *29*, 176–178, 1999.

R. Röthlisberger, R. Mulvaney, and E. W. Wolff, British Antarctic Survey, High Cross, Madingley Road, Cambridge CB3 0ET, England, UK.

M. Bigler and S. Sommer, Climate and Environmental Physics, University of Bern, Sidlerstr. 5, 3012 Bern, Switzerland.

M. Hutterli, Department of Hydrology and Water Resources, University of Arizona, Harshbarger Building 11, Tucson, Arizona 85721, USA.

J. Jouzel, IPSL/Laboratoire des Sciences du Climat et de l'Environnement, CEA/DSM CE Saclay, 91191 Gif-sur-Yvette, France.

GEOPHYSICAL RESEARCH LETTERS, VOL. 30, NO. 5, 1216, doi:10.1029/2003GL016936, 2003

Correction to "Dust and sea salt variability in central East Antarctica (Dome C) over the last 45 kyrs and its implications for southern high-latitude climate" by R. Röthlisberger et al.

Received 16 January 2003; published 6 March 2003.

INDEX TERMS: 3344 Meteorology and Atmospheric Dynamics: Paleoclimatology; 0368 Atmospheric Composition and Structure: Troposphere—constituent transport and chemistry; 1620 Global Change: Climate dynamics (3309); 9310 Information Related to Geographic Region: Antarctica; 9900 Corrections.
Citation: Röthlisberger, R., R. Mulvaney, E. W. Wolff, M. A. Hutterli, M. Bigler, S. Sommer, and J. Jouzel, Correction to ''Dust and sea salt variability in central East Antarctica (Dome C) over the last 45 kyrs and its implications for southern high-latitude climate'' by R. Röthlisberger et al., *Geophys. Res. Lett.*, *30*(5), 1216, doi:10.1029/2003GL016936, 2003.

[1] In the paper "Dust and sea salt variability in central East Antarctica (Dome C) over the last 45 kyrs and its implications for southern high-latitude climate" by Regine Röthlisberger, Robert Mulvaney, Eric W. Wolff, Manuel A. Hutterli, Matthias Bigler, Stefan Sommer, and Jean Jouzel [*Geophys. Res. Lett.*, *29*(20), 1963, doi:10.1029/2002GL015186, 2002], an incorrect version of Figure 1 was published. The correct Figure 1 and its caption appear below.

[2] The following reference appeared incorrectly. The correct version follows: Delmonte, B., J. R. Petit, and V. Maggi, Glacial to Holocene implications of the new 27,000-year dust record from the EPICA Dome C (East Antarctica) ice core, *Clim. Dyn.*, *18*(8), 647–660, doi: 10.1007/s00382-001-0193-9, 2002. Consequently, the correct citations for this reference appear below.

[3] In paragraph [7], the last sentence should read as follows: The changes seen in nss-Ca^{2+} concentrations agree with insoluble dust measurements [*Delmonte et al.*, 2002], with particle number and mass concentration changing by a factor of 50 from the LGM to the Holocene and a factor of 2 from the ACR to the Holocene.

[4] In paragraph [9], the fifth sentence should read as follows: These results are supported by dust particle measurements [*Delmonte et al.*, 2002], which showed a slightly smaller particle mode and a smaller geometric standard deviation of the particle size distribution in the glacial than in the Holocene, indicative of a tendency to longer transport paths and less meridional transport. The sixth sentence should read as follows: On the other hand, based on GCM simulations *Krinner and Genthon* [2002] concluded that the dust transport from Patagonia to Dome C was faster during the LGM, in contrast to the studies by *Lunt and Valdes* [2001] and *Delmonte et al.* [2002].

[5] The following acknowledgment was incorrectly published. In paragraph [15], the first sentence should read as follows: **Acknowledgments.** This work is contribution No. 49 to the "European Project for Ice Coring in Antarctica" (EPICA), a joint ESF (European Science Foundation)/EC scientific programme, funded by the European Commission and national contributions from Belgium, Denmark, France, Germany, Italy, the Netherlands, Norway, Sweden, Switzerland, and the United Kingdom.

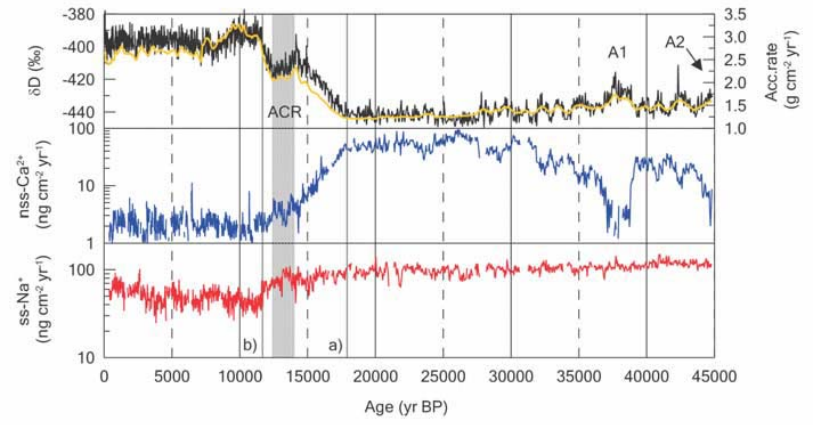

Figure 1. Fluxes of ss-Na^{+} and nss-Ca^{2+}, as well as the δD and the accumulation rate (yellow line, [*Schwander et al.*, 2001]) from the top 780 m of the EPICA Dome C deep ice core at 55 cm resolution. The vertical grey lines refer to the beginning (a) and the end (b) of the Transition, the shaded area corresponds to the Antarctic Cold Reversal (ACR).

0094-8276/03/2003GL016936$05.00

2.3 The Eemian interglacial represented in the chemical ice core record from Dome C, Antarctica

Matthias Bigler, Regine Röthlisberger, Fabrice Lambert, Thomas F. Stocker, Eric W. Wolff, Emiliano Castellano, Roberto Udisti

Earth and Planetary Science Letters
2004, in preparation

The Eemian interglacial represented in the chemical ice core record from Dome C, Antarctica

Matthias Bigler[1], Regine Röthlisberger[1], Fabrice Lambert[1], Thomas F. Stocker[1],
Eric W. Wolff[2], Emiliano Castellano[3], Roberto Udisti[3]

[1] Climate and Environmental Physics, Physics Institute, University of Bern, Switzerland
[2] British Antarctic Survey, Cambridge, United Kingdom
[3] Department of Chemistry, University of Florence, Italy

Abstract

The Eemian interglacial period as reflected in the chemical ice core record from Dome C, Antarctica, shows a very stable behaviour. However, while the two last glacial maxima were very similar, the conditions during the Eemian differed from the Holocene. During the early Eemian, lower sea salt (ss-Na^+) fluxes compared to the Holocene are observed that point to a reduced sea ice production rate at that time. On the other hand, continental aerosol (nss-Ca^{2+}) fluxes did not reach the low Holocene levels during the early-mid Eemian, probably indicating wetter climatic conditions for southern South America compared to a drier, Holocene-like period during the late Eemian and the first stage of Inception I. This transition from the Eemian into the last glacial period is gradual and less abrupt than both, Termination II and I. During transitions, the flux changes differ strongly for different species; the largest changes are observed in nss-Ca^{2+}, moderate changes in the marine sea salt proxy sodium ss-Na^+, and the least changes in ammonium (NH_4^+), which remained almost constant over glacial-interglacial periods. The different flux changes and the slightly lower relative variability of the annually resolved data during glacial maxima point to considerable changes at the different sources rather than strong modifications of transport patterns. Concerning the sequence of events we found, that nss-Ca^{2+} starts in the early stages of terminations coincident with δD, while the flux of ss-Na^+ remains high, presumably until the local temperature (δD) falls bellow a certain threshold. Only then is a relationship between δD and sea ice production rate established. In contrast, ss-Na^+ increases steadily already during the Eemian, reaching full glacial values within Inception I, while nss-Ca^{2+} remains at interglacial flux levels far into Inception I, pointing to a decoupling of the southern South American and Antarctic climate at that time.

1 Introduction

The characterisation of the Eemian interglacial period (Marine Isotope Stage MIS 5e) and the preceding Termination II is an important issue to understand the climate system of the earth. The Eemian has often been referred to as an analogue of the present warm period, the Holocene. Although other interglacial periods may show a greater similarity to the Holocene [*Loutre and Berger*, 2003], the Eemian plays a key role in paleoclimatology due to its better availability and resolution in different climate records [*van Kolfschoten et al.*, 2003]. However, data for the Eemian climate are still not abundant enough to build a complete picture. Global model simulations of Eemian climate together with local paleodata suggest that it may have been around 1°C warmer (global annual mean) compared to the modern pre-industrial climate [*Rahmstorf*, 2002]. In Antarctica, the temperature offset was

probably even higher, especially during the early Eemian [*Petit et al.*, 1999], estimated to +3°C [*Jouzel et al.*, 2003], derived from water-isotope measurements (δD) on the East Antarctic plateau.

Of particular interest are investigations of the Eemian with regard to its stability and the shape of its transitions: The first issue addresses whether the Eemian was characterised by stable climatic conditions like the Holocene or by several abrupt cooling events as reported for example in *Ninnemann et al.* [1999]. The second question is focusing mainly on determining how climate responded at the onset and at the end of the last interglacial, in view of an improved understanding of the governing processes and in order to better predict the future behaviour of the current warm period.

The ionic composition of the ice provides an excellent resource for investigating changes in the source strength and transport patterns in the atmosphere [*Legrand and Mayewski*, 1997]. However there is still a lack of high-resolution chemical ice core time series covering the Eemian. This gap can be closed with the present study, discussing new records of sodium Na^+, calcium Ca^{2+}, ammonium NH_4^+ and nitrate NO_3^- from the EPICA Dome C deep ice situated on the East Antarctic plateau.

2 Acquisition and reduction of chemical ice core data

In the frame of the European Project for Ice Coring in Antarctica (EPICA) several field campaigns have been carried out at Dome Concordia (Dome C) since 1995 [*EPICA community members*, in press]. The Dome C drill site is situated on the East Antarctic Plateau at 75°06'S, 123°21'E and 3233 m above sea level. A mean annual surface temperature of –54.5°C and a present time-day accumulation rate of 25 kg m^{-2} a^{-1} characterize it. Apart from drilling, logging and packing, some analyses of the ice core have been done already in the field, amongst them measurements of the water-soluble sodium Na^+, calcium Ca^{2+}, ammonium NH_4^+ and nitrate NO_3^- ion concentrations in ng g^{-1} with a Continuous Flow Analysis system (CFA) as described in *Röthlisberger et al.* [2000a]. Detection limits are 4 ng g^{-1} for Na^+, 0.4 ng g^{-1} for Ca^{2+}, 0.1 ng g^{-1} for NH_4^+, and 3 ng g^{-1} for NO_3^-, respectively. The CFA data agree well with ion-chromatography measurements [*Littot et al.*, 2002] with the exception of NH_4^+, for which ion-chromatography is prone to contaminations at such low levels.

The dating of the upper part of the core (EDC96) is according the time scale EDC1 [*Schwander et al.*, 2001], the lower part (EDC99) uses EDC2 [*EPICA community members*, in press]. The temporal resolution of the data is roughly annual or higher which allows calculating annual mean values, although they are not based on counting individual layers. We applied a Gaussian filter to the annual mean data with a cut off period of 2000 years in order to show long-term patterns of the data. For this study, we focus on two time periods: On the one hand, from 150 ka before present (BP) to 100 ka BP, covering the penultimate glacial maximum (GM II), Termination II, the Eemian interglacial period, and Inception I, and on the other hand from 30 ka BP to present, including the last glacial maximum (GM I), Termination I and the present interglacial Holocene. The two sections are presented in Figure 1 together with deuterium measurements (δD), a proxy for the temperature at the drill site [*EPICA community members*, in press; *Jouzel et al.*, 2001].

Both, Na^+ and Ca^{2+}, have a marine and a continental source. The marine source is clearly dominating during interglacial periods, providing almost all of the total Na^+ and a significant fraction of the total Ca^{2+}. Under glacial conditions, the continental source becomes more important, contributing almost all of the total Ca^{2+} and some of the total Na^+. Based on the seawater ratio (Ca^{2+}/Na^+) = 0.038 [*Bowen*, 1979] and on the continental aerosol ratio (Na^+/Ca^{2+}) = 1.0 [*Bigler et al.*, in preparation], sea-salt sodium (ss-Na^+) and non-sea-salt calcium (nss-Ca^{2+}) were calculated. The uncertainty of the (Na^+/Ca^{2+}) ratio of the continental aerosol is fairly large [*Bigler et al.*, in preparation], and different values have been used up to now, often relying on the ratio in mean crust [*Bowen*, 1979]. In order to take this uncertainty into account, we show the total Na^+ and ss-Na^+ in Figure 2. As the influence of this uncertainty is limited to the ss-Na^+ during glacial maxima, the main points of the paper are not affected by the uncertainty of the correction.

Considering the very low accumulation rate at Dome C it is appropriate to use fluxes instead of concentrations because they are more representative of atmospheric concentrations when dry deposition is dominant. To calculate fluxes, we used accumulation rates emerging from the timescales EDC1 and EDC2. Although the accuracy of accumulation rate estimates based on isotope measurements have been questioned [see for example *Udisti et al.*, 2004], it remains the best guess with regard to its homogeneity over the whole data set. Our results would not be affected by reasonable deviations of the true accumulation rate from the accumulation rate used. Gaussian filtered fluxes of ss-Na^+, nss-Ca^{2+}, NH_4^+ and NO_3^- are shown in Figure 2 along with the δD (for references see above). Na^+, Ca^{2+} and NH_4^+ are deposited irreversibly, and hence their fluxes reflect changes of source and transport, whereas NO_3^- is deposited reversibly and therefore subjected to post-depositional effects. So, NO_3^- represents not an unambiguous atmospheric signal.

Statistical parameters of the annual mean data for different time periods are summarized in Table 1 (rounded to two digits). Quantile-quantile-plots from data of GM II in Figure 3 show, that the concentration measurements are represented by a log-normal rather than a normal distribution. However, even the latter one does not fit perfectly, especially for high Ca^{2+} and NO_3^- values, which exceed the expected ones from the theoretical log-normal distribution; by contrast, low concentration levels of Na^+ and NH_4^+ are lower than expected. With mean μ and variance σ^2 of the logarithmised data, the median and the variation coefficient of log-normal distributed data are given as follows:

$$\text{median} = 10^{\mu}$$

$$\text{variation coefficient} = \sqrt{10^{\sigma^2} - 1}$$

Variation coefficients, which give the relative variability, are calculated only for the original data and not for ss-Na^+ and nss-Ca^{2+}, due to their interdependence in the calculation and slight uncertainties of the depth assignment between both species, which would introduce a certain degree of artificial variation. A visualisation of the flux changes and the variation coefficients over different climatic periods can be found in Figure 4.

3 Flux levels over glacial-interglacial periods

3.1 General behaviour during glacial-interglacial periods and terminations

The high flux medians of ss-Na^+, nss-Ca^{2+} and NH_4^+ agree strikingly well over the last two glacial maxima, GM II and I (Figures 2 and 4, Table 1), pointing to comparable climatic conditions during these extremely cold periods.

During transitions, changes in the flux differ strongly for different species. But comparing Termination II and I for any particular species the changes are quite similar: The ss-Na^+ flux changes roughly by a factor 2 (GM II – early and mid Eemian: 2.5; GM I – early and mid Holocene: 1.8), whereas it is one order of magnitude larger for nss-Ca^{2+} flux (GM II – mean Eemian: 16; GM I – mean Holocene: 28). Surprisingly, the NH_4^+ flux remains nearly constant over both Terminations, considering the general variability and the measurement uncertainties (GM II – mean Eemian: 1.6; GM I – mean Holocene: 1.2). It is obvious that such huge differences in the flux change between different species cannot be explained by changes of the transport pattern during glacial-interglacial periods only, but that considerable modifications at the source of the particular species have occurred. Indications pointing to a less important role of the transport pattern as often assumed, is given as well by the observation of slightly decreased relative variability of the annually resolved Na^+, Ca^{2+} and NH_4^+ data throughout glacial maxima (Table 1, Figure 4).

At first sight, the two last interglacial periods, the Holocene and the Eemian, compare quite well and show a remarkably stable behaviour. Instabilities of the climate resulting in imprints in the chemical ice core records cannot be observed, not even in the annually resolved data (Figure 1). However, there are greater differences between both warm periods compared to the difference of the glacial extremes.

Because the differences in the ss-Na^+ and the nss-Ca^{2+} record are opposite, they are rather related to source effects than to modifications of the transport. Specific features concerning the flux levels for both interglacial periods are discussed in the following sections.

3.2 ss-Na^+ – a marine proxy related to the sea ice production rate

The good correlation of proxy data like δD and ss-Na^+ from the East Antarctic plateau with marine sediment records was noted earlier [*Kanfoush et al.*, 2002; *Mortyn et al.*, 2003]. In these records each interglacial period exhibits low ice-rafted debris and high foraminiferal abundance during the respective early part, indicating relatively warm sea-surface temperatures and reduced influence of sea ice. Changes in these proxies in the course of interglacial periods indicate a return to more glacial-like conditions. The ss-Na^+, originating from frost flowers rather than from bubble bursting over the open ocean according to recent publications, is used as a proxy for the sea ice production rate and probably also extent [*Rankin et al.*, 2000; *Wolff et al.*, 2003]. Interpretations of the ss-Na^+ in this work rest on these latest findings.

The δD record of Dome C points to significantly higher temperatures especially during the early Eemian [*Jouzel et al.*, 2003]. It is plausible that the source areas of ss-Na^+ in the south polar ocean were exposed to warmer temperatures as well diminishing the sea ice production rate. The observed 30% lower flux of ss-Na^+ (in the opposite direction than nss-Ca^{2+}) from Dome C in the early Eemian compared to the early Holocene could therefore be related to a lesser sea ice production rate at this time. Apart from the lower level in the early Holocene, the pattern within both interglacial periods is very similar, showing a gradual increase in ss-Na^+ concentrations (Figure 2, Table 1) related to growing winter sea ice production as reported for the Holocene [*Wolff et al.*, 2003, and references therein]. A slightly higher gradient towards the end of the Eemian can be observed, turning into a steady increase during Inception I.

The correlation of the ss-Na^+ with the local Antarctic temperature proxy δD shown in Figure 5a is based on averaged data (7 bag means, equivalent to 3.85 m); additional data from the last glacial period reaching back to 78 ka BP (not shown in this paper) is used to account for the whole glacial range of both proxies. During the interglacial periods, an anti-correlation between the Dome C site temperature proxy and ss-Na^+ is found ($R^2 = 0.48$). The appearance of this correlation is strengthened due to the extended range of observed temperature and ss-Na^+ values in the Eemian. So, under interglacial conditions, temperature variations recorded in Dome C are related with the sea ice production rate. On the other hand, ss-Na^+ and δD show almost no correlation during glacial periods, pointing to a minor relationship between ss-Na^+ and the local Antarctic temperature. This could be an indication of ss-Na^+ and therefore the glacial sea ice production rate reaching some sort of a maximum that is almost independent from further cooling. Additionally as reported in *Vimeux et al.* [2002], moister transport and the sea salt transport to the ice sheet maybe controlled by processes in different latitudes.

3.3 nss-Ca^{2+} – a continental proxy related to the southern South American climate

The most likely source of continental aerosols, and hence nss-Ca^{2+}, is southern South America, particularly Patagonia and the southern Argentinean Pampa [*Bigler et al.*, in preparation; *Delmonte et al.*, in press; *Röthlisberger et al.*, 2002b]. Opposite to the observations of ss-Na^+, the general level of the nss-Ca^{2+} flux is higher during the Eemian than during the Holocene. The minimum early in the interglacial periods, which was suggested to be an indication of wetter conditions at the dust source area in the early Holocene [*Delmonte et al.*, 2002], is doubled in the Eemian (Figure 2, Table 1). The same holds true for the flux levels in the mid Holocene and Eemian, respectively. After maximum interglacial values in the mid Eemian, a decreasing trend is observed towards the end of the Eemian and far into Inception I with Holocene-similar values. If the hypothesis is correct, that the changes of nss-Ca^{2+} levels recorded in Dome C can be interpreted as changes of southern South American climate, this pattern can be explained as the early and mid Eemian were drier than the Holocene maintaining a slightly higher degree of dust mobilization as a precursor for higher values at Dome C.

On the other hand the subsequent lower, Holocene-like levels during the late Eemian and in the early Inception I point to wetter climatic conditions, similar to the Holocene, preventing an efficient dust mobilization [*Röthlisberger et al.*, 2002b]. Therefore, the southern South American climate was probably slightly more variable during the Eemian than during the Holocene. Unfortunately there is very little known about the climate of the Eemian interglacial in southern South America from other paleorecords (personal communication *Andreas Schellenberger*, Institute of Geography, University of Bern). Most of the records do not date back to the Eemian, contain gaps, or lie too much to the north. *Clapperton* [1993] reported the Eemian as probably little different from much of the Holocene. However there is evidence from a general circulation model that moisture transport from ocean to land decreased globally during the Eemian interglacial period with respect to the Holocene [*Montoya et al.*, 2000].

The above-discussed pattern is seen in the Ca^{2+} concentration record too (Figure 1), but it is further amplified by the changes in accumulation rate and by the differentiation between the marine and the continental contribution to the total Ca^{2+}, when considering nss-Ca^{2+} fluxes. Examining the correlation of the nss-Ca^{2+} flux with δD (Figure 5b; for details see section 3.2), almost no correlation is found for warm periods, whereas in glacial times the correlation is very good ($R^2 = 0.72$). This implies that the relation between climate in the nss-Ca^{2+} source region and the temperature on the East Antarctic plateau is strong under glacial but uncoupled under interglacial conditions.

3.4 NH_4^+ – a marine proxy for biogenic emissions

In Greenland, ice cores contain a spiky pattern of NH_4^+ allowing for the reconstruction of boreal zone forest fires [*Legrand et al.*, 1992], whereas the background levels were related to continental biogenic soil emissions with almost no marine contribution [*Fuhrer et al.*, 1996]. Compared to this, the knowledge of the NH_4^+ sources, responsible for the low level depositions in central Antarctic deep ice cores, is still limited. However, NH_4^+ does certainly not act as a significant neutralizer of sulphur-derived aerosol at high southern latitudes. At coastal stations, summer maxima of NH_4^+ coincided with peaks of sulphur containing species provided by marine biogenic emissions, pointing to remote marine emissions with a weak additional contribution from the polar ocean [*Legrand et al.*, 1998; *Legrand et al.*, 1999].

In the high-resolution record from Dome C, the NH_4^+ concentration and flux levels are very low, and there are hardly any spikes observed. NH_4^+ recorded on the East Antarctic ice sheet has therefore a completely different behaviour than in Greenland. The most striking feature of our NH_4^+ measurements is, that there are almost no flux changes between glacial and interglacial periods (Figure 2, Table 1). Such behaviour can hardly be explained by attributing NH_4^+ to a continental source, bearing in mind that nss-Ca^{2+} flux changed dramatically over glacial-interglacial transitions. Although the seasonality of NH_4^+ is presumably different from ss-Na^+ and nss-Ca^{2+} [*Sommer et al.*, 2000], the characteristic of the NH_4^+ signal resembles more the marine ss-Na^+ than the continental nss-Ca^{2+}: The variability of the signal (variation coefficient, Figure 4), as well as the log-normal distribution (Figure 3) of NH_4^+ are more like the ss-Na^+ than the nss-Ca^{2+}. Due to significantly smaller changes in the glacial-interglacial NH_4^+ flux compared to the presumed sea ice proxy ss-Na^+, the main source lies probably further north than for ss-Na^+. Furthermore, there are no correlations found between local temperature in Dome C and the NH_4^+ flux for both interglacial and glacial periods as shown in Figure 5c (for details see section 3.2). We therefore assume that the southern hemispheric oceans, and neither a continental source nor the south polar ocean, seem to be the most probable source for the small amount of NH_4^+ deposited on the East Antarctic plateau, which is in agreement with previous findings [*Legrand et al.*, 1999].

3.5 NO_3^- – related to the accumulation rate during interglacial periods

NO_3^- is hard to interpret because it is reversibly deposited. Concentration levels measured in ice cores are strongly affected by the local temperature, accumulation rate and the coinciding dust content [*Röthlisberger et al.*, 2002a; *Röthlisberger et al.*, 2000b]. As main sources in central East Antarctic ice

cores the NO_3^- production in the stratosphere, tropospheric lightning and an organic origin are discussed.

During glacial periods, lower temperatures and the reaction of NO_3^- with nss-Ca^{2+} or dust reduce or prevent NO_3^- from being lost despite lower accumulation rates, leading to higher levels as well as higher variability [Röthlisberger et al., 2000b]. This increase in the NO_3^- variability during glacial periods compared to interglacial periods is unique compared to the irreversibly deposited species that show a slight decrease in their variation coefficients (Figure 4, Table 1). Despite similar local temperature and nss-Ca^{2+}, the flux level of NO_3^- is significantly lower in GM II than in GM I, which could indicate different NO_3^- source strengths.

On the other hand, accumulation rate and temperature control NO_3^- preservation, when nss-Ca^{2+} is low [*Röthlisberger et al.*, 2000b]. However, because the temperature difference between Eemian and Holocene (present-day mean annual surface temperature of –54.5°C) probably does not exceed +3°C [*Jouzel et al.*, 2003], the temperature effect can be neglected and different NO_3^- levels can qualitatively be explained with the direct or indirect effect of accumulation rate. Such an accumulation rate dependency is of interest in the context of this past accumulation rate reconstruction: The flux of NO_3^- (Figure 2, Table 1) but also the concentration (Figure 1) is significantly higher during the whole Eemian compared to the Holocene. Even the NO_3^- peak related to an accumulation rate maximum in the early Holocene is lower than all the value throughout the Eemian interglacial. A similar peak in NO_3^- in the early Eemian reaches twice the value of the early Holocene. This result is an independent, qualitative indication for higher accumulation rates during the whole Eemian, in good agreement with the commonly used δD-derived accumulation rates. The same result is found when examining the (Cl^-/Na^+) ratios as in *Röthlisberger et al.* [2003]. Accumulation rates derived directly from isotope measurements are thus a reasonable first order estimate of the true accumulation rate, although some uncertainty may exist [*Udisti et al.*, 2004].

The ambivalent behaviour of NO_3^- shows up in Figure 5d (for details see section 3.2). The correlation between NO_3^- and δD is good during warm periods due to the temperature-accumulation effect on the preservation of NO_3^- ($R^2 = 0.75$). During cold periods, a correlation with δD is found ($R^2 = 0.61$), even though this is not the result of temperature and accumulation changes, but of the reaction of NO_3^- with dust, itself well correlated with δD, which led to irreversible deposition.

During Transition II, Inception I, within the early glacial I and during Transition I (137-129 ka, from 113 ka on and 16-12 ka) NO_3^- shows minima: The dust level within these periods is already low, the accumulation rate still low, so that NO_3^- losses are pronounced. However, to estimate the accumulation rate quantitatively, the understanding of the air-snow-transfer of NO_3^- needs further improvement concerning measurements and modelling [*Röthlisberger et al.*, 2002a].

4 Sequence of marine and continental signals

4.1 Time references

The beginning of Termination II and I is set at the onset of the δD increase and the nss-Ca^{2+} decrease, at 137 ka BP and 18 ka BP, respectively. For the end of the terminations and the beginning of the interglacial periods the turning point after the δD increase and the ss-Na^+ decrease coincides: For the Eemian at 128 ka BP, for the Holocene at 11.5 ka BP. We chose three sections for each of the two examined interglacial periods (early, mid and late) according to the ages and given in Table 1. The end of the Eemian and the beginning of Inception I are assigned to the turning point of the δD record before the distinct decrease around 116 ka BP. At that point, no conspicuous marker is found in the CFA measurements. We set the end of Inception I and the beginning of the Glacial I to 107 ka BP, because a first glacial minimum is reached at this time by δD, coincident with a nss-Ca^{2+} peak of approximately 100 $\mu g\ m^{-2}\ a^{-1}$.

This timing of the Eemian from 128 ka BP to 116 ka BP is in agreement for example with uranium and thorium ages from fossil reefs along the continental margin of Western Australia which resulted in 128 ± 1 ka BP to 116 ± 1 ka BP with the major episode of reef building from 128 ka BP to 121 ka BP [*Stirling et al.*, 1998]. Additionally, stalagmites from southern Tasmania, Australia, revealed the fastest growth between 129 ± 2 ka and 122 ± 1 ka [*Zhao et al.*, 2001].

4.2 Termination II and I

As mentioned above, the beginning of Termination II and I is coincident for nss-Ca^{2+} and δD. Termination II starts abruptly for nss-Ca^{2+} around 137 ka BP, continued by a moderate decrease together with a weak δD increase from 137 to 134 ka BP. A stronger decrease in nss-Ca^{2+} then follows in a second stage of the Termination II from 133-130 ka BP, reaching Eemian values while δD is still increasing towards Eemian peak values. Termination I shows a gradual decrease in nss-Ca^{2+} from 18 to 11 ka BP, somewhat weakened during the Antarctic Cold Reversal (ACR). Average Holocene nss-Ca^{2+} values were reached almost coincident with the plateau in δD.

The situation is completely different for ss-Na^{+} fluxes, which remains on glacial levels for most part of both Terminations. Not until nss-Ca^{2+} has undergone most of the flux change ss-Na^{+} begins its gradual decrease around 132 ka BP during Termination II and after 13.2 ka BP during Termination I. Interglacial levels are reached at the same time as δD.

This pattern for nss-Ca^{2+} and ss-Na^{+} was explained in *Röthlisberger et al.* [2002b] for Termination I to the extent that most of the nss-Ca^{2+} flux change can be attributed to changes in the southern South American dust source region, whereas the simultaneous decrease of nss-Ca^{2+} and ss-Na^{+} after the ACR could partly be related to a reorganisation of the atmospheric transport. As the general pattern for Termination II is very similar to Termination I, the same mechanism could be responsible.

At the beginning of a termination, nss-Ca^{2+} originating from southern South America reacts immediately and sensitively to the changing climatic conditions. The source area seems to undergo climatic changes, which efficiently reduce the potential of dust mobilization. Similar patterns are observed during glacial warm events (e.g. A1 to A4, data not shown), when nss-Ca^{2+} shows dips in flux and concentration, reaching almost interglacial levels [*Röthlisberger et al.*, submitted].

The start of a termination has no immediate effect on ss-Na^{+} flux, changes occur only after several thousand years delay. The sea ice production rate remains almost unchanged, even though the South American continent to the North and Antarctica to the South of the sea salt source area are both experiencing the onset of the termination. This could be an indication together with the observations reported in section 3.2 that small temperature variations during glacial periods have no significant influence on sea ice production, which is also evident from the glacial warm events (A1 to A4), revealing only very small changes in the ss-Na^{+} flux compared to nss-Ca^{2+}. We assume that a certain threshold level in the temperature has to be exceeded before the sea ice production rate collapses and turns towards interglacial levels. This explains the absence of distinct ss-Na^{+} flux changes during glacial warm events and the delayed start of terminations for this proxy.

4.3 Inception I

Inception I as recorded in the Dome C ice core showed no abrupt events and was generally much more gradual than both terminations. This is in contrast to for example a Chinese stalagmite record [*Yuan et al.*, 2004] where Inception I around 120 ± 1 ka BP lasting less than 300 years was of similar abruptness as Termination I at 129 ± 1 ka BP lasting 200 years.

It is most noticeable that nss-Ca^{2+} remains on interglacial levels far into Inception I between 115-110 ka BP, reaching even lower levels than in the early and mid Eemian, whereas ss-Na^{+} has already increased and reached full glacial values around 111 ka BP. This indicates that southern South American interglacial climate lasted longer compared to the duration imprinted in the Antarctic Dome C temperature record or the ss-Na^{+} record, which remained at low interglacial levels for a quite short

time interval only. Looking at the nss-Ca^{2+} record, glacial conditions seem to build up much more slowly in southern South America than in Antarctica, evolving not until the sea ice production rate has reached full glacial values. But this result can hardly be compared to direct evidence from South America as mentioned in section 3.3, because it is not even clear yet how extensive Andean glaciers were during the early cold part of the last glacial period [*Clapperton*, 1993].

5 Conclusion

The last two glacial maxima are very similar in chemical ice core data from Dome C, Antarctica. During Termination II and I, changes in the flux of irreversibly deposited water-soluble ions develop very differently, which is mainly related to source modifications: While the dust proxy nss-Ca^{2+} is extremely lowered, ss-Na^{+}, a proxy for the sea ice production rate, decreases only moderately and NH_4^{+}, whose sources are assumed to be marine biogenic emissions, remains nearly constant. This could be, together with the observed decrease in relative variability of the annually resolved data during glacial maxima, an indication of only small changes in glacial-interglacial transport patterns.

Furthermore the high-resolution data point to very stable climatic conditions during the Eemian interglacial period, which is known from water-isotope records like δD as slightly warmer compared to the Holocene. Based on δD, higher accumulation rates are found as well in the Eemian. This finding is supported by increased NO_3^{-} preservation, which is strongly affected by accumulation rate dependent post-depositional losses under interglacial conditions. Furthermore, the sea ice production rate was smaller in the early Eemian than in the early Holocene based on the ss-Na+ record; however a distinct increase of ss-Na^{+} is observed during both interglacial periods. On the other hand, the southern South American climate during the Eemian seems to be slightly more variable, with drier conditions especially at the beginning and subsequently a wetter climate lasting far into Inception I. This transition into the last glacial period shows up very gradually and less abruptly than both Termination II and I.

The marine proxy ss-Na^{+} and the continental nss-Ca^{2+} show quite a different behaviour: ss-Na^{+} reacts slowly during Terminations II and I, but very sensitive at Inception I. Correlation with local temperature under interglacial periods and warm transitions is strong, while no significant correlation is found under glacial conditions. This points to the presence of a temperature threshold below which the sea ice production rate is independent from temperature variations, like for example during the Antarctic glacial warm events. Meanwhile, nss-Ca^{2+} is strongly correlated with the Antarctic temperature under glacial conditions, undergoing severe flux changes during the glacial warm events, and subsequently reacting immediately and sensitively to the onset of Termination II and I. However no correlation of nss-Ca^{2+} and δD is found during interglacial periods, and during most of Inception I, nss-Ca^{2+} remains on interglacial levels, pointing to an uncoupling of the climate of southern South America and Antarctica.

In the future, it will be possible to further examine the described mechanisms and observations based on chemical ice core data from several additional glacial-interglacial cycles preserved in the Dome C ice core. This could give additional insights into the coupling of southern mid- and high latitudes over glacial-interglacial transitions. A better and more quantitative understanding of post-depositional effects affecting reversibly deposited species could provide accumulation rate estimates during interglacial periods that are independent from δD. Furthermore, additional examination of the continental aerosol composition will improve the accuracy of the source assignment for constituents of the continental and the marine aerosol. Both will improve the flux calculations that are essential to examine climatic mechanisms related to ice core records.

Acknowledgements

This work is contribution XX to the "European Project for Ice Coring in Antarctica" (EPICA), a joint ESF (European Science Foundation) / EC scientific programme, funded by the European Commission and by national contributions from Belgium, Denmark, France, Germany, Italy, Netherlands, Norway, Sweden, Switzerland and the United Kingdom. We thank all the scientists involved in the fieldwork to obtain this chemical ice core data set.

References

Bigler, M., R. Röthlisberger, F. Lambert, T.F. Stocker, G.C. Littot, E.W. Wolff, and D. Wagenbach, The continental contribution to the water-soluble aerosol deposited on the East Antarctic plateau (EPICA Dome C), in preparation.

Bowen, H.J.M., *Environmental Chemistry of the Elements*, Academic Press, London, 1979.

Clapperton, C., *Quaternary geology and geomorphology of South America*, 779 pp., Elsevier, Amsterdam, 1993.

Delmonte, B., I. Basile-Doelsch, J.-R. Petit, V. Maggi, M. Revel-Rolland, A. Michard, E. Jagoutz, and F. Grousset, Comparing the EPICA and Vostok dust records during the last 220,000 years: stratigraphical correlation and provenance in glacial periods, *Earth-Science Reviews*, in press.

Delmonte, B., J.R. Petit, and V. Maggi, Glacial to Holocene implications of the new 27000-year dust record from the EPICA Dome C (East Antarctica) ice core, *Climate Dynamics*, *18* (8), 647-660, 2002.

EPICA community members, Eight glacial cycles from an Antarctic ice core, *Nature*, in press.

Fuhrer, K., A. Neftel, M. Anklin, T. Staffelbach, and M. Legrand, High-resolution ammonium ice core record covering a complete glacial-interglacial cycle, *Journal of Geophysical Research*, *101* (D2), 4147-4164, 1996.

Jouzel, J., V. Masson, O. Cattani, S. Falourd, M. Stievenard, B. Stenni, A. Longinelli, S.J. Johnsen, J.P. Steffenssen, J.R. Petit, J. Schwander, R. Souchez, and N.I. Barkov, A new 27 ky high resolution East Antarctic climate record, *Geophysical Research Letters*, *28* (16), 3199-3202, 2001.

Jouzel, J., F. Vimeux, N. Caillon, G. Delaygue, G. Hoffmann, V. Masson-Delmotte, and F. Parrenin, Magnitude of isotope/temperature scaling for interpretation of central Antarctic ice cores, *Journal of Geophysical Research - Atmospheres*, *108* (D12), 2003.

Kanfoush, S.L., D.A. Hodell, C.D. Charles, T.R. Janecek, and F.R. Rack, Comparison of ice-rafted debris and physical properties in ODP Site 1094 (South Atlantic) with the Vostok ice core over the last four climatic cycles, *Palaeogeography Palaeoclimatology Palaeoecology*, *182* (3-4), 329-349, 2002.

Legrand, M., M. de Angelis, T. Staffelbach, A. Neftel, and B. Stauffer, Large perturbations of ammonium and organic acids content in the Summit-Greenland ice core. Fingerprint from forest fires?, *Journal of Geophysical Research*, *19* (5), 473-475, 1992.

Legrand, M., F. Ducroz, D. Wagenbach, R. Mulvaney, and J. Hall, Ammonium in coastal Antarctic aerosol and snow: Role of polar ocean and penguin emission, *Journal of Geophysical Research*, *103* (D8), 11,043-11,056, 1998.

Legrand, M., and P. Mayewski, Glaciochemistry of polar ice cores: A review, *Reviews of Geophysics*, *35* (3), 219-243, 1997.

Legrand, M., D. Wagenbach, and B. Jourdain, Origins of ammonium in Antarctic air and snow deposits, *EOS Transactions, American Geophysical Union*, *80* (46), 198, 1999.

Littot, G.C., R. Mulvaney, R. Röthlisberger, R. Udisti, E.W. Wolff, E. Castellano, M. de Angelis, M.E. Hansson, S. Sommer, and J.P. Steffenssen, Comparison of analytical methods used for measuring major ions in the EPICA Dome C (Antarctica) ice core, *Annals of Glaciology*, *35*, 299-305, 2002.

Loutre, M.F., and A. Berger, Marine Isotope Stage 11 as an analogue for the present interglacial, *Global and Planetary Change*, *36* (3), 209-217, 2003.

Montoya, M., H. von Storch, and T.J. Crowley, Climate simulation for 125 kyr BP with a coupled ocean-atmosphere general circulation model, *Journal of Climate*, *13* (6), 1057-1072, 2000.

Mortyn, P.G., C.D. Charles, U.S. Ninnemann, K. Ludwig, and D.A. Hodell, Deep sea sedimentary analogs for the Vostok ice core, *Geochemistry Geophysics Geosystems*, *4*, 2003.

Ninnemann, U.S., C.D. Charles, and D.A. Hodell, Origin of global millennial scale climate events: Constraints from the southern ocean deep sea sedimentary record, in *Mechanisms of global climate change at milennial time scales*, American Geophysical Union, 1999.

Petit, J.R., J. Jouzel, D. Raynaud, N.I. Barkov, J.-M. Barnola, I. Basile, M. Bender, J. Chappellaz, M. Davis, G. Delaygue, M. Delmotte, V.M. Kotlyakov, M. Legrand, V.Y. Lipenkov, C. Lorius, L. Pépin, C. Ritz, E. Saltzman, and M. Stievenard, Climate and atmospheric history of the past 420,000 years from the Vostok ice core, Antarctica, *Nature*, *399*, 429-436, 1999.

Rahmstorf, S., Ocean circulation and climate during the past 120,000 years, *Nature*, *419*, 207-214, 2002.

Rankin, A.M., V. Auld, and E.W. Wolff, Frost flowers as a source of fractionated sea salt aerosol in the polar regions, *Geophysical Research Letters*, *27* (21), 3469-3472, 2000.

Röthlisberger, R., M. Bigler, M. Hutterli, S. Sommer, B. Stauffer, H.G. Junghans, and D. Wagenbach, Technique for continuous high-resolution analysis of trace substances in firn and ice cores, *Environmental Science & Technology*, *34* (2), 338-342, 2000a.

Röthlisberger, R., M. Bigler, E.W. Wolff, F. Joos, E. Monnin, and M.A. Hutterli, Ice core evidence for the extent of past atmospheric CO_2 change due to iron fertilisation, *Geophysical Research Letters*, submitted.

Röthlisberger, R., M.A. Hutterli, E.W. Wolff, R. Mulvaney, H. Fischer, M. Bigler, K. Goto-Azuma, M.E. Hansson, U. Ruth, M.L. Siggaard-Andersen, and J.P. Steffensen, Nitrate in Greenland and Antarctic ice cores: A detailed description of post-depositional processes, *Annals of Glaciology*, *35*, 209-216, 2002a.

Röthlisberger, R., R. Mulvaney, E.W. Wolff, M.A. Hutterli, M. Bigler, M. de Angelis, M.E. Hansson, J.P. Steffensen, and R. Udisti, Limited dechlorination of sea-salt aerosols during the last glacial period: Evidence from the European Project for Ice Coring in Antarctica (EPICA) Dome C ice core, *Journal of Geophysical Research - Atmospheres*, *108* (D16), 2003.

Röthlisberger, R., R. Mulvaney, E.W. Wolff, M.A. Hutterli, M. Bigler, S. Sommer, and J. Jouzel, Dust and sea salt variability in central East Antarctica (Dome C) over the last 45 kyrs and its implications for southern high-latitude climate, *Geophysical Research Letters*, *29* (20), 2002b.

Röthlisberger, R., E.W. Wolff, R. Mulvaney, M. Hutterli, and S. Sommer, Factors controlling nitrate concentration in a deep ice core: evidence from the Dome C deep ice core, *Journal of Geophysical Research*, *105* (D16), 20565-20572, 2000b.

Schwander, J., J. Jouzel, C.U. Hammer, J.R. Petit, R. Udisti, and E. Wolff, A tentative chronology for the EPICA Dome Concordia ice core, *Geophysical Research Letters*, *28* (22), 4243-4246, 2001.

Sommer, S., D. Wagenbach, R. Mulvaney, and H. Fischer, Glacio-chemical study spanning the past 2 kyr on three ice cores from Dronning Maud Land, Antarctica. 2. Seasonally resolved chemical records, *Journal of Geophysical Research*, *105* (D24), 29423-29433, 2000.

Stirling, C.H., T.M. Esat, K. Lambeck, and M.T. McCulloch, Timing and duration of the Last Interglacial: evidence for a restricted interval of widespread coral reef growth, *Earth and Planetary Science Letters*, *160* (3-4), 745-762, 1998.

Udisti, R., S. Becagli, E. Castellano, B. Delmonte, J. Jouzel, J.R. Petit, J. Schwander, B. Stenni, and E.W. Wolff, Stratigraphic correlations between the European Project for Ice Coring in Antarctica (EPICA) Dome C and Vostok ice cores showing the relative variations of snow accumulation over the past 45 kyr, *Journal of Geophysical Research*, *109* (D8), 2004.

van Kolfschoten, T., P.L. Gibbard, and K.-L. Knudsen, The Eemian interglacial: A global perspective. Introduction, *Global and Planetary Change*, *36* (3), 147-149, 2003.

Vimeux, F., K.M. Cuffey, and J. Jouzel, New insights into southern hemisphere temperature changes from Vostok ice cores using deuterium excess correction, *Earth and Planetary Science Letters*, *203* (3-4), 829-843, 2002.

Wolff, E.W., A.M. Rankin, and R. Röthlisberger, An ice core indicator of Antarctic sea ice production?, *Geophysical Research Letters*, *30* (22), 2003.

Yuan, D., H. Cheng, R.L. Edwards, C.A. Dykoski, M.J. Kelly, M. Zhang, J. Qing, Y. Lin, Y. Wang, J. Wu, J.A. Dorale, Z. An, and Y. Cai, Timing, duration, and transitions of the last interglacial Asian Monsoon, *Science*, *304* (5670), 575-578, 2004.

Zhao, J.X., Q.K. Xia, and K.D. Collerson, Timing and duration of the Last Interglacial inferred from high resolution U-series chronology of stalagmite growth in Southern Hemisphere, *Earth and Planetary Science Letters*, *184* (3-4), 635-644, 2001.

		Late Holocene 1 – 5 ka BP	**Mid Holocene** 5 – 9 ka BP	**Early Holocene** 9.5 – 11.5 ka BP	**Glacial Maximum I** 18 – 27 ka BP	**Late Eemian** 116 – 120 ka BP	**Mid Eemian** 120 – 124 ka BP	**Early Eemian** 126 – 128 ka BP	**Glacial Maximum II** 137 – 146 ka BP
Na^+	concentration median (ng g^{-1})	20	18	14	100	18	12	7.7	95
	concentration variation coefficient (%)	27	26	26	16	20	22	29	12
	flux median (µg m^{-2} a^{-1})	520	470	380	1300	510	380	290	1300
ss-Na^+	concentration median (ng g^{-1})	19	17	14	58	17	11	6.9	56
	flux median (µg m^{-2} a^{-1})	500	440	370	740	480	340	260	790
Ca^{2+}	concentration median (ng g^{-1})	1.5	1.4	1.0	44	1.6	1.8	1.0	41
	concentration variation coefficient (%)	26	25	29	23	20	24	32	18
	flux median (µg m^{-2} a^{-1})	39	37	28	560	47	53	39	570
nss-Ca^{2+}	concentration median (ng g^{-1})	0.74	0.77	0.51	42	0.96	1.3	0.76	38
	flux median (µg m^{-2} a^{-1})	20	20	14	530	28	40	28	540
NH_4^+	concentration median (ng g^{-1})	0.76	0.74	0.65	1.8	0.48	0.55	0.38	1.7
	concentration variation coefficient (%)	29	28	30	15	26	25	29	14
	flux median (µg m^{-2} a^{-1})	20	19	17	23	14	17	14	24
NO_3^-	concentration median (ng g^{-1})	14	–	17	50	19	22	21	36
	concentration variation coefficient (%)	19	–	21	27	16	11	21	23
	flux median (µg m^{-2} a^{-1})	360	–	450	640	560	670	780	500

Table 1. Mass concentration medians, variation coefficients and flux medians of the last two interglacial periods and the preceding glacial maxima from the EPICA Dome C ice core. All values are based on the log-normal distributed annual mean data and are rounded to two digits.

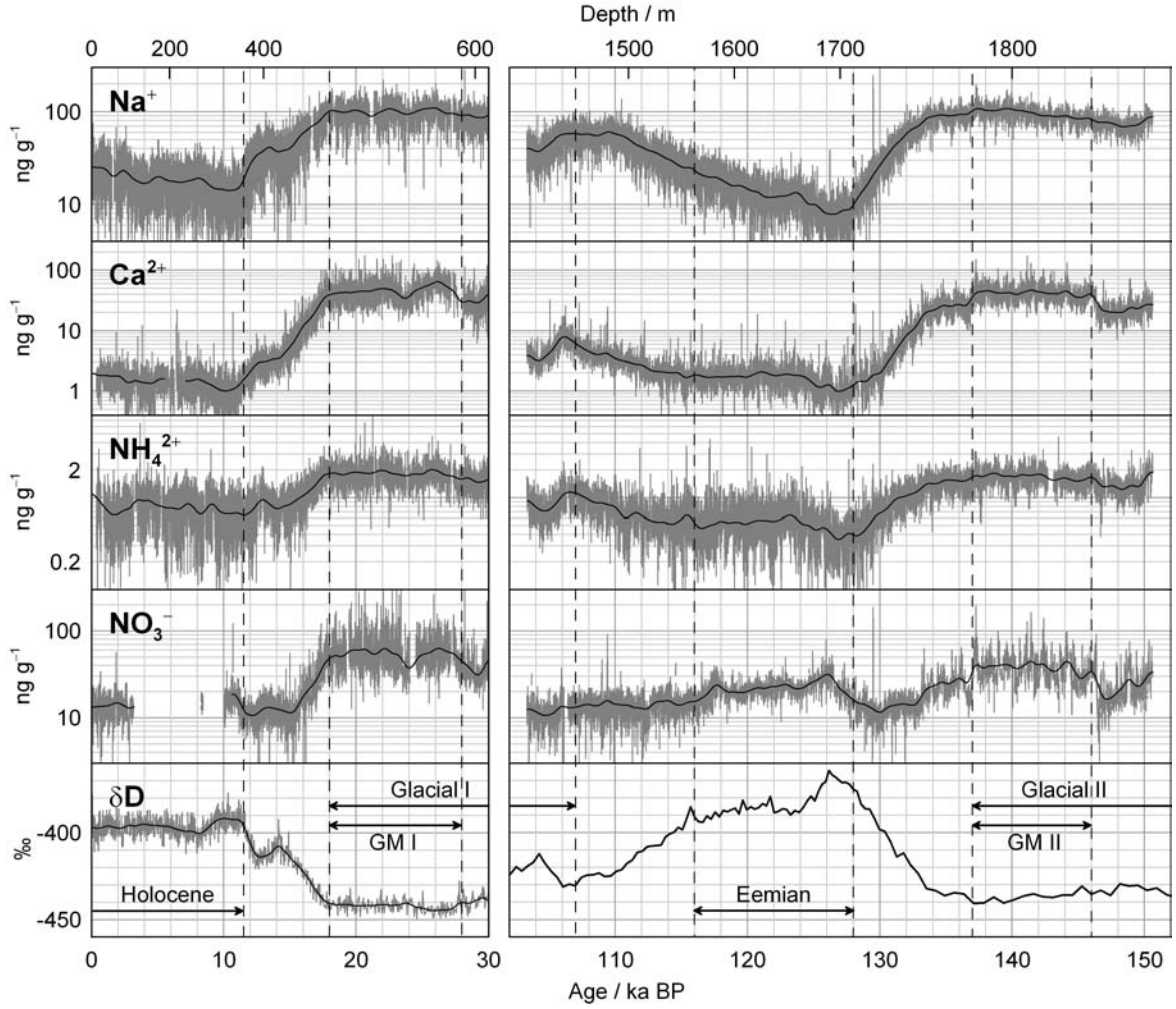

Figure 1. Na^+, Ca^{2+}, NH_4^+ and NO_3^- measurements (concentrations in ng g^{-1}) from the EPICA Dome C deep ice core in formal annual resolution (grey lines) and Gaussian-filtered (cut off period 2000a; black lines), along with δD (in ‰) [*EPICA community members*, 2004; *Jouzel et al.*, 2001], around the two interglacial periods (Holocene, Eemian).

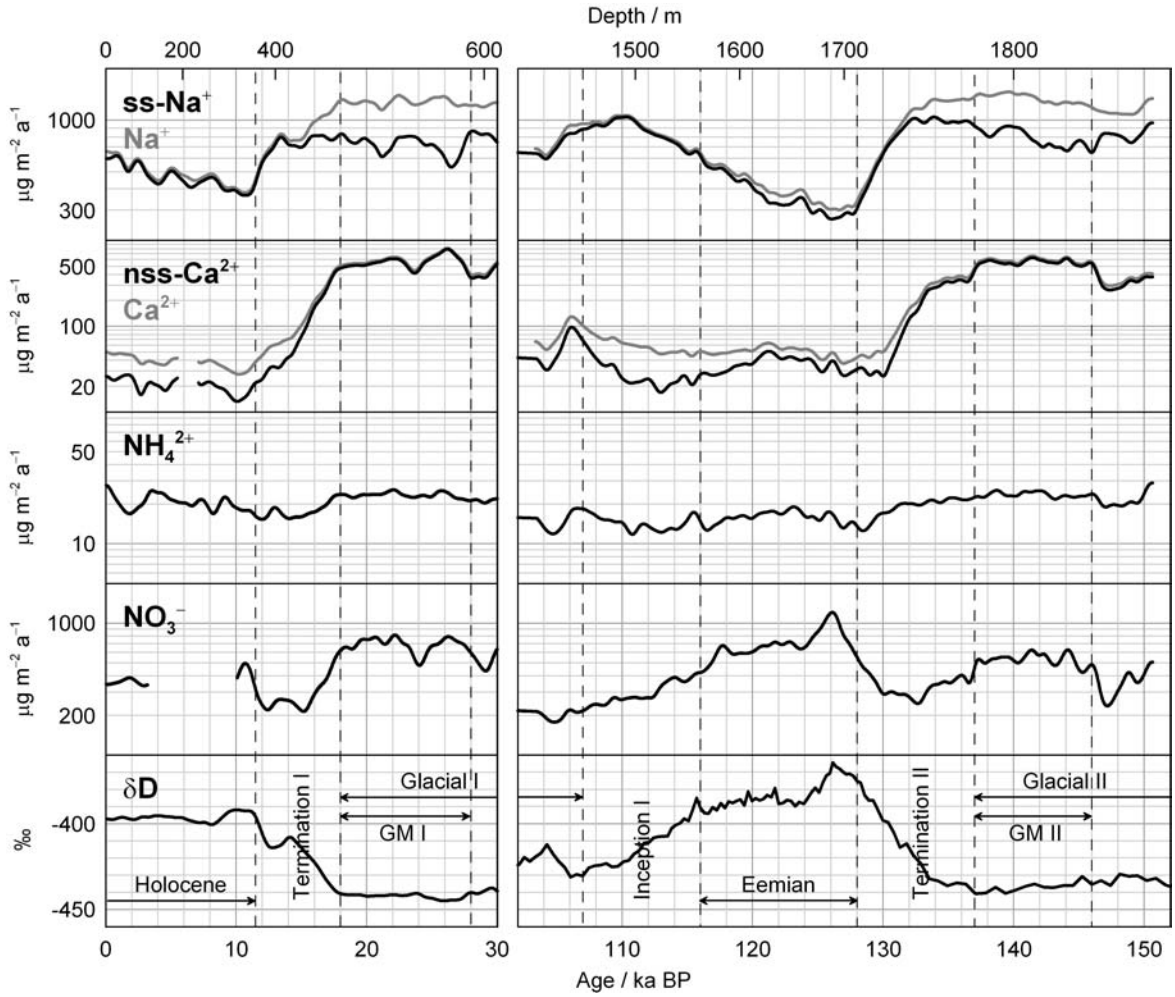

Figure 2. Fluxes of ss-Na^+, Na^+, nss-Ca^{2+}, Ca^{2+}, NH_4^+ and NO_3^- (in µg m^{-2} a^{-1}) from the EPICA Dome C deep ice core filtered (Gaussian-filter, cut off period 2000a) along with δD (in ‰) [*EPICA community members*, 2004; *Jouzel et al.*, 2001], around the two interglacial periods (Holocene, Eemian). In contrast to the other records, NO_3^- is subjected to post-depositional effects, therefore fluxes do not represent an atmospheric signal.

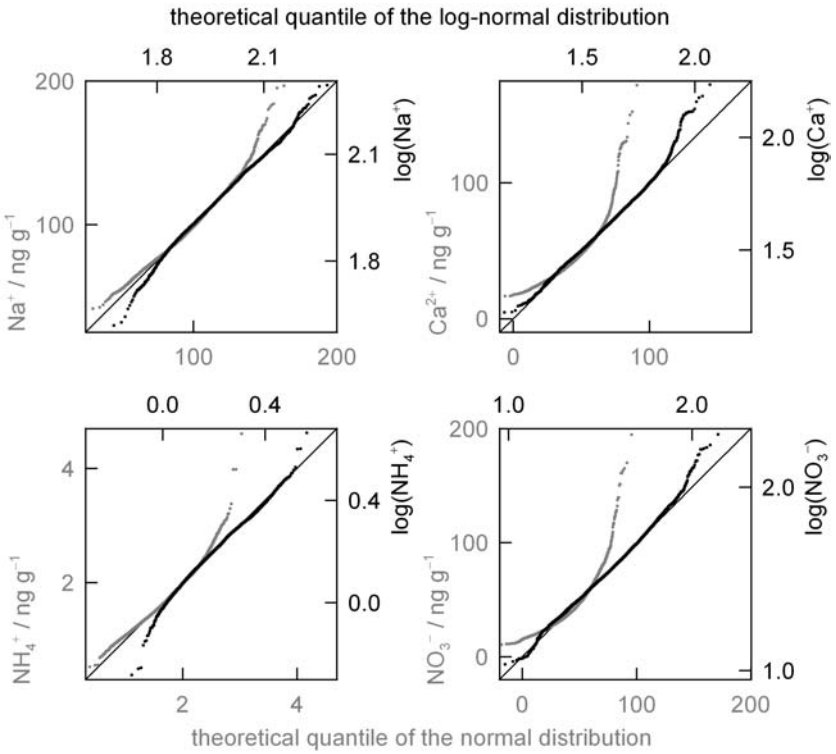

Figure 3. Quantile-quantile-plot of Na^+, Ca^{2+}, NH_4^+ and NO_3^- to examine the statistical distribution of the measurements, exemplarily for GM II. Although not perfect, log-normal distributions (black) fit better to the ideal diagonal than normal distributions (grey). Deviations at low concentration levels can be observed for Na^+ and NH_4^+, whereas Ca^{2+} and NO_3^- reveal more high peaks than expected from the theoretical distribution.

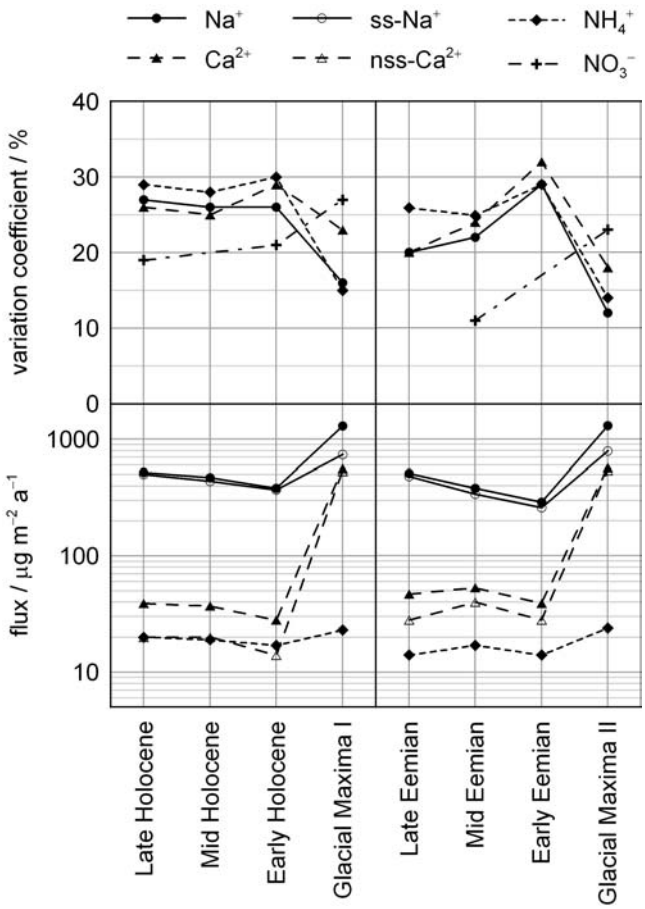

Figure 4. Variation coefficients of Na^+, Ca^{2+}, NH_4^+ and NO_3^- (in %, upper panel) and fluxes of Na^+, ss-Na^+, Ca^{2+}, nss-Ca^{2+} and NH_4^+ (in µg m^{-2} a^{-1}, lower panel) within different parts of the Holocene and Eemian interglacial periods and the preceding glacial maxima GM I and II.

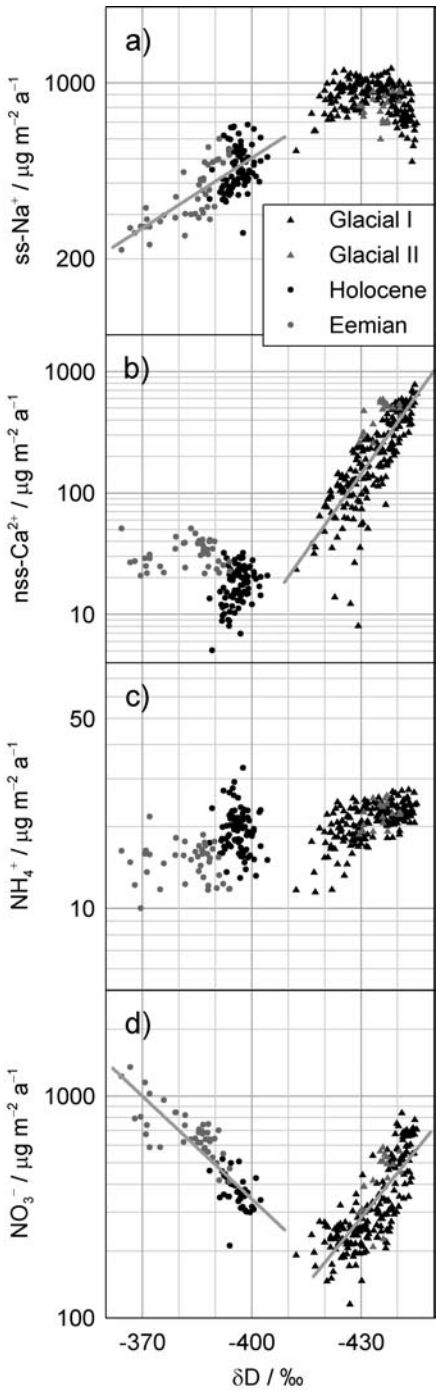

Figure 5. Correlation of a) ss-Na^+, b) nss-Ca^{2+}, NH_4^+ c) and d) NO_3^- (in ng g^{-1}, on a log-scale) with δD (in ‰) based on approximately 4m-mean values; linear fits of the logarithmised data in light grey. ss-Na^+ is well anti-correlated in warm, interglacial periods, whereas nss-Ca^{2+} shows a good anti-correlation during cold glacial periods. No correlation is shown for NH_4^+, neither in glacial nor in interglacial periods. However, attention has to be paid concerning NO_3^-: During interglacial periods NO_3^- preservation correlates with the accumulation rate, whereas it is correlated to the dust input for glacial periods.

2.4 Ice core evidence for the extent of past atmospheric CO_2 change due to iron fertilisation

Regine Röthlisberger, Matthias Bigler, Eric W. Wolff,
Eric Monnin, Fortunat Joos, Manuel A. Hutterli

Geophysical Research Letters
2004, submitted

Ice core evidence for the extent of past atmospheric CO_2 change due to iron fertilisation

R. Röthlisberger,[1,2] M. Bigler,[3] E. W. Wolff,[1] F. Joos,[3] E. Monnin,[3] M. A. Hutterli[3]

An extended high-resolution ice core record of dust deposition over the past 60 ka from Dome C, Antarctica, is presented. The data are in conflict with the idea that changes in aeolian iron input into the Southern Ocean were the major cause for the 80 ppm glacial-interglacial CO_2 increase. During the deglaciation, the CO_2 increase shows a linear relationship with the fall of the logarithm of the nss-Ca^{2+} flux, a proxy for dust deposition. However, the very large variations in the nss-Ca^{2+} flux related to the glacial Antarctic warm events A1 to A4 were accompanied by small CO_2 variations only. Our data-based analysis suggests that decreased Southern Ocean dust deposition caused at most a 20 ppm increase in CO_2 at the last glacial-interglacial transition. Rapid decreases in dust deposition to the northern Pacific could have been responsible for a maximum of 8 ppm in addition.

Introduction

The concentration of CO_2 in the atmosphere over the last 420 kyr has alternated between about 180 ppm in glacial maxima and 280 ppm in interglacials [*Petit et al.*, 1999]. These changes act as a major amplifier in the climate system, contributing to the strong glacial-interglacial contrast that is observed. Determining the causes of the CO_2 increase at glacial terminations, such as the ∼80 ppm increase at the last one (Fig. 1), is one of the major challenges in understanding the Earth system. Here we use high-resolution chemical data from an Antarctic ice core to set limits on one of the most pervasive mechanisms that has been proposed, iron fertilisation of the oceans.

The ocean is the most important control on atmospheric CO_2 concentrations on glacial-interglacial timescales [*Sigman and Boyle*, 2000; *Archer et al.*, 2000]. The equilibrium partial pressure of CO_2 in seawater depends on the concentration of dissolved inorganic carbon (DIC) amongst other factors. In high-latitude surface waters, particularly in the Southern Ocean and in the North Pacific, the concentrations of nutrients and DIC remain high and chlorophyll levels low throughout the year. Iron concentrations in these high-nutrient low-chlorophyll (HNLC) regions are very low. Several field experiments demonstrate that addition of iron stimulates biological productivity and reduces surface water pCO_2 in the Southern Ocean and other HNLC regions [*Boyd et al.*, 2000; *Tsuda et al.*, 2003]. Consequently, it has been suggested that enhanced aeolian iron deposition into the Southern Ocean was the primary cause for the observed low glacial CO_2 values [*Martin*, 1990].

Different model analyses focusing on a range of iron-related marine biogeochemical processes yield ambiguous results, explaining little [*Bopp et al.*, 2003] up to all [*Matsumoto et al.*, 2002] of the observed 80 ppm CO_2 increase during past deglaciations. Several processes other than iron fertilisation may be responsible for the low glacial CO_2 concentrations [*Sigman and Boyle*, 2000; *Archer et al.*, 2000; *Broecker and Henderson*, 1998].

Here we analyse changes in atmospheric CO_2 concentrations [*Indermühle et al.*, 2000] and aeolian dust deposition as recorded in Antarctic ice cores (Fig. 1). The strategy is to estimate data-based bounds for the contribution of iron fertilisation to atmospheric CO_2 variations during periods where variations in aeolian dust supply are large, but changes in other parameters affecting atmospheric CO_2 remained modest. For the first time, chemical data are available at a resolution capable of assessing the role of dust on CO_2 over the past 60 ka, i.e. covering the period of the last four glacial Antarctic warm events and the last deglaciation.

Data

The chemical ice core records from Dome C have been obtained by a Continuous Flow Analysis (CFA) system, as described in [*Röthlisberger et al.*, 2000]. Back to 45 kyr B.P. the data originate from the EDC96 ice core, mainly analysed during the 97/98 and 98/99 field seasons [*Röthlisberger et al.*, 2002]. Data reaching further back in time were obtained from EDC99 during the 01/02 field season. The Dome C EDC96 records are displayed on the EDC1 timescale [*Schwander et al.*, 2001], EDC99 records on the EDC2 timescale (pers. comm. Jakob Schwander, University of Bern). Temporal resolution of the chemical records is of the order of at most a few years. Presented here are 50-year averages of the high-resolution data. For comparison, the widely-cited dust record from Vostok, Antarctica [*Petit et al.*, 1999] includes only approximately 80 data points over the past 60 kyr.

The CO_2 data covering 8 to 22 kyr B.P. were measured in the air bubbles of the EPICA Dome C ice core [*Monnin et al.*, 2001] (EDC96), whilst from 20 to 60 kyr B.P. they originate from the Taylor Dome ice core [*Indermühle et al.*, 2000]. The Dome C deuterium record [*Stenni et al.*, 2003], an indicator of local Antarctic temperature, is so far only published back to 45 kyr B.P., but a comparison of Vostok isotopic records with the Taylor Dome CO_2 data [*Indermühle et al.*, 2000] has shown that the variation over events A2 to A4 were similar in amplitude and timing to event A1. The data from Taylor Dome are transferred to the EDC2 timescale using CH_4 to synchronise the records [*Brook et al.*, 2000] (J. Flückiger, University of Bern, unpublished data). Due to the uncertainty of Δage and of the CH_4 synchronisation, the exact timing of the CO_2 variation

[1]British Antarctic Survey, Natural Environment Research Council, Cambridge, United Kingdom

[2]Now at NCCR Climate, University of Bern, Bern, Switzerland.

[3]Climate and Environmental Physics, University of Bern, Bern, Switzerland.

0094-8276/04/$5.00

relative to the changes in Antarctic temperature, nss-Ca^{2+} and Na^+ remains elusive.

We use the non-sea-salt calcium flux (nss-Ca^{2+}) as a proxy for dust and the sodium (Na^+) flux as a first-order estimate of sea ice coverage [*Wolff et al.*, 2003]. Changes in transport efficiency could alter the measured nss-Ca^{2+} flux at Dome C. However, it has been shown that changes at the source were the dominant cause for the observed nss-Ca^{2+} variations [*Röthlisberger et al.*, 2002]. Hence, the nss-Ca^{2+} flux represents the magnitude of dust deposition to the Southern Ocean.

Glacial period

During events A2 to A4 the nss-Ca^{2+} flux was reduced from high glacial values to levels similar to those of the Antarctic Cold Reversal (ACR), i.e. only approximately twice the Holocene level (Fig. 1). At event A1, nss-Ca^{2+} flux was reduced even further. These strong changes in dust deposition were accompanied by changes in atmospheric CO_2 of up to 20 ppm [*Indermühle et al.*, 2000]. Changes in other parameters potentially affecting atmospheric CO_2 were much smaller during this time interval than during the transition. This suggests that changes in aeolian iron deposition to the Southern Ocean of glacial-interglacial magnitude have a limited effect on atmospheric CO_2.

Potentially, other factors could have masked an impact of iron fertilisation on atmospheric CO_2 during the A1 to A4 events. However, SST variations and changes in the North Atlantic thermohaline circulation have likely contributed to the observed CO_2 variations, suggesting that the net impact of aeolian iron deposition to the Southern Ocean is even smaller than the observed CO_2 variations.

Earlier studies [*Stocker and Johnsen*, 2003] link the Antarctic warm phases to the Dansgaard-Oeschger warm/cold cycles recorded in Greenland ice cores and to changes in the North Atlantic thermohaline circulation invoking a 'thermal bipolar seesaw'. Model results [*Marchal et al.*, 1999; *Scholze et al.*, 2003] suggest that a collapse of the North Atlantic Deep Water formation and associated Northern Hemisphere cooling and Southern Hemisphere warming and biogeochemical changes lead to a release of carbon both from the ocean and the land biosphere. Thus, the reorganizations in the North Atlantic thermohaline circulation and associated changes in sea surface temperature and on land have contributed to the observed high CO_2 levels during the Antarctic warm events.

Regardless of the mechanism responsible for the Antarctic warm phases, the related sea surface temperature (SST) increase in the Southern Hemisphere must have led to decrease in the solubility of CO_2 in seawater and to outgassing to the atmosphere. Data-based global reconstructions of the spatio-temporal variability in SST over A1 to A4 are missing and a data-based quantification of the impact of SST variations, complementing model-based analyses [*Marchal et al.*, 1999], is therefore currently not possible. A recent record from the southwest Pacific east of New Zealand [*Pahnke et al.*, 2003] estimates a 3°C change in SST over A1 to A4. However, variations of similar amplitude are observed during the period from 60 to 20 kyr B.P. that are not accompanied by similar CO_2 changes.

Turning to sea ice, there is no evidence from the Na^+ flux for significant changes in sea ice production over A1 to A4 [*Wolff et al.*, 2003]. This suggests a small contribution from changing sea ice coverage of the Southern Ocean to the glacial CO_2 variations.

The periods of low nss-Ca^{2+} were shorter during A1 to A4 than during the transition and atmospheric CO_2 might not have reached a new equilibrium. The glacial nss-Ca^{2+} variations occurred on a multi-millennia time scale, implying that atmospheric CO_2 must have fully responded to processes with time scales of up to a millennium. The time scales governing nutrient supply from sub-surface waters and export of biogenic material to the abyss, the coupling between high- and low-latitude ocean processes, and the response of atmospheric CO_2 are in the range of decades to centuries [*Joos et al.*, 1991; *Matsumoto et al.*, 2002]. On the other hand, the effect on CO_2 of a potential readjustment of the ocean's alkalinity budget and the calcite lysocline [*Archer et al.*, 2000] and changes in the whole ocean nitrate inventory, e. g. in response to iron-stimulated changes in the calcite to organic matter rain ratio or changes in nitrate fixation [*Broecker and Henderson*, 1998], would accrue on a multi-millenia time scale only. However, observed changes in the lysocline depth [*Broecker and Henderson*, 1998] and co-limitation of biological production by phosphate suggest a limited role for these slow-response scenarios. The Vostok results [*Petit et al.*, 1999] corroborate this analysis: During the last three glacial periods, atmospheric CO_2 decreased from interglacial concentrations to 230 ppm before the onset of high dust deposition in the Vostok core.

In conclusion, the observed change of 20 ppm CO_2 during the Antarctic warm events A1 to A4 likely represents an upper boundary for the effect of reduced iron fertilisation due to a reduction in dust input into the Southern Ocean.

Transition

Transferring this insight to the situation during the transition implies that reduced iron fertilisation of the Southern Ocean led to at most a 20 ppm increase in CO_2 over the first half of the transition (from 18 to 14 kyr B.P.), corresponding to the period of largest reduction in dust (interval I and II in Fig. 2). Over the same period, CO_2 increased by 40 ppm, i.e. other factors, including their interplay with iron fertilisation, must have accounted for at least 20 ppm. Since the dust flux changed little during interval IV, and since dust in event A1 already reached (albeit temporarily) Holocene levels, it is unlikely that much of the CO_2 increase in interval IV was connected to changing iron fertilisation.

The different relationship between CO_2 and dust over A1 to A4 compared to the transition is shown in Fig. 3. As an estimate of a maximum effect and in order to avoid a large scatter due to the uncertainty in the synchronisation of the two ice core records, we compare the maxima of the CO_2 concentration with the minima of the nss-Ca^{2+} flux and vice versa. For the transition, we selected data at the boundaries of the intervals indicated in Fig. 2; these CO_2 and nss-Ca^{2+} data originate from the same ice core, therefore the uncertainty in matching the corresponding data points is small. The slope during the glacial period, being itself an upper limit of the effect of dust on atmospheric CO_2, is much smaller than during the transition. The difference between the glacial relationship and the one derived from the data of the transition reflects the amount of CO_2 changes that needs to be caused by other factors.

At the end of interval II and again at the end of interval IV of the transition, CO_2 concentrations increased by 6 - 8 ppm within less than a few centuries [*Monnin et al.*, 2001], coeval with the large changes in CH_4 that occurred at the warming into the Bølling (corresponding to the end of interval II) and the warming after the Younger Dryas (end of interval IV). This implies that these two increases are due to a northern hemisphere, rather than a Southern Ocean, process. By matching the methane records from Dome C and Greenland, we can precisely align these two periods with datasets from Greenland ice cores (Fig. 2). The two warming events were

accompanied by large and rapid decreases in the dust input to Greenland. The dust found in Greenland ice cores originates from Asia [*Biscaye et al.*, 1997] and is transported by the westerlies over the northern Pacific and North America to Greenland. The rapid decrease by an order of magnitude suggests that also dust fallout en route was reduced significantly. This could have had a considerable effect on the northern Pacific productivity. While glacial dust supply prevented iron limitation, the decrease in dust at the end of interval II and IV led to conditions similar to today, i.e. a significant iron deficit [*Tsuda et al.*, 2003]. The suddenly decreased iron supply would be a relatively fast mechanism influencing the carbon cycle and raises the possibility that changes in dust deposition to the northern Pacific were the factor leading to these observed 8 ppm increases in CO_2. However, the increase in dust at the onset of the Younger Dryas did not leave a reverse imprint on the CO_2 concentrations. One possibility is that the increased dust did have a reverse effect, acting on a longer timescale, and that this was masked by the overlying process that led to the observed increase at a rate of 20 ppm/kyr during interval IV. Based on the ammonium record from the Greenland GRIP ice core [*Fuhrer et al.*, 1996], the North American biosphere evolved rapidly during interval III. If other regions showed a similar development during this period, this could have contributed to the observed temporary stabilisation of the CO_2 concentrations during this interval.

Conclusions

Data from Greenland and Antarctic ice cores suggest that the overall effect of iron fertilisation on glacial-interglacial CO_2 changes is limited in extent and time. Changes of iron supply to the Southern Ocean probably contributed at most 20 ppm to the CO_2 increase between 18 and 14 kyr B.P. and were negligible thereafter. Reduction of the dust input into the northern Pacific was much faster, but has a smaller effect on CO_2 of up to 8 ppm only. The remaining 50 ppm of increase must thus be ascribed to other processes, possibly acting in concert with iron fertilisation.

Acknowledgments. This work is contribution No. x to the "European Project for Ice Coring in Antarctica" (EPICA), a joint ESF (European Science Foundation)/EC scientific programme, funded by the European Commission and by national contributions from Belgium, Denmark, France, Germany, Italy, the Netherlands, Norway, Sweden, Switzerland and the United Kingdom. Thanks to Thomas Stocker for valuable discussion and Jakob Schwander for his support with the Dome C chronology. Jacqueline Flückiger and Renato Spahni are acknowledged for providing unpublished methane data. M.H. was supported by the EC project PACLIVA(EVR1-2002-000413).

References

Archer, D. E., A. Winguth, D. Lea, and N. Mahowald, What caused the glacial/interglacial atmospheric pCO_2 cycles?, *Rev. Geophys.*, *38*(2), 159–189, 2000.

Biscaye, P. E., F. E. Grousset, M. Revel, S. Van der Gaast, G. Zielinski, A. Vaars, and G. Kukla, Asian provenance of glacial dust (stage 2) in the Greenland Ice Sheet Project 2 Ice Core, Summit, Greenland, *J. Geophys. Res.*, *102*(C12), 26,765–26,781, 1997.

Bopp, L., K. E. Kohfeld, C. Le Quéré, and O. Aumont, Dust impact on marine biota and atmospheric CO_2 during glacial periods, *Paleoceanogr.*, *18*(2), 1046, doi:10.1029/2002PA000,810, 2003.

Boyd, P. W., et al., A mesoscale phytoplankton bloom in the polar Southern Ocean stimulated by iron fertilization, *Nature*, *407*, 695–702, 2000.

Broecker, W. S., and G. M. Henderson, The sequence of events surrounding Termination II and their implications for the cause of glacial-interglacial CO_2 changes, *Paleoceanogr.*, *13*(4), 352–364, 1998.

Brook, E. J., S. Harder, J. P. Severinghaus, E. J. Steig, and C. M. Sucher, On the origin and timing of rapid changes in atmospheric methane during the last glacial period, *Global Biogeochem. Cyc.*, *14*(2), 559–572, 2000.

Fuhrer, K., A. Neftel, M. Anklin, T. Staffelbach, and M. Legrand, High-resolution ammonium ice core record covering a complete glacial-interglacial cycle, *J. Geophys. Res.*, *101*(D2), 4147–4164, 1996.

Indermühle, A., E. Monnin, B. Stauffer, T. F. Stocker, and M. Wahlen, Atmospheric co2 concentration from 60 to 20 kyr BP from the Taylor Dome ice core, Antarctica, *Geophys. Res. Lett.*, *27*(5), 735–738, 2000.

Joos, F., J. L. Sarmiento, and U. Siegenthaler, Estimates of the effect of Southern Ocean iron fertilization on atmospheric CO2 concentrations, *Nature*, *349*, 772–774, 1991.

Marchal, O., T. F. Stocker, F. Joos, A. Indermühle, T. Blunier, and J. Tschumi, Modelling the concentration of atmospheric CO2 during the Younger Dryas climate event, *Clim. Dyn.*, *15*, 341–354, 1999.

Martin, J. H., Glacial-interglacial CO2 change: The iron hypothesis, *Paleoceanogr.*, *5*, 1–13, 1990.

Matsumoto, K., J. L. Sarmiento, and M. A. Brzezinski, Silicic acid leakage from the Southern Ocean: A possible explanation for glacial atmospheric pCO_2, *Global Biogeochem. Cyc.*, *16*(3), 10.1029/2001GB001,442, 2002.

Monnin, E., A. Indermühle, A. Dällenbach, J. Flückiger, B. Stauffer, T. F. Stocker, D. Raynaud, and J.-M. Barnola, Atmospheric CO_2 Concentrations over the Last Glacial Termination, *Science*, *291*, 112–114, 2001.

Pahnke, K., R. Zahn, H. Elderfield, and M. Schulz, 340,000-Year Centennial-Scale Marine Record of Southern Hemisphere Climatic Oscillation, *Science*, *301*, 948–952, 2003.

Petit, J. R., et al., Climate and atmospheric history of the past 420,000 years from the Vostok ice core, Antarctica, *Nature*, *399*, 429–436, 1999.

Röthlisberger, R., M. Bigler, M. Hutterli, S. Sommer, B. Stauffer, H. G. Junghans, and D. Wagenbach, Technique for continuous high-resolution analysis of trace substances in firn and ice cores, *Environ. Sci. Technol.*, *34*, 338–342, 2000.

Röthlisberger, R., R. Mulvaney, E. W. Wolff, M. A. Hutterli, M. Bigler, S. Sommer, and J. Jouzel, Dust and Sea-Salt Variability in Central East Antarctica (Dome C) over the Last 45 kyrs and its Implications for Southern High-Latitude Climate, *Geophys. Res. Lett.*, *29*(20), 1963, doi:10.1029/2002GL015,186, 2002.

Scholze, M., W. Knorr, and M. Heimann, Modelling terrestrial vegetation dynamics and carbon cycling for an abrupt climate change event, *The Holocene*, *13*(3), 327–333, 2003.

Schwander, J., J. Jouzel, C. U. Hammer, J. R. Petit, R. Udisti, and E. Wolff, A tentative chronology for the EPICA Dome Concordia ice core, *Geophys. Res. Lett.*, *28*(22), 4243–4246, 2001.

Sigman, D. M., and E. A. Boyle, Glacial/interglacial variations in atmospheric carbon dioxide, *Nature*, *407*, 859–869, 2000.

Stenni, B., et al., A late-glacial high resolution site and source temperature record derived from the EPICA Dome C isotope records (East Antarctica), *Earth Planet. Sci. Lett.*, *217*(1-2), 183–195, 2003.

Stocker, T. F., and S. Johnsen, A minimum thermodynamic model for the bipolar seesaw, *Paleoceanogr.*, *18*(4), 1087, doi:10.1029/2003PA000,920, 2003.

Tsuda, A., et al., A mesoscale iron enrichment in the western subarctic Pacific induces a large centric diatom bloom, *Science*, *300*, 958–961, 2003.

Wolff, E. W., A. M. Rankin, and R. Röthlisberger, An ice core index of Antarctic sea ice production?, *Geophys. Res. Lett.*, *30*(22), 2158, doi:10.1029/2003GL018,454, 2003.

R. Röthlisberger, British Antarctic Survey, Natural Environment Research Council, Madingley Road, Cambridge CB3 0ET,

United Kingdom. Now at NCCR Climate, University of Bern, Erlachstr. 9a, 3012 Bern, Switzerland. (regine@giub.unibe.ch)

E. W. Wolff, British Antarctic Survey, Natural Environment Research Council, Madingley Road, Cambridge CB3 0ET, United Kingdom.

M. Bigler, F. Joos, E. Monnin, M. A. Hutterli, Climate and Environmental Physics, University of Bern, Sidlerstr. 5, 3012 Bern, Switzerland.

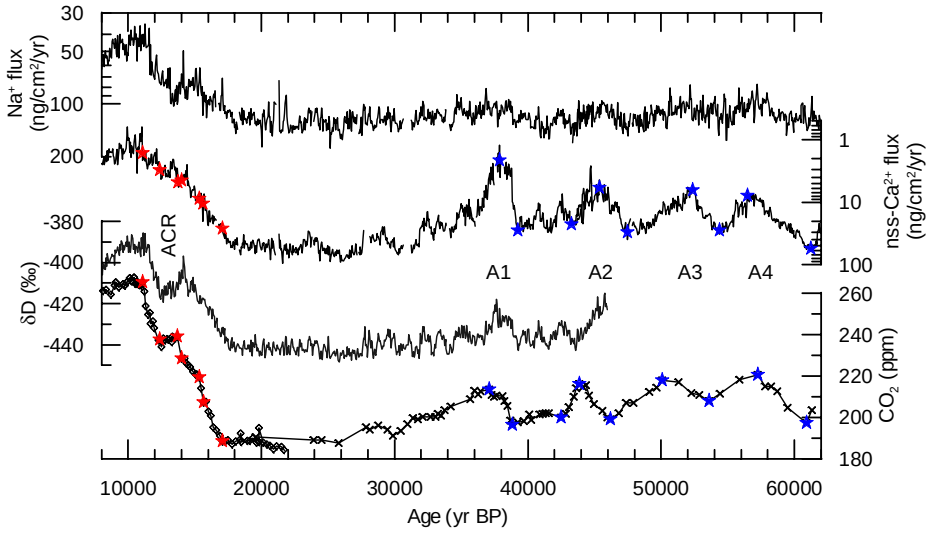

Figure 1. Dome C ice core records covering 10 to 60 kyr B.P. CO_2 concentrations were measured in the Dome C ice core (diamonds) and in the Taylor Dome ice core (crosses). Note that the y-axes of Na^+ and nss-Ca^{2+} are reversed. ACR marks the Antarctic Cold Reversal, A1 to A4 the last four warm events of the last glacial period in Antarctica. Red and blue stars refer to the bold symbols used in Fig. 3

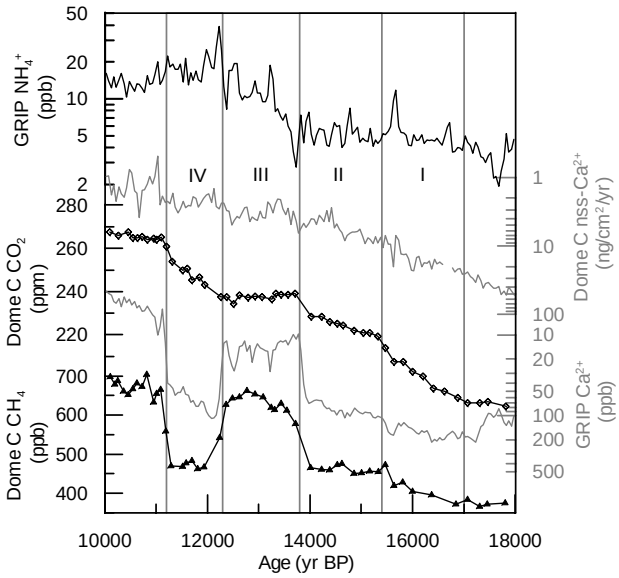

Figure 2. Comparison of Dome C CO_2 and CH_4 records with Greenland and Antarctic aerosol records over the transition from the last glacial period into the Holocene. The intervals I to IV correspond to the periods of different rates of change in CO_2 concentrations as indicated in [*Monnin et al.*, 2001] . Note that the y-axes of the two Ca^{2+} records are reversed.

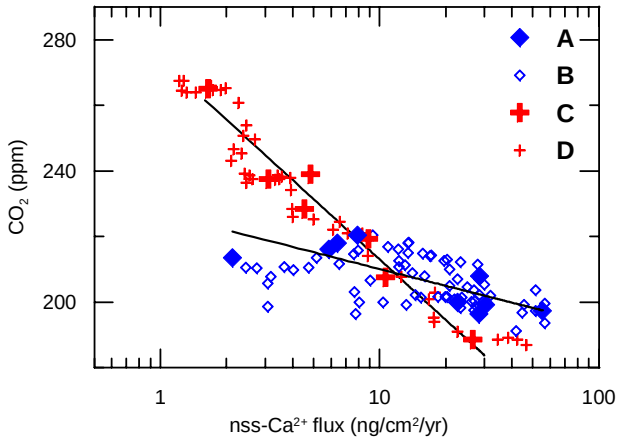

Figure 3. Empirical relationships between CO_2 and nss-Ca^{2+} flux at Dome C for different climatic periods. **A** concentration minima and maxima over A1 to A4 (blue stars in Fig. 1). **B** CO_2 and corresponding nss-Ca^{2+} flux (250yr averages) over the period from 30 to 60 kyr B.P. **C** concentrations at the boundaries of intervals I to IV (red stars in Fig. 1). **D** CO_2 and corresponding nss-Ca^{2+} flux over the period 10 to 18 kyr B.P. The linear fits were calculated based on A and C, with $r^2 = 0.66$ and $r^2 = 0.96$ respectively.

2.5 Continuous record of microparticle concentration and size distribution in the central Greenland NGRIP ice core during the last glacial period

Urs Ruth, Dietmar Wagenbach, Jørgen Peder Steffensen, Matthias Bigler

Journal of Geophysical Research
108(D3), 4098, 2003

JOURNAL OF GEOPHYSICAL RESEARCH, VOL. 108, NO. D3, 4098, doi:10.1029/2002JD002376, 2003

Continuous record of microparticle concentration and size distribution in the central Greenland NGRIP ice core during the last glacial period

Urs Ruth[1] and Dietmar Wagenbach
Institute of Environmental Physics, University of Heidelberg, Heidelberg, Germany

Jørgen P. Steffensen
Department of Geophysics, University of Copenhagen, Copenhagen, Denmark

Matthias Bigler
Department of Climate and Environmental Physics, University of Bern, Bern, Switzerland

Received 26 March 2002; revised 29 July 2002; accepted 12 September 2002; published 5 February 2003.

[1] A novel laser microparticle detector used in conjunction with continuous sample melting has provided a more than 1500 m long record of particle concentration and size distribution of the NGRIP ice core, covering continuously the period approximately from 9.5–100 kyr before present; measurements were at 1.65 m depth resolution, corresponding to approximately 35–200 yr. Particle concentration increased by a factor of 100 in the Last Glacial Maximum (LGM) compared to the Preboreal, and sharp variations of concentration occurred synchronously with rapid changes in the $\delta^{18}O$ temperature proxy. The lognormal mode μ of the volume distribution shows clear systematic variations with smaller modes during warmer climates and coarser modes during colder periods. We find $\mu \approx 1.7$ μm diameter during LGM and $\mu \approx 1.3$ μm during the Preboreal. On timescales below several 100 years μ and the particle concentration exhibit a certain degree of independence present especially during warm periods, when μ generally is more variable. Using highly simplifying considerations for atmospheric transport and deposition of particles we infer that (1) the observed changes of μ in the ice largely reflect changes in the size of airborne particles above the ice sheet and (2) changes of μ are indicative of changes in long range atmospheric transport time. From the observed size changes we estimate shorter transit times by roughly 25% during LGM compared to the Preboreal. The associated particle concentration increase from more efficient long range transport is estimated to less than one order of magnitude. *INDEX TERMS:* 0305 Atmospheric Composition and Structure: Aerosols and particles (0345, 4801); 0322 Atmospheric Composition and Structure: Constituent sources and sinks; 0368 Atmospheric Composition and Structure: Troposphere—constituent transport and chemistry; *KEYWORDS:* mineral dust, ice cores, size distribution, continuous flow analysis, atmospheric circulation, paleoclimate

Citation: Ruth, U., D. Wagenbach, J. P. Steffensen, and M. Bigler, Continuous record of microparticle concentration and size distribution in the central Greenland NGRIP ice core during the last glacial period, *J. Geophys. Res.*, *108*(D3), 4098, doi:10.1029/2002JD002376, 2003.

1. Introduction

[2] Ice cores provide a wealth of paleoclimatic information including records of windblown mineral aerosol (hereinafter dust). Among all deposited components this atmospheric constituent has a special quality because not only its concentration but also the size distribution of its insoluble fraction is preserved. As East Asian deserts have been identified as the dominant source area for dust transported to Greenland [*Biscaye et al.*, 1997; *Kahl et al.*, 1997; *Svensson et al.*, 2000; *Bory et al.*, 2002], archives may hold specific information about atmospheric transport in particular. Particulates found in Greenland ice overwhelmingly derive from the insoluble fraction of dust (hereinafter particles) [e.g., *Thompson*, 1977].

[3] Dust concentrations in ice cores vary by a factor of $\approx$100 between the Holocene and the Last Glacial Maximum (LGM) in central Greenlandic ice [*Steffensen*, 1997; *Fuhrer et al.*, 1999]. Continuous particle and Ca^{2+} measurements in the Renland ice core [*Hansson*, 1994] and continuous Ca^{2+} measurements in the GISP2 and GRIP ice cores [*Mayewski et al.*, 1994; *Fuhrer et al.*, 1999] have shown that during rapid climatic transitions the dust concentration varied synchronously with the $\delta^{18}O$ temperature proxy. Explana-

[1]Also at Alfred-Wegener-Institute for Polar and Marine Research, Bremerhaven, Germany.

0148-0227/03/2002JD002376$09.00

tions for the pronounced increase in dust concentration in cold periods include changed atmospheric conditions [*Petit et al.*, 1981, 1990] and intensified sources [*Fuhrer et al.*, 1999]. Further specification of this general inference, however, remains difficult as the observed dust concentrations are a combined result of a number of entangled mechanisms ranging from dust mobilization in the source areas over uplift and long range transport to deposition onto the ice sheet. *Fuhrer et al.* [1999] discussed some of the relevant processes, but the fact that changes of source aridity, surface wind speed, uplift, transport, and deposition may all have varied jointly on similar timescales [*Porter and Zhisheng*, 1995; *Wang et al.*, 2001] makes it very difficult to assess their relative importance. As yet, only limited clarification can be expected from modeling approaches because current dust models, although having improved considerably, still are unable to reproduce accurately the change in dust concentration observed in polar ice cores and cannot confidently resolve the individual processes involved [*Andersen et al.*, 1998; *Mahowald et al.*, 1999; *Tegen and Rind*, 2000]. Also, models do not provide an adequate description of the mixing mechanisms in the lower atmospheric boundary layer over ice sheets which play an important role in dust deposition.

[4] Size distribution measurements on particles in polar ice cores have shown that the bulk of the particle volume can be described by a single lognormal distribution with a modal diameter around 1.5 to 2.0 μm [*Royer et al.*, 1983]. This mode is found to be fairly robust in remote regions worldwide [*Zdanowicz et al.*, 1998]. But small systematic shifts have been observed on various timescales in ice cores from Greenland as well as from Antarctica [e.g., *Steffensen*, 1997; *Delmonte et al.*, 2002]. As particle size distributions may be indicative of atmospheric transport times it may be possible to use this information to gain further insights into the past dust cycle. But size distribution measurements are scarce. So far they have been performed only in a discontinuous spot check manner using microscopy or the well established Coulter counting technique. For Greenland, *Steffensen* [1997] found a tendency towards larger modal diameters for colder climates, which are also associated with higher dust concentrations in ice cores.

[5] The interpretation of particle size measurements is not straightforward. Dry and wet removal during long range transport is generally size fractionating [*Junge*, 1977]; as well, in-cloud processing may occur [*Wurzler et al.*, 2000], and particles may be further size-fractionated on transfer from air to snow [*Unnerstad and Hansson*, 2001]. Quantification of these processes is difficult, and our current understanding about how different climatic situations may have influenced the particle size distribution is limited. Also, the forward modelling of particle size distributions is not very accurate. Dust modules for general circulation models (GCM) work with one or only few size classes (e.g. four classes covering the range from 1 to 100 μm [*Tegen and Fung*, 1994]) and cannot resolve fine shifts of the mode.

[6] So far, no continuous ice core record of particle size distribution covering the last glacial period has been published. Here we present a comprehensive particle profile from the North Greenland Ice Core Project (NGRIP) deep ice core, drilled at (75.1N, 42.3W) in central Greenland about 300 km north of the summit region. The record is from 1405 m to 2930 m depth and spans the period from ≈9.5 kyr to ≈100 kyr before present (bp), i.e. it includes the Pleistocene to Holocene transition and most of the last glacial period. The core was analyzed continuously for insoluble particle concentration and size distribution using a new laser based sensor coupled to a continuous flow system. To interpret the observed changes in particle size, we present a simple model picture that describes the modification of a particle size distribution during long range transport and deposition.

2. Methods

2.1. Measurements

[7] The measurement procedure and the laser based particle detector have already been described by *Ruth et al.* [2002] and therefore are only briefly outlined here. However, the particle size calibration will be covered in greater detail. The measurements took place in a warm laboratory (18°C) during the NGRIP-2000 field campaign. Continuous sections of ice core were melted in a controlled fashion along the core direction, and the melt water was passed through established continuous flow analysis (CFA) systems [e.g., *Röthlisberger et al.*, 2000; M. Bigler, dissertation in preparation, University of Berne] and to a particle counter. For decontamination purposes the abutting faces of the core sections were carefully cleaned using a stainless steel microtome blade. In addition, the melter had two concentric sections, and only the uncontaminated meltwater from the inner section was used for the analyses as described by *Röthlisberger et al.* [2000]. Peristaltic pumps and teflon tubings were used to feed the water into the detection units. Debubblers were used to eliminate air bubbles.

[8] In our measuring procedure the size distribution data were accumulated over 1.65 m intervals (corresponding to approximately 35–200 yr, see below), while the particle concentration also was recorded at an effective depth resolution of 1.0 cm [*Ruth et al.*, 2002]. Count rates were converted to concentrations using regular flow rate measurements. To avoid coincidence distortion of the particle counting the sample flow of glacial age ice was reduced to approximately 0.15 ml min^{-1}; however, to maintain an optimal flow rate of 1.5 ml min^{-1} through the detector the sample was added to prefiltered (0.2 μm) carrier water (dilution). Dilution was performed below 1494.9 m depth, i.e. for ice from the Younger Dryas period and older; in this case, the volume of ice core liquid consumed for each 1.65 m section was approximately 6 ml.

2.2. Size Calibration of the Particle Sensor

[9] The particle detection is based on laser light attenuation by single particles. The sample water is pumped through an illuminated detection cell, where each particle is detected as a negative peak of transmitted light. The peaks are counted and sorted by height into channels, that can be adjusted to appropriate size intervals. Twelve channels were used in this application.

[10] The interrelation of peak height and particle size is complex as both geometric shadowing and scattering processes are involved. Shadowing depends on geometric particle cross section, and therefore on a combination of

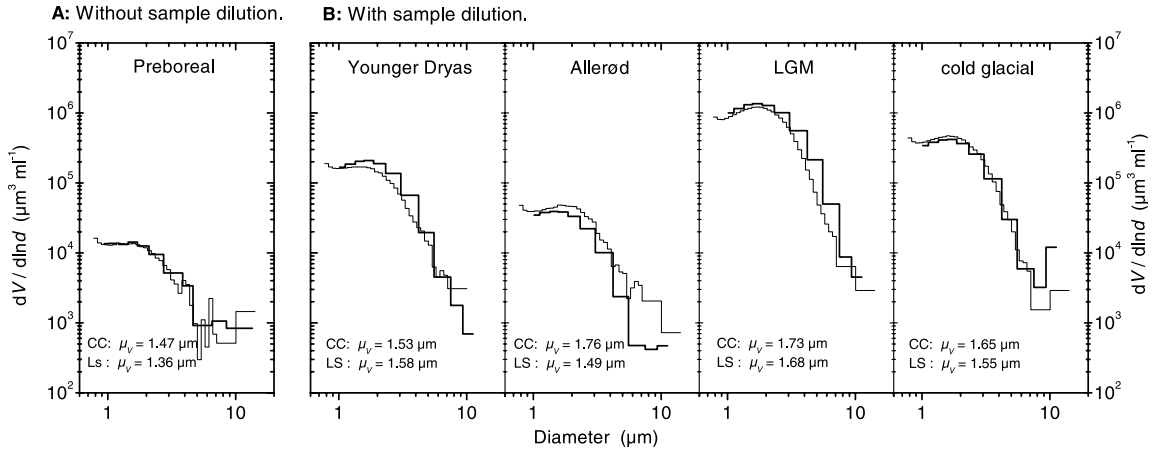

Figure 1. Size distributions by volume used for calibration. Coulter Counter (CC) data in thin lines, laser sensor (LS) data in bold lines. The laser sensor data is shown after the adjustment of its size axis. The rise at the left end of the Coulter Counter curves is due to noise as the lower size limit is reached. Listed is also the lognormal mode μ of the distributions as derived from CC and LS data. Calibration for measurements without sample dilution is based on the Preboreal sample (A); calibration for measurements with sample dilution is based on the other four samples (B).

particle volume, shape and orientation. Scattering in addition depends on optical particle properties and features nonlinearities between particle size and scattered light intensity. Only for particles larger than $\approx$7 µm diameter geometric shadowing dominates enough to allow a calibration with latex spheres of known diameter. In the remaining main part of the spectrum scattering becomes increasingly important, and a size calibration with latex spheres is inaccurate because dust particles have different scattering properties than latex spheres of identical volume, predominantly due to their nonspherical shape [*Saey*, 1998].

[11] Therefore, a size calibration was achieved indirectly through comparison with measurements obtained using a Coulter Counter, which measures the particle volume directly and independently of shape. At selected depths, NGRIP ice core samples were also measured with a Coulter Counter, and the laser sensor size axis was adjusted until the laser sensor and Coulter Counter data showed optimal correspondence. Samples from five different climatic periods (Preboreal Holocene, Younger Dryas (YD), Allerød, LGM, and pre-LGM cold glacial (CG)) were used for the calibration, thus the full concentration range was covered. Hereby the lower detection limit was recognized at 1.0 µm diameter, and proper sizing showed possible between 1.0 and 11 µm. The total particle concentrations agreed within approximately 5% to Coulter Counter measurements.

[12] During the calibration process it was discovered that the dilution setup had had a modifying influence on the size distribution, probably due to coagulation of particles in a mixing cell with turbulent flow. Therefore, the measurements of Preboreal Holocene ice (undiluted) and glacial age ice (diluted) were calibrated separately. Figure 1 shows the volume distribution spectra used for the two calibrations. The Preboreal sample was used to calibrate the measurements above 1494.9 m depth, that were done undiluted (A). For the calibration of the measurements below this depth the other four samples were used altogether for one separate calibration (B). After the adjustment of the laser sensor size axis, the data sets of the two counters show good accordance. Differences between the laser sensor and the Coulter Counter data may result from the fact that the Coulter Counter data covers only 0.55 m out of the 1.65 m long section measured with the laser sensor so that the underlying size distributions possibly indeed slightly differed in the respective samples. For calibration (B) the differences in the underlying sample populations may be expected to counterbalance each other as several samples could be used for one calibration.

2.3. Data Parametrization

[13] A lognormal function was used to parametrize the volume distribution data:

$$\frac{dV}{d\ln d} = \frac{V_0}{\sqrt{2\pi}\ln\sigma} e^{-\frac{1}{2}\left(\frac{\ln d - \ln\mu}{\ln\sigma}\right)^2},$$

where V_0 is the amplitude, μ the mode and σ the standard deviation of the distribution. Because the width of the size channels was quite large the fit procedure iteratively accounted for the modeled distribution within each channel. Furthermore, the relative quadratic error was minimized thus assigning equal weights to all channels. The first nine channels were considered for fitting, i.e. particles between 1.0 µm and 7.5 µm diameter.

[14] Other parameters are sometimes used to characterize a particle size distribution: The volume V_c of coarse particles ($d > d_c$) is used as well as the relative coarseness as V_c/V_{tot}; d_c was chosen as 7.5 µm in our study. The parameters 'mean volume diameter' (MVD) and 'mean number diameter' (MND) as e.g. used by *Zielinski* [1997] denote the mean diameter with respect to volume or number. These parameters highly depend on the covered size range and thus are intercomparable only for identically treated data sets. Furthermore, the MVD was found to be ambiguous in our data:

At high concentrations it tended to be in phase with changes of the mode μ and in antiphase with the relative coarseness (i.e. it depended on the size of small particles); yet at low concentrations it tended to be in antiphase with the mode and in phase with relative coarseness (i.e. it depended on the abundance of large particles). For these reasons, neither MND nor MVD are used in this study.

[15] Because a considerable portion of the mass is contributed by the small particles below the detection limit of approximately 1.0 μm, mass concentrations reported in this paper are derived as follows: For $d > \mu$ the total measured particle volume $V_m^{d>\mu}$ is taken by summation of all relevant channels or fractions thereof; for $d < \mu$ the volume is taken from the fitted lognormal distribution, i.e. $V_{tot} = V_m^{d>\mu} + 0.5 \cdot V_0$. Subsequently, the total mass concentration is inferred by assuming a material density of 2.6 g cm^{-3} [*Sugimae*, 1984].

2.4. Measurement Errors

[16] Occasionally, sections were affected from system malfunction and were excluded from further processing. A few sections showed a very high concentration of large particles possibly resulting from contamination and were also excluded. The measurement blank for small particles was below 15% of the count rate for most low concentration samples and was negligible in high concentration samples. For coarse particles ($d > 7.5$ μm) the blank relative to sample count rates was higher and more variable; since for these particles counting statistics also deteriorate, caution must be taken when interpreting the volume of the coarse fraction. The error on the total number concentration for all particles is predominantly due to flow rate uncertainties and is estimated to typically 5%–10%. The uncertainty of total volume or mass concentration as due to flow rate and size calibration uncertainties is estimated to be about 15%–20%.

[17] The exact determination of the particle sizes is hindered by the influence of the flow set up on the size distribution, which may not be constant and therefore not at all times be fully compensated for by the calibration. Further, the calibration is affected from the fact that the Coulter Counter data covers only part of the sample population measured with the laser sensor, which may explain the difference of about 0.1 μm between the fit parameter μ when derived from the Coulter Counter or the laser sensor data (see Figure 1). The difference in μ that result from using calibration A or B for any given sample was typically around 0.04 μm. The analytical uncertainty of the fit is variable and lies in the range from 0.01 μm to 0.1 μm diameter. We therefore estimate the possible error for μ to be generally around 0.1 μm diameter; it may be larger for the Holocene samples, where only one calibration sample exists and also the uncertainty of the fit is large. Double measurements on ice from the YD-Holocene transition, one time performed without and the other time with the dilution setup, yielded a discrepancy in μ of up to 0.1 μm, which supports the above estimates.

3. Results

3.1. Size Distributions

[18] Four individual volume size distributions are shown in Figure 2 for illustration. They are representative for different climatic periods, namely LGM (a), Stadial (S) S9 (b), Interstadial (IS) IS10 (c), and Preboreal Holocene (d). The samples span a concentration range of more than two orders of magnitude for particles smaller than 7.5 μm. For coarse particles larger than 7.5 μm the concentration range of the four samples is less than one order of magnitude and is not strictly correlated to the concentration of small particles.

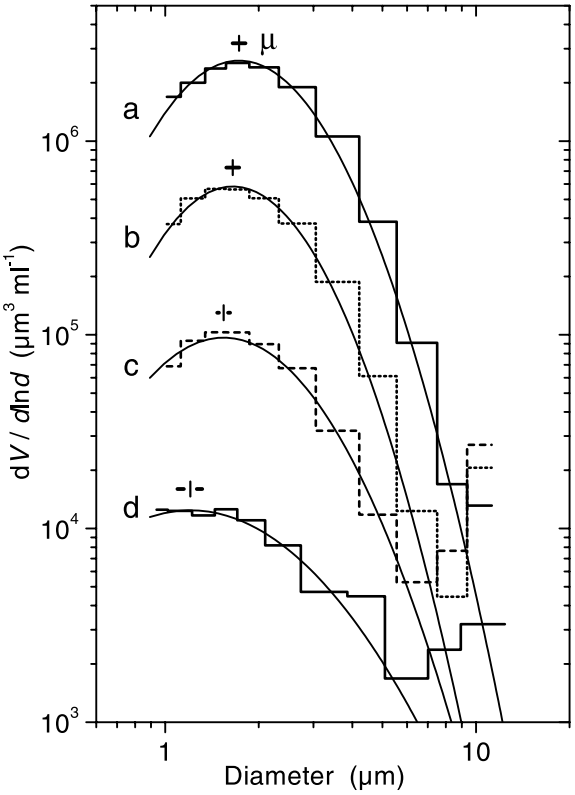

Figure 2. Individual size distributions by volume from different climatic periods along with lognormal fits. a: 1831.50–1833.15 m (LGM); b: 2075.70–2077.35 m (S9); c: 2121.90–2123.55 m (IS10); d: 1460.25–1461.90 m (Preboreal). Indicated is the position of the mode and the uncertainty of the fit [a: (1.73 ± 0.02) μm; b: (1.65 ± 0.06) μm; c: (1.54 ± 0.05) μm; d: (1.21 ± 0.11) μm].

[19] The respective lognormal fits are also shown in Figure 2, and the position and uncertainty of the mode μ are indicated. The fits describe the measured distributions very well for high concentration samples. For low concentration samples the description is still satisfactory, however deviations of the data from the ideal model distribution are larger. It may also be noticed that with higher concentrations the mode tends to get coarser whereas the width of the distribution tends to decrease.

3.2. Profiles

[20] Particle concentration and size distribution parameters of all samples are plotted as depth profiles in Figure 3. Shown are the insoluble particle number concentration C_N, mass concentration C_M, lognormal mode μ of the volume distribu-

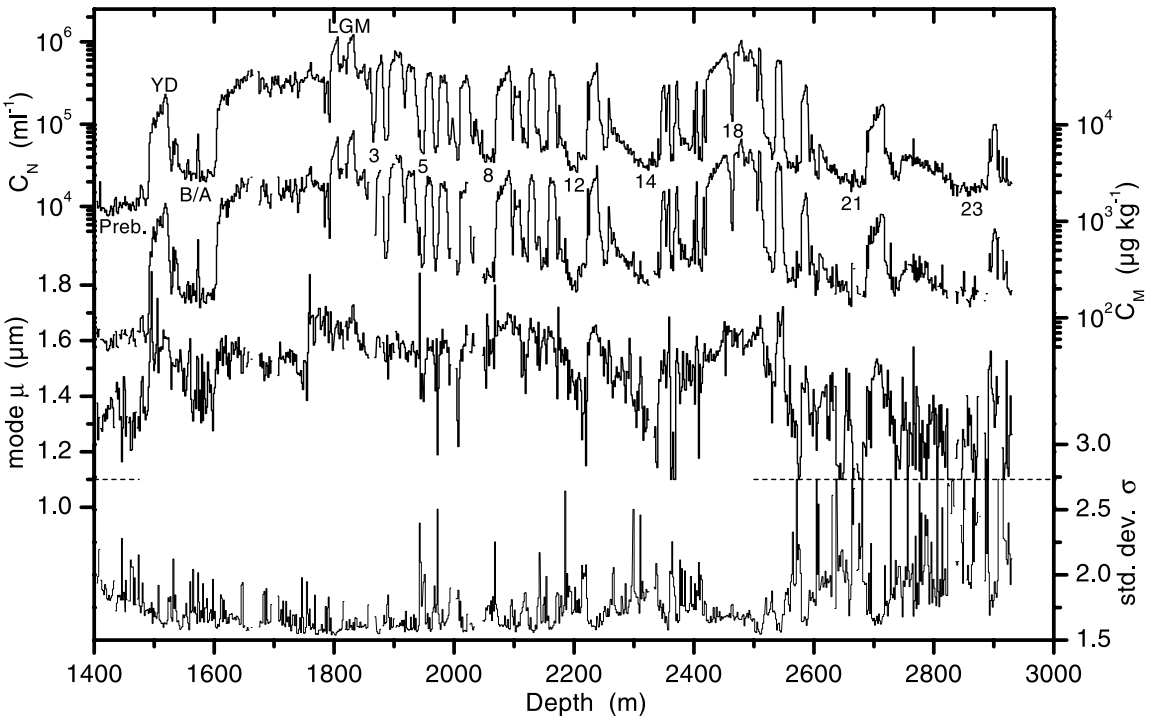

Figure 3. Profiles of microparticle concentration and lognormal size distribution parameters µ (diameter) and σ. Number concentration is based on counts of particles larger 1.0. Gaps arise either from missing data or from data that did not allow for a proper lognormal fit. Selected climatic periods are labeled: Preb = Preboreal Holocene, YD = Younger Dryas, B/A = Bølling/Allerød, LGM = Last Glacial Maximum; numbers refer to Dansgaard/Oeschger-events. The data of the bottom two panels was truncated at the dashed line indicated.

tion, and lognormal standard deviation σ. The concentration profiles clearly exhibit all climatic events known from the Greenlandic GRIP and GISP2 deep ice core records [*Johnsen et al.*, 1997; *Grootes and Stuiver*, 1997], some of which have been labeled in the figure. In particular, the stadial-interstadial fluctuations (or Dansgaard-Oeschger (D/O)-events) are clearly resolved. Periods of low particle concentrations correspond to warm phases while cold phases correspond to high particle concentrations. Concentrations are lowest during Preboreal Holocene ($C_N \approx 1 \cdot 10^4$ ml^{-1} or $C_M \approx 70$ µg kg^{-1}) and highest during LGM ($C_N \approx 1 \cdot 10^6$ ml^{-1} or $C_M \approx 8000$ µg kg^{-1}). This compares well to the reported particle mass concentrations from the GRIP core of 50 µg kg^{-1} and 8000 µg kg^{-1} for Preboreal and peak-LGM respectively [*Steffensen*, 1997]; discrepancies may be due to differences in the methods of measurement and data evaluation and need not be of geographical origin. The relative changes of the mass concentrations we observe across D/O-transitions range from a factor of 5 to 18 and are typically around 8.

[21] As expected, the overall appearance of the particle concentration profile closely resembles the continuous Ca^{2+} concentration profile from the GRIP core [*Fuhrer et al.*, 1999]. This means that the soluble and insoluble fractions of dust varied largely alike. However, systematic changes of the Ca^{2+}/particle ratio by a factor ≤ 2 have been observed [*Steffensen*, 1997; *Ruth et al.*, 2002].

[22] The close correspondence of the particle profile to the GRIP Ca^{2+} or $\delta^{18}O$ profiles permits to establish a provisional timescale for our NGRIP particle profile by matching respective climatic events and transferring the GRIP SS09 timescale [*Johnsen et al.*, 1997] to the NGRIP core. Thereby we infer that the time spanned by each 1.65 m section ranges from 35 to 200 years. We also infer that the concentration changes at D/O-transitions may have happened within 100 years or less.

[23] The mode µ of the particle size distribution shows considerable systematic variability throughout the record, and most major climatic events as identified from the concentration profiles are also visible in the size distribution. These are, in particular, the YD and B/A periods, and the most prominent D/O-events; but also smaller D/O-events or the LGM as a whole are identifiable in the profile. Typical values for µ in the Preboreal are around 1.3 µm diameter; and peak values exceed 1.7 µm during LGM. Typical values within the Pleistocene are around 1.6 µm during cold periods and may decrease to values around 1.4 µm or less during interstadial warm periods. A marked increase of the mode can be noticed between 2600 m and 2500 m depth, which corresponds to the transition from Marine Isotope Stage (MIS) 5 to MIS 4. Below this depth (i.e. during MIS 5) µ is generally about 0.2 µm smaller than above. During corresponding periods

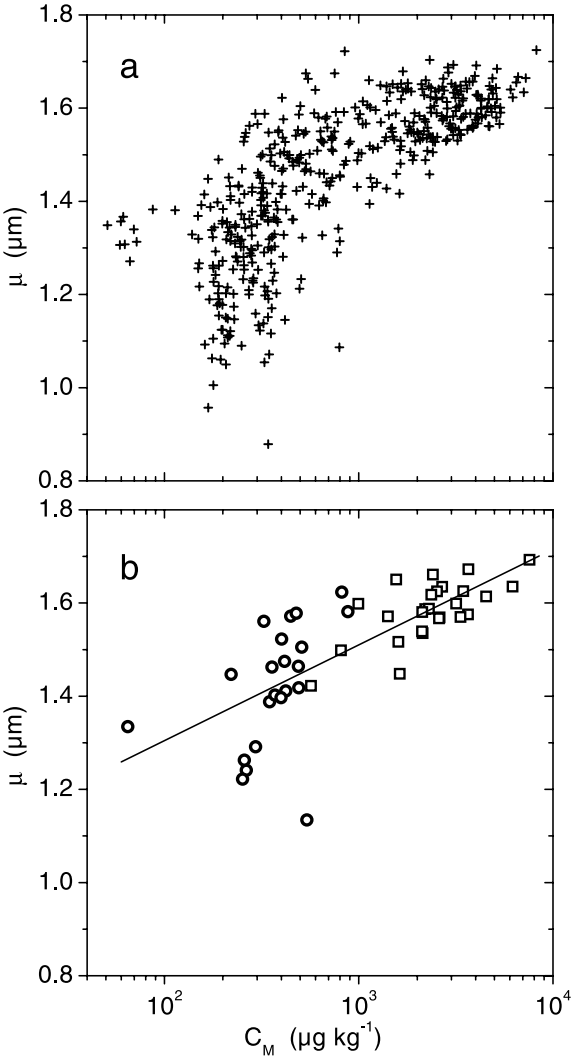

Figure 4. Correlation of the mode μ and the mass concentration C_M. a: All data has been averaged such that each data point represents 200 years. b: All data has been averaged over climatic periods; circles denote warm periods, squares denote cold periods. A logarithmic trend line is also shown.

we find modes that are smaller than those of *Steffensen* [1997] by 0.2 μm.

[24] The switching of the mode between states may happen as fast as the concentration changes, but it is not always as evident. Further, μ tends to be more variable (point-to-point variation) when dust concentrations are low. This higher variability persists even when the data are averaged over equally long time periods; so it is not a consequence from formal counting statistics nor from the fact that low concentration samples systematically cover shorter time spans.

[25] The lognormal standard deviation also shows systematic variations. It ranges from about 1.55 during LGM to more than 2 during the warm periods of MIS 5 (below 2550 m depth). This indicates that in warm climates the mode was more variable *within* the 35–200 year period covered by each 1.65 m section. At these times μ shows a large point-to-point variability, which suggests increased variability also on longer timescales, however only with marginal significance.

3.3. Systematic Changes of the Mode

[26] Figure 3 shows that the mode tends to increase with larger particle concentrations. A systematic plot of these two parameters is shown in Figure 4a, where data are averaged to 200 years resolution to reduce the point-to-point scatter for periods with higher layer thickness (and thus less time spanned by each sample). A clear positive correlation is exhibited. It also can be noted that the spread of the mode is smaller by a factor of 3 for high compared to low particle concentrations. Coarser modes and smaller spread for high concentration samples are also observed if the data are averaged over climatic periods (Figure 4b).

3.4. Detailed Profile Section

[27] A closer look at rapid transitions may bring further insights into the dust regime. Figure 5 shows the enlarged profile from IS 9 through IS 12 with size distribution parameters, particle concentration, and $\delta^{18}O$ (isotope data: personal communication from NGRIP-members, unpublished data). Cold periods very clearly show high particle concentrations and vice versa. Further, almost all high concentration periods are concurrent with large modes;

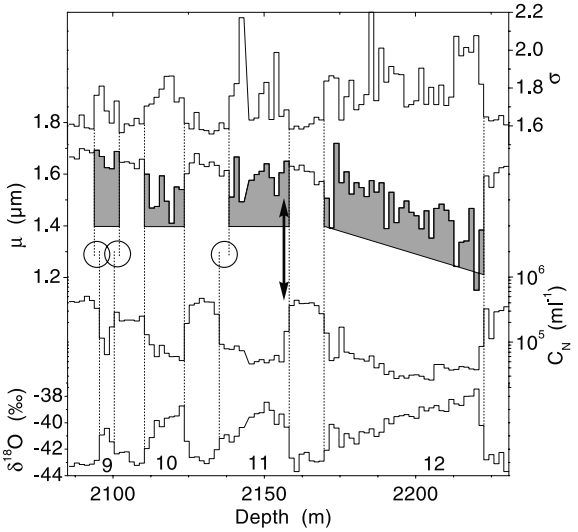

Figure 5. Detail from profiles showing various rapid D/O-transitions. Shown are size distribution parameters σ and μ, number concentration C_N, and $\delta^{18}O$ (data is personal communication from NGRIP-members). Shaded areas emphasize interstadials as inferred from the profiles of μ and σ. Circles mark instances where the timing of a transition may be inferred differently from μ and σ or respectively from V_N and $\delta^{18}O$. The arrow points to a transition where μ seemingly shows other timing than σ and C_N. Numbers in the bottom panel indicate interstadials.

however, not all periods with low concentrations are accompanied by smaller modes, and during low concentration periods the mode is more variable. This shows an independence of μ and V which is especially pronounced during warm periods.

[28] The fact that the mode is more variable during warm periods may cause confusion when determining the exact point of a transition. One such occasion at the beginning of IS 11 is marked in Figure 5 with an arrow. Here, the size distribution shifts synchronously with the concentration into the "warm"-state as can be seen from the profile of σ. However, its increased variability allows the mode to stay large for two more samples (corresponding to roughly 200 years). Only the increased values for σ show that the individual dust events contributing to the multiyear samples were already more variable with respect to particle size, as is typical for warm periods. Therefore, D/O-transitions seem to show more clearly in σ than in μ.

[29] Another observation is that there may indeed be a difference in the particular time when a transition occurs in the concentration and in the size distribution of particles (circles in Figure 5). No systematic leads or lags seem to occur, but shifts range up to ±200 years. This again shows some independence of the processes influencing the particle concentration or size distribution. The independence is observed especially during warm periods, and it vanishes if the data are averaged for several centuries.

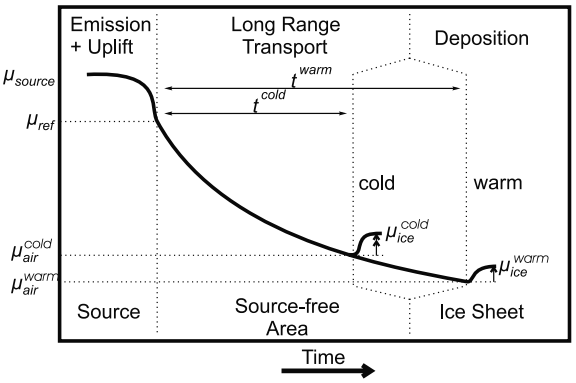

Figure 6. Conceptual illustration of the model picture. The airborne particle size distribution with mode μ_{source} at the source is changed rapidly during uplift until μ_{ref} is reached. Here, per definition, long range transport across source-free areas starts. During long range transport the mode decreases slowly owing to size fractionating depletion processes. Because the transit time t during cold climates is shorter than during warm climates the mode μ_{air} of airborne particles at the ice sheet is larger during cold climates. During deposition the mode is shifted slightly towards larger particles leading to μ_{ice}. Upper indices '*cold*' and '*warm*' denote cold and warm climatic states, respectively.

4. A Simple Model Picture

[30] The atmospheric dust cycle starts with the production of wind-erodible material in the source areas by weathering processes [*Pye*, 1987]. The amount of dust entrained into the atmosphere depends on the frequency and strength of surface winds [*Gillette et al.*, 1980], the mobility of the dust, and the size of the source areas. The geographical overlap of source regions and long range transport zones may be another important factor [*Chylek et al.*, 2001]. The transport of dust depends on long range atmospheric circulation patterns, which in turn are influenced by e.g. global heat distribution or the ice cover of land and ocean [*Krinner and Genthon*, 1998]. Transport efficiency depends on processes removing aerosol en route. Finally, air-to-snow transfer of dust depends on wet and dry deposition processes [*Davidson et al.*, 1996].

[31] From ice cores and from other paleoclimatic archives it has been inferred that atmospheric circulation during the last glacial period differed from present day's [e.g., *Janecek and Rea*, 1985; *Rea*, 1994; *Kapsner et al.*, 1995; *Lamy et al.*, 1999; *Lagroix and Banerjee*, 2002]; in particular, an increased westerly flow has been proposed for both the northern and the southern hemispheres. On the hypothesis that transit times control the size distribution, we will estimate in the following the degree to which transport needs to have been faster to explain the observed size changes of particles. First however, we will investigate the extent to which the observed changes may be due to changed deposition conditions during different climates. Hereby, our very simple approach clearly is far from capturing reality in its complexity; but at least the direction of the various effects and rough estimates of their magnitudes may be attained.

[32] For comparison of two climatic states in the following sections we use the upper index '*cold*' to denote a cold state and the upper index '*warm*' to denote a warm state. A conceptual illustration of our model picture sketched in Figure 6.

4.1. Size Fractionation During Deposition

[33] Particles are transferred from the air to the snow by dry and wet deposition [see, e.g., *Alley et al.*, 1995]. Wet deposition includes all precipitation related events and is described by an effective wet deposition velocity v_w. Dry deposition processes include all sinks not directly related to precipitation, i.e. mainly sedimentation, impaction, and snow drift scavenging, and are summarized as an effective total dry deposition velocity v_d. We consider only multiyear means (disregarding e.g. changed seasonality of precipitation [*Werner et al.*, 2000]) and assume that the precipitation rate equals the accumulation rate; then the deposition flux f may be expressed as $f = (v_w + v_d)\, c_{air} = (\varepsilon A + v_d)\, c_{air}$ with

ε: scavenging ratio, i.e. particle concentration in new snow divided by c_{air},
A: snow accumulation rate (in water equivalent), and
c_{air}: airborne particle concentration.

[34] As a first order approximation particle size fractionation by dry deposition may be described by $v_d = kd^n$ (d: particle diameter, k and n: constants), although for large particles v_d may be rate limited through insufficient vertical mixing. Wet deposition may be regarded as so efficient that at least for sufficiently high precipitation rates its size fractionating potential [*Junge*, 1977] is canceled; thus we assume ε independent from particle size. In this picture the size distribution is shifted towards larger particles by dry

deposition but not by wet deposition; consequently the degree of modification depends on the ratio of dry and wet deposition fluxes. Therefore, a change in the snow accumulation rate will change the archived particle size distribution [see also *Unnerstad and Hansson*, 2001].

[35] Assuming a unimodal, lognormal distribution defined by $\langle \mu_{air}, \sigma \rangle$, the size distribution of particles in the air will transform during deposition as $\langle \mu_{air}, \sigma \rangle \cdot (v_w + v_d)$. The mode μ_{ice} of the size distribution in the ice is found at the maximum of this product and is given by

$$\ln\left(\frac{\mu_{ice}}{\mu_{air}}\right) = n\sigma_g^2 \frac{v_d}{v_w + v_d} = n\sigma_g^2 \frac{k\mu_{ice}^n}{A\varepsilon + k\mu_{ice}^n}$$

where $\sigma_g = \ln \sigma$. The maximum shift in modal particle size occurs if only dry deposition is active. In that extreme case $\frac{\mu_{ice}}{\mu_{air}} = \exp(n\sigma_g^2)$; and with $n = 2$ (sedimentation) and $\sigma = 1.7$ a ratio of $\approx$1.7 is obtained.

[36] Because the accumulation rate varied under different past climates the particle size distribution shifts during deposition were also different. To calculate the size shift for two different accumulation rates we choose $\mu_{air} = 1.4$ μm and assume constant values for n ($n = 2$), σ ($\sigma = 1.7$), k ($k = 8.3 \cdot 10^7$ m^{-1}s^{-1} from *Fuchs* [1964]), and ε. The values vor ε are not well known, but $0.2 \cdot 10^6 \leq \varepsilon \leq 2.0 \cdot 10^6$ seems probable as *Davidson et al.*, [1996] find $\varepsilon = (0.65 \pm 0.31) \cdot 10^6$ for Ca^{2+} at Summit. For $A^{warm} = 0.2$ ma^{-1} and $A^{cold} = 0.5\ A^{warm}$, which reflects LGM vs. Preboreal accumulation changes [*Johnsen et al.*, 1997], we obtain a difference $\Delta = (\mu_{ice}^{cold} - \mu_{air}^{cold}) - (\mu_{ice}^{warm} - \mu_{air}^{warm})$ of $\Delta = 0.08$ μm for $\varepsilon = 0.2 \cdot 10^6$ and $\Delta = 0.01$ μm for $\varepsilon = 2.0 \cdot 10^6$, which typically is about 1/4 of the absolute shifts $\mu_{ice} - \mu_{air}$ in our calculations. Similar results are achieved if more realistic calculations of v_d are used [*Sehmel*, 1980].

[37] These calculated differences only account for roughly 3% to 20% of the observed change of μ of μ_{ice} of approximately 0.4 μm. We therefore conclude that the observed differences of μ during different climatic periods predominantly result from changed airborne size distributions over Greenland. This also holds true if typical coatings of soluble salts (e.g. $CaCO_3$) are assumed around the airborne particles.

4.2. Size Fractionation During Emission and Long-Range Transport

4.2.1. Emission

[38] Surface wind speed mainly influences the abundance of particles greater than 10 μm diameter but has little effect on the size distribution of particles that may be carried long distances [*Gillette et al.*, 1974; *D'Almeida and Schütz*, 1983]. Because we consider only particles smaller than 10 μm we therefore assume that the size distribution of airborne particles above the ground is independent from the source strength. The mode of this distribution be μ_{source}.

4.2.2. Long-Range Transport

[39] The change of particle concentration during long range transport can be described by the term $f \cdot e^{-t/\tau}$, with

- t: transit time between free troposphere at source and deposition onto the ice sheet
- τ: residence time governed by depletion processes en route, and
- f: correction factor in our one-dimensional approach to account for external mixing with particle free air (dilution).

We assume $\tau(d) = \frac{H}{\tilde{v}_w + \tilde{v}_d}$, where H denotes the mixing height, $\tilde{v}_w$ describes the depletion process en route due to wet depletion and $\tilde{v}_d$ due to dry depletion. Dry depletion again is assumed to be size fractionating according to $\tilde{v}_d = kd^n$, and $\tilde{v}_w$ again is assumed to be so efficient that its size fractionating effect is overridden.

[40] Following the motion of an air parcel $\langle \mu_0, \sigma \rangle$ transforms as $\langle \mu_0, \sigma \rangle \cdot f \cdot e^{-t\frac{\tilde{v}_w + \tilde{v}_d}{H}}$. The resulting distribution is not exactly lognormal; however, the new mode μ is characterized by:

$$\ln\left(\frac{\mu}{\mu_0}\right) = -n \cdot \sigma_g^2 \cdot \frac{t}{\tau} \frac{\tilde{v}_d}{\tilde{v}_w + \tilde{v}_d} \tag{1}$$

which reflects that μ decreases with time during transport. Simultaneously, the distribution gets narrower, i.e. σ_g also decreases. Consequently, the change of μ occurs more rapidly at the beginning, when σ_g is large.

[41] We now compare the size change during long range transport under a cold and warm climatic state starting from a common reference size distribution with the mode $\mu_{ref} = \mu_{ref}^{cold} = \mu_{ref}^{warm}$ in the free troposphere upon uplift. With the assumption of identical initial widths of distributions ($\sigma_g^{cold} = \sigma_g^{warm}$), dry deposition mechanisms ($n^{cold} = n^{warm}$), dry deposition strengths ($\tilde{v}_d^{cold} = \tilde{v}_d^{warm}$), and mixing heights ($H^{cold} = H^{warm}$) the ratio $\frac{\mu_{air}^{cold}}{\mu_{air}^{warm}}$ of the airborne modes at the ice sheet can be deduced from equation 1 as

$$\ln\left(\frac{\mu_{air}^{cold}}{\mu_{air}^{warm}}\right) = -\ln\left(\frac{\mu_{air}^{warm}}{\mu_{ref}^{warm}}\right)\left[1 - \frac{t^{cold}}{t^{warm}}\right] \tag{2}$$

thus linking $\mu_{air}^{cold}/\mu_{air}^{warm}$ with t^{cold}/t^{warm} (Figure 7). Since we have only limited knowledge about μ_{ref}, three different values have been applied for $\mu_{air}^{warm}/\mu_{ref}^{warm}$: All are based on $\mu_{air}^{warm} = 1.3$ μm, which is the average mode we observed for the Preboreal; based on data from *D'Almeida and Schütz* [1983] and *Wagenbach and Geis* [1989] μ_{ref}^{warm} has been taken as 2.5 μm, 3.2 μm and 4.0 μm respectively.

[42] In Figure 7 typical ratios of $\mu_{air}^{cold}/\mu_{air}^{warm}$ as based on our measurements have been marked for LGM vs. Preboreal and Stadial vs. Interstadial after a 10% correction for different deposition scenarios was made. With the assumption that differences in long range transport account for these size changes the implied ratio of transit times can be read from Figure 7. Our model suggests $t^{cold}/t^{warm} \approx 0.75$ for the LGM vs. Preboreal and $t^{cold}/t^{warm} \approx 0.9$ for the Stadial vs. Interstadial comparisons respectively. These reasonable values support the hypothesis that a variable transit time may indeed have caused the observed particle size changes.

4.3. Implications From Size Changes for Concentration Changes

[43] The estimated ratio of transit times t^{cold}/t^{warm} imposes limits on dust concentration change associated with changed long range transport. The concentration change

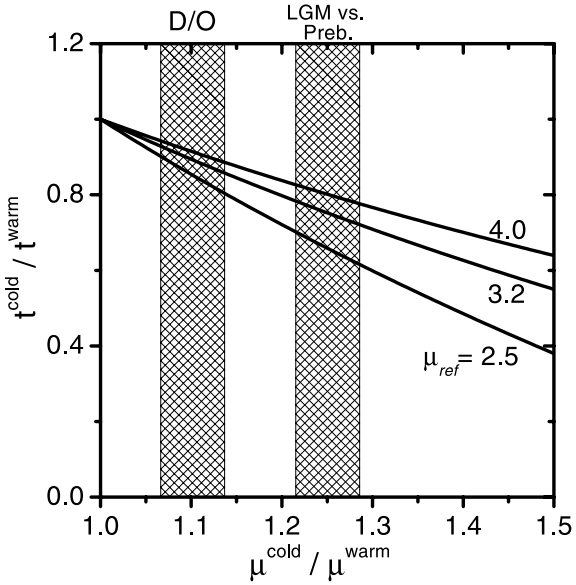

Figure 7. Implications from observed size changes μ^{cold}/μ^{warm} for the change in transit times t^{cold}/t^{warm}. Curves consider different scenarios for μ_{ref}. Shaded areas mark LGM vs. Preboreal and Stadial vs. Interstadial (D/O) changes, respectively.

resulting from varying long range transport between cold and warm periods may be assessed as $(\frac{C^{cold}}{C^{warm}}) = \frac{f^{cold}}{f^{warm}} \cdot \exp(\frac{t^{warm}}{\tau^{warm}}(1 - \frac{\tau^{warm}}{\tau^{cold}}\frac{t^{cold}}{t^{warm}}))$. To calculate C^{cold}/C^{warm} as a function of t^{cold}/t^{warm} a number of parameters must be estimated. For dilution with particle free air $f \sim 1/s$ is taken where s is the transversal width of the airborne dust plume. Assuming $s = \sqrt{D/t}$ and no change of eddy diffusion constants D yields $f^{cold}/f^{warm} = (t^{cold}/t^{warm})^{-1/2}$. The scaling factor t^{warm}/τ^{warm} can be estimated from equation 1 by taking $\frac{\mu}{\mu_0} = \frac{\mu_{air}^{warm}}{\mu_{ref.}^{warm}} \approx \frac{1.3\mu m}{3.2\mu m}$, $n = 2$ (sedimentation), $\sigma_g = \ln 1.7$, and by assuming $\tilde{v}_d \approx \tilde{v}_w$ during warm climates, which renders $\frac{t^{warm}}{\tau^{warm}} = 3.2$.

[44] In Figure 8 the resulting C^{cold}/C^{warm} is shown as a function of t^{cold}/t^{warm} for two different assumptions of τ^{warm}/τ^{cold}. First, $\tau^{warm}/\tau^{cold} = 1$ is taken for curve (A), i.e. C^{cold}/C^{warm} resulting from changed transit times only. For curve (B) the residence times were also varied, which is more realistic; to estimate τ^{warm}/τ^{cold} in this case it was assumed that $H^{cold} = H^{warm}$, and $\tilde{v}_d^{cold} = \tilde{v}_d^{warm}$; $\tilde{v}_w^{cold}/\tilde{v}_w^{warm}$ was interpolated between 1 (no change) and 0.5 (for LGM vs. Preboreal) to account for reduced wet depletion en route during LGM [*Andersen and Ditlevsen*, 1998]. This leads to $\tau^{Preb}/\tau^{LGM} = 0.75$ and gives values for C^{cold}/C^{warm} of ≈5 for LGM vs. Preboreal and ≈2 for a typical D/O transition.

[45] Compared to the observed concentration increases in our data of 100-fold from Preboreal to LGM it is evident even from our rough estimate that other processes must have contributed more effectively to the concentration increase than did changes of atmospheric circulation. These other processes may have included source strength intensification through an increased frequency of dust storms, higher surface wind speeds or increased source aridity, as these do not cause a change of the size distribution.

[46] The increase of airborne dust concentration due to higher wind speed and a reduced hydrological cycle during the LGM compared to present day has been calculated by *Andersen and Ditlevsen* [1998] as well as *Tegen and Rind* [2000]; their calculations suggest increases of 2-fold and 4-fold, respectively. The similarity of these values to our own estimates, which are based only on the observed size changes and a number of independent assumptions, supports the hypothesis that changes in transit times may have controlled the size distribution of microparticles in polar ice cores.

5. Comparison With Other Ice Core Records

[47] Much attention has been given to the question "whether particles were larger during Holocene or LGM". However, this unspecific formulation allows for several confusions. Firstly, the answer depends on the size parameter considered because various size parameters behaved differently. In our data set we find instances where, for example, the mode increases, absolute coarseness stays unchanged, relative coarseness decreases, and the mean volume diameter remains unchanged. Therefore, the size parameter considered must always be specified. Secondly, the stated question may be confused with the one "whether particles were larger in conjunction with high

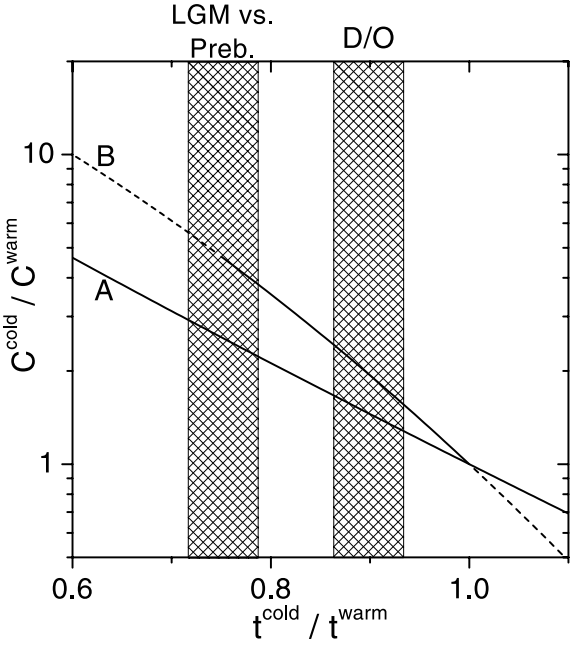

Figure 8. Proposed concentration change C^{cold}/C^{warm} as a function of changed transit time t^{cold}/t^{warm} for two scenarios of τ^{cold}/τ^{warm}. (A): no change of residence times; (B): reduction of wet removal during LGM as described in the text; extrapolations are dashed. Shaded areas mark probable values for t^{cold}/t^{warm} for LGM vs. Preboreal and D/O transitions as inferred from Figure 7.

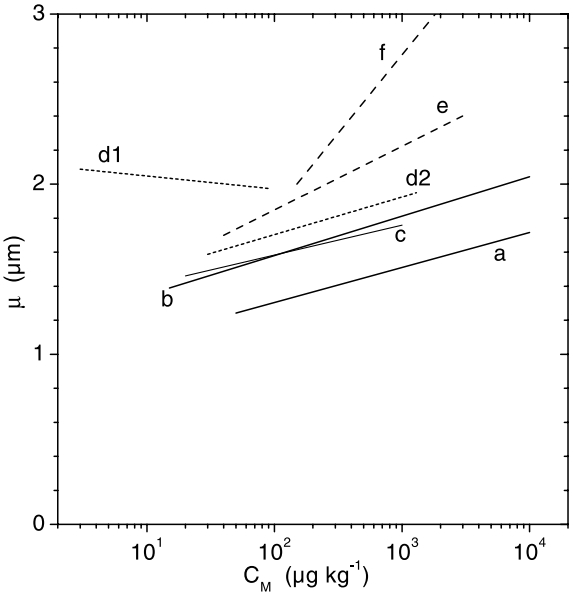

Figure 9. Correlation of C_M and μ in different ice cores from Greenland (solid lines) and from Antarctica (broken lines). a: NGRIP (this work); b: GRIP [*Steffensen*, 1997]; c: Dye3 [*Steffensen*, 1995]; d1: EPICA Dome-C, Holocene data until mid-transition (younger than ≈14.5 kyr bp) [*Delmonte et al.*, 2002]; d2: EPICA Dome-C, glacial age data starting mid-transition (older than ≈14.5 kyr bp) [*Delmonte et al.*, 2002]; e: Dome-C (Holocene and glacial samples) [*Petit et al.*, 1981]; f: Vostock (Holocene and glacial samples) [*De Angelis et al.*, 1984]. For (e) and (f) mass concentrations were inferred from the number concentrations reported using a conversion deduced from *Delmonte et al.* [2002].

or with low particle concentrations"; the necessity for this differentiation has become apparent at least for Antarctica from recent work (see below).

[48] Regarding the dependance of the mode on particle concentration, observations from the Greenlandic Dye3 [*Steffensen*, 1995] and GRIP [*Steffensen*, 1997] ice cores during the last glacial resemble each other closely with respect to both rate of increase as well as absolute level (see Figure 9). In the NGRIP core we find a similar rate of increase, but a lower absolute level, which may be due to methodical or unknown geographical differences. For Antarctica, in early size distribution measurements, *Petit et al.* [1981] and *De Angelis et al.* [1984] did not perform lognormal fits, but their examination of the data suggested increasing modes with increasing particle concentration (Figure 9). Both find this trend for glacial as well as for Holocene samples. However, new Antarctic data by *Delmonte et al.* [2002] contains increasing modes with increasing concentration only for glacial ice older than the Antarctic Cold Reversal (older than ≈14.5 kyr bp). Yet unexplained, the opposite behavior is clearly exhibited for ice younger than ≈14.5 kyr bp; and although particle modes increase with concentration in Pleistocene ice they are still larger during Holocene than during LGM, which may be an important clue for the understanding of past southern hemisphere climate. This probably had not been observed in the earlier Antarctic work [*Petit et al.*, 1981; *De Angelis et al.*, 1984] due to limited number and nonrepresentative selection of samples. For Greenland such a split behavior is not observed based on the very few Holocene measurements published [*Steffensen*, 1997; *Zdanowicz et al.*, 2000]. The larger absolute values of μ in Antarctica compared to Greenland may result from higher contribution of size fractionating dry deposition due to a lower accumulation rate at the Antarctic sites.

[49] Regarding the relative coarseness of particles in ice cores, a greater relative abundance of large particles concurrent with high concentrations had been reported for Antarctica [*Petit et al.*, 1981] but a smaller one for Greenland [*Steffensen*, 1997]. However, like *Steffensen* [1997], also *Delmonte et al.*, [2002] find fewer large particles during times of high concentrations. Since these new data have a higher resolution than those of *Petit et al.* [1981], the disagreement seems to be resolved. Also we find relatively less large particles at high concentrations, so that it seems evident that relative coarseness changed similarly in Greenland and Antarctica. Although findings for Greenland and Antarctica are in accordance at least during the glacial epoch the atmospheric systems transporting dust to the polar ice sheets may have behaved very differently in the northern and southern hemispheres; whereas in Antarctica the abundance of large particles clearly must be driven by atmospheric transport, in Greenland also other causes such as varying contributions of proximal sources or of biological particles may be important.

6. Conclusions

[50] A laser microparticle detector was used for very efficient counting and sizing of windblown dust particles in the NGRIP ice core. A more than 1500 m long continuous profile of particle concentration and size distribution is provided spanning the period approximately from 9.5–100 kyr bp. The laser sensor was easy to handle and proved suitable for field usage. It was possible to calibrate the laser sensor for proper sizing of windblown dust particles. In future usage the flow system between melter and sensor should be as short as possible and kept unchanged throughout the measurements. Calibrations may be achieved indirectly by forced agreement to Coulter counter measurements but should be based on multiple, identical samples from different climatic periods, and should be verified.

[51] We find particle concentrations higher by a factor of 100 during LGM than during the Preboreal and concentration changes by typically a factor of 8 at the sharp transitions of D/O-events. The mode μ of the lognormal size distribution varies systematically with a tendency towards smaller particles during warmer climates. During warmer climates the variability of the mode is higher, and the standard deviation σ also increases. The latter may be due to increased variability of the size distributions in events contributing particles for each multiyear sample.

[52] We base our interpretation of the particle size distribution on a highly simplified, but quantitative model of atmospheric transport and deposition of dust. From this we

suggest the mode of the distribution as indicating atmospheric transit times during transport from the source to the ice sheet. Larger modes may indicate shorter transit times, which may result from higher advection velocities and/or shorter transport routes, i.e. changed atmospheric circulation patterns. Both may be related to changes in the position of the Polar Front. From our data we estimate a ≈25% shorter transit time during LGM than during the Preboreal. We infer that circulation changes alone cannot account for the observed particle concentration increase by a factor of 100. Therefore, other processes such as source intensification might predominately have caused this increase. The synchronism of respective changes in the source areas with changes of large scale atmospheric circulation patterns suggests strong mediating mechanisms.

[53] During warm periods a tendency towards longer transit times is inferred; and transit times were much more variable during these periods. Conversely, atmospheric circulation appears to have been more stable when providing faster transport during cold climates. This may reveal the variability of the Polar Front with respect to the source areas: During cold periods the Polar Front may have always been located far enough south to provide fast transport from the East Asian source areas to Greenland. During warmer periods, the Polar Front may have been located generally further north but was subject to occasional southward excursions.

[54] The variability of transit times during warm periods is - on timescales of up to several 100 years - not connected to concentration changes, which may be controlled by variable source strength. This possible independence between dust production processes and long range transport times may also be evident from occasional timing differences of particle concentration and size distribution parameters at rapid climatic transitions. This supports our notion that source processes by themselves do not influence the size distribution of particles carried to Greenland. It further suggests that source processes and long range transport are two independent results from environmental forcings.

[55] Clearly, the interpretation of particle size distributions in ice cores is limited through inadequate understanding of size fractionating processes. More accurate model calculations for long range transport and particle deposition are needed to check our findings and to draw more differentiated conclusions from the size distribution data. Particle size distribution measurements at high depth resolution may assist the understanding of rapid climate transitions during the last glacial period. Furthermore, closer investigation of size distributions in Greenland during the Holocene are desirable for a comparison to the newest Antarctic results. As insights on variability, timing and the systematics of changes are benefits from continuous measurements, these should always be preferred over discontinuous measurements.

[56] **Acknowledgments.** The North-GRIP project is directed and organized by the Department of Geophysics at the Niels Bohr Institute for Astronomy, Physics and Geophysics, University of Copenhagen. It is being supported by funding agencies in Denmark(SNF), Belgium (NFSR), France (IFRTP and INSU/CNRS), Germany (AWI), Iceland (RannIs), Japan (MECS), Sweden (SPRS), Switzerland (SNF) and the United States of America (NSF). We wish to thank all the funding bodies and field participants. Regine Röthlisberger is acknowledged for her exceptional dedication in running the CFA-lab in the field. Two anonymous reviewers, Hubertus Fischer and John Robbins are thanked for their helpful comments to the manuscript.

References

Alley, R., R. Finkel, K. Nishuzumi, S. Anandakrishnan, C. A. Shuman, G. Mershon, G. A. Zielinski, and P. A. Mayewski, Changes in continental and sea-salt atmospheric loadings in central greenland during the most recent deglaciation: Model-based estimates, *J. Glaciol.*, *41*, 503–514, 1995.

Andersen, K. K., and P. D. Ditlevsen, Glacial-interglacial variations of meridional transport and washout of dust: A one-dimensional model, *J. Geophys. Res.*, *103*(D8), 8955–8962, 1998.

Andersen, K. K., A. Armengaud, and C. Genthon, Atmospheric dust under glacial and interglacial conditions, *Geophys. Res. Lett.*, *25*(13), 2281–2284, 1998.

Biscaye, P. E., F. E. Grousset, M. Revel, S. Van der Gaast, G. A. Zielinski, A. Vaars, and G. Kukla, Asian provencance of glacial dust (stage 2) in the Greenland Ice Sheet Project 2 ice core, Summit, Greenland, *J. Geophys. Res.*, *102*(C12), 26,765–26,781, 1997.

Bory, A. J.-M., A. Biscaye, A. Svensson, and F. E. Grousset, Seasonal variability in the origin of recent atmospheric mineral dust at NorthGRIP, Greenland, *Earth Planet. Sci. Lett.*, *196*, 123–134, 2002.

Chylek, P., G. Lesins, and U. Lohmann, Enhancement of dust source area during past glacial periods due to changes of the Hadley circulation, *J. Geophys. Res.*, *106*(D16), 18,477–18,485, 2001.

D'Almeida, G. A., and L. Schütz, Number, mass and volume distributions of mineral aerosol and soils of the Sahara, *J. Clim. Appl. Meteorol.*, *22*, 233–243, 1983.

Davidson, C. I., M. H. Bergin, and H. D. Kuhns, The deposition of particles and gases to ice sheets, in *Chemical Exchange Between the Atmosphere and Polar Snow*, edited by E. W. Wolff and R. C. Beales, pp. 275–306, Springer-Verlag, New York, 1996.

De Angelis, M., M. Legrand, J. R. Petit, N. I. Barkov, Y. S. Korotkevitch, and V. M. Kotlyakov, Soluble and insoluble impurities along the 950 m deep Vostok ice core (Antarctica)–Climatic implications, *J. Atmos. Chem.*, *1*, 215–239, 1984.

Delmonte, B., J. R. Petit, and V. Maggi, Glacial to Holocene implications of the new 27,000-year dust record from the EPICA Dome C (East Antarctica) ice core, *Clim. Dyn.*, *18*(8), 647–660, 2002.

Fuchs, N. A., *The Mechanics of Aerosols*, Pergamon, New York, 1964.

Fuhrer, K., E. W. Wolff, and S. J. Johnsen, Timescales for dust variability in the Greenland Ice Core Projct (GRIP) ice core in the last 100,000 years, *J. Geophys. Res.*, *104*(D24), 31,043–31,052, 1999.

Gillette, D. A., I. H. J. Blifford, and D. W. Fryrear, The influence of wind velocity on the size distributions of aerosols generated by the wind erosion of soils, *J. Geophys. Res.*, *79*(D27), 4068–4075, 1974.

Gillette, D. A., J. Adams, A. Endo, and D. Smith, Threshold velocities for input of soil particles into the air by desert soils, *J. Geophys. Res.*, *85*(C10), 5621–5630, 1980.

Grootes, P. M., and M. Stuiver, Oxygen 18/16 variability in Greenland snow and ice with 10-3- to 10-5- year time resolution, *J. Geophys. Res.*, *102*(C12), 26,455–26,470, 1997.

Hansson, M. E., The Renland ice core: A nothern hemisphere record of aerosol composition over 120,000 years, *Tellus, Ser. B*, *46*, 390–418, 1994.

Janecek, T. R., and D. K. Rea, Quaternary fluctuations in the northern hemisphere trade winds and westerlies, *Quat. Res.*, *24*, 150–163, 1985.

Johnsen, S. J., et al., The $\delta^{18}O$ record along the Greenland Ice Core Project deep ice core and the problem of possible Eemian climatic instability, *J. Geophys. Res.*, *102*(C12), 26,397–26,410, 1997.

Junge, C. E., Processes responsible for the trace content in precipitation, in *Isotopes and Impurities in Ice and Snow*, *IAHS-AISH Publ. 118*, Int. Assoc. Hydrol. Sci., Grenoble, 1977.

Kahl, J. D. W., D. A. Martinez, H. Kuhns, C. I. Davidson, J.-L. Jaffrezo, and J. M. Harris, Air mass trajectories to Summit, Greenland: A 44-year climatology and some episodic events, *J. Geophys. Res.*, *102*(C12), 26,861–26,875, 1997.

Kapsner, W. R., R. B. Alley, C. A. Shuman, S. Anandakrishnan, and P. M. Grootes, Dominant influence of atmospheric circulation on snow accumulation in Greenland over the past 18,000 years, *Nature*, *373*, 52–54, 1995.

Krinner, G., and C. Genthon, GCM simulations of the Last Glacial Maximum surface climate of Greenland and Antarctica, *Clim. Dyn.*, *14*, 741–758, 1998.

Lagroix, F., and S. K. Banerjee, Paleowind directions from the magnetic fabric of loess profiles in central Alaska, *Earth Planet. Sci. Lett.*, *195*, 99–112, 2002.

Lamy, F., D. Hebbeln, and G. Wefer, High-resolution marine records of climatic change in mid-latitude Chile during the last 28,000 years based on terrigenous sediment parameters, *Quat. Res.*, *51*, 83–93, 1999.

Mahowald, N., K. Kohfeld, M. Hansson, Y. Balkanski, S. P. Harrison, I. C. Prentice, M. Schulz, and H. Rodhe, Dust sources and deposition during the last glacial maximum and current climate: A comparison of model results with paleodata from ice cores and marine sediments, *J. Geophys. Res.*, *104*(D13), 15,895–15,916, 1999.

Mayewski, P. A., et al., Changes in atmospheric circulation and ocean ice cover over the North Atlantic during the last 41,000 years, *Science*, *263*, 1747–1751, 1994.

Petit, J.-R., M. Briat, and A. Royer, Ice age aerosol content from East Antarctic ice core samples and past wind strength, *Nature*, *293*, 391–394, 1981.

Petit, J. R., L. Mounier, J. Jouzel, Y. S. Korotkevich, V. I. Kotlyakov, and C. Lorius, Palaeoclimatological and chronological implications of the Vostok core dust record, *Nature*, *343*, 56–58, 1990.

Porter, S. C., and A. Zhisheng, Correlation between climate events in the North Atlantic and China during the last glaciation, *Nature*, *375*, 305–308, 1995.

Pye, K., *Aeolian Dust and Dust Deposits*, Academic, San Diego, Calif., 1987.

Rea, D. K., The paleoclimatic record provided by Aeolian deposition in the deep sea: The geologic history of wind, *Rev. Geophys.*, *32*(2), 159–195, 1994.

Röthlisberger, R., M. Bigler, A. Hutterli, S. Sommer, B. Stauffer, H. G. Junghans, and D. Wagenbach, Technique for continious high-resolution analysis of trace substances in firn and ice cores, *Environ. Sci. Technol.*, *34*, 338–342, 2000.

Royer, A., M. De Angelis, and J. R. Petit, A 30,000 year record of physical and optical properties of microparticles from an East Antarctic ice core and implications for paleoclimate reconstruction models, *Clim. Change*, *4*, 381–412, 1983.

Ruth, U., D. Wagenbach, M. Bigler, J. P. Steffensen, and R. Röthlisberger, High resolution dust profiles at NGRIP: Case studies of the calcium-dust relationship, *Ann. Glaciol.*, *35*, in press, 2002.

Saey, P., Concentration and size distribution of microparticles in Alpine and polar ice cores (in German), M.Sc. thesis, Univ. of Heidelberg, Heidelberg, Germany, 1998.

Sehmel, G. A., Particle and gas dry deposition: A review, *Atmos. Environ.*, *14*, 983–1011, 1980.

Steffensen, J. P., Microparticles and chemical impurities in ice cores from Dye 3, South Greenland and their interpretation in palaeoclimatic reconstructions, Ph.D. thesis, Univ. of Copenhagen, Copenhagen, 1995.

Steffensen, J. P., The size distribution of microparticles from selected segments of the Greenland Ice Core Project ice core representing different climatic periods, *J. Geophys. Res.*, *102*(C12), 26,755–26,763, 1997.

Sugimae, A., Elemental constituents of atmospheric particulates and particle density, *Nature*, *307*, 145–147, 1984.

Svensson, A., P. E. Biscaye, and F. E. Grousset, Characterization of late glacial continental dust in the Greenland Ice Core Project ice core, *J. Geophys. Res.*, *105*(D24), 4637–4656, 2000.

Tegen, I., and I. Fung, Modeling of mineral dust in the atmosphere: Sources, transport, and optical thickness, *J. Geophys. Res.*, *99*(D11), 22,897–22,914, 1994.

Tegen, I., and D. Rind, Influence of the latitudinal temperature gradient on soil dust concentration and deposition in Greenland, *J. Geophys. Res.*, *105*(D6), 7199–7212, 2000.

Thompson, L. G., Variations in microparticle concentration, size distribution, size distribution and elemental composition found in Camp Century, Greenland, and Byrd Station, Antarctica, deep ice cores, in *Isotopes and Impurities in Snow and Ice*, *IAHS-AISH Publ. 118*, pp. 351–363, Int. Assoc. Hydrol. Sci., Grenoble, 1977.

Unnerstad, L., and M. Hansson, Simulated airborne particle size distributions over Greenland during Last Glacial Maximum, *Geophys. Res. Lett.*, *28*(2), 287–290, 2001.

Wagenbach, D., and K. Geis, The mineral dust record in a high altitude Alpine glacier (Colle Gnifetti, Swiss Alps), in *Paleoclimatology and Paleometeorology: Modern and Past Patterns of Global Atmospheric Transprot*, edited by M. Leinen and M. Sarnthein, pp. 543–564, Kluwer Acad., Norwell, Mass., 1989.

Wang, Y. J., H. Cheng, R. L. Edwards, Z. S. An, J. Y. Wu, C.-C. Shen, and J. A. D'Orale, A high-resolution absolute-dated late pleistocene Monsoon record from Hulu cave, China, *Science*, *294*, 2345–2348, 2001.

Werner, M., U. Mikolajewicz, M. Heimann, and G. Hoffmann, Borehole versus isotope temperatures on Greenland: Seasonality does matter, *Geophys. Res. Lett.*, *27*(5), 723–726, 2000.

Wurzler, S., T. G. Reisin, and Z. Levin, Modification of mineral dust particles by cloud processing and subsequent effects on drop size distributions, *J. Geophys. Res.*, *105*(D4), 4501–4512, 2000.

Zdanowicz, C. M., G. A. Zielinski, and C. P. Wake, Characteristics of modern atmospheric dust deposition in snow on the Penny ice cap, Baffin Island, Arctic Canada, *Tellus, Ser. B*, *50*, 506–520, 1998.

Zdanowicz, C. M., G. A. Zielinski, and C. P. Wake, A holocene record of atmospheric dust deposition on the Penny ice cap, Baffin Island, Canada, *Quat. Res.*, *53*, 62–69, 2000.

Zielinski, G. A., Paleoenvironmental implications of the insoluble microparticle record in the GISP2 (Greenland) ice core during the rapidly changing climate of the Pleistocene-Holocene transition, *Geol. Soc. Am. Bull.*, *109*(5), 547–559, 1997.

M. Bigler, Department of Climate and Environmental Physics, University of Bern, CH-3012 Bern, Switzerland.

U. Ruth and D. Wagenbach, Institute of Environmental Physics, University of Heidelberg, 69120 Heidelberg, Germany. (urs.ruth@urz.uni-heidelberg.de)

J. Steffensen, Department of Geophysics, University of Copenhagen, DK-2100 Copenhagen, Denmark.

2.6 High resolution microparticle profiles at NGRIP: Case studies of the calcium-dust relationship

Urs Ruth, Dietmar Wagenbach, Matthias Bigler,
Jørgen Peder Steffensen, Regine Röthlisberger

Annals of Glaciology
35, 237–242, 2002

Annals of Glaciology 35 – Paper 35A042 – Ruth and others

High resolution microparticle profiles at NGRIP: case studies of the calcium - dust relationship

Urs Ruth[1,2], Dietmar Wagenbach[1], Matthias Bigler[3], Jørgen P. Steffensen[4], Regine Röthlisberger[3], and Heinz Miller[2]

[1]Institut für Umweltphysik, University of Heidelberg, Germany
[2]Alfred Wegener Institut für Polar- und Meeresforschung, Bremerhaven, Germany
[3]Climate and Environmental Physics, University of Bern, Switzerland
[4]Department of Geophysics, University of Copenhagen, Denmark

ABSTRACT

A novel flow-through microparticle detector was deployed concurrently with continuous flow analyses of major ions during the NGRIP 2000 field season. The easy handling detector performs continuous counting and sizing. In this deployment the lower size detection limit was conservatively set to 1.0 μm equivalent spherical particle diameter, and a depth resolution of ≤ 1 cm was achieved for microparticle concentrations. The dust concentration usually followed the Ca^{2+} variability. Here results are presented from an inspection of the Ca/dust mass ratio in 23 selected intervals, 1.65m long each, covering different climatic periods including Holocene and last glacial maximum (LGM). A (Ca^{2+})/(insoluble dust) mass ratio of 0.29 was found for Holocene and 0.11 for LGM. Changes of the Ca/dust ratio also occur on an annual to multi-annual time scale exhibiting the same pattern, i.e. a lower Ca/dust ratio for higher crustal concentrations. Moreover, the Ca^{2+}/dust ratio may increase significantly during episodic events such as volcanic horizons due to enhanced dissolution of $CaCO_3$. This questions the notion of deploying Ca2+ as a quantitative mineral dust reference species and stresses the importance of variable source properties or fractionating processes during transport and deposition.

INTRODUCTION

The atmospheric mineral dust load, mainly composed of insoluble mineral particles, is an important part of Earth's climatic system as it is involved in direct and indirect radiative forcing processes (e.g. Tegen and Fung, 1994). Equally, the amount, size distribution and composition of dust deposited on polar ice sheets may hold valuable information about both, positions and climatic conditions of source areas, as well as about long range transport and deposition processes (Biscaye and others, 1997; Fuhrer and others, 1999). Over the last climatic cycle, Greenland as well as Antarctic mineral dust records exhibit changes on a huge dynamic range (e.g. Hansson, 1994; Steffensen, 1997; Petit and others, 1999). In Greenland these changes occurred very rapidly and were coinciding with changes in $\delta^{18}O$ at rapid climatic transitions within the last Pleistocene as has been inferred from high resolution measurements of Ca^{2+} and ECM on the GRIP and GISP2 ice cores (Taylor and others, 1997; Fuhrer and others, 1999).

The concentration of Ca ions (Ca^{2+}) is often being used as a proxy parameter for total mineral dust in ice cores as it represents the major part of the readily dissolved fraction of the dust aerosol. But the soluble proportion of dust is not constant over different climatic periods (Steffensen, 1997), so using Ca^{2+} as a proxy may give a distorted view of the total dust concentration. However, also dust measurement techniques have specific disadvantages. Only low resolution profiles or selected continuous sections have been measured for insoluble microparticles using the well established Coulter counting technique (e.g. Steffensen, 1997) because it requires extensive sample preparation and handling. And high resolution continuous dust measurements using 90° laser light scattering off melt water (Hammer and others, 1985) or off ice (Ram and Koenig, 1997) yield no size distribution information or are difficult to calibrate.

Here we introduce a novel laser sensor device for microparticle measurements deployed for continuous recordings of microparticle

concentration and size distribution during the North Greenland Ice Core Project (NGRIP) 2000 field season. Apart from the methodical aspects, we present and discuss case studies of the dust concentration focussing on the Ca^{2+}/dust ratio under inconspicuous conditions as well as in volcanic horizons.

EXPERIMENTAL SETUP

During the NGRIP 2000 field season, extensive scientific processing was performed shortly after retrieval of the ice core. This included the operation of a warm laboratory for continuous flow analyses (CFA) of Ca^{2+}, Na^{+}, NH_4^{+}, SO_4^{2-}, NO_3^{-}, H_2O_2 and HCHO concentrations, and of electrolytical conductivity (Röthlisberger and others, 2000). Concurrently, continuous microparticle counting and sizing was performed. Discrete liquid samples were collected at 55 cm resolution for subsequent ion chromatography (IC) analysis; and over selected depths, discrete samples for IC and acidity measurements at approx. 6 cm resolution were also collected by an automatic sampler. The contamination free sample water for all these analyses was drawn from the inner area of a melt head, where the ice was melted at approx. 4 cm min^{-1}. For an overview of the setup see Figure 1. By these means the core was continuously analyzed from approx. 1400 m to 2930 m depth.

The particle sensor

The particle sensor, for general purpose laboratory applications, is from Klotz GmbH, Bad Liebenzell, Germany, and was specifically modified in collaboration with the Institut for Environmental Physics of the University of Heidelberg (Saey, 1998; Armbruster, 2000). The sample water is pumped through the detection cell, where it is illuminated by a 1.5 µm by 250 µm wide laser light beam of 670 nm wavelength. The transmitted light is measured by a photo diode detector (see Figure 2). When a particle passes through the detection area the transmitted light is attenuated by shadowing and scattering which results in a negative peak of transmitted light. The peak is counted and sorted by height into 32 bins, that can be adjusted to appropriate size intervalls.

The inter-relation of peak height and particle size is complex. Geometric shadowing is combined with scattering processes, both depending not only on particle volume but also on particle shape, material and orientation. A size calibration was achieved by measuring NGRIP ice core samples from different climatic periods with a Coulter counter and tying the laser sensor measurements of identical depths to the Coulter counter spectra. The calibration measurements showed the particle detection limit to be approx. 0.8 µm of spherical equivalent particle diameter. For our measurements, we used 1.0 µm diameter as the lower detection limit to be safely above the level of detector noise.

In our measuring procedure, size distributions were averaged over 1.65 m intervals. Respective results including size calibration will be presented elsewhere (Ruth, in preparation). The bulk particle number concentration was obtained continuously. To do so, the momentary count rate, converted to an analogue output signal, was recorded and the flow rate regularly measured. The continuously recorded data was later reduced to 1 mm depth intervals. Dust mass concentrations were inferred by integrating the particle size distributions that were obtained for each 1.65 m section and a material density of 2.7 g cm^{-3}; on average, this yielded that 1000 count ml^{-1} are equivalent to 5.6 µg kg^{-1}. For each section, the relative error of particle mass is about 15% due to size calibration uncertainties and varying pump rates.

To avoid coincidence distortion of the measurements the output signal is cut off by the counter electronics if the counting rate exceeds 4000 particles s^{-1}, so the sample flow needs to be decreased for high particle concentrations. However, as flow rates below 1 ml min^{-1} increase the sample dispersion in the flow system, the sample water from glacial age ice, which has a considerably higher dust concentration, was diluted with 0.2 µm prefiltered carrier water. Hereby an effective sample flow of approx. 0.15 ml min^{-1} could be established while keeping the flow through the sensor above 2 ml min^{-1}. The dilution setup allowed for measuring concentrations lower than 15 µg kg^{-1} and in excess of 15,000 µg kg^{-1}, thus, covering the full

dynamic range from Holocene to last glacial maximum (LGM). When used without the dilution system, the detection limit in terms of minimal count rate was about 200 particles ml^{-1}; this value however is dependent on the flow rate.

As used in our setup, the depth resolution of the microparticle measurement – expressed as the observed 1/e-depth of a step signal – is ≤ 1 cm. It is generally similar to the depth resolution of most other CFA-components, often slightly better. Apart from the melt rate, the depth resolution is limited by the conical surface of the melt head, by dead volumes and by longitudinal sample dispersion in the flow system. The impairment in depth resolution from using the dilution system was around 10%. In ice with low particle concentration, the counting statistics also impose a limit on the depth resolution by raising the error of a data point if the number of counts for this data point is low, thus, demanding an increase of interval width for each data point. However, the contribution of this statistical effect is more than one order of magnitude less than that of the mentioned physical factors.

Microparticle concentrations are reported here for the size fraction from 1.0 μm to 11.5 μm equivalent spherical diameter in $\mu g\ kg^{-1}$. The mass fraction not measured below 1.0 μm accounts for about 10% assuming a typical lognormal volume distribution.

List of samples

From the whole NGRIP core profile 23 sections, each 1.65 m long, are taken for this study. These sections cover depths from 1420 m to 2921 m and represent various climatic periods including Holocene and LGM. For all sections $\delta^{18}O$ data are already available (personal communication from NGRIP members, 2000). For some sections acidity and standard IC anion data is also available and will be included in our discussion. Table 1 gives an overview of all selected sections, many of which contain volcanic horizons.

RESULTS AND DISCUSSION

A: The high resolution profiles

Articulate variations of the dust concentration are observed throughout large sections of the core. Figure 3 shows two 1.65 m long sections of the microparticle and Ca^{2+} profiles, one out of the Holocene and one out of the LGM. Typical peak heights for microparticles are about 6 times (Ca^{2+}: 4 times) the background value in the Holocene and about 2.2 times (Ca^{2+}: 2.0 times) in the LGM section. Based on a preliminary estimate of annual layer thicknesses λ, which was done by applying the GRIP ages from Johnson and others (1997) to identified horizons in the NGRIP core, we expect that the variations may correspond to annual variations in the Holocene section; in the LGM section partly annual and partly multi-annual variations may be resolved. The insoluble dust profile, therefore, may assist the dating by annual layer counting based on other high resolution profiles, such as ECM, Ca^{2+}, Na^{+}, or visual stratigraphy (e.g. Meese and others, 1997).

B: Variation of the Ca^{2+}-to-dust ratio

Normally, a good correspondence is observed between insoluble microparticle and Ca^{2+} concentrations for Holocene ice as well as for glacial age ice. The correlation coefficients for the two examples shown in Figure 3 are 0.92 (Holocene) and 0.89 (LGM) after slight smoothing of both signals (see below). A similarly high correlation is found throughout the whole core. This at first sight may be seen as a general confirmation for the use of Ca^{2+} concentrations as a proxy for the insoluble mineral dust variability.

A more detailed examination of the Ca^{2+}/dust ratio reveals, however, distinct differences between the Holocene and the glacial section. To inspect these, the Ca^{2+}/dust ratio was calculated for each data point and smoothed to weaken artifacts arising from incorrect peak phasings and from different peak shapes caused by signal noise, different sample dispersion or different response characteristics of the two detection systems. For the smoothing a 5.0 cm wide hanning window was used, i.e. a gliding

average using a cosinusoidal weighting function. The smoothed Ca^{2+}/dust ratio is included in Figure 3. It varies significantly on the same depth scale as peaks occur in the crustal concentrations and tends to be enhanced during low dust levels. The (mean Ca^{2+}) / (mean dust) ratio of the two sections are ~ 0.29 for Holocene and ~ 0.11 for LGM, which is similar to earlier findings from Steffensen (1997) based on established Coulter counter and standard IC measurements.

For all ice core sections listed in Table 1 the Ca^{2+}/dust mean ratios were calculated; hereby horizons with strong acid inputs, that showed unusually high Ca^{2+}/dust values (see below), were excluded. Figure. 4 shows the such derived (mean Ca^{2+}) / (mean dust) ratios plotted against $\delta^{18}O$; mean microparticle concentrations are also shown. A gradual trend to lower mean ratios for isotopically colder samples is exhibited. It can be excluded that the observed trend is an artifact arising from possibly higher relative errors of the measurements for isotopically warmer samples, which have lower concentrations of Ca^{2+} and dust; even Holocene concentrations are well above detection limit, and both systems responded very linearly to sample concentrations. Also the Ca^{2+} fraction derived from sea salt aerosol does not contribute significantly.

In order to compare the measured R_0 = (Ca^{2+})/(insoluble dust) ratios with data on the elemental composition of airborne mineral dust or source material, the ratios R_0 need to be converted to R = (total Ca) / (total dust). It is: $R = a\dfrac{1}{(bR_0)^{-1} + c}$, where a = (total Ca) / (Ca^{2+}) ≈ 1 is the ratio of total Ca to dissolved Ca^{2+}, $b \approx 0.9$ is the correction for the dust fraction not measured below 1.0 μm, and $c = 2.5$ is the mass ratio of $CaCO_3$ to Ca, assuming that the dissolved dust fraction predominantly consisted of $CaCO_3$ or of species with similar mass. This approximation yields ratios of 0.16 for Holocene and 0.08 for LGM. This Holocene value is in weak agreement with a mean ratio of 0.09 (range: 0.06 – 0.18) deduced from measurements of total Ca and Al in recent Greenland firn by atomic absorption spectroscopy (Boutron, 1978), but it is larger than the value of 0.05 deduced from total Ca and Al analyses in Summit aerosol by Colin and others (1997). For comparison to both references, the reported Al masses were used to infer the total dust mass by assuming a crustal abundance of 8%.

The trend to lower observed values of Ca^{2+}/dust for lower $\delta^{18}O$ remains under dispute as several explanations may be invoked. These include possible changes of source areas and properties, or of fractionating transformation and removal processes during long range transport or deposition (e.g. Hansson, 1994; Wurzler and others, 2000). The observed effect may also possibly be explained by slower dissolution of Ca^{2+} due to alkaline conditions of glacial ice, which would lead to lower observed Ca^{2+} concentrations by the immediate CFA-detection method used here.

Changes of mineral dust source areas are a controversial topic in the literature. De Angelis and others (1997) – by comparing their Ca^{2+}/Mg^{2+} ratios to Bowen (1979) – deduce mean sediment sources for present day and marine carbonate sources for the last glacial. Biscaye and others (1997) – based on mineralogical and isotopic studies – propose no significant change of source area during times of variable dust fluxes within the last glacial. Hinkley and others (1997) – on the basis of mineralogical studies – presume a present day tropospheric background aerosol uniformly composed of average crustal rock and not of carbonates. Maggi (1997) finds that weathering processes may have been changed with climate; but little is known about how this might have affected the relative abundances of $CaCO_3$ or $CaSO_4$ in the dust aerosol (Pye, 1987). A comparison of our data with Ca abundances in crustal material (Bowen, 1979) (see Table 2) suggests that marine carbonates or limestone sediments could have contributed significantly only during Holocene and that that during LGM mean crust and other sediments would have dominated. Various soils could have contributed at all times.

In the data presented here, it may be noteworthy that the variations of the Ca^{2+}/dust ratio that occur on an annual to multi-annual scale follow the same pattern as the variations just discussed on a long time scale. As can be seen in Figure 3 the Ca^{2+}/dust ratio is small during large dust concentrations, which at least for the

Holocene may be driven by variability in the transport efficiency as known for the Arctic Haze phenomenon (Rahn and Borys, 1977). It seems possible that also on an annual time scale these variations may be attributed to changing source areas or may be closely linked to changing fractionation processes during long range transport.

C: Special events in the microparticle and Ca^{2+} profiles

Figure 5 shows an example of a 1.65 m long section from the time between GRIP interstadials 1 and 2 which exhibits several anomalies (denoted by $\alpha - \delta$). Event α is a strong dust layer (note that the microparticle concentration got cut off by the detector electronics). Event δ is an increase of the Ca^{2+}/dust ratio caused by a Ca^{2+} peak that has no corresponding microparticle peak; only NO_3^- exhibits a pronounced peak that may be related (e.g. Wolff, 1984). Events β and γ arise from two very strong Ca^{2+} peaks coinciding with only small insoluble dust peaks; they have a Ca^{2+}/dust ratio about 100% and 200% higher than the typical value. Coinciding are very strong peaks in SO_4^{2-} and also enhancements of ECM, acidity, and F^- (not shown) indicating volcanic horizons. These phenomena were observed during cold glacial times predominately, but they also occured during warm interstadials.

From our size distribution measurements we can rule out that the observed increase of the Ca^{2+}/dust ratio during events β and γ is only an artifact resulting from a dust size distribution severely shifted towards larger particles during these events. High inputs of acid however may lead to enhanced Ca^{2+}/dust ratios by promoting the rapid dissolution of calcite particles or $CaCO_3$ coatings. Indeed, all 13 anomalous Ca^{2+}/dust enhancements investigated in this study are accompanied by a clear SO_4^{2-} peak, indicating a strong input of acid (see Table 1).

An ionic balance was evaluated using major ion concentrations and acidity data for 10 of these sections, and it was found to be rather constant – not zero, at a low $\mu eq\ kg^{-1}$ level – across the disturbed horizons, which indicates that no unmeasured ionic species contributed substantially during these events. From the ionic balance, of course, it still cannot be distinguished to which extent SO_4^{2-} derived from H_2SO_4 or from mineral $CaSO_4$. But it seems much more probable that during volcanic events the predominant part of SO_4^{2-} originates from volcanic H_2SO_4 and that the Ca^{2+} peak is produced by enhanced dissolution of $CaCO_3$ during in-cloud processing or pre-analytical sample melting.

CONCLUSIONS

The novel particle sensor proved to be a reliable tool even under field conditions; it provided the total particle concentration at ≤ 1 cm depth resolution backed up by size distribution information. Thus, calibrated records of insoluble particle mass concentrations are obtained. Variations of the Ca/dust mass ratio were seen during long term climatic changes as well as on annual or multiannual time scales. This suggests variable source properties or variable fractionation during transfer, which should be investigated in more detail. If Ca^{2+} measurements are used as a quantitative proxy for mineral dust care must be taken when considering data across climatic transitions, at volcanic horizons, or at subseasonal resolution.

A dedicated investigation of Ca ion solubility in glacial meltwater and its implications for the CFA and IC analytical methods is essential as we are currently limited in our interpretation by this uncertainty. To elucidate possible variations in dust source areas and properties, or of changes in fractionation processes during long range transport, routine analysis of crustal reference elements like Al are needed as they would help to infer the total – i.e. soluble and insoluble – crustal concentration.

ACKNOLEDGEMENTS

The North-GRIP project is directed and organised by the Department of Geophysics at the Niels Bohr Institute for Astronomy, Physics and Geophysics, University of Copenhagen. It is being supported by funding agencies in Denmark

(SNF), Belgium (NFSR), France (IFRTP and INSU/CNRS), Germany (AWI), Iceland (RannIs), Japan (MECS), Sweden (SPRS), Switzerland (SNF) and the United States of America (NSF). We wish to thank all the funding bodies and field participants. Chris Zdanowicz is thanked for his helpful comments to improve the manuscript.

REFERENCES

Armbruster, M., 2000, *Stratigraphical dating of high alpine ice cores over the last 1000 years (in German)*, M.Sc. thesis, Institut für Umweltphysik, University of Heidelberg, Heidelberg.

Biscaye, P. E., F. E. Grousset, M. Revel, S. Van der Gaast, G. A. Zielinski, A. Vaars, and G. Kukla, 1997, Asian provencance of glacial dust (stage 2) in the Greenland Ice Sheet Project 2 Ice Core, Summit, Greenland, *Journal of Geophysical Research*, 102 (C12), 26765-26781.

Boutron, C., 1978, *Influences of aerosols of natural and antropogenic origin on the chemistry of polar snows (in French)*, Ph.D thesis, , University of Grenoble, Grenoble.

Bowen, H. J. M., 1979, *Environmental Chemistry of the Elements*, Academic Press, London.

Colin, J. L., B. Lim, E. Herms, F. Genet, E. Drab, J. L. Jaffrezo, and C. I. Davidson, 1997, Air-to-snow mineral transfer - crustal elements in aerosols, fresh snow and snowpits on the Greenland ice sheet, *Atmospheric Environment*, 31 (20), 3395-3406.

De Angelis, M., J. P. Steffensen, M. Legrand, H. Clausen, and C. Hammer, 1997, Primary aerosol (sea salt and soil dust) deposited in Greenland ice during the last climatic cycle: Comparison with east Antarctic records, *Journal of Geophysical Research*, 102 (C12), 26681-26698.

Fuhrer, K., E. W. Wolff, and S. J. Johnsen, 1999, Timescales for dust variability in the Greenland Ice Core Projct (GRIP) ice core in the last 100,000 years, *Journal of Geophysical Research*, 104 (D24), 31043-31052.

Hammer, C. U., H. B. Clausen, W. Dansgaard, A. Neftel, P. Kristinsdottir, and E. Johnson, 1985, Continuous impurity analysis along the Dye 3 deep core, in C.C.J. Langway, H. Oeschger, and W. Dansgaard (Eds.) *Greenland Ice Core: Geophysics, Geochemistry, and the Environmentl*, Geophysical Monograph 33, American Geophysical Union, Washington, 90-94.

Hansson, M. E., 1994, The Renland ice core. A Northern Hemisphere record of aerosol composition over 120,000 years, *Tellus*, 46B, 390-418.

Hinkley, T., F. Pertsiger, and L. Zavjalova, 1997, The modern atmospheric background dust load: recognition in Central Asian snowpack, and compositional contraints, *Geophysical Research Letters*, 24 (13), 1607-1610.

Johnsen, S. J., H. B. Clausen, W. Dansgaard, N. S. Gundestrup, C. U. Hammer, U. Andersen, K. K. Andersen, C. S. Hvidberg, D. Dahl-Jensen, J. P. Steffensen, H. Shoji, A. E. Sveinbjörnsdòttir, J. W. C. White, J. Jouzel, and D. Fisher, 1997, The $d^{18}O$ record along the Greenland Ice Core Project deep ice core and the problem of possible Eemian climatic instability, *Journal of Geophysical Research*, 102 (C12), 26397-26410.

Maggi, V., 1997, Mineralogy of atmospheric microparticles deposited along the Greenland Ice Core Project ice core, *Journal of Geophysical Research*, 102 (C12), 26725-26734.

Meese, D. A., A. J. Gow, R. B. Alley, G. A. Zielinski, P. M. Grootes, M. Ram, K. C. Taylor, P. A. Mayewski, and J. F. Bolzan, 1997, The Greenland Ice Sheet Project 2 depth-age scale: Methods and results, *Journal of Geophysical Research*, 102 (C12), 26411-26423.

Petit, J. R., J. Jouzel, D. Raynaud, N. I. Barkov, J.-M. Barnola, I. Basile, M. Bender, J. Chappellaz, M. Davis, G. Delaygue, M. Delmotte, V. M. Kotlyakov, M. Legrand, V. Y. Lipenkov, C. Lorius, L. Pépin, C. Ritz, E. Saltzmann, and M. Stievenard, 1999, Climatic and atmospheric history of the past 420,000 years from the Vostok ice core, Antarctica, *Nature*, 399, 429-436.

Pye, K., 1987, *Aeolian dust and dust deposits*, Academic Press, London.

Rahn, K. A., and R. D. Borys, 1977, The Asian source of Arctic haze bands, *Nature*, 268, 713-715.

Ram, M., and G. Koenig, 1997, Continuous dust concentration profile of pre-Holocene ice from the Greenland Ice Sheet Projct 2 ice core: Dust stadials, interstadials, and the Eemian, *Journal of Geophysical Research*, 102 (C12), 26641-26648.

Röthlisberger, R., M. Bigler, M. Hutterli, S. Sommer, and B. Stauffer, 2000, A technique for contiunuous high resolution analysis of trace substances in firn and ice cores, *Environmental Science & Technology*, 34, 338-342.

Saey, P., 1998, *Concentration and size distribution of microparticles in alpine and polar ice cores (in German)*, M.Sc. thesis, Institut für Umweltphysik, University of Heidelberg, Heidelberg.

Steffensen, J. P., 1997, The size distribution of microparticles from selected segments of the Greenland Ice Core Project ice core representing different climatic periods, *Journal of Geophysical Research*, 102 (C12), 26,755-726,763.

Taylor, K. C., R. B. Alley, G. W. Lamorey, and P. Mayewski, 1997, Electrical measurements on the Greenland Ice Sheet Project 2 Core, *Journal of Geophysical Research*, 102 (C12), 26511-26517.

Tegen, I., and I. Fung, 1994, Modeling of mineral dust in the atmosphere: Sources, transport, and optical thickness, *Journal of Geophysical Research*, 99 (D11), 22897-22914.

Wolff, G. T., 1984, On the nature of nitrate in coarse continental aerosols, *Atmospheric Environment*, 18 (5), 977-981.

Wurzler, S., T. G. Reisin, and Z. Levin, 2000, Modification of mineral dust particles by cloud processing and subsequent effects on drop size distributions, *Journal of Geophysical Research*, 105 (D4), 4501-4512.

FIGURES AND TABLE S

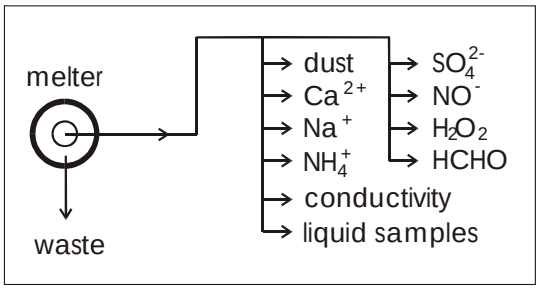

Figure 1. Flowchart of the analytical setup (highly simplified).

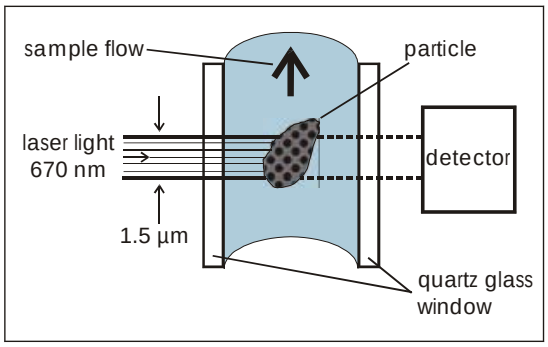

Figure 2. Detection cell of the laser sensor (schematic). The cross section of the cell is 230 µm × 250µm; the laser beam is 250 µm × 1.5 µm wide.

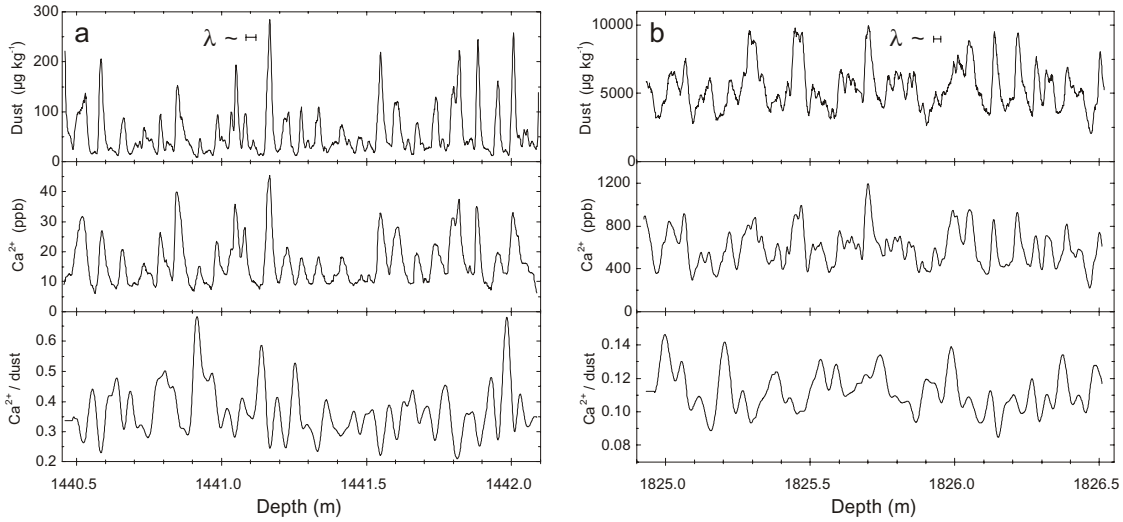

Figure 3. Examples of the insoluble dust and the Ca^{2+} measurements: (a) is in Holocene, (b) is during LGM. Also shown is the Ca^{2+}/dust ratio, which is smoothed (see text). A preliminary estimate of annual layer thicknesses λ is included. Note the different scales in all panels for (a) and (b).

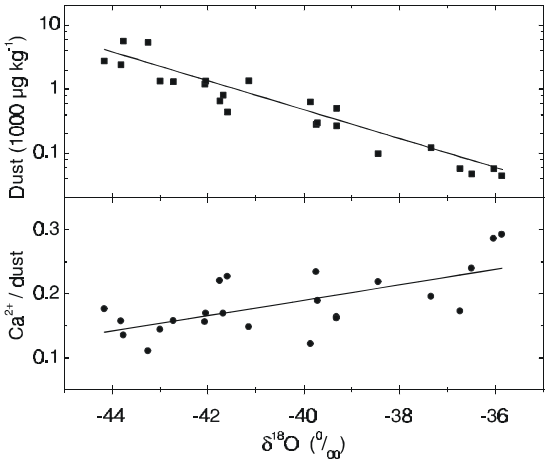

Figure 4. Ca^{2+}/dust ratio and mean dust concentration for all 23 sections plotted against $\delta^{18}O$. Each data point represents a 1.65 m long intervall.

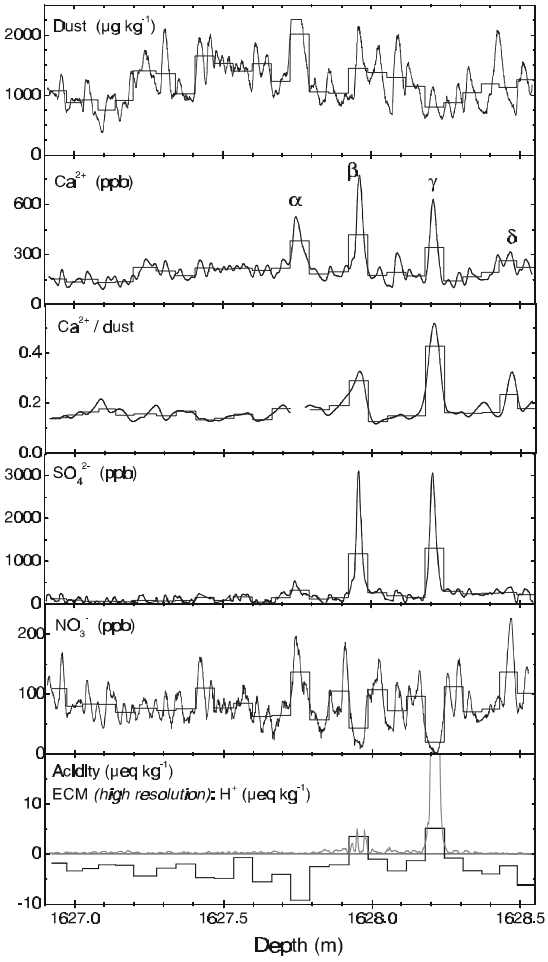

Figure 5. Examples of anomalous events in the microparticle and Ca^{2+} profiles. The sample is from the cold stadial between IS 1 and 2. The data for dust, Ca^{2+}, SO_4^{2-}, and NO_3^- were obtained by CFA; the Ca^{2+}/dust ratio was smoothed (see text); acidity was measured at approx. 6 cm depth resolution; in the same panel the ECM data is shown in high resolution (preliminary calibration). The fine histogram style lines represent the high resolution data reduced to the resolution of the acidity measurement. Labeled Ca^{2+} peaks refer to events discussed in text.

mid-depth (m)	climatic period	$\delta^{18}O$ (‰)	mean dust (µg kg^{-1})	mean Ca^{2+}/ mean dust	unusual Ca^{2+}/dust	ECM peak	SO_4^{2-} peak
1424.8	hol	-35.87	44	0.29	-	na	-
1441.3	hol	-36.04	57	0.29	-	na	-
1459.4	hol	-36.74	58	0.17	+	na	+
1479.2	hol	-38.45	99	0.22	-	na	+
1486.9	hol	-36.60	48	0.24	-	na	-
1627.7	c-1/2	-42.07	1200	0.16	+	+	+
1642.6	c-1/2	-42.05	1347	0.17	+	+	+
1688.8	c-1/2	-42.73	1318	0.16	+	+	+
1716.8	c-1/2	-41.15	1353	0.15	+	+	+
1805.9	LGM	-43.76	5589	0.14	-	-	+
1825.7	LGM	-43.25	5373	0.11	-	-	-
1855.4	LGM	-43.00	1337	0.14	+	+	+
1895.0	c-4/5	-44.16	2755	0.18	-	-*	+
1931.3	c-4/5	-43.82	2418	0.16	+	+	+
2252.5	IS13	-41.59	440	0.23	+	+	+
2254.2	IS13	-39.75	280	0.23	+	+	+
2390.0	IS16	-39.72	298	0.19	+	+	+
2399.9	c-16/17	-41.68	810	0.17	-	-*	+
2708.5	c-21/22	-41.76	650	0.22	+	-	+
2901.5	c-pre23	-39.86	634	0.12	-	-	-
2904.8	c-pre23	-39.32	502	0.16	+	-	+
2918.0	w-23/5e1	-37.34	122	0.20	-	-	-
2921.3	c-post5e1	-39.32	268	0.16	+	-	+

Table. 1. Overview of the NGRIP core sections used for this study. All sections are 1.65 m long. The climatic period is preliminary; it was determined by matching the NGRIP dust profile to the GRIP $\delta^{18}O$ profile (Johnson and others, 1997). The NGRIP $\delta^{18}O$ values given are from personal communication from NGRIP members (2000). hol: Holocene; IS n: GRIP interstadial n; c m/n: cold stadial between SI m and SI n; LGM: last glacial maximum; pre23c: cold stage before IS23; w23/5e1: intermittent warm stage between IS23 and 5e1; post5e1: cold stage after 5e1. na: data not available; '+': existing; '-': not existing; '-': no ECM peak observed but a visible ash layer.*

Mean crust (igneous rocks)	0.041
Mean sediment	0.066
Marine carbonates	0.203
Mean limestone	0.340
Soils	0.015 (0.0007 – 0.50)

Table. 2. Mean weight fractions of Ca in different types of crust material (adapted from Bowen, 1978).

2.7 Sulphate record from a northeast Greenland ice core over the last 1200 years based on Continuous Flow Analysis

Matthias Bigler, Dietmar Wagenbach, Hubertus Fischer
Heinz Miller, Stefan Sommer, Bernhard Stauffer

Annals of Glaciology
35, 250–256, 2002

Annals of Glaciology 35 2002

Sulphate record from a northeast Greenland ice core over the last 1200 years based on continuous flow analysis

MATTHIAS BIGLER,[1] DIETMAR WAGENBACH,[2] HUBERTUS FISCHER,[3] JOSEF KIPFSTUHL,[3] HEINRICH MILLER,[3] STEFAN SOMMER,[1] BERNHARD STAUFFER[1]

[1]*Climate and Environmental Physics, Physics Institute, University of Bern, Sidlerstrasse 5, CH-3012 Bern, Switzerland*
E-mail: bigler@climate.unibe.ch

[2]*Institut für Umweltphysik, University of Heidelberg, Im Neuenheimer Feld 229, D-69120 Heidelberg, Germany*

[3]*Alfred Wegener Institute for Polar and Marine Research, Columbusstrasse, D-27515 Bremerhaven, Germany*

ABSTRACT. A 150 m deep ice core from the low-accumulation area of northeast Greenland was analyzed for sulphate, calcium, sodium and electrolytical meltwater conductivity at a depth resolution of approximately 1 cm by continuous flow analysis (CFA). The calcium and sodium profiles are used to establish a relatively precise ice-core chronology by annual-layer counting back to AD 830. Inspection of the novel CFA method for sulphate revealed relative errors typically around 15%, but at least $\pm 20\,ng\,g^{-1}$, for concentrations $<130\,ng\,g^{-1}$, and a current detection limit for routine ice-core analyses of $40\,ng\,g^{-1}$. Annual sulphate peaks are shown to occur over almost the entire core, with only a small shift in seasonality between the modern and pre-industrial sections. Inspection of volcanic horizons allowed more accurate timing of these peaks and clear identification of calcium-rich events. Disregarding clear volcanic peaks, significant long-term changes of sulphate are only seen over the industrial period. However, a higher frequency of important volcanic inputs was identified around AD 1200.

INTRODUCTION

Sulphate components constitute a major part of the submicron aerosol body and thus contribute significantly to direct and indirect aerosol radiative forcing. While ice-core studies clearly show that anthropogenic sulphur-dioxide emission controls the modern sulphate budget of the Northern Hemisphere (Neftel and others, 1985; Mayewski and others, 1990; Fischer and others, 1998b), much less is known about the natural sulphate source apportionment (mainly with respect to marine dimethyl sulphide, soil dust, sea salt and volcanoes) and about the possible long-term sulphate variability during the pre-industrial era. For sulphate, glaciochemical ice-core studies from Greenland have been evaluated in detail mainly over the last 200 years (with only few records available back to 500 years (e.g. Fischer and others, 1998b)). Time series from the Greenland Summit exist over the entire Holocene (and beyond) in up to biannual (Mayewski and others, 1997) and in small sections at seasonal resolution (Legrand and others, 1997). They were examined, however, mainly in view of strong volcanic inputs (Zielinski and others, 1994; Zielinski, 1995) or Holocene/Pleistocene changes of atmospheric sulphur species (Legrand and others, 1997). Here we report on detailed continuous high-resolution sulphate analyses on an ice core from northeast Greenland going back to approximately AD 830. This record covers both the Little Ice Age and the Medieval Warming. Evaluation of our dataset, which stands out as the first long-term sulphate record in sub-seasonal resolution, is mainly aimed at: (1) assessment of the reliability of the newly applied continuous flow analyses (CFA) for sulphate (even at relatively low levels), (2) the deployment of our high-resolution sulphate record for the examination of distinct peaks such as volcanic horizons made up by H_2SO_4, and (3) inspection of the last 1200 year period for possible long-term perturbation in the background sulphate level.

METHODS

Sample collection and processing

Within the North Greenland Traverse (NGT) project, 13 ice cores covering mainly the last 500 years were drilled, along with numerous shallow firn cores and snow-pit samplings (Fischer and others, 1998a). To use the potential of the high depth resolution of the CFA system, we selected one of the deeper cores (150 m) situated in the less explored low-accumulation area of northeast Greenland, hereafter denoted as B20 (78°50′ N, 36°30′ W; 2150 m a.s.l.). For the geographical position of B20 in relation to other drill sites see Figure 1.

Core sections, $3 \times 3\,cm^2$ and 110 cm long, were transported to the Bern laboratory where they were continuously melted on a special firn melt head (Röthlisberger and others, 2000), as an important part of the core consists of porous firn. The uncontaminated meltwater from the central part of the melt head, which has not been exposed to the ambient atmosphere, was permanently drained off, debubbled and split into nine substreams at a flow rate of $0.9\,mL\,min^{-1}$ each for concurrent online chemical analyses by CFA.

Chemical analyses

For the chemical measurements, a CFA system was used as described in detail by Röthlisberger and others (2000). It essentially consists of fluorescence or absorption spectrometric detection systems for sulphate, nitrate, calcium,

Fig. 1. Geographical position of the B20 ice core in relation to other NGT drill sites and Summit.

sodium, ammonium and hydrogen peroxide. In addition, the electrolytical meltwater conductivity was measured continuously as an estimate for the total ion concentration.

The newly developed sulphate detection system is described by Röthlisberger and others (2000). The detection principle is based on a standard photometric flow-injection method using methylthymol blue (MTB) (Madsen and Murphy, 1981) which was adapted to the existing CFA system. Thereby sulphate is indirectly determined by competitive reaction of MTB with barium ions. The resulting absorbance at 608 nm of MTB–barium complexes decreases as sulphate concentration increases.

The sensitivity of the sulphate determination is strongly affected by the quality of the MTB reagent and by the regularity of the various flow rates. The detection limit (calculated as three times the standard deviation of the baseline noise) is about 40 ng g^{-1}, which is higher by up to a factor of four than the lowest concentration levels expected in Greenland ice. The maximum of the linear range of the calibration curve approaches 6000 ng g^{-1} and exceeds the maximum values of the measured samples by up to a factor of five. By evaluating multiple measurements on the same core section, we estimate the total uncertainty of a single data point selected out of the continuous record to be about 15%, but at least ± 20 ng g^{-1}, for concentrations < 130 ng g^{-1}. This is still above the typical uncertainty of around 10% achieved for all other CFA detection systems described by Röthlisberger and others (2000). With a melting rate of approximately 3.5 cm min^{-1} and a temporal resolution of typically 20 s associated with the continuous sulphate signal (corresponding to the time needed to drop to 1/e of the signal of a sulphate standard solution measurement after switching back to blank), the characteristic depth resolution is estimated to be about 1 cm.

Possible additional errors in the sulphate determination could be: (1) baseline distortion due to small uncontrollable flow-rate changes and due to flow interruption during valve switches, leading to transient systematic errors in both directions; (2) deviations from the required 1:1 molar ratio of MTB and barium in the reagent, causing a slightly smaller slope of the calibration curve for low sulphate concentrations which resulted in an underestimation for concentration levels < 200 ng g^{-1} and an overestimation for higher values; and (3) disproportionate occurrence of gaps in the dataset at low concentration levels due to unreliable readings close to the detection limit, leading to systematic higher overall means. A formal assessment of the sulphate data reliability, particularly at lower concentration levels, remains difficult at this stage. The same holds true for a realistic quantification of the uncertainties encountered. In more recent deployments of the CFA system, these systematic errors have been lowered by using non-linear calibration curves and by decoupling the automatic valve from the detection unit.

Dating and data reduction

Dating of the core has been based on the identification of well-known historic volcanic layers characterized, among other things, by high sulphate concentrations. Only the very distinct sulphate signals were used: Katmai, Alaska (AD 1912); Tambora, Indonesia (AD 1815); Laki, Iceland (1783 AD); Huaynaputina, Peru (AD 1600); unknown source (AD 1259); and Eldgja, Iceland (AD 934) (Fig. 2). On the other hand, annual-layer counting was also possible, due to the high depth resolution of the record, even though the annual snow accumulation is only around 100 mm w.e. a^{-1}. A first criterion for setting annual marks is the increase of the calcium signal occurring around spring. In case of ambiguities, the typical winter to early-spring peak of the sodium signal was also used. The dating uncertainty between the reference horizons is estimated to be ± 5 years.

Following Sommer and others (2000), the intervals between two annual marks were divided into 12 equidistant parts for which mean values from the included data points were calculated. In this way, CFA time series at a formal monthly resolution were generated.

Calculation of the sea-salt sulphate fraction by means of the sodium record gave on average a contribution to the total sulphate of only 8% during the pre-industrial epoch (this fraction is even lower in recent times). Here, we report total sulphate concentrations, i.e. without sea-salt correction.

RESULTS AND DISCUSSION

Sulphate mean values and seasonal features

Our sulphate CFA record is presented in Figure 2 at monthly resolution over the period from AD 830 to present. Sodium and calcium are also shown, because they are associated with the rather constant sea-salt and crustal sulphate sources. Sulphate shows the well-known anthropogenic increase in the course of the 20th century, and some very strong peaks obviously caused by volcanic deposits. In addition, the snow-accumulation rate as derived from annual-layer counting is shown in Figure 2. The long-term mean annual layer thickness λ is fairly constant at 9.9 ± 3.8 cm w.e. except for an excursion between AD 900 and 1300. A similar deviation can be seen in the accumulation-rate record from the NGT core B18 (Schwager, 2000), about 200 km south of B20, but not at other NGT positions. However, the long-term accumulation-rate changes are rather small and, according to the deposition model by Fischer and others (1998a), have only a minor influence on the mean sulphate concentrations (not more than 7%). Other physical characteristics (e.g. elevation and distance from the coast) are negligible for this interior area of Greenland.

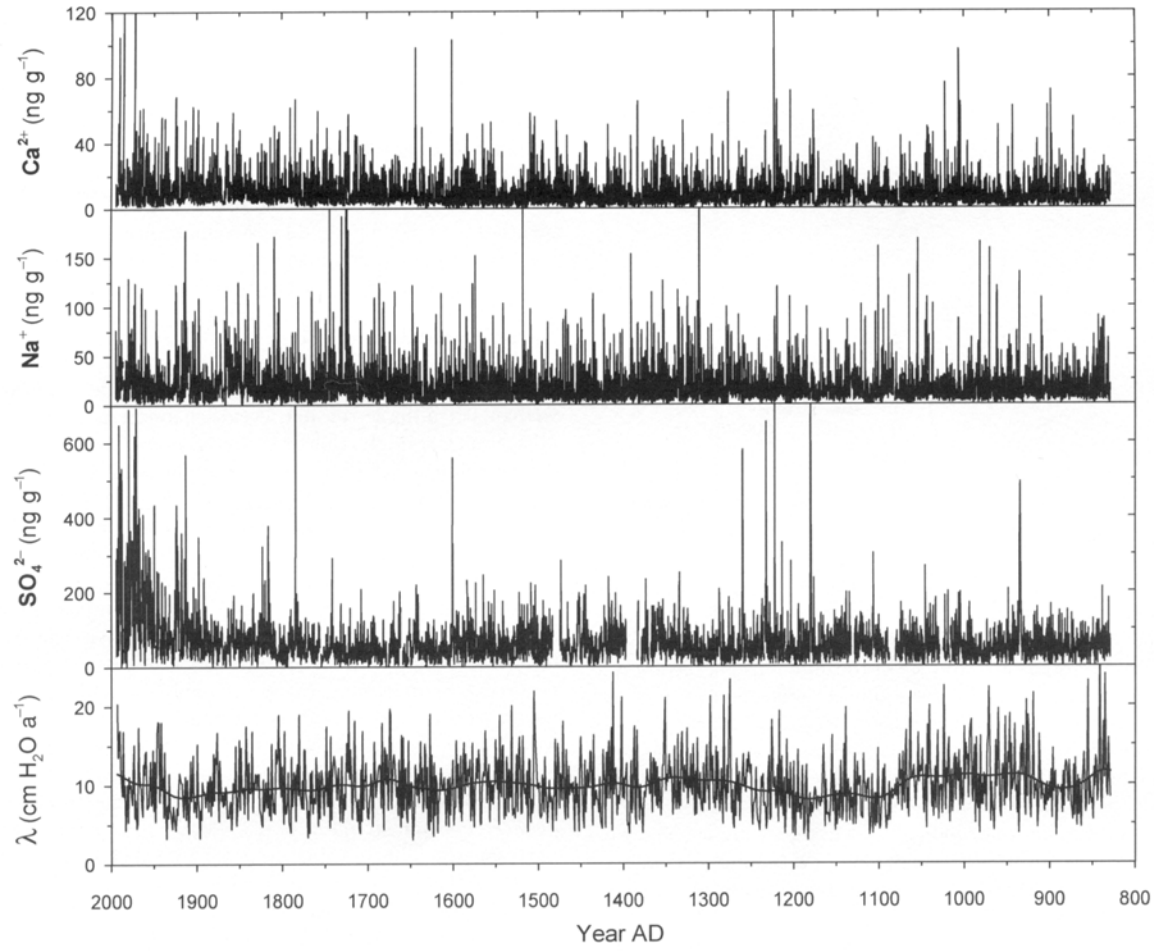

Fig. 2. Raw data of ion records at (formal) monthly resolution from B20 ice core from northeast Greenland. Annual layer thickness λ has been smoothed by applying a low-pass filter (Gaussian filter with cut-off frequency of 100 years; bold line) to display long-term changes in the snow accumulation rate.

For comparisons of our mean sulphate values from the upper part of our core with those observed at Summit and North Greenland, the most prominent volcanic peaks were removed. It turned out that anthropogenic means (1850–1992) available from adjacent NGT cores (B18: 119 ng g^{-1}; B20: 114 ng g^{-1}; and B21: 114 ng g^{-1}; values for B18 and B21 from Fischer and others, 1998b) are in perfect agreement, confirming that there are no analytical problems at higher concentration levels. A higher value with respect to Summit (67 ng g^{-1}: EUROCORE; personal communication from M. Legrand, 2001) can be fully explained by the difference in accumulation rates (Fischer and others, 1998a). In the pre-industrial era back to AD 1500, however, the B20 mean data appear to be systematically higher by about 20% than those of adjacent NGT cores B18 and B21, even after correction of the small accumulation effect. The remaining systematic overestimation of low background sulphate values is likely to be explained by analytical effects of the CFA sulphate detection method as described above.

To illustrate in more detail the sulphate variability on the multi-annual scale, an expanded view is given in Figure 3, along with calcium (which has served as the main dating component) and the electrolytical conductivity. The sulphate noise level is obviously larger than the calcium one, particularly at lower concentrations. On the other hand, the electrolytical conductivity profile frequently corresponds to the sulphate variability even at lower levels. This indicates a possible overestimation of the detection limit given above as 40 ng g^{-1}. Furthermore the periodically occurring sulphate peaks, found in the range of up to 200 ng g^{-1} almost every year concurrently with the annual calcium peaks, suggest a persistent reliable seasonal sulphate signal can be detected with CFA. Note that no clear volcanic event was identified in the core section shown in Figure 3.

In order to evaluate the seasonal timing of the sulphate signal, we used our formal monthly values as described above. Because the accumulation distribution in the course of the year is not the same for each year, we stacked the individual months over long pre-industrial and industrial time intervals, respectively, to minimize the uncertainties (for details and accuracy of this method see Sommer and others, 2000). Note, however, that this method cannot account for a systematic seasonal bias in the annual cycle of snow accumulation, so each interval does not truly represent a single month. The adjustment of these formal months to calendar months was accomplished by setting the marks in the increasing calcium flank as February. Figure 4 illustrates mean seasonal cycles of sulphate for the industrial

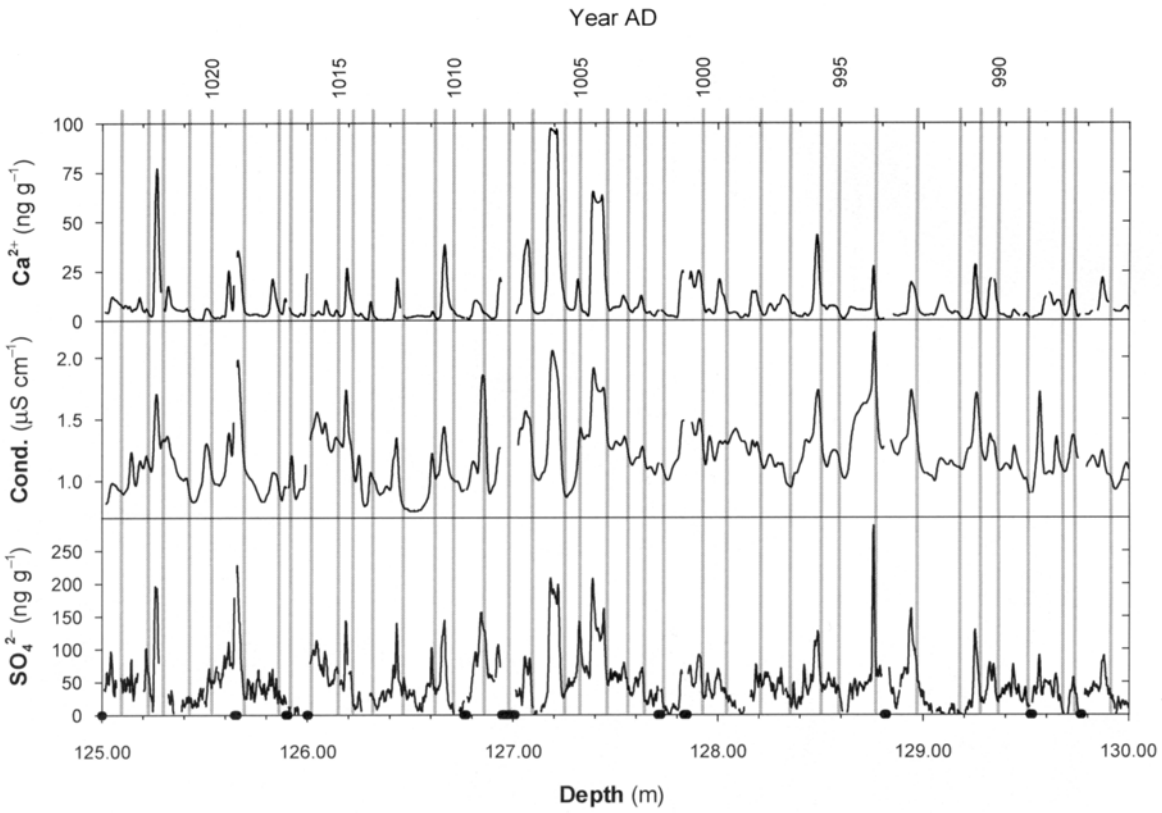

Fig. 3. Expanded view on a B20 core section. Vertical bars indicate annual layering used for dating; dots at the depth scale indicate core breaks.

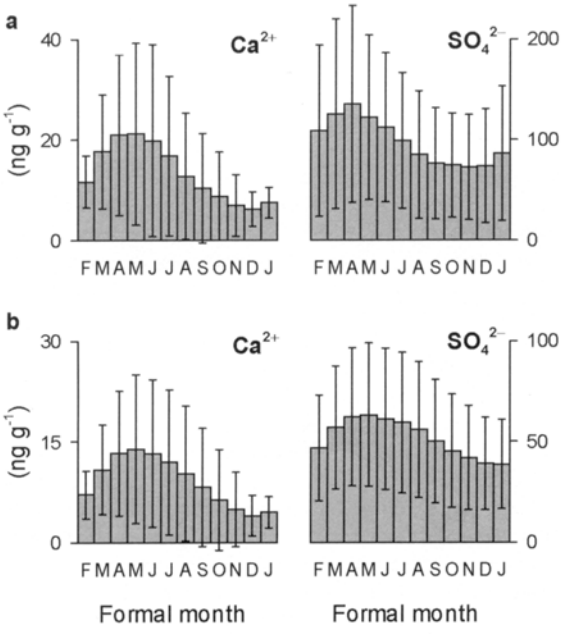

Fig. 4. Mean annual cycles of calcium and sulphate observed in B20 ice core (a) for the industrial era AD 1850–1994, and (b) for the pre-industrial era AD 830–1850. Bars correspond to a 1σ standard error.

and pre-industrial eras, along with calcium serving as the seasonal reference species. These seasonal cycles are in good agreement with the present state of knowledge. At higher sulphate levels during the industrial era (Fig. 4a), the seasonality is mainly driven by the Arctic haze, leading to a sulphate maximum during spring (Laj and others, 1992; Whitlow and others, 1992; Dibb and Jaffrezo, 1997). At lower sulphate levels in pre-industrial epochs, the extension of this peak towards summer (Fig. 4b) is consistent with the findings of Legrand and others (1997) reported for a short 11 year period around AD 1200, though at much lower time resolution. It appears that the main feature of seasonal cycles can be reliably reproduced, although we may expect the seasonal amplitude to be biased by an analytical systematic overestimation of sulphate minima, particularly during the pre-industrial core section with lower mean values.

We may summarize that systematic effects, particularly at lower sulphate levels, lead to an overestimation of overall mean values. The highly resolved sulphate, however, captures main features such as the typical seasonality quite well. It is not yet known whether weak long-term changes in the pre-industrial era might also be resolved.

Examination of episodic sulphate events

The examination of episodic volcanic events is a straightforward application of a sulphate record at sub-annual resolution. Due to associated high concentration levels, the analytical inaccuracy is of minor importance here. Different types of volcanic events are presented in Figure 5.

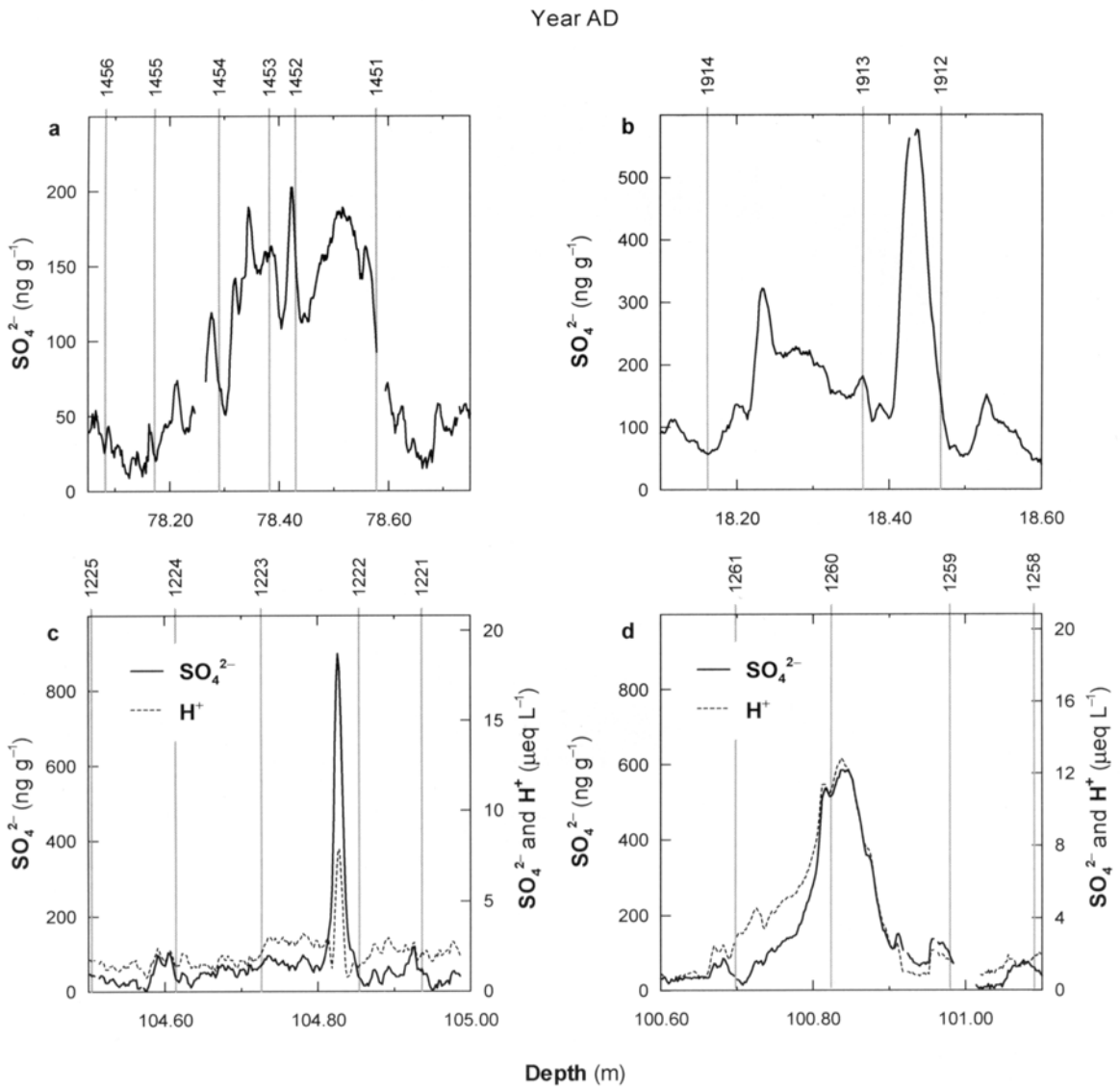

Fig. 5. Examples of distinct sulphate peaks from B20 ice core at sub-seasonal resolution: (a) multi-annual feature possibly from Kuwae (AD 1452 ± 10); (b) Katmai (AD 1912) possibly followed by Hekla (AD 1913); (c) short-pulse feature, possibly from Hekla (AD 1222) or Reykjaneshryggur (AD 1223); (d) unknown source (AD 1259) with bipolar occurrence. The H^+ concentration is derived from the ion-balanced CFA components (for explanations see text).

Figure 5a shows a broad peak over several years, probably representing the huge Kuwae eruption (volcanic explosivity index (VEI) 6) which occurred in AD 1452 ± 10 in the southwest Pacific region (Simkin and Siebert, 1994). The typical input from stratospheric material during spring and summer (Beer and others, 1991) shows up for another 3 years after the major event. Following Simkin and Siebert (1994), this event is possibly overlaid by another eruption that occurred in the same time period (Aniakchak, Alaska, VEI 5, 1450?).

In Figure 5b the potential of resolved sub-annual structures is demonstrated since two eruptions fit the two peaks appearing in AD 1912 and 1913: Katmai, Alaska (VEI 6, starting on 6 June 1912), and afterwards Hekla, Iceland (VEI 2, starting on 25 April 1913). A Mexican eruption in January 1913 is the only other significant one known in this time period.

A spike of very short sub-annual duration is presented in Figure 5c. Most likely it was produced from the AD 1222 eruption of Hekla or the AD 1223 eruption of the submarine Reykjaneshryggur, Iceland (VEI 2). The short distance to Greenland suggests that the accompanying extraordinary calcium spike reaching 140 ng g^{-1} might be related to volcanic-ash deposits. Because of the almost identical depth resolution of the other CFA components, concurrent peaks are emphasized. For this purpose the H^+ concentration was derived from the ion balance (driven here by the major species sulphate and calcium) of CFA components. Missing Cl^-, Mg^{2+} and K^+ contributions were inferred from Na^+ assumed to be totally marine and from Ca^{2+} assumed to be totally crustal-derived. H^+ gave a relatively low value for this event (see Fig. 5c) which might not show up in an ECM record (Clausen and others, 1997).

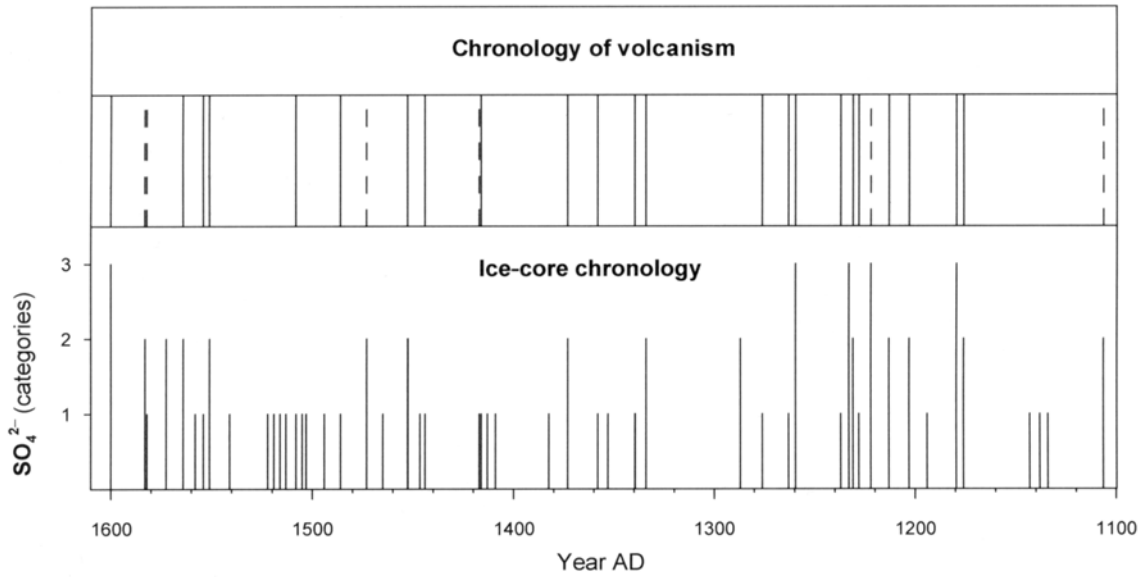

Fig. 6. Comparison of volcanic ice-core events from B20 arranged according to three categories (for details see text) with a chronology of volcanism. Full lines indicate obvious assignments, and dashed lines ambiguous ones.

A prominent volcanic event also seen in many other ice cores from Greenland and Antarctica is the eruption of an unknown source in AD 1259 ± 10 (Fig. 5d). Because no outstanding input of calcium occurred at the same time, the estimated H^+ profile closely follows the sulphate signal at a micro-equivalent ratio near unity. The high depth resolution not only helps to distinguish more clearly between adjacent events, but also allows accurate calculation of inventories in kg sulphate km^{-2}. We calculated an inventory of a volcanic event as the integral over the sulphate peak minus the prevailing mean background concentration weighted with the particular mean density at this depth. Integral limits are the feet of the volcanic peak where the sulphate concentration values exceed the mean background level. We estimated the inventories of the AD 1259 event and the AD 1912 Katmai eruption to be 41 and 10 kg km^{-2}, respectively, which are noticeably lower values than those from Summit based on ECM records (161 and 15 kg km^{-2}, respectively, for GRIP; Clausen and others, 1997) or on biannual sulphate records (145 and 27 kg km^{-2}, respectively, for GISP2; Zielinski, 1995). One reason for this may be better determination of the peak feet, and thus a clearer separation of a volcanic event from the background level, due to a high-resolution sulphate dataset. But the main reason for discrepancies in the inventory values seems to be spatial deposition differences which need to be carefully assessed when, for example, the optical depth of the atmosphere based on ice-core data is calculated.

Refined volcanic chronology

Another application of high-resolution sulphate records leads to a refined volcanic chronology. To explore this possibility, we first compiled a list of possible volcanic ice-core events

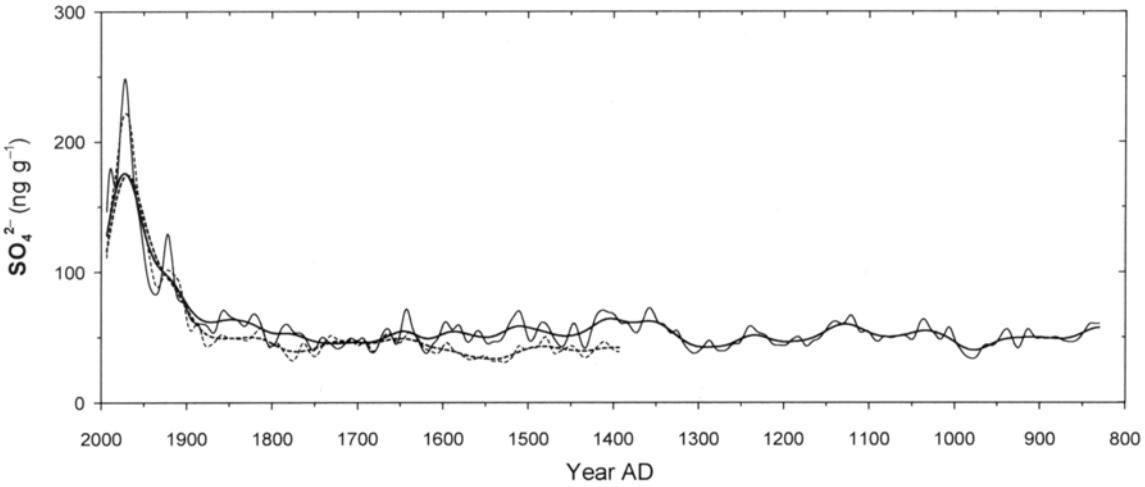

Fig. 7. Low-pass filtered sulphate records from B20 (solid lines) and from B21 (dashed lines). Bold lines correspond to 100 year, thin lines to 30 year cut-off frequencies of the Gaussian filter.

during the time period AD 1100–1600 according to three different categories (see Fig. 6, lower plot): peaks with non-sea-salt sulphate values of (1) 150–200 ng g^{-1}, (2) 200–400 ng g^{-1} and (3) > 400 ng g^{-1}. Then we independently picked out from Simkin and Siebert (1994) all listed eruptions with a VEI $\geqslant 5$ (including Plinian ones), all Northern Hemispheric eruptions with a VEI of 4, all Icelandic eruptions in view of their geographical proximity, and all unknown sources detected in other ice cores. From this list we eliminated all eruptions showing a dating uncertainty of $> \pm 10$ years. Subsequently we assigned our ice- core candidates to the literature-based list. If the assignment was consistent with the maximum dating uncertainty of ± 5 years, we marked it in Figure 6 in the upper plot with a vertical line; if the assignment was ambiguous we indicated this with a dashed line. Nearly 60% of our candidates have been assigned, and about 45% of the events from the literature-based list have been hit. Different assignment qualities showed up for different time periods: a relatively good agreement was found for AD 1150–1400 but a poor one around AD 1500. Noticeable is the 120 year period of more frequent stronger events around AD 1200.

A high-resolution sulphate record leads to a refined volcanic chronology since even very narrow volcanic spikes can be recognized as the relatively accurately dated Icelandic volcanoes. Compared to ECM profiling, the advantages of direct sulphate analyses are the low risk of interference from concurrent species and the more accurate calibration procedure in terms of volcanic sulphate.

Long-term sulphate changes

To extract long-term sulphate variations from B20 in the pre-industrial era, we looked at strongly smoothed sulphate records over the entire period. We removed strong episodic sulphate peaks in categories 2 and 3 according to the procedure presented above, and calculated annual means which were low-pass filtered afterwards (Gaussian filter with cut-off frequencies of 30 and 100 years, respectively).

For comparison we used the same filter procedures on annually resolved raw data from B21 (Fischer and others, 1998b) in which episodic events have already been removed. Figure 7 shows the long-term variations of both cores: B20 which reaches back to AD 830, and B21 which covers the more recent period starting in AD 1400. The deviation between the two records is comparable to the variability seen within the extended B20 period back to AD 830. We thus conclude that the observed long-term changes over the first half of the last millennium may not be significant with respect to the stated analytical precision of the CFA sulphate method, nor to the typical glacio-meteorological noise demonstrated by Fischer and others (1998b) for ice-core records in the NGT area. Note that this assessment holds true for the background sulphate record only where we eliminated volcanic events in advance of low-pass filtering. As in the previous section (see Fig. 6), we noticed a 120 year period around AD 1200 with frequent strong sulphate peaks mainly identified as volcanic horizons. This suggests higher atmospheric sulphate loads during this period, though they are a highly episodic feature.

ACKNOWLEDGEMENTS

The ice core was recovered by the Alfred Wegener Institute (AWI), Bremerhaven, Germany, in the frame of the NGT project. The analyses have been supported by the Swiss National Science Foundation, the Bundesamt für Bildung und Wissenschaft and the University of Bern. We thank B. Mieding (AWI, Bremerhaven) and M. Legrand (Laboratoire de Glaciologie et Géophysique de l'Environnement, Grenoble, France) for providing data.

REFERENCES

Beer, J. *and 15 others*. 1991. Seasonal variations in the concentrations of ^{10}Be, Cl^-, NO_3^-, SO_4^{2-}, H_2O_2, ^{210}Pb, ^3H mineral dust and $\delta^{18}O$ in Greenland snow. *Atmos. Environ., Ser. A*, **25**(5–6), 899–904.

Clausen, H. B. *and 6 others*. 1997. A comparison of the volcanic records over the past 4000 years from the Greenland Ice Core Project and Dye 3 Greenland ice cores. *J. Geophys. Res.*, **102**(C12), 26,707–26,723.

Dibb, J. E. and J.-L. Jaffrezo. 1997. Air–snow exchange investigations at Summit, Greenland: an overview. *J. Geophys. Res.*, **102**(C12), 26,795–26,807.

Fischer, H., D. Wagenbach and J. Kipfstuhl. 1998a. Sulfate and nitrate firn concentrations on the Greenland ice sheet. 1. Large-scale geographical deposition changes. *J. Geophys. Res.*, **103**(D17), 21,927–21,934.

Fischer, H., D. Wagenbach and J. Kipfstuhl. 1998b. Sulfate and nitrate firn concentrations on the Greenland ice sheet. 2. Temporal anthropogenic deposition changes. *J. Geophys. Res.*, **103**(D17), 21,935–21,942.

Laj, P., J. M. Palais and H. Sigurðsson. 1992. Changing sources of impurities to the Greenland ice sheet over the last 250 years. *Atmos. Environ.*, **26A**(14), 2627–2640.

Legrand, M. *and 6 others*. 1997. Sulfur-containing species (methanesulfonate and SO_4) over the last climatic cycle in the Greenland Ice Core Project (central Greenland) ice core. *J. Geophys. Res.*, **102**(C12), 26,663–26,679.

Madsen, B. C. and R. C. Murphy. 1981. Flow injection and photometric determination of sulphate in rainwater with methylthymol blue. *Anal. Chem.*, **53**(12), 1924–1926.

Mayewski, P. A., W. B. Lyons, M. J. Spencer, M. S. Twickler, C. F. Buck and S. Whitlow. 1990. An ice core record of atmospheric response to anthropogenic sulphate and nitrate. *Nature*, **346**(6284), 554–556.

Mayewski, P. A. *and 6 others*. 1997. Major features and forcing of high-latitude Northern Hemisphere atmospheric circulation using a 110,000-year-long glaciochemical series. *J. Geophys. Res.*, **102**(C12), 26,345–26,366.

Neftel, A., J. Beer, H. Oeschger, F. Zürcher and R.C. Finkel. 1985. Sulphate and nitrate concentrations in snow from south Greenland, 1895–1978. *Nature*, **314**(6012), 611–613.

Röthlisberger, R. *and 6 others*. 2000. Technique for continuous high-resolution analysis of trace substances in firn and ice cores. *Environ. Sci. Technol.*, **34**(2), 338–342.

Schwager, M. 2000. Ice core analysis on the spatial and temporal variability of temperature and precipitation during late Holocene in North Greenland. (Ph.D. thesis, University of Bremen. Alfred Wegener Institute for Polar and Marine Research.)

Simkin, T. and L. Siebert. 1994. *Volcanoes of the world. Second edition*. Tucson, AZ, Geoscience Press.

Sommer, S., D. Wagenbach, R. Mulvaney and H. Fischer. 2000. Glacio-chemical study spanning the past 2 kyr on three ice cores from Dronning Maud Land, Antarctica. 2. Seasonally resolved chemical records. *J. Geophys. Res.*, **105**(D24), 29,423–29,433.

Whitlow, S., P. A. Mayewski and J. E. Dibb. 1992. A comparison of major chemical species seasonal concentration and accumulation at the South Pole and Summit, Greenland. *Atmos. Environ.*, **26A**(11), 2045–2054.

Zielinski, G. A. 1995. Stratospheric loading and optical depth estimates of explosive volcanism over the last 2100 years derived from the Greenland Ice Sheet Project 2 ice core. *J. Geophys. Res.*, **100**(D10), 20,937–20,955.

Zielinski, G. A. *and 8 others*. 1994. Record of volcanism since 7000 B.C. from the GISP2 Greenland ice core and implications for the volcano–climate system. *Science*, **264**(5161), 948-952.

2.8 Limited dechlorination of sea salt aerosols during the last glacial period – Evidence from the EPICA Dome C ice core

Regine Röthlisberger, Rob Mulvaney, Eric W. Wolff, Manuel A. Hutterli, Matthias Bigler, Martine de Angelis, Margareta E. Hansson, Jørgen Peder Steffensen, Roberto Udisti

Journal of Geophysical Research
108(D16), 4526, 2003

JOURNAL OF GEOPHYSICAL RESEARCH, VOL. 108, NO. D16, 4526, doi:10.1029/2003JD003604, 2003

Limited dechlorination of sea-salt aerosols during the last glacial period: Evidence from the European Project for Ice Coring in Antarctica (EPICA) Dome C ice core

Regine Röthlisberger,[1,2] Robert Mulvaney,[1] Eric W. Wolff,[1] Manuel A. Hutterli,[3] Matthias Bigler,[3] Martine de Angelis,[4] Margareta E. Hansson,[5] Jørgen P. Steffensen,[6] and Roberto Udisti[7]

Received 17 March 2003; revised 5 June 2003; accepted 17 June 2003; published 30 August 2003.

[1] Chloride (Cl^-) and sodium (Na^+) in ice cores originate mainly from sea salt, and one would thus expect the Cl^-/Na^+ ratio to reflect the seawater ratio. However, at Dome C, a low-accumulation site in East Antarctica, this is not the case in present-day snow. Instead, a Cl^- excess relative to Na^+ is observed in surface snow, and within a few meters depth the Cl^- concentration decreases, and the Cl^-/Na^+ ratio becomes significantly lower than the seawater ratio. Aerosol studies at coastal Antarctic sites have shown that the reaction of sea-salt aerosols with nitric and sulphuric acid leads to the formation of HCl that eventually escapes the sea-salt aerosol. The observed decrease in Cl^- concentrations in the uppermost snow layers is due to reemission of HCl from the snow. Postdepositional loss of HCl depends among other factors on the accumulation rate at the site, with lower accumulation rates leading to larger losses. During the Last Glacial Maximum (LGM) the Cl^-/Na^+ ratio is relatively stable and close to the seawater ratio, despite the even lower accumulation rate during that time. The likely explanation for this conflicting observation is that high levels of dust neutralized nitric and sulphuric acids during the LGM which in turn reduced the formation of HCl from sea-salt aerosol. With less or no HCl formed, postdepositional loss would be prevented, keeping the Cl^-/Na^+ ratio close to that of sea water. *INDEX TERMS:* 0368 Atmospheric Composition and Structure: Troposphere—constituent transport and chemistry; 0305 Atmospheric Composition and Structure: Aerosols and particles (0345, 4801); 1615 Global Change: Biogeochemical processes (4805); 3344 Meteorology and Atmospheric Dynamics: Paleoclimatology; 9310 Information Related to Geographic Region: Antarctica; *KEYWORDS:* sea-salt aerosol, ice core records, Antarctica

Citation: Röthlisberger, R., R. Mulvaney, E. W. Wolff, M. A. Hutterli, M. Bigler, M. de Angelis, M. E. Hansson, J. P. Steffensen, and R. Udisti, Limited dechlorination of sea-salt aerosols during the last glacial period: Evidence from the European Project for Ice Coring in Antarctica (EPICA) Dome C ice core, *J. Geophys. Res.*, *108*(D16), 4526, doi:10.1029/2003JD003604, 2003.

1. Introduction

[2] Ice cores offer a unique possibility to reconstruct variations of past atmospheric aerosol concentrations, transport and transformation during transport. Cl^- and Na^+ have been used as indicators of sea-salt aerosols, as they are the main constituents of sea salt and are routinely analyzed in chemical ice core analysis. Usually, sea-salt aerosol is believed to originate from open water and it was assumed that sea ice extent would influence the source area in the vicinity of the Antarctic continent. More recently, evidence for an additional sea-salt aerosol source, particularly in winter, has been presented [*Wagenbach et al.*, 1998]. On the basis of the chemical signature of atmospheric aerosols, back trajectory calculations and satellite imagery, *Rankin et al.* [2002] showed that frost flowers, which form from the brine on new sea ice, are the dominant contributors to coastal Antarctic sea-salt aerosol. Sea-salt aerosols from frost flowers are slightly depleted in Na^+, but this depletion is limited to approximately 10%. So whether the sea-salt aerosol is produced over open water or fresh sea ice, one would expect a Cl^-/Na^+ ratio close to the one found in seawater.

[3] Other sources than sea salt are known to contribute to the Na^+ and Cl^- concentrations of polar snow, which could potentially change the Cl^-/Na^+ ratio in snow and ice

[1]British Antarctic Survey, Cambridge, United Kingdom.
[2]Now at NCCR Climate, University of Bern, Bern, Switzerland.
[3]Climate and Environmental Physics, University of Bern, Bern, Switzerland.
[4]Laboratoire de Glaciologie et Géophysique de l'Environnement (LGGE), CNRS, Grenoble, France.
[5]Physical Geography and Quaternary Geology, University of Stockholm, Stockholm, Sweden.
[6]Department of Geophysics, University of Copenhagen, Copenhagen, Denmark.
[7]Department of Chemistry, University of Florence, Sesto Fiorentino, Italy.

0148-0227/03/2003JD003604$09.00

compared to the ratio found in seawater. Some Na^+ and a negligible amount of Cl^- comes along with mineral dust. Our analytical method only accounts for the soluble fractions, i.e., dust is unlikely to contribute to the Na^+ concentrations measured. However, there remains some uncertainty due to insufficient knowledge of the availability of Na^+ from minerals. Nevertheless, even if all Na^+ of the mineral dust would be dissolved during analysis, the terrestrial contribution to Na^+ at Dome C would be below 10% during the Holocene and below 25% in the Last Glacial Maximum (LGM) (based on an average crustal Ca^{2+}/Na^+ ratio of 1.78 [*Bowen*, 1979]). For Cl^-, an additional source is HCl of volcanic origin. Such emissions are easily identified as they are fairly episodic and normally coincide with prominent SO_4^{2-} peaks.

[4] Past studies presenting Na^+ and Cl^- concentrations in Antarctic snow and ice have shown that the Cl^-/Na^+ ratio is very different from the seawater ratio [*Legrand et al.*, 1988; *Legrand and Delmas*, 1988a] with values at a single site sometimes being higher and sometimes lower than in seawater. A mechanism based on the reaction of sea-salt aerosol with acids leading to the formation of HCl has been proposed [*Legrand and Delmas*, 1988b]. Postdepositional HCl losses in surface snow have been observed on the East Antarctic plateau [*Wagnon et al.*, 1999], resulting in Cl^-/Na^+ ratios below the seawater ratio at a few meters depth. During the last glacial period, these losses seem less pronounced or absent, which has been assigned to shorter atmospheric residence times of the sea-salt aerosol [*Legrand and Delmas*, 1988b] allowing for less formation of HCl. However, there is no evidence for significantly shorter transport times during the last glacial period [*Lunt and Valdes*, 2001; *Krinner and Genthon*, 2003], and a recent study of dust particle sizes even tended to longer atmospheric residence times of the particles deposited at Dome C during the LGM [*Delmonte et al.*, 2002]. Thus no consistent explanation for the variation of the Cl^-/Na^+ ratio has been found so far.

[5] The present work identifies the mechanisms leading to changes in the Cl^-/Na^+ ratio preserved in Antarctic ice cores and describes the changing interplay of these factors over glacial-interglacial cycles. In order to explain the various determining factors, we use the new record from Dome C (75°06′S, 123°24′E) back to 45 kyr B.P. This section has been drilled and analyzed in the framework of the European Project for Ice Coring in Antarctica (EPICA) from 1996 to 1999.

2. Methods

[6] The chemical analysis of the ice core from Dome C was done by continuous flow analysis (CFA) for Na^+ and Ca^{2+} [*Röthlisberger et al.*, 2000a], fast ion chromatography (FIC) for Cl^- and SO_4^{2-} [*Udisti et al.*, 2000] and standard ion chromatography (IC) for all major ions [*Littot et al.*, 2002]. CFA and FIC were done in the field during the core processing campaigns. These two methods are based on a continuous sample obtained by melting a subsection of the ice core on a melter where the outer, possibly contaminated part of the sample, is discarded. CFA uses spectrophotometric methods for the determination of Na^+ and Ca^{2+} which produce data at a spatial resolution of the order of 1 cm (i.e., 0.35 yr during the Holocene and 0.9 yr during the LGM). FIC takes one sample every minute which is then analyzed by ion chromatography, which results in a spatial resolution of approximately 4 cm. IC analysis on discrete samples was done in five European laboratories after retrograding of the core. Detailed description of the methods can be found in the references cited above. Generally, we used 55-cm averages of the high-resolution records.

[7] In this study, we present Cl^- and Na^+ data from the IC analysis of discrete samples in order to compare Cl^- and Na^+ data that were measured on exactly the same sample. However, using CFA or FIC data leads to the same conclusions. The Ca^{2+} record shown was measured by CFA. The advantage of one method over the other and the agreement between the methods used is discussed in detail by *Littot et al.* [2002].

[8] On the basis of the sulphate record [*Udisti et al.*, 2000], we identified sections with volcanic input and checked for indication of significant amounts of Cl^- of volcanic origin. However, there were few events that showed markedly elevated Cl^- concentrations and the impact on the 55-cm averages was negligible. Therefore, we did not correct the record for potential volcanic Cl^-.

3. Observations

[9] The detailed Cl^- and Na^+ records from Dome C showed several different regimes with respect to the Cl^-/Na^+ ratio. At the snow surface, a considerable surplus of Cl^- relative to Na^+ is observed (Figure 1). However, in the first few meters, the Cl^- concentrations decrease steadily and at about 4 m depth, a Cl^- deficit relative to Na^+ is observed. This deficit is maintained throughout most of the Holocene, except for the time period between 8.8 and 11.3 kyr B.P. (Figure 2), where some excess Cl^- is observed. The excess during this early Holocene period is smaller than the excess found at the surface, but still remarkably high considering the rest of the Holocene. During the Last Glacial Maximum (18 to 24 kyr B.P.) the Cl^-/Na^+ ratio was rather constant and close to the ratio observed in seawater [*Bowen*, 1979]. In contrast to that, the Cl^-/Na^+ ratio showed large fluctuations in the earlier glacial period (35 to 45 kyr B.P.). Similar to the Cl^- concentrations also the nss-Ca^{2+} (nss$-Ca^{2+} = Ca_{tot}^{2+} - 0.038 * Na^+$) concentrations changed dramatically during this period, while the Na^+ concentrations were relatively stable. During the Eemian, the previous warm period, excess Cl^- was found in the Vostok ice core [*Legrand et al.*, 1988], contrasting the distinct Cl^- deficit observed during most of the Holocene in Vostok as well as in Dome C.

4. Discussion

[10] In the following sections, we discuss the main phenomena of the Cl^-/Na^+ ratio of the Dome C record, namely the observed Cl^- excess in surface snow and in the early Holocene, the depletion of Cl^- in the uppermost meters of the snowpack, and the stable Cl^-/Na^+ ratio close to the seawater ratio during the LGM. The factors responsible for these three aspects allow a consistent explanation of the Cl^-/Na^+ ratio observed in Antarctic ice cores.

4.1. Surface Excess of Cl^-

[11] Several studies have emerged lately showing considerable Cl^- depletion of sea-salt aerosols in coastal Antarctica during the summer months [*Kerminen et al.*, 2000; *Wagenbach et al.*, 1998]. Similar results have been

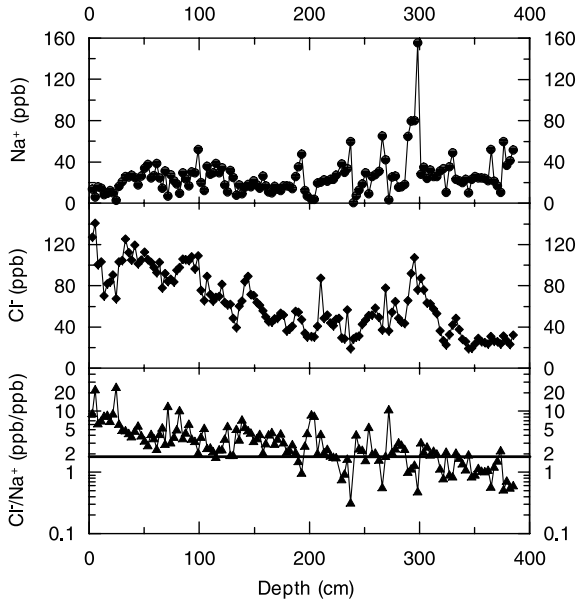

Figure 1. Cl^- and Na^+ concentrations and Cl^-/Na^+ ratio in the top 4 m of snow at Dome C, Antarctica. The thick horizontal line in the bottom graph reflects the Cl^-/Na^+ ratio in seawater. See color version of this figure in the HTML.

reported for South Pole summer aerosols [*Arimoto et al.*, 2001]. Recently, these findings have been confirmed in the context of a comprehensive, year-round aerosol monitoring campaign at the French station Dumont d'Urville, coastal Antarctica [*Jourdain and Legrand*, 2002]. The depletion during summer ranged from 10% to 90%, depending on the total sea-salt aerosol load and the aerosol size. On the basis of size-segregated analyses of the aerosols, HNO_3 accounted for some if not for most of the dechlorination of the aerosol [*Jourdain and Legrand*, 2002; *Kerminen et al.*, 2000] and sulphur species, mainly H_2SO_4, for the remainder. Dechlorination can likely occur both during transport and in the snowpack after deposition. This would then allow dechlorination even of sea salt deposited in winter, when atmospheric acidity in the coastal regions is low.

[12] The product of this dechlorination, HCl, has been measured in the atmosphere at Dumont d'Urville during a year-round monitoring campaign [*Jourdain and Legrand*, 2002]. It showed highest atmospheric HCl levels in summer, when dechlorination of the aerosol is most pronounced. The HCl concentrations matched the observed losses fairly well, with HCl only slightly exceeding the Cl^- deficit in the aerosol, which was attributed to a slightly longer atmospheric lifetime of HCl compared to sea-salt aerosol.

[13] This difference in atmospheric lifetime could partly explain the excess Cl^- observed in surface snow at inland Antarctic sites. While the sea-salt concentrations in snow drop rapidly with distance from the coast, the concentrations of sulphate, which is related to smaller aerosols, decrease more slowly [*Minikin et al.*, 1994]. HCl is either in the gas phase or associated to a smaller aerosol mode than Na^+ and most likely behaves similar to sulphur species, i.e., due to the longer atmospheric lifetime being transported more easily over long time periods. This results in the tendency to higher Cl^-/Na^+ ratios at sites further on the Antarctic plateau (Figure 3). The longer the transport route, the more transport favors Cl^- over coarse sea-salt particles and relatively more excess Cl^- arrives at the site.

[14] During winter however, no dechlorination of the sea-salt aerosol is observed at coastal Antarctica [*Jourdain and Legrand*, 2002]. On the contrary, a slight excess of Cl^- was observed arising from sea-salt aerosol produced from frost flowers. *Wagenbach et al.* [1998] reported a Na^+ depletion in winter aerosol at coastal Antarctica of up to 10%, which would contribute to the Cl^- excess at inland sites.

4.2. Postdepositional Loss of HCl

[15] As a result of the processes described, what is transported inland is sea-salt aerosol that is partly dechlorinated, along with HCl in the gas phase or on smaller aerosols. However, it has been shown that HCl is reversibly deposited to the snow surface: Although excess Cl^- is found in surface snow, part of it is released back into the boundary layer atmosphere. At some sites (e.g., Vostok [*Wagnon et al.*, 1999], Dome C (Figure 1)), this leads gradually to Cl^-/Na^+ ratios below the seawater ratio at a few meters depth, i.e., most of the initially deposited HCl has been reemitted and no longer balances the Cl^- deficit in sea-salt aerosol. Cl^-/Na^+ ratios below the seawater ratio are sustained during most of the Holocene (Figure 2, or for Vostok see [*Legrand et al.*, 1988]).

[16] Detailed investigations of postdepositional effects on other reversibly deposited substances (formaldehyde (HCHO) and hydrogen peroxide (H_2O_2)) have shown that apart from temperature also accumulation rate is a crucial factor for preservation in snow [*Hutterli et al.*, 2003]. There is a critical accumulation rate, below which most or all of the excess substance is released into the atmosphere again. Although the quantitative knowledge of the postdepositional processes affecting Cl^- is less advanced than for HCHO and H_2O_2, Cl^- profiles from other Antarctic sites indicate that the postdepositional losses are most pronounced at sites with accumulation rates below 4 g cm^{-2} yr^{-1} (see data archived at the National Snow and Ice Data Center, http://www.nsidc.org). At South Pole, for example, where the accumulation rate is estimated to be around 8 g cm^{-2} yr^{-1}, the Cl^-/Na^+ ratio does not drop below 1.8 [*Whitlow et al.*, 1992].

[17] Comparing the Dome C Holocene Cl^-/Na^+ record with the accumulation rate supports the hypothesis of accumulation rate dependent preservation of Cl^- (Figure 2). The accumulation rate [*Schwander et al.*, 2001], which has been derived from the deuterium record δD, was elevated during the early Holocene, approaching the estimated critical accumulation rate for the preservation of Cl^- of 4 g cm^{-2} yr^{-1}. During this period, the Cl^-/Na^+ ratio was again higher than the sea water ratio but considerably lower than in the uppermost snow layers (Figure 1), i.e., some HCl probably still escaped the snowpack after deposition. But HCl losses were reduced compared to the more recent Holocene due to the increased accumulation rate that preserved some excess Cl^-. This effect also explains the observed Cl^- excess in the Vostok record of the Eemian: The accumulation rate was higher during the Eemian than during the Holocene (above 3 g cm^{-2} yr^{-1}, F. Parrenin, personal communication, 2002), leading to better preservation of Cl^- in the snow.

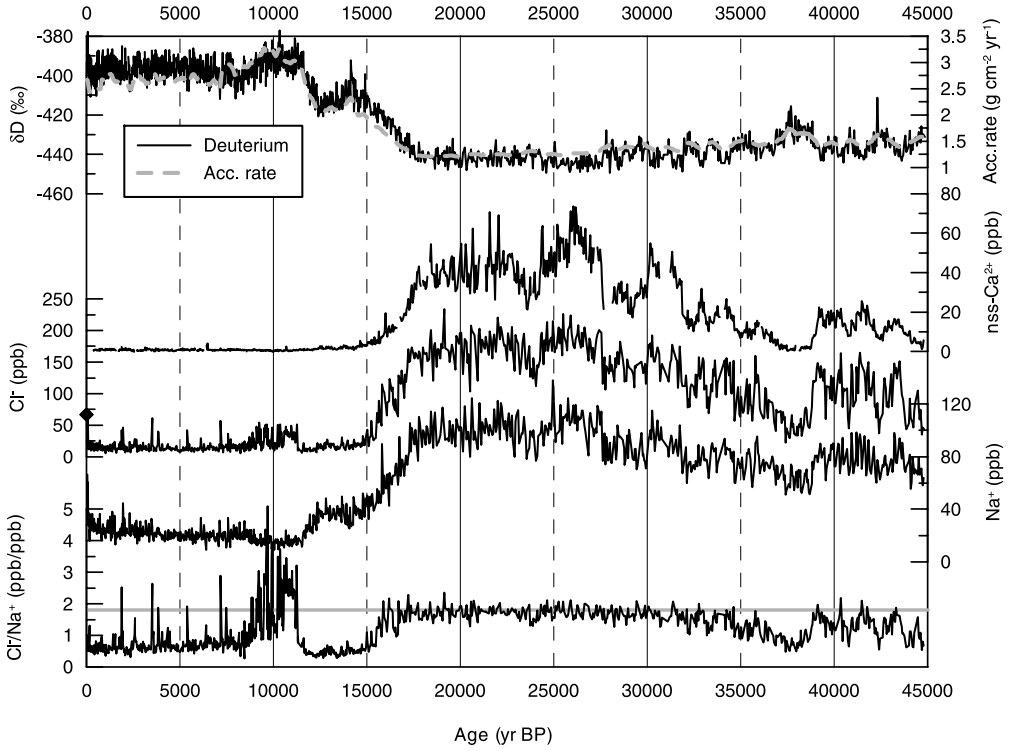

Figure 2. Cl^-/Na^+, Na^+, Cl^- and nss-Ca^{2+} records covering the past 45 kyr B.P. at 55 cm resolution together with δD [*Jouzel et al.*, 2001] and accumulation rate (yellow) [*Schwander et al.*, 2001]. The thick horizontal line in the bottom graph reflects the Cl^-/Na^+ ratio in seawater. The blue diamond on the left hand y axis corresponds to the Cl^-/Na^+ ratio averaged over the top 55 cm of the pit. See color version of figure in the HTML.

[18] In Figure 4a, the relationship between the Cl^-/Na^+ ratio and the accumulation rate is shown. The lowest Cl^-/Na^+ ratio is observed during the Antarctic Cold Reversal (ACR), and with increasing accumulation rate, the Cl^-/Na^+ ratio increased as well. However, the fact that the Cl^-/Na^+ ratio was higher during the glacial period than during the ACR despite even lower accumulation rates seems inconsistent with the postulated relationship between Cl^-/Na^+ and accumulation rate and is discussed in the following section.

4.3. Limited HCl Formation Due to High Dust Levels

[19] As seen in Figures 2 and 4a, the Cl^-/Na^+ ratio was higher during the last glacial period than during the ACR and most of the recent Holocene. In the LGM the Cl^-/Na^+ ratio remained fairly stable at the level of the seawater ratio. If the reactions between sea-salt aerosols and acids in the atmosphere were still responsible for significant dechlorination of sea-salt aerosol during the LGM, it would be very unlikely to result in a Cl^-/Na^+ ratio at Dome C that is so close to the seawater ratio. We therefore suggest that the dechlorination of sea-salt aerosol was suppressed during the LGM, limiting the formation of HCl which could escape the snowpack after deposition.

[20] It has been suggested that shorter residence times reduced the reaction between sea-salt aerosol and H_2SO_4 [*Legrand and Delmas*, 1988b], but there is no indication for significant changes in residence time. The size distribution of dust particles of the LGM suggests a tendency to longer residence times during this period [*Delmonte et al.*, 2002] and current transport models give no evidence for significantly faster transport in the LGM either [*Lunt and Valdes*, 2001; *Krinner and Genthon*, 2003].

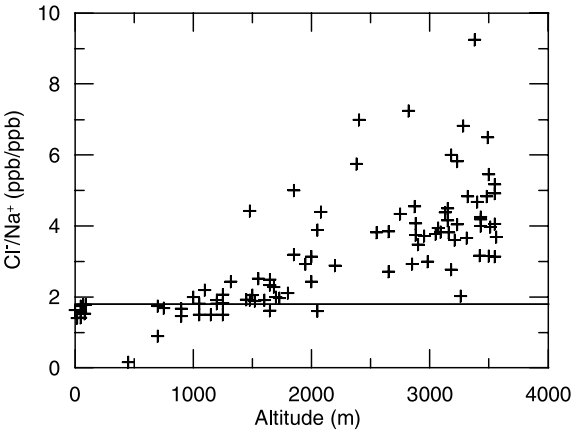

Figure 3. Cl^-/Na^+ ratio in surface snow along the 1990 International Trans-Antarctic Expedition (data from *Qin et al.* [1999]). See color version of this figure in the HTML.

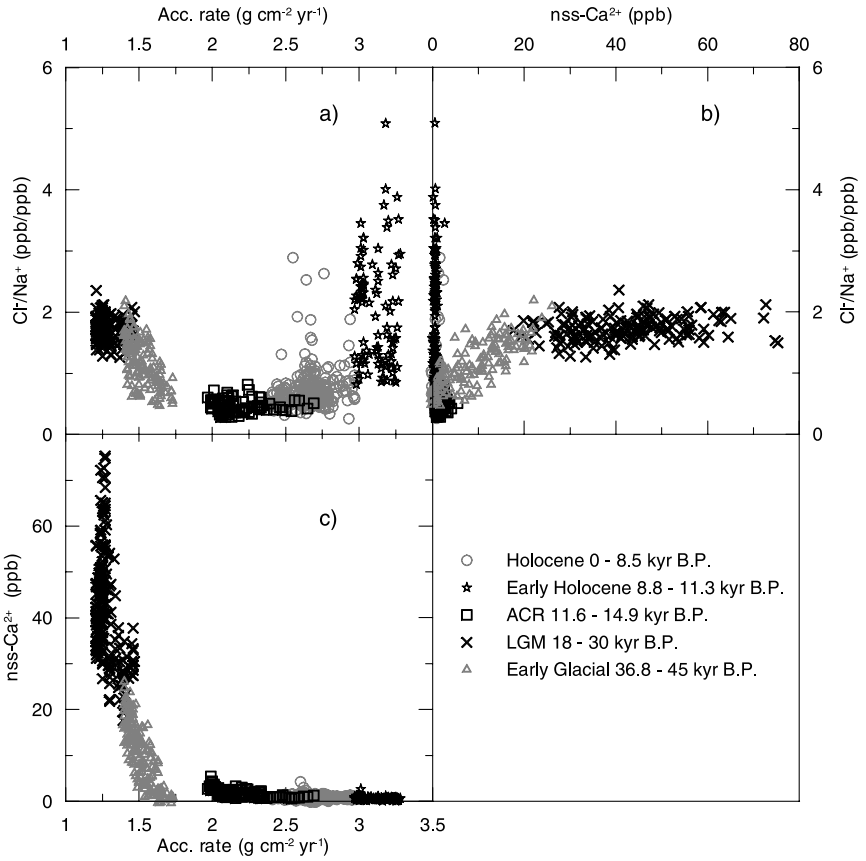

Figure 4. Relationships between the Cl^-/Na^+ ratio, accumulation rate and nss-Ca^{2+} at Dome C during different periods (55-cm averages). ACR covers the period of the Antarctic cold reversal during the transition from the LGM to the Holocene. See color version of this figure in the HTML.

[21] The Cl^-/Na^+ ratio remained close to the seawater ratio during periods with high nss-Ca^{2+} concentration (a proxy for dust) as seen in Figure 2. It is known that uptake on dust is an efficient pathway for HNO_3 removal [*Hanisch and Crowley*, 2001] and there is evidence for such reactions to have happened during the LGM in Antarctica [*Röthlisberger et al.*, 2000b]. It is conceivable that H_2SO_4 is neutralized as well, but unlike for HNO_3, this has no effect on the preservation of SO_4^{2-} in snow and can thus not be inferred from ice core records. Studies regarding the agents responsible for the dechlorination of sea salt are not yet fully conclusive: *Kerminen et al.* [2000] found that H_2SO_4 causes slightly more of the observed dechlorination than HNO_3, and that even MSA (methane sulphonic acid) contributes to some extent. *Jourdain and Legrand* [2002], on the other hand, attribute most of the dechlorination to HNO_3, with little effect of the sulphur compounds.

[22] During the LGM, the Na^+ flux at Dome C doubled, whereas the dust flux was more than 20 times higher than during the Holocene [*Röthlisberger et al.*, 2002a]. Such a high dust load could reduce the atmospheric lifetime of HNO_3 by a factor of 25 [*Röthlisberger et al.*, 2002b] and could make the effect of dechlorination caused by HNO_3 negligible. On the basis of the balance of anions and cations, we estimate that the dechlorination is equally caused by HNO_3 and H_2SO_4 under present-day conditions. By eliminating the effect of HNO_3 under glacial conditions, dechlorination would be reduced by a factor of 2. On the other hand, the SO_4^{2-} flux during the LGM was comparable to the Holocene flux [*Traversi et al.*, 2002]. Given the greatly enhanced abundance of dust relative to sea salt during the LGM, it seems likely that some of the H_2SO_4 reacted with dust which led to a further reduction in dechlorination.

[23] In Figure 4b, the relationship between the Cl^-/Na^+ ratio and nss-Ca^{2+} is shown. During the LGM, the Cl^-/Na^+ ratio is fairly constant, independent of the nss-Ca^{2+} level. It seems as if a critical atmospheric dust level to prevent significant dechlorination is reached when nss-Ca^{2+} concentrations at Dome C are around 20 ppbw. In the earlier part of the glacial period, however, dust levels drop markedly (see Figures 2 and 4c and *Röthlisberger et al.* [2002a]), leading to the formation and subsequent postdepositional loss of HCl. During the transition and the Holocene, dust levels are extremely low and have no impact on the Cl^-/Na^+ ratio.

5. Conclusions

[24] The key to understanding the Cl^-/Na^+ ratio of the Dome C ice core record lies in the formation of HCl and the subsequently partly independent transport of Cl^- and Na^+

as well as the postdepositional formation and reemission of HCl from the snow pack.

[25] We have shown that, under present-day conditions, significant excess of Cl^- over Na^+ is found at inland Antarctic sites due to the formation of gas-phase HCl and the subsequent fractionation processes during long-range transport, due to Na^+ depletion of winter sea-salt aerosol and due to redeposition of HCl that has been emitted from deeper snow layers. During the LGM the formation of HCl was strongly reduced due to high dust levels relative to sea salt that neutralized HNO_3 and H_2SO_4 to some extent. Therefore, no HCl that could be reemitted was formed and the Cl^-/Na^+ ratio at Dome C remained close to the sea water ratio. In the earlier part of the glacial period, dust levels dropped and accordingly, dechlorination of sea salt increased again, leading to the formation and postdepositional loss of HCl.

[26] At sites with very low accumulation rates, the reemission of HCl from the surface snow might contribute to the abundance of HCl at the air-snow interface. The reemission of HCl is highly dependent on the accumulation rate, apart from other factors such as for example temperature. At accumulation rates below 4 g cm^{-2} yr^{-1}, the postdepositional losses lead to a Cl^- deficit relative to Na^+ below the surface layers, as observed at Dome C during the later part of the Holocene. The strong accumulation rate dependency is most likely the reason for the increase in the Cl^-/Na^+ ratio to values above the seawater ratio during the early Holocene and the Eemian. This dependency could, if quantified, serve as an independent indicator of changes in accumulation rate within a small sensitive range. If additional substances with different accumulation sensitivities are combined, one might achieve an estimate of the accumulation rate. However, a prerequisite for this is a quantitative understanding of the postdepositional processes affecting Cl^-. For this purpose, atmospheric measurements combined with surface snow analyses at inland sites (e.g., Dome C) as well as laboratory studies are needed.

[27] **Acknowledgments.** This work is contribution 62 to the "European Project for Ice Coring in Antarctica" (EPICA), a joint ESF (European Science Foundation)/EC scientific programme, funded by the European Commission and by national contributions from Belgium, Denmark, France,Germany, Italy, Netherlands, Norway, Sweden, Switzerland and the United Kingdom. R.R. thanks the Swiss National Foundation for financial support.

References

Arimoto, R., A. S. Nottingham, J. Webb, C. A. Schloesslin, and D. D. Davis, Non-sea salt sulfate and other aerosol constituents at the South Pole during ISCAT, *Geophys. Res. Lett.*, *28*, 3645–3648, 2001.

Bowen, H. J. M., *Environmental Chemistry of the Elements*, Academic, San Diego, Calif., 1979.

Delmonte, B., J. R. Petit, and V. Maggi, Glacial to Holocene implications of the new 27,000-year dust record from the EPICA Dome C (East Antarctica) ice core, *Clim. Dyn.*, *18*, 647–660, 2002.

Hanisch, F., and J. N. Crowley, Heterogeneous reactivity of gaseous nitric acid on Al_2O_3, $CaCO_3$, and atmospheric dust samples: A Knudsen cell study, *J. Phys. Chem. A*, *105*, 3096–3106, 2001.

Hutterli, M. A., J. R. McConnell, R. C. Bales, and R. W. Stewart, Sensitivity of hydrogen peroxide (H_2O_2) and formaldehyde (HCHO) preservation in snow to changing environmental conditions: Implications for ice core records, *J. Geophys. Res.*, *108*(D1), 4023, doi:10.1029/2002JD002528, 2003.

Jourdain, B., and M. Legrand, Year-round records of bulk and size-segregated aerosol composition and HCl and HNO_3 levels in the Dumont d'Urville (coastal Antarctica) atmosphere: Implications for sea-salt aerosol fractionation in the winter and summer, *J. Geophys. Res.*, *107*(D22), 4645, doi:10.1029/2002JD002471, 2002.

Jouzel, J., et al., A new 27 ky high resolution East Antarctic climate record, *Geophys. Res. Lett.*, *28*, 3199–3202, 2001.

Kerminen, V. M., K. Teinilä, and R. Hillamo, Chemistry of sea-salt particles in the summer Antarctic atmosphere, *Atmos. Environ.*, *34*, 2817–2825, 2000.

Krinner, G., and C. Genthon, Tropospheric transport of continental tracers towards Antarctica under varying climatic conditions, *Tellus, Ser. B*, *55*, 54–70, 2003.

Legrand, M., and R. J. Delmas, Soluble impurities in four Antarctic ice cores over the last 30,000 years, *Ann. Glaciol.*, *10*, 116–120, 1988a.

Legrand, M., and R. J. Delmas, Formation of HCl in the Antarctic atmosphere, *J. Geophys. Res.*, *93*, 7153–7168, 1988b.

Legrand, M., C. Lorius, N. I. Barkov, and V. N. Petrov, Vostok (Antarctica) ice core: Atmospheric chemistry changes over the last climatic cycle (160,000 years), *Atmos. Environ.*, *22*, 317–331, 1988.

Littot, G. C., et al., Comparison of analytical methods used for measuring major ions in the EPICA Dome C (Antarctica) ice core, *Ann. Glaciol.*, *35*, 299–305, 2002.

Lunt, D. J., and P. J. Valdes, Dust transport to Dome C, Antarctica at the Last Glacial Maximum and present day, *Geophys. Res. Lett.*, *28*, 295–298, 2001.

Minikin, A., D. Wagenbach, W. Graf, and J. Kipfstuhl, Spatial and seasonal variations of the snow chemistry at the central Filchner-Ronne ice shelf, Antarctica, *Ann. Glaciol.*, *20*, 283–290, 1994.

Qin, D., P. Mayewski, R. Jiawen, X. Cunde, and S. Junying, The Weddell Sea region: An important precipitation channel to the interior of the Antarctic ice sheet as revealed by glaciochemical investigation of surface snow along the longest trans-Antarctic route, *Ann. Glaciol.*, *29*, 55–60, 1999.

Rankin, A. M., E. W. Wolff, and S. Martin, Frost flowers: Implications for tropospheric chemistry and ice core interpretation, *J. Geophys. Res.*, *107*(D23), 4683, doi:10.1029/2002JD002492, 2002.

Röthlisberger, R., M. Bigler, M. Hutterli, S. Sommer, B. Stauffer, H. G. Junghans, and D. Wagenbach, Technique for continuous high-resolution analysis of trace substances in firn and ice cores, *Environ. Sci. Technol.*, *34*, 338–342, 2000a.

Röthlisberger, R., M. A. Hutterli, S. Sommer, E. W. Wolff, and R. Mulvaney, Factors controlling nitrate in ice cores: Evidence from the Dome C deep ice core, *J. Geophys. Res.*, *105*, 20,565–20,572, 2000b.

Röthlisberger, R., R. Mulvaney, E. W. Wolff, M. A. Hutterli, M. Bigler, S. Sommer, and J. Jouzel, Dust and sea-salt variability in central East Antarctica (Dome C) over the Last 45 kyrs and its implications for southern high-latitude climate, *Geophys. Res. Lett.*, *29*(20), 1963, doi:10.1029/2002GL015186, 2002a.

Röthlisberger, R., et al., Nitrate in Greenland and Antarctic ice cores: A detailed description of post-depositional processes, *Ann. Glaciol.*, *35*, 209–216, 2002b.

Schwander, J., J. Jouzel, C. U. Hammer, J. R. Petit, R. Udisti, and E. Wolff, A tentative chronology for the EPICA Dome Concordia ice core, *Geophys. Res. Lett.*, *28*, 4243–4246, 2001.

Traversi, R., S. Becagli, E. Castellano, A. Migliori, M. Severi, and R. Udisti, High resolution Fast Ion Chromatography (FIC) measurements of chloride, nitrate and sulphate along the EPICA Dome C ice core, *Ann. Glaciol.*, *35*, 291–298, 2002.

Udisti, R., S. Becagli, E. Castellano, R. Mulvaney, J. Schwander, S. Torcini, and E. Wolff, Holocene electrical and chemical measurements from the EPICA-Dome C ice core, *Ann. Glaciol.*, *30*, 20–26, 2000.

Wagenbach, D., F. Ducroz, R. Mulvaney, L. Keck, A. Minikin, M. Legrand, J. S. Hall, and E. W. Wolff, Sea-salt aerosol in coastal Antarctic regions, *J. Geophys. Res.*, *103*, 10,961–10,974, 1998.

Wagnon, P., R. J. Delmas, and M. Legrand, Loss of volatile acid species from upper firn layers at Vostok, Antarctica, *J. Geophys. Res.*, *104*, 3423–3431, 1999.

Whitlow, S., P. A. Mayewski, and J. E. Dibb, A comparison of major chemical species seasonal concentration and accumulation at the South Pole and Summit, Greenland, *Atmos. Environ., Part A*, *26*, 2045–2054, 1992.

M. Bigler and M. A. Hutterli, Climate and Environmental Physics, University of Bern, Sidlerstrasse 5, 3012 Bern, Switzerland.

M. de Angelis, Laboratoire de Glaciologie et Géophysique de l'Environnement, CNRS, BP96 38402 St. Martin d'Hères, France.

M. E. Hansson Physical Geography and Quaternary Geology, Stockholm University, 106 91, Stockholm, Sweden.

R. Mulvaney and E. W. Wolff, British Antarctic Survey, Natural Environment Research Council, Madingley Road, Cambridge CB3 0ET, UK.

R. Röthlisberger, NCCR Climate, University of Bern, Erlachstrasse 9a, 3012 Bern, Switzerland. (regine@giub.unibe.ch)

J. P. Steffensen, Department of Geophysics, University of Copenhagen, Juliane Maries Vej 30, 2100 Copenhagen, Denmark.

R. Udisti, Department of Chemistry, University of Florence, Via della Lastruccia 3, 50019 Sesto Fiorentino, Italy.

2.9 Nitrate in Greenland and Antarctic ice cores: A detailed description of post-depositional processes

Regine Röthlisberger, Manuel A. Hutterli, Eric W. Wolff,
Rob Mulvaney, Hubertus Fischer, Matthias Bigler,
Kumiko Goto-Azuma, Margareta E. Hansson, Urs Ruth,
Marie-Louise Siggaard-Andersen, Jørgen Peder Steffensen

Annals of Glaciology
35, 209–216, 2002

Annals of Glaciology 35 2002

Nitrate in Greenland and Antarctic ice cores: a detailed description of post-depositional processes

Regine RÖTHLISBERGER,[1,2] Manuel A. HUTTERLI,[3] Eric W. WOLFF,[2] Robert MULVANEY,[2] Hubertus FISCHER,[4] Matthias BIGLER,[1] Kumiko GOTO-AZUMA,[5] Margareta E. HANSSON,[6] Urs RUTH,[4,7] Marie-Louise SIGGAARD-ANDERSEN,[8] Jørgen P. STEFFENSEN[8]

[1]*Climate and Environmental Physics, University of Bern, Sidlerstrasse 5, CH-3012 Bern, Switzerland*
[2]*British Antarctic Survey, Natural Environment Research Council, Madingley Road, Cambridge CB3 0ET, England*
E-mail: rro@bas.ac.uk
[3]*Department of Hydrology and Water Resources, University of Arizona, Tucson, AZ 85721-0011, U.S.A.*
[4]*Alfred Wegener Institute for Polar and Marine Research, P.O. Box 120161, D-27515 Bremerhaven, Germany*
[5]*National Institute of Polar Research, 9-10, Kaga 1-chome, Itabashi-ku, Tokyo 173-8515, Japan*
[6]*Department of Physical Geography and Quaternary Geology, Stockholms Universitet, S-106 91 Stockholm, Sweden*
[7]*Institut für Umweltphysik, Universität Heidelberg, Im Neuenheimer Feld 299, D-69120 Heidelberg, Germany*
[8]*Department of Geophysics, The Niels Bohr Institute for Astronomy, Physics and Geophysics, University of Copenhagen, Juliane Maries Vej 30, DK-2100 Copenhagen, Denmark*

ABSTRACT. A compilation of nitrate (NO_3^-) data from Greenland has shown that recent NO_3^- concentrations reveal a temperature dependence similar to that seen in Antarctica. Except for sites with very low accumulation rates, lower temperatures tend to lead to higher NO_3^- concentrations preserved in the ice. Accumulation rate, which is closely linked to temperature, might influence the concentrations preserved in snow as well, but its effect cannot be separated from the temperature imprint. Processes involved in NO_3^- deposition are discussed and shown to be temperature- and/or accumulation-rate-dependent. Apart from scavenging of nitric acid (HNO_3) during formation of precipitation, uptake of HNO_3 onto the ice crystal's surface during and after precipitation seems to contribute further to the NO_3^- concentrations found in surface snow. Post-depositional loss of NO_3^- from the top snow layers is caused by release of HNO_3 and by photolysis of NO_3^-. It is suggested that photolysis accounts for considerable losses at sites with very low accumulation rates. Depending on the site characteristic, and given that the temperature and accumulation-rate dependence is quantified, it should be possible to infer changes in atmospheric HNO_3 concentrations.

INTRODUCTION

The nitrate (NO_3^-) record in polar ice cores is expected to contain information about past atmospheric concentrations of nitrogen oxides ($NO_x = NO + NO_2$) due to the close link between NO_3^- and NO_x. The increase in atmospheric NO_x concentrations in the Northern Hemisphere caused by rising fossil-fuel combustion since approximately 1940, for example, is reflected in higher NO_3^- concentrations in Greenland snow (Neftel and others, 1985). However, past studies have shown that factors other than atmospheric NO_x concentrations also influence NO_3^- records (Wolff, 1995). In Greenland as well as in Antarctica, reversible deposition of NO_3^- and net losses in the top snow layers have been observed. It has been suggested that either re-evaporation of nitric acid (HNO_3) (Dibb and others, 1998; Mulvaney and others, 1998; Röthlisberger and others, 2000a) or photolysis of NO_3^- in the top few centimetres of the snowpack (Honrath and others, 2000; Jones and others, 2000) causes such post-depositional alterations.

In earlier studies, relationships between NO_3^- and accumulation rate have been proposed (Herron, 1982; Legrand and Kirchner, 1990; Yang and others, 1995), with generally higher accumulation rates associated with lower NO_3^- concentrations and higher NO_3^- depositional fluxes. In a more recent study based on a macroscopic deposition model, Fischer and others (1998) found a second-order polynomial dependence of average firn concentration and inverse snow accumulation.

Based on a compilation of NO_3^- data from more than 50 Antarctic sites covering various temperature and accumulation regimes, it has recently been suggested that temperature is also a key parameter in defining NO_3^- concentrations in Antarctic snow and ice, with lower temperatures leading to higher NO_3^- concentrations preserved in the snow (Röthlisberger and others, 2000a). Elevation has also been linked to NO_3^- concentrations, for both Greenland and Antarctica (Mulvaney and Wolff, 1994; Yang and others, 1996), but no statistically significant relationship has been found in a more recent study (Kreutz and Mayewski, 1999). The inherent connection between temperature, accumulation rate and elevation makes it difficult to distinguish between the separate effects, and no firm conclusions about their relative importance have yet been reached.

Here, we provide a detailed description of the processes involved in NO_3^- re-emission and a discussion of how temperature and accumulation rate affect those processes. In analogy to the compilation of NO_3^- data from Antarctic

Table 1. Temperature, accumulation rate and NO_3^- concentration for Greenland locations used in this study

Site (source)	*Location*	*Altitude*	*Temperature*	*Accumulation*	*NO_3^- pre-1940*		*NO_3^- post-1970*	
					Concentration	*Number of years*	*Concentration*	*Number of years*
		m	°C	g cm^{-2} a^{-1}	ppb		ppb	
1988-8[1]	64.6° N, 43.7° W	2550	−19.9	57			94	2
1988-7[1]	64.8° N, 44.1° W	2745	−22.0	38			90	3
Dye 3 18C[2], 20D[3]	65.0° N, 44.9° W	2617	−22.3	41	53,55	174[a],30[c]	100,122,132	15,5,15
Dye 3[2,4]	65.2° N, 43.8° W	2491	−20.0	49	44,52,52	10[b],11[b],220[h]	86,114,137	6,7,2
1988-4[1]	66.6° N, 45.5° W	2130	−18.6	30			117	2
1988-5[1]	67.0° N, 44.5° W	2250	−20.3	33			115	4
1988-6[1]	67.2° N, 43.8° W	2450	−21.6	36			108	6
EGIG T05[5]	69.9° N, 47.3° W	1910	−18.0	46			118	5
EGIG T09[5]	70.0° N, 46.3° W	2170	−20.0	41			134	9
EGIG T13[5]	70.2° N, 45.0° W	2380	−22.6	46			107	8
Milcent[2]	70.3° N, 44.6° W	2410	−22.0	49	61	7[g]		
EGIG T17[5]	70.4° N, 44.1° W	2530	−23.8	44			117	9
EGIG T21[5]	70.6° N, 43.0° W	2700	−24.8	44			112	9
Site A[2,6]	70.6° N, 35.8° W	3092	−29.4	29	45,64,70	3[d],2[c],19[b]		
Site D[6]	70.6° N, 39.6° W	3018	−28.3	34	73	19[b]		
EGIG T27[5]	70.8° N, 41.6° W	2870	−26.6	39			113	9
EGIG T31[5]	70.9° N, 40.6° W	2970	−27.5	34			133	10
EGIG T41[5]	71.1° N, 37.9° W	3150	−29.5	25			144	12
Crête[2]	71.1° N, 37.3° W	3172	−30.0	28	60,80	60[c],2[g]		
EGIG T43[5]	71.1° N, 37.3° W	3172	−30.1	23			144,146	8,14
EGIG T47[5]	71.2° N, 36.0° W	3099	−29.9	22			143	8
Renland[7,8]	71.3° N, 26.7° W	2340	−18.0	42	64,88	5[g],9[c]		
EGIG T53[5]	71.4° N, 32.5° W	2864	−28.0	23			134	9
1987-2[1]	71.6° N, 38.1° W	3157	−30.4	25			128	5
EGIG NST08[5]	71.9° N, 37.8° W	3220	−31.0	23			153	5
1987-3[1]	71.9° N, 39.8° W	3145	−30.3	30			123	2
1987-5[1]	72.0° N, 37.5° W	3187	−31.5	22			130	6
EGIG T61[5]	72.2° N, 32.3° W	2812	−28.8	19			144	8
1987-1[1]	72.3° N, 37.9° W	3170	−31.3	22			124	10
1987-4[1]	72.4° N, 40.2° W	3146	−31.5	27			130	5
GISP2 ATM[1]	72.4° N, 38.8° W	3200	−32.0	24			120,130,135,138	3,5,9,3
EGIG T66[5]	72.5° N, 30.8° W	2678	−25.7	17			159	6
GISP2[1,9,10]	72.6° N, 38.5° W	3200	−31.0	22	61,70	410[a],650[a]	108,125,126,135,136,149,149,167	30,7,3,6,6,2,2,4
GRIP[5,11,12]	72.6° N, 37.6° W	3232	−31.6	20	68	30[c]	130,138,142	5,9,21
1987-7[1]	72.6° N, 35.9° W	3190	−33.1	18			157	8
1990-2[1]	72.8° N, 36.5° W	3200	−33.8	17			136	1
1987-6[1]	73.0° N, 37.7° W	3224	−33.8	17			148	8
NGT01[13]	73.0° N, 37.7° W	3223	−34.3	16			143	13
NGT03 B16[13]	73.9° N, 37.6° W	3040	−34.6	12	85	40[a]	132	23
North Central[2]	74.6° N, 39.6° W	2930	−32.0	13	83,112	9[f],21[b]	164	5
NGT05[13]	74.9° N, 37.6° W	2873	−35.3	11			189	12
NGRIP[8,14]	75.1° N, 42.1° W	2978	−30.9	17	81	156[a]	149,161	5,11
NGT12[13]	75.7° N, 36.4° W	2671	−34.2	10			161	14
NGT14 B18[13]	76.6° N, 36.4° W	2508	−35.0	10	73	40[a]	128	23
Camp Century[2]	77.2° N, 61.1° W	1880	−24.4	35	46,65,71	10[g],13[d],100[h]	120	2
1988-1[1]	77.2° N, 60.7° W	1650	−24.6	29			101	7
1988-2,3[1]	77.2° N, 59.2° W	1700	−23.7	31			96,107	4,2
Camp Century II[2]	77.2° N, 60.8° W	1910	−24.7	35	52	13[b]		
NGT37 B26[15]	77.3° N, 49.2° W	2598	−30.0	18	69	440[a]	110	24
NGT18[13]	77.5° N, 36.4° W	2319	−32.6	11			158	14
NGT23 B20[16]	78.8° N, 36.5° W	2147	−31.5	10	83	1130[a]	155	24
NGT27 B21[13]	80.0° N, 41.1° W	2185	−29.6	11	80	40[a]	126	24
Hans Tausen[8]	80.5° N, 37.5° W	1271	−21.0	10	74	30[c]	91	3

Notes: [1]Yang and others (1996), data obtained from http://nsidc.org. [2]Clausen and Langway (1989). [3]Mayewski and others (1990). [4]Neftel and others (1985). [5]Fischer and Wagenbach (1996). [6]Steffensen (1988). [7]Hansson (1994). [8]H. B. Clausen, personal communication (2001). [9]Yang and others (1995). [10]University of Arizona, unpublished data. [11]Clausen and others (1997). [12]Steffensen and others (1996). [13]Fischer and others (1998). [14]L. B. Larsen, personal communication (2001). [15]Hausbrand (1998). [16]Bigler (2000). [a]Continuous record up to 1940. [b]20th century, before 1940. [c]19th century. [d]18th century. [e]11th to 18th century. [f]15th century. [g]13th century. [h]Holocene.

sites, NO_3^- data from many Greenland sites have been gathered in order to illustrate the effect of temperature. Also, we outline how calcium (Ca^{2+}) can inhibit NO_3^- re-emission.

Another aspect that has been discussed lately is the effect on NO_3^- concentrations of snow layers containing large amounts of sulphuric acid (H_2SO_4) of volcanic origin. Most studies focused on a few well-known volcanic eruptions during the Holocene which showed post-depositional displacement of NO_3^- away from the H_2SO_4 peak. This behaviour has been found in single events in Greenland and Antarctica (Legrand and Kirchner, 1990; Clausen and others, 1997; Röthlisberger and others, 2000a). However, the mechanisms leading to this effect are only vaguely understood, and hypotheses have not been tested on a large number of cases, because of a lack of sufficient high-resolution data.

In this paper, new high-resolution data from the North-

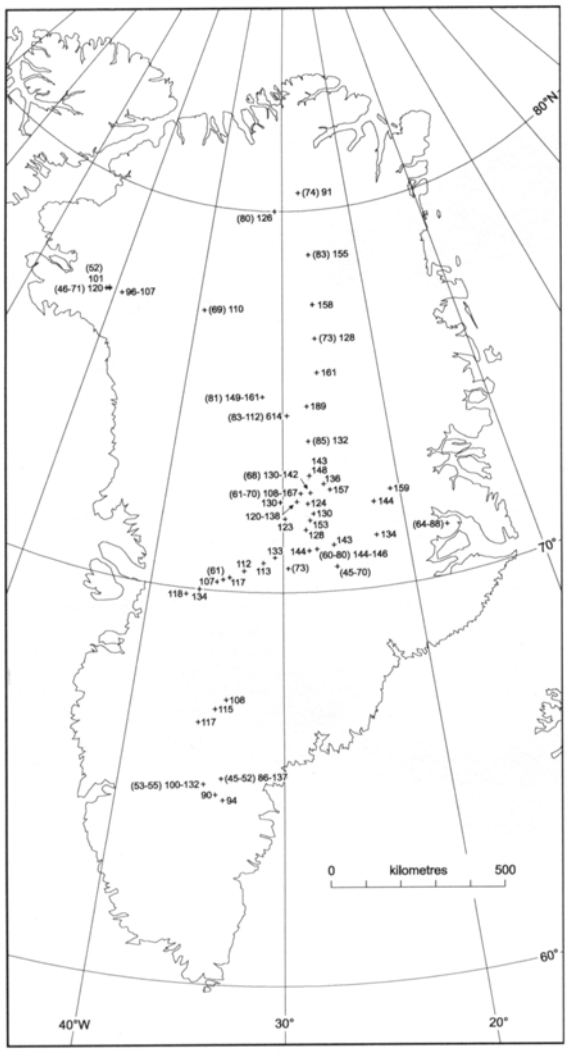

Fig. 1. Spatial distribution of NO_3^- across Greenland. Concentrations in snow deposited before 1940 are shown in parentheses; the other values correspond to concentrations in snow deposited after 1970. All concentrations are in ppb.

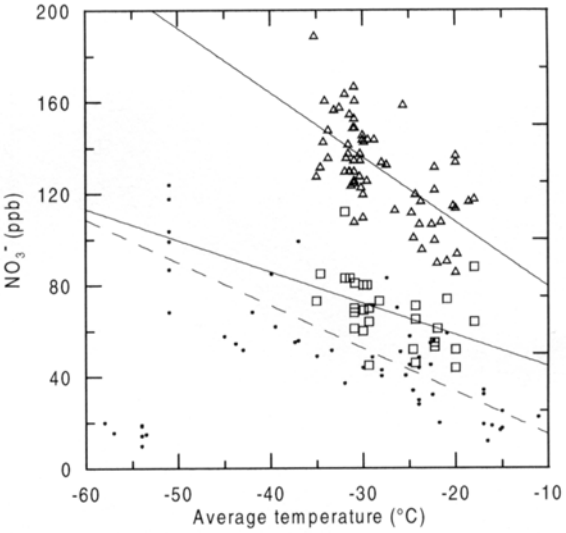

Fig. 2. NO_3^- concentrations vs average temperatures in Greenland and Antarctica with linear trends (triangles: post-1970; squares: pre-1940; solid lines: Greenland; dots and dashed line: Antarctica). The data points at temperatures below −52°C correspond to sites with very low accumulation rates and are not used for the calculation of the linear fit shown.

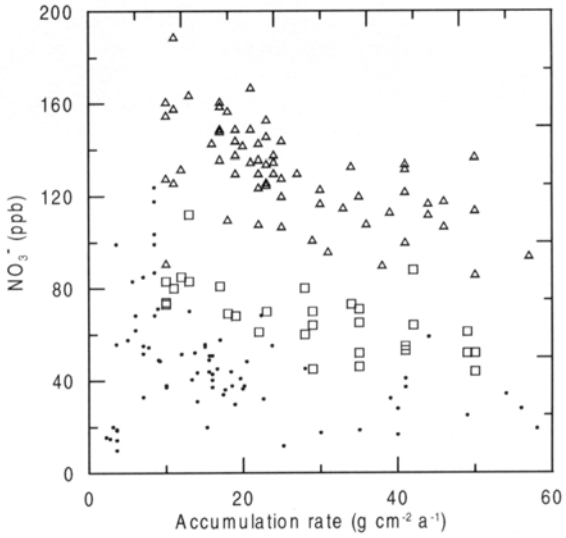

Fig. 3. NO_3^- concentrations vs accumulation rate in Greenland and Antarctica (triangles: post-1970; squares: pre-1940; dots: Antarctica).

GRIP (North Greenland Ice Core Project) ice core are used to investigate in more detail the effect of volcanic H_2SO_4 on NO_3^-. Volcanic events from the early Holocene, the Last Glacial Maximum (LGM) and some earlier glacial periods are compared and a hypothesis of the mechanism is given.

DATA

Many of the NO_3^- data used in this paper are compiled from earlier studies (see Table 1 for sources). Furthermore, data from selected sections of the NorthGRIP ice core (75.1° N, 42.05° W; 2978 m a.s.l.) are presented. These sections were analyzed during the NorthGRIP 2000 field season with a continuous flow analysis (CFA) system, as described in Röthlisberger and others (2000b). Among other compounds, nitrate (NO_3^-), sulphate (SO_4^{2-}) and calcium (Ca^{2+}) have been measured at a resolution of approximately 1 cm.

NO_3^-, TEMPERATURE AND ACCUMULATION RATE

In Figure 1, average NO_3^- concentrations for different Greenland locations are indicated. In order to account for the anthropogenic increase in NO_3^- concentrations in Greenland, the data have been split into two separate sets, one indicating concentrations from before 1940, which are unaffected by the anthropogenic emissions, and one from after 1970. The data and their sources are listed in Table 1. For both pre-1940 and post-1970, a decreasing trend in NO_3^- concentration with increasing temperature is found (Fig. 2). A similar trend has been found in Antarctica (Röthlisberger and others, 2000a),

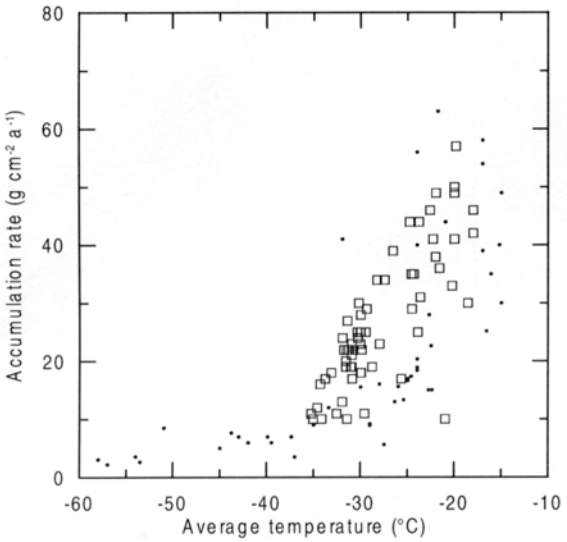

Fig. 4. Accumulation rate vs average temperatures in Greenland and Antarctica (squares: Greenland; dots: Antarctica).

where also generally higher concentrations are found at sites with lower temperatures, except for very low-accumulation sites (e.g. Dome C). At Dome C, the concentrations in the top few centimetres can be very high (up to 1000 ppb), but at greater depths, only 15 ppb are preserved, despite the low temperatures (annual mean temperature ≈ −54°C).

When NO_3^- concentrations are plotted against accumulation rate, higher NO_3^- concentrations are found at sites with lower accumulation rates (Fig. 3), but again, NO_3^- concentrations at very low-accumulation sites do not agree with the general trend. Considering the close relationship between temperature and accumulation rate (Fig. 4), it seems difficult to separate their effects on NO_3^- concentrations. Only a detailed consideration of the underlying microphysical processes allows for assigning a temperature or accumulation-rate dependence.

In the following discussion, we analyze the temperature and accumulation-rate dependence of processes involved in NO_3^- deposition and re-emission, aiming for a better understanding of:

the cause of the relationship between NO_3^- concentrations and mean annual temperature and accumulation rate at a site

the generally higher NO_3^- levels in summer snow than in winter snow

the net loss of NO_3^- from snow after deposition.

NO_3^- can either be predominantly incorporated in the bulk or be adsorbed to the surface of a snow crystal, depending on the deposition pathway. In a cloud with a liquid-water content of >0.01 g m^{-3} and pH > 1, HNO_3 would be completely dissolved in water droplets due to its high solubility, leaving virtually no HNO_3 in the gas phase (Seinfeld and Pandis, 1998). Thus, in the case of liquid or mixed clouds, essentially all HNO_3 is removed from the gas phase independent of the cloud temperature. While there is no specific information about the conditions at cloud level, typical liquid-water contents of 0.1 g m^{-3} and initial HNO_3 concentrations of 20 pptv in the air would lead to NO_3^- concentrations of

Table 2. Estimates of NO_3^- concentrations in snow due to different deposition mechanisms

	Summit		*Neumayer*		*South Pole*	
	Summer	*Winter*	*Summer*	*Winter*	*Summer*	*Winter*
Pressure (Pa)	67 000		99 000		68 000	
Accumulation rate (g cm^{-2} a^{-1})	20		34		8.5	
Temperature (K)	259	230	269	247	246	208
Relative humidity	0.75	0.75	0.8	0.8	0.75	0.6
HNO_3 atm. (pptv)	20	1	6	1	20	1
NO_3^- snow (ppbw)	120		50		100	
Co-condensation (ppbw)	7	9	1	2	26	160
Solubility in ice (ppbw)	19	29	8	12	40	150
Surface uptake (ppbw)		1900		780	840	3300
Dry deposition (ppbw)	30	2	8	1	77	5

Note: The meteorological data are from automatic weather stations; the atmospheric HNO_3 summer concentrations are from Dibb and others (1994) and Jones and others (1999). For South Pole, atmospheric concentrations of the same order of magnitude as in Summit have been assumed. The HNO_3 winter concentration has only been measured at Neumayer and has been found to be approximately 1 pptv (personal communication from R. Weller, 2001). In the absence of measurements for the other sites, we assume the winter concentrations at Summit and South Pole are the same as in Neumayer. The calculations for co-condensation and solubility in ice are based on Thibert and Dominé (1998). Surface uptake was estimated using a linear regression through the values for temperature-dependent uptake found by Abbatt (1997) and assuming a typical surface area of 4000 m^2 m^{-3} (Narita, 1971). Temperatures higher than 248 K have not been included in the study of surface uptake, so the estimates for surface uptake in Summit and Neumayer during summer are missing. Dry deposition was calculated assuming a dry-deposition velocity of 0.5 cm s^{-1} (Hauglustaine and others, 1994).

approximately 350 ppbw in fresh snow. On the other hand, the co-condensation of HNO_3 and water (H_2O) molecules on ice crystals (Thibert and Dominé, 1998) would lead to a bulk concentration of 20 ppbw only. In the absence of liquid water, i.e. in ice clouds, the high NO_3^- concentrations found in surface snow could not be explained. However, Abbatt (1997) observed a temperature dependence of adsorption of HNO_3 on ice surfaces with higher uptake at lower temperatures. For typical summer temperatures at South Pole (246 K; data obtained from http://www.cmdl.noaa.gov), the uptake capacity on fresh snow crystals exceeds the amount of HNO_3 available in the cloud, implying that at very cold temperatures where ice clouds predominate, essentially all HNO_3 in a cloud is bound to the surface of the snow crystal. While co-condensation, riming and adsorption of HNO_3 determine the distribution of NO_3^- within the ice crystal, its concentration is defined by the initial atmospheric concentration of HNO_3 and the amount of condensed water in the cloud. An imprint of temperature is expected for surface uptake and co-condensation, but not for the HNO_3 taken up in liquid cloud droplets. Based on the results of Abbatt (1997), the snow crystals are expected to efficiently scavenge atmospheric HNO_3 on their way to the surface, potentially further increasing the NO_3^- concentration of the fresh snow.

Once on the ground, the formation of surface hoar frost (co-condensation), rime (deposition of supercooled fog droplets) as well as dry deposition (adsorption of HNO_3 onto the crystal's surface) leads to additional NO_3^- deposition to surface snow. For a given atmospheric HNO_3 concentration, the hoar-frost NO_3^- concentration is determined by the water-

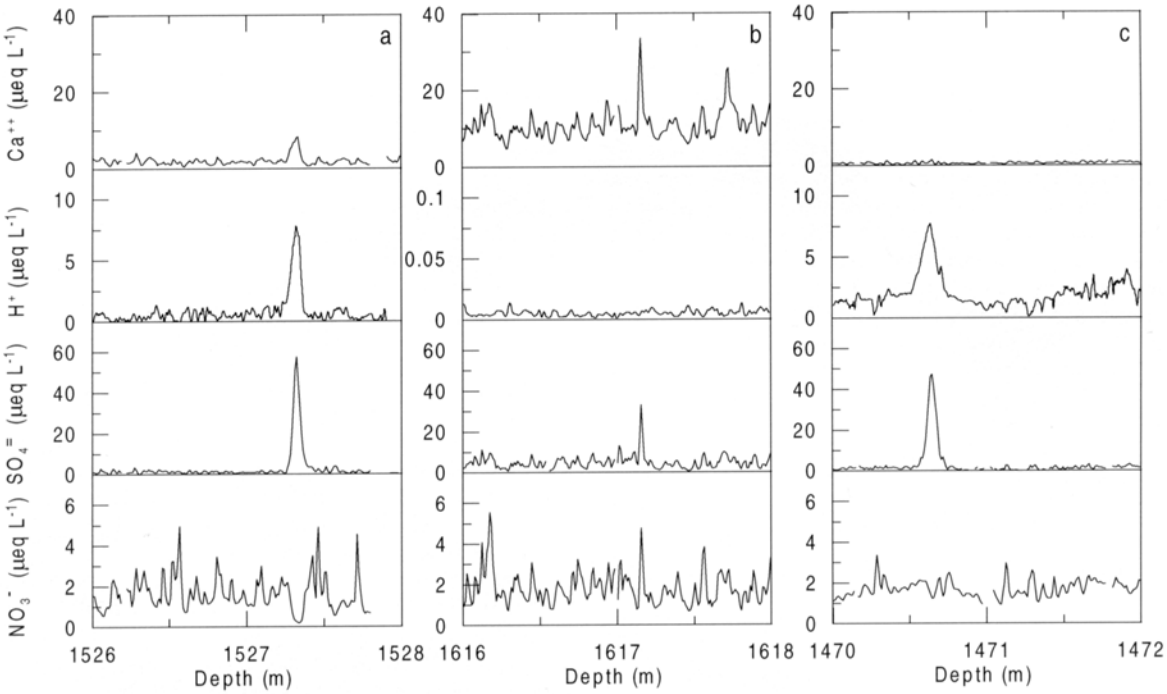

Fig. 5. Examples of the influence of volcanic H_2SO_4 on NO_3^- in the NorthGRIP ice core. H^+ concentrations have been inferred from electrical conductivity measurements on the solid ice. Due to very low H^+ concentrations, the scale of the y axis had to be adjusted for the section shown in (b). Of 28 events selected with SO_4^{2-} concentrations exceeding 20 μeqL^{-1}, 14 showed a pattern similar to (a), 12 similar to (b), and 2 similar to (c). The data are shown against depth, as the absolute age is not critical to the illustration of the effect and an absolute time-scale is not yet available.

vapour concentration (Thibert and Dominé, 1998), which is mainly a function of temperature T. Assuming that the relative humidity at the site is similar throughout the year, the NO_3^- concentration should depend linearly on $1/T$ in a first-order approach. However, assuming that the HNO_3 concentrations in the atmosphere as in Table 2 are representative for the site, the estimated concentrations resulting from co-condensation are lower than observed surface snow concentrations, thus leading to dilution of the surface snow (Table 2). Rime deposition, on the other hand, which is likely to remove all HNO_3 from the air, shows concentrations similar to those in fresh snow, provided that the atmospheric HNO_3 concentration is similar to that at cloud level. A net dry deposition of HNO_3 (adsorption of HNO_3 onto snow crystals) has the potential to increase the NO_3^- concentration in snow. However, it will only contribute where the surface is undersaturated, i.e. at very cold sites and during winter. The contribution in winter is small, due to low atmospheric HNO_3 concentrations. During the summer, the contribution of dry deposition to the NO_3^- concentrations in snow at South Pole might be considerable. However, according to Hauglustaine and others, (1994), the dry-deposition velocity of 0.5 cm s^{-1} for HNO_3 on snow has to be considered as an upper limit. At sites with higher accumulation rates, a specific surface snow layer is buried more rapidly, leaving less time to adsorb additional HNO_3 from the atmosphere, given that no saturation has been reached. Therefore, a tendency to higher concentrations at lower accumulation rates is expected.

Besides the diluting effect of co-deposition, processes capable of reducing the NO_3^- concentration in snow are desorption of HNO_3 from the snow crystal (Dibb and others, 1998; Mulvaney and others, 1998; Röthlisberger and others, 2000a) and photolysis (Honrath and others, 2000; Jones and others, 2000). In both cases, the NO_3^- ion has to be at the surface of a snow crystal, since photolysis of NO_3^- in the bulk is not effective (Dubowski and others, 2001). If a NO_3^- ion recombines with a H^+ ion to form HNO_3, it then may desorb into the firn air and eventually diffuse into the air above the snow. Diffusion of NO_3^- in ice has been investigated by Thibert and Dominé (1998), who found that diffusion of NO_3^- in ice is slower at colder temperatures, with the diffusion coefficient D given by $D = 1.37 \times 10^{-2610/T}$ $cm^2 s^{-1}$, with T being the temperature in K. During the summer, the typical time a NO_3^- molecule needs to reach the ice surface (diffusion length of 40 μm, corresponding to an average crystal radius (Harder and others, 1996)) is of the order of a couple of hours (e.g. Neumayer) to a few days (e.g. South Pole).

The solubility of NO_3^- in ice has been determined for various temperatures (Thibert and Dominé, 1998). For summer conditions, not only the surface snow but also deeper layers are supersaturated with respect to the solubility of NO_3^- in ice (Table 2). In the case of South Pole, the surface remains undersaturated, suggesting that NO_3^- that is expelled from the bulk is simply transferred to the surface without affecting the NO_3^- concentration. At warmer sites (e.g. Neumayer or Summit), the ice surface also might become supersaturated during the summer, leading to release of HNO_3 from the snow into the interstitial air. From a thermodynamic point of view, warmer temperatures during the summer should facilitate the release of HNO_3 from the ice surface. But according to the uptake experiment of Abbatt (1997), only up to 25% of the

HNO_3 that has been taken up is released again afterwards. However, his study emphasized the uptake rather than the release of HNO_3, and a temperature dependence of the release has not been discussed. Once released from the snow crystal's surface, the HNO_3 molecule might make its way out of the snowpack, leading to a net loss of NO_3^- in the snow. The molecular diffusion of HNO_3 in the interstitial air is temperature-dependent as well, but probably this is not the limiting factor controlling the transfer out of the snowpack. It is conceivable that temperature-dependent, repeated adsorption and subsequent desorption of a HNO_3 molecule on ice crystals will determine the removal from the snowpack.

Photolysis of NO_3^- in the top snow layers results in the production of nitrogen dioxide (NO_2) and hydroxyl radical (OH). NO_2 is expected not to interact with the surrounding snow but to be mixed into the boundary layer rather quickly, leading to a NO_3^- depletion in surface snow. The influence is presumably largest at low-accumulation sites, where surface snow is exposed to sunlight for a long time. Furthermore, photolysis should become more efficient at lower latitudes due to more incoming ultraviolet radiation. At Dome C, the top few centimetres of snow seem to reach saturated surface coverage (concentrations in the range of several hundred ppbw) (Röthlisberger and others, 2000b). Deeper layers are then dramatically undersaturated considering surface coverage and solubility in the bulk. No quantitative estimate has yet been made of how much NO_3^- can be lost by photolysis. It therefore remains unclear whether photolysis alone can account for the NO_3^- profile seen in the snow at Dome C. The estimate of the maximum surface uptake relies very much on the surface area in snow and might change due to recrystallization, which has not yet been taken into account.

Although elevation may affect the atmospheric HNO_3 concentration, there is no obvious mechanism by which it can have a direct physical influence on post-depositional processes. A minor influence is expected on the photolysis rate due to changes in the irradiance with altitude and on the gas-phase diffusion due to lower pressure, but both effects might only slightly modulate the changes in NO_3^- concentrations.

INTERACTIONS OF NO_3^- WITH DUST

Recent studies have reported that NO_3^- and Ca^{2+} concentrations are correlated in ice from the last glacial period from Vostok and Dome C, Antarctica (Legrand and others, 1999; Röthlisberger and others, 2000a). During the last glacial period, the Ca^{2+} deposited on the East Antarctic plateau is mainly of terrestrial origin and can thus be used as a proxy for dust. It has been suggested that the reaction of HNO_3 and $CaCO_3$ to form $Ca(NO_3)_2$ prevents NO_3^- from being released from the snow into the gas phase.

In principle, the reaction could take place in the atmosphere or in the snow. For it to occur in the atmosphere, high dust concentrations would need to be in the same season as the maximum nitrate concentrations. A recent paper that studied the reaction of $CaCO_3$ with HNO_3 derived a formula for the lifetime for removal of HNO_3 by dust (Hanisch and Crowley, 2001). Based on this, and using very rough estimates for the surface area of dust (assuming spherical particles of 1 μm diameter, a typical density of 2 g cm^{-3}, and atmospheric dust concentrations of 10 ng m^{-3}), we can estimate a HNO_3 lifetime vs removal by dust in the present-day Antarctic atmosphere of around 50 days. This is unlikely to be important relative to other removal processes. However, this could be reduced to 2 days under the dustier conditions of the LGM, and in Greenland under LGM conditions one could estimate a lifetime for this removal of only a few hours. It seems possible therefore that under LGM conditions much of the atmospheric HNO_3 could be converted to aerosol calcium nitrate in the atmosphere. In addition, the reaction to form $Ca(NO_3)_2$ might take place in the snow, in which case HNO_3 has to make its way to the snow layer where the Ca^{2+} has been deposited and, if Ca^{2+} is inside the snow grain rather than on its surface, diffuse through it.

INFLUENCE OF VOLCANIC H_2SO_4 ON NO_3^-

As shown lately in an Antarctic high-resolution record from Dome C (Röthlisberger and others, 2000a), H_2SO_4 of volcanic origin can cause NO_3^- to move in the ice. Several examples of very low NO_3^- concentrations coinciding with H_2SO_4 peaks and increased NO_3^- concentrations above and below this layer have been found in the Dome C as well as the NorthGRIP record (Fig. 5a). At Dome C, the effect is first seen at 12 m depth, where the deposits of the Tambora (Indonesia) eruption (AD 1815) are located. This indicates that the processes involved take place or at least start in the firn.

Our hypothesis of the mechanism for NO_3^- displacement in the firn relies on processes similar to those described above, as it includes diffusion of HNO_3 in the firn air. The high concentration of H_2SO_4 in a volcanic layer causes the equilibrium of $H^+ + NO_3^- \rightleftharpoons HNO_3$ to shift towards the righthand side, as a large amount of H^+ from the H_2SO_4 is present. Therefore, a locally elevated concentration of HNO_3 in the firn air is caused, which prompts gas-phase diffusion of the HNO_3 away from the volcanic layer towards either side. In an adjacent layer with no excessive H_2SO_4, HNO_3 favours dissociation into H^+ and NO_3^-, thus maintaining the gradient in the firn air by removing HNO_3 from the gas phase. It is possible that the movement of NO_3^- progresses via a different mechanism in the ice after pore close-off, possibly by diffusion of ions in the veins.

Figure 5b shows an event where no NO_3^- displacement occurred. In this section, large amounts of alkaline material are present in the ice, as seen by the high Ca^{2+} and negligible H^+ concentrations. In the context of the above hypothesis, the high concentrations of alkaline material (presumably $CaCO_3$) neutralize the H_2SO_4 and prevent the formation of HNO_3. The assumption that in this case H_2SO_4 undergoes some reactions is supported by the significantly narrower SO_4^{2-} peak compared to the ones seen in acid ice (personal communication from P. Barnes, 2001).

Our hypothesis is challenged by the example shown in Figure 5c. Although much excess H_2SO_4 is present and far too little Ca^{2+} to compensate, no marked NO_3^- displacement is seen. It is possible that the Ca^{2+} was unable to neutralize the H_2SO_4, but that it managed to bind NO_3^-, thus preventing it from being transferred into the gas-phase. The occurrence of ice layers limiting HNO_3 diffusion in the interstitial air is rather unlikely in NorthGRIP.

CONCLUSIONS

The spatial distribution of nitrate concentrations in Greenland is shown to be strongly related to site temperature, just as it is

for Antarctica. Because temperature and snow-accumulation rate are so closely linked, we cannot determine which of these factors is the one exerting physical control on the concentrations seen. In either case, the relationship changes at the very lowest accumulation rates, where it is clear that post-depositional losses are the dominant control on the subsurface concentration.

By examining the individual processes that could contribute to the nitrate concentration in snow, we find that many of them are indeed temperature-dependent, with higher concentrations predicted at lower temperatures, as observed. Some processes could also depend on the accumulation rate, if a longer exposure time at the surface allows additional uptake. Of the processes identified, either uptake by liquid droplets in cloud, if present, or uptake onto the ice surface in the cloud or after deposition can lead to concentrations in fresh snow that are as high as or higher than those observed. However, the role of surface uptake at higher temperatures, as encountered in coastal Antarctica and in Greenland in summer, needs to be quantified. Co-condensation of nitric acid and water, and dissolution of nitric acid within the ice lattice appear to give concentrations that are too low compared to those observed. This suggests tentatively that surface uptake and retention might be rather important in determining the concentrations we see. This process has a temperature dependence (approximately threefold greater uptake at −55°C compared to −25°C (Abbatt, 1997)) similar to that seen in Figure 2. However, according to Abbatt (1997), the uptake is not dependent on the nitric acid concentration in air. The higher nitrate concentrations in post-1970 Greenland snow compared to pre-1940 snow suggest that the snow concentration is somehow related to atmospheric concentrations, and we suggest that this is simply a question of limited supply to the ice surface, because nitric acid is scavenged so efficiently. In that case, a temperature- and accumulation-rate-corrected Holocene nitrate ice-core record of a site with adequate snow-accumulation rate should reflect the flux of nitrate to the surface, which should in turn be related to atmospheric NO_x input.

For sites with very low accumulation rate, losses, possibly due to photolysis, control the concentration seen in the Holocene in such a dominant way that it is unlikely that information about atmospheric nitrate or NO_x can be extracted. Once the ice becomes less acidic (in the last glacial period), the concentration of nitrate seems to be strongly controlled by the calcium or dust content of the atmosphere, and the deposition processes might be significantly altered. The ratio of nitrate to dust might give clues to the past nitrate content of the atmosphere, although in this case it is probable that the nitrate uptake is determined by the content of the atmosphere over the whole transport route of dust from its source to the deposition site, and is not closely related to the local nitrate concentration at the ice-core site.

A number of laboratory and field experiments would help to test the above hypotheses. Laboratory uptake experiments, similar to those carried out at 248 K and below (Abbatt, 1997), are needed at higher temperatures, appropriate to summer temperatures at coastal Antarctic or Greenland sites. Laboratory experiments would also allow an assessment of whether photolysis can account for the magnitude of nitrate losses at low-accumulation sites. Field measurements of the nitric acid content of the atmosphere are lacking for most sites, and particularly for winter. Experiments that follow the evolution of concentration from fresh snow to depth in individual layers are also required.

In summary, the factors that control nitrate concentration in ice cores are complex, and interpretation is likely to involve different factors for different locations and time periods. However, if the factors controlling deposition and loss can be better understood, it may still be possible, in some cases, to reconstruct information about the important NO_x cycle in the past.

ACKNOWLEDGEMENTS

This work was supported by a fellowship of the Swiss National Science Foundation. We thank H. B. Clausen and L. B. Larsen for providing unpublished nitrate data. Thanks to NorthGRIP participants and supporters as well as its funding agencies.

REFERENCES

Abbatt, J. P. D. 1997. Interaction of HNO_3 with water–ice surfaces at temperatures of the free troposphere. *Geophys. Res. Lett.*, **24**(12), 1479–1482.

Bigler, M. 2000. Entwicklung und Anwendung einer neuen Methode zur kontinuierlichen, hochaufgelösten Messung der Sulfatkonzentration an alpinen und polaren Eisbohrkernen. (M.Sc. thesis, University of Bern.)

Clausen, H. B. and C. C. Langway, Jr. 1989. The ionic deposits in polar ice cores. *In* Oeschger, H. and C. C. Langway, Jr, *eds. The environmental record in glaciers and ice sheets*. Chichester, etc., John Wiley and Sons, 225–247.

Clausen, H. B. *and 6 others*. 1997. A comparison of the volcanic records over the past 4000 years from the Greenland Ice Core Project and DYE 3 Greenland ice cores. *J. Geophys. Res.*, **102**(C12), 26,707–26,723.

Dibb, J. E., R. W. Talbot and M. H. Bergin. 1994. Soluble acid species at Summit, Greenland. *Geophys. Res. Lett.*, **21**(15), 1627–1630.

Dibb, J. E., R. W. Talbot, J. W. Munger, D. J. Jacob and S. M. Fan. 1998. Air–snow exchange of HNO_3 and NO_y at Summit, Greenland. *J. Geophys. Res.*, **103**(D3), 3475–3486.

Dubowski, V., A. J. Colussi and M. R. Hoffmann. 2001. Nitrogen dioxide release in the 302 nm band photolysis and spray-frozen aqueous nitrate solutions: atmospheric implications. *J. Phys. Chem., Ser. A*, **105**(20), 4928–4932.

Fischer, H. and D. Wagenbach. 1996. Large-scale spatial trends in recent firn chemistry along an east–west transect through central Greenland. *Atmos. Environ.*, **30**(19), 3227–3238.

Fischer, H., D. Wagenbach and J. Kipfstuhl. 1998. Sulfate and nitrate firn concentrations on the Greenland ice sheet. 1. Large-scale geographical deposition changes. *J. Geophys. Res.*, **103**(D17), 21,927–21,934.

Hanisch, F. and J. N. Crowley. 2001. Hetereogeneous reactivity of gaseous nitric acid on Al_2O_3, $CaCO_3$, and atmospheric dust samples: a Knudsen cell study. *J. Phys. Chem., Ser. A*, **105**(13), 3096–3106.

Hansson, M. E. 1994. The Renland ice core: a Northern Hemisphere record of aerosol composition over 120 000 years. *Tellus*, **46B**(5), 390–418.

Harder, S. L., S. G. Warren, R. J. Charlson and D. S. Covert. 1996. Filtering of air through snow as a mechanism for aerosol deposition to the Antarctic ice sheet. *J. Geophys. Res.*, **101**(D13), 18,729–18,743.

Hauglustaine, D. A., C. Granier, G. P. Brasseur and G. Mégie. 1994. The importance of atmospheric chemistry in the calculation of radiative forcing on the climate system. *J. Geophys. Res.*, **99**(D1), 1173–1184.

Hausbrand, R. 1998. Direktmessung der Azidität in einem Eisbohrkern aus Nordwestgrönland. (M.Sc. thesis, University of Heidelberg.)

Herron, M. M. 1982. Impurity sources of F^-, Cl^-, NO_3^- and SO_4^{2-} in Greenland and Antarctic precipitation. *J. Geophys. Res.*, **87**(C4), 3052–3060.

Honrath, R. E., S. Guo, M. C. Peterson, M. P. Dziobak, J. E. Dibb and M. A. Arsenault. 2000. Photochemical production of gas phase NO_x from ice crystal NO_3^-. *J. Geophys. Res.*, **105**(D19), 24,183–24,190.

Jones, A. E. *and 8 others*. 1999. Oxidized nitrogen chemistry and speciation in the Antarctic troposphere. *J. Geophys. Res.*, **104**(D17), 21,355–21,366.

Jones, A. E., R. Weller, E. W. Wolff and H.-W. Jacobi. 2000. Speciation and rate of photochemical NO and NO_2 production in Antarctic snow. *Geophys. Res. Lett.*, **27**(3), 345–348.

Kreutz, K. J. and P. A. Mayewski. 1999. Spatial variability of Antarctic surface snow glaciochemistry: implications for paleoatmospheric circulation reconstructions. *Antarct. Sci.*, **11**(1), 105–118.

Legrand, M. R. and S. Kirchner. 1990. Origins and variations of nitrate in south polar precipitation. *J. Geophys. Res.*, **95**(D4), 3493–3507.

Legrand, M., E. Wolff and D. Wagenbach. 1999. Antarctic aerosol and snowfall chemistry: implications for deep Antarctic ice-core chemistry. *Ann. Glaciol.*, **29**, 66–72.

Mayewski, P. A., W. B. Lyons, M. J. Spencer, M. S. Twickler, C. F. Buck and S.

Whitlow. 1990. An ice core record of atmospheric response to anthropogenic sulphate and nitrate. *Nature*, **346**(6284), 554–556.

Mulvaney, R. and E. W. Wolff. 1994. Spatial variability of the major chemistry of the Antarctic ice sheet. *Ann. Glaciol.*, **20**, 440–447.

Mulvaney, R., D. Wagenbach and E. Wolff. 1998. Postdepositional change in snowpack nitrate from observation of year-round near-surface snow in coastal Antarctica. *J. Geophys. Res.*, **103**(D9), 11,021–11,031.

Narita, H. 1971. [Specific surface of deposited snow. II.] *Low Temp. Sci., Ser. A*, **29**, 69–79. [In Japanese with English summary.]

Neftel, A., J. Beer, H. Oeschger, F. Zürcher and R.C. Finkel. 1985. Sulphate and nitrate concentrations in snow from south Greenland, 1895–1978. *Nature*, **314**(6012), 611–613.

Röthlisberger, R., M. A. Hutterli, S. Sommer, E. W. Wolff and R. Mulvaney. 2000a. Factors controlling nitrate in ice cores: evidence from the Dome C deep ice core. *J. Geophys. Res.*, **105**(D16), 20,565–20,572.

Röthlisberger, R. *and 6 others*. 2000b. Technique for continuous high-resolution analysis of trace substances in firn and ice cores. *Environ. Sci. Technol.*, **34**(2), 338–342.

Seinfeld, J. H. and S. N. Pandis. 1998. *Atmospheric chemistry and physics: from air pollution to climate change*. New York, John Wiley and Sons.

Steffensen, J. P. 1988. Analysis of the seasonal variation in dust, Cl^-, NO_3^-, and SO_4^{2-} in two central Greenland firn cores. *Ann. Glaciol.*, **10**, 171–177.

Steffensen, J. P., H. B. Clausen and J. M. Christensen. 1996. On the spatial variability of impurity content and stable isotopic composition in recent Summit snow. *In* Wolff, E.W. and R. C. Bales, *eds. Chemical exchange between the atmosphere and polar snow*. Berlin, etc., Springer-Verlag, 607–615. (NATO ASI Series I: Global Environmental Change 43.)

Thibert, E. and F. Dominé. 1998. Thermodynamics and kinetics of the solid solution of HNO_3 in ice. *J. Phys. Chem., Ser. B*, **102**, 4432–4439.

Wolff, E.W. 1995. Nitrate in polar ice. *In* Delmas, R. J., *ed. Ice core studies of global biogeochemical cycles*. Berlin, etc., Springer-Verlag, 195–224. (NATO ASI Series I: Global Environmental Change 30.)

Yang, Q. *and 7 others*. 1995. A global perspective of nitrate flux in ice cores. *J. Geophys. Res.*, **100**(D3), 5113–5121.

Yang, Q., P. A. Mayewski, E. Linder, S. Whitlow and M. Twickler. 1996. Chemical species spatial distribution and relationship to elevation and snow accumulation rate over the Greenland ice sheet. *J. Geophys. Res.*, **101**(D13), 18,629–18,637.

2.10 Technique for Continuous High-Resolution Analysis of Trace Substances in Firn and Ice Cores

Regine Röthlisberger, Matthias Bigler, Manuel A. Hutterli, Stefan Sommer, Bernhard Stauffer, Hans G. Junghans, Dietmar Wagenbach

Environmental Science and Technology
2(34), 338–342, 2000

Technique for Continuous High-Resolution Analysis of Trace Substances in Firn and Ice Cores

REGINE RÖTHLISBERGER,* MATTHIAS BIGLER, MANUEL HUTTERLI,† STEFAN SOMMER, AND BERNHARD STAUFFER

Climate and Environmental Physics, Physics Institute, University of Bern, Sidlerstrasse 5, 3012 Bern, Switzerland

HANS G. JUNGHANS AND DIETMAR WAGENBACH

Institut für Umweltphysik, University of Heidelberg, Heidelberg, Germany

The very successful application of a CFA (Continuous flow analysis) system in the GRIP project (Greenland Ice Core Project) for high-resolution ammonium, calcium, hydrogen peroxide, and formaldehyde measurements along a deep ice core led to further development of this analysis technique. We included methods for continuous analysis of sodium, nitrate, sulfate, and electrolytical conductivity, while the existing methods have been improved. The melting device has been optimized to allow the simultaneous analysis of eight components. Furthermore, a new melter was developed for analyzing firn cores. The system has been used in the frame of the European Project for Ice Coring in Antarctica (EPICA) for in-situ analysis of several firn cores from Dronning Maud Land, Antarctica, and for the new ice core drilled at Dome C, Antarctica.

Introduction

During the last few decades, ice core analyses have become increasingly important in understanding global climate change: In ice cores, a wealth of information about past climate is archived at an extraordinarily high temporal resolution. In particular, the study of soluble chemical trace substances in ice cores provides a unique tool for obtaining information on changes of the atmospheric aerosol load over the last several hundred thousand years (*1*). Usually such analyses have been carried out on discrete samples by ion chromatography. However, this is very time-consuming, and thus the spatial resolution is limited by the maximum amount of samples that can be analyzed.

Continuous flow analysis (CFA) allowed fast analysis of ammonium, calcium, formaldehyde, and hydrogen peroxide along the GRIP ice core with an extraordinarily high spatial resolution (*2*, *3*). The analysis was carried out in the field; hence, the risk of contamination due to sample handling, storage, or transport could be minimized.

CFA is based on a steady sample flow combined with an immediate detection of the compounds of interest. For detection, we used mainly fluorescence and absorption spectrometric methods adapted from flow injection analysis (FIA). To obtain a continuous sample stream, a subsection of the ice core is melted continuously on a melting device where the sample is permanently drained off by a peristaltic pump and led into the analytical system.

With the prospect of EPICA, we aimed at lower detection limits of the existing four components with respect to the extremely low concentration levels in Antarctic ice. Also, we wanted to extend the number of compounds to be analyzed, and we wanted to apply this technique to porous firn cores.

In this paper, we describe an improved system capable of simultaneous analysis of eight compounds in firn or ice cores. The new system has been used for analysis of firn cores from Dronning Maud Land, Antarctica, during the reconnaissance in 1997/1998 and for the new deep ice core from Dome C, Antarctica, 1997/1998 and 1998/1999 in the frame of EPICA. A total of 20 m of ice core could be analyzed daily with a depth resolution of approximately 1 cm. Data acquisition as well as data processing was done with a laptop computer running Labview (National Instruments). A detailed discussion of the data will be published elsewhere.

Melting Devices

For all analyses with the described CFA system, we used a small heated room (25 °C) adjacent to a cold room for ice core processing (−20 °C). The melter was mounted in the cold room with a piece of ice (approximately 1 m long, cross-section typically 3 × 3 cm) placed above, so that the ice sample was melted at one end. The meltwater was led through a hole in the wall into the heated laboratory for analysis.

One of the main advantages of such a CFA system is the very efficient decontamination of the sample. This is achieved by the melter, which separates the meltwater into a clean inner and a possibly contaminated outer fraction (*2*). The melting progress was registered by an optical encoder. This information was used to accurately assign the measured concentrations to the corresponding depths.

Dome C Melter. As a result of the additional compounds analyzed with the new CFA system, the water consumption increased from 3.6 to 7 mL/min. Therefore, the melter was enlarged by expanding the central area to a diameter of 20 mm. The melter is made of aluminum, ensuring high thermal conductivity, and surface-coated with PTFE. It is heated to a constant temperature of about 35 °C, depending on the desired melting speed, with a thermostat controlling the electrical heat source of 800 W.

Firn Melter. With the melter described above, it is more difficult to analyze firn cores. Due to capillary forces in the porous firn, meltwater is soaked up into layers above the melting head. Thus, the spatial resolution of the measurement decreases, and it is even possible that contaminated water from the core surface reaches the inner part of the melter. To avoid such effects, a melter for firn cores was designed (Figure 1). It consists of a flat surface with many radial narrow slits. These slits cause a capillary force downward into the melter, which is higher than the one of the porous firn, and thus prevents meltwater from being drawn up into the firn. Below these 0.2 mm wide slits, a specific geometry similar to the design of the Dome C melter allows a separation of the meltwater into inner and outer fractions. Since a capillary force can only be generated by a moistened surface, the aluminum-made melter is hardcoated instead of having a hydrophobic PTFE surface coating. The melter is heated by two 350-W heat sources, analogous to the Dome C melter.

* Corresponding author phone: +41 31 631 4465; fax: +41 31 631 8742; e-mail: regine@climate.unibe.ch.

† Present address: Department of Hydrology and Water Resources, University of Arizona, Tucson, AZ.

10.1021/es9907055 CCC: $19.00
Published on Web 12/10/1999

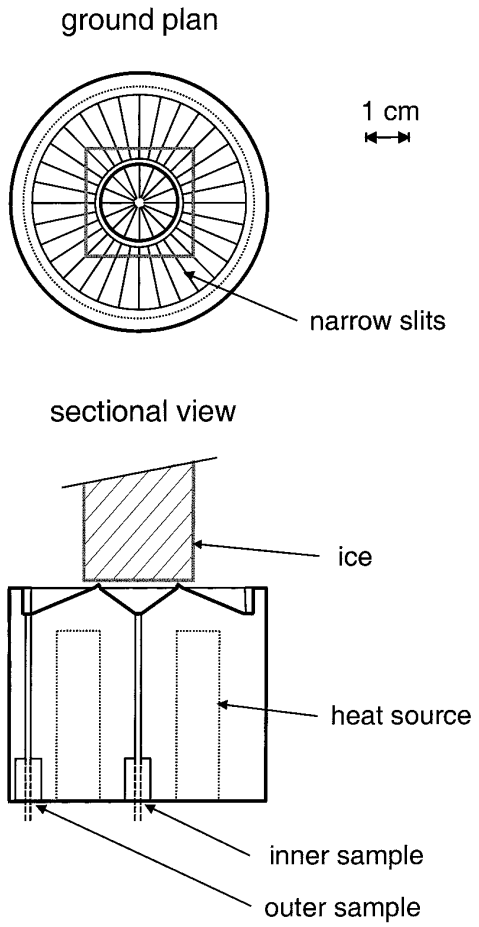

FIGURE 1. Firn melter.

Continuous Flow Analysis

All analytical systems operate continuously, and an automated set of valves controls whether meltwater from the ice core or blank or standard solution is analyzed. This configuration prevents air from entering the detectors before and after each piece of ice (*2*). Most of the tubing (including reaction loops of different lengths) was made of PTFE (0.5 mm i.d.). We used Tygon pump tubing for the peristaltic pumps, except for sulfate, where we used Ismaprene pump tubing. A short piece of microporous polypropylene membrane tubing (Accurel) was inserted before each detector (indicated as small gray boxes in Figure 2) to remove air bubbles.

For all systems, we used Milli-Q water for blank solutions and preparation of standard and reagent solutions. See Table 1 for the reagent composition (and also Table 1 in ref *2* for NH_4^+, H_2O_2, and HCHO reagents).

To characterize the system performance, we determined the detection limit and the temporal resolution for each component. The detection limit is calculated as three times the standard deviation of the blank, and the temporal resolution corresponds to the time needed to reach 1/e of the drop of a step function. The values are summarized in Table 2. Given a meltspeed of typically 4 cm/min, this results in a depth resolution of approximately 1 cm. For a detailed setup of each component, see Figure 2.

NH_4^+, H_2O_2, and HCHO. The fluorimetric methods for the determination of ammonium, hydrogen peroxide, and formaldehyde were adopted from Sigg et al. (*2*). The concentrations of the fluorescent complexes are measured with self-built fluorescence spectrometers with either a cadmium lamp (NH_4^+, H_2O_2) or a phosphor-coated mercury lamp with its emission maximum at 406 nm (HCHO). To improve the detection limit, we developed a new flow cell (18 μL) with mirrored inside surfaces to increase the excitation and emission of the fluorescence light. To prevent scattered light from entering the detector, all surfaces except the windows facing the light source and the detector were blackened. Due to these changes, the detection limit of the existing systems was lowered by a factor of 2.

Ca^{2+}. We chose a fluorimetric method (*4*) for the analysis of calcium with a lower detection limit and with a smaller flow cell than the absorption method previously used (*2*). The reagent was merged to the sample stream protected from daylight to prevent photolytic decomposition of the fluorescent complexes. The fluorescence light was detected in a self-built fluorescence spectrometer with a cadmium lamp and a flow cell as mentioned above. The setup showed a linear behavior in the concentration range from 0.1 to 100 ppb. If necessary, higher concentrations could be measured by increasing the concentration of Quin-2 in the reagent.

Na^+. A method for the detection of sodium was developed according to an enzymatic FIA method described by Quiles et al. (*5*). The photometric determination of sodium is based on the absorbance of *o*-nitrophenol produced by hydrolysis of *o*-nitrophenyl-β-D-galactopyranoside (ONPG) catalyzed by β-galactosidase. Since the enzyme activity depends on the sodium concentration in the medium, the sodium concentration can be determined by monitoring the *o*-nitrophenol concentration. We built an immobilized enzyme reactor (IMER, approximately 1 cm length, 1.2 mm i.d.), where the reaction of ONPG and β-galactosidase occurred. To achieve maximal absorption of the *o*-nitrophenol, the pH of the solution was raised to 9 with an Accurel membrane hanging in a closed container above 40 mL of ammonia solution (25% v/v). The absorption spectrometer consists of a phosphor-coated mercury lamp (emission maximum at 406 nm), an interference filter from ORIEL (410 nm, 10 nm bandwidth), a flow cell from Hellma (100 μL, 3 mm light path, no. 176.002-QS), and a photosensor module from Hamamatsu (H5701-50). The setup showed a linear behavior in the concentration range from 1 to 100 ppb. The method can also be used for concentrations up to 500 ppb; however, above 100 ppb, the response is not linear any more.

Enzyme Immobilization for the Na^+ Detection. All chemicals are from Merck if not stated otherwise. First, the controlled pore glass (CPG, Sigma, pore size 240 Å, 120−200 mesh) was cleaned in nitric acid (5%, 80 °C, 30 min), then thoroughly rinsed with Milli-Q water, and dried in an oven at 95 °C. In a second step, 5 mL of 3-aminopropyltriethoxysilane was added to 45 mL of ethanol and heated to 40 °C. CPG was added and whirled gently every 15 min for 5 h. Then, the CPG was rinsed with ethanol and dried in an oven at 50 °C. Next, the CPG was added into glutaraldehyde solution (2.5 mL of glutaraldehyde 50% in a 0.1 M phosphate buffer of pH 7) for 1 h. Every 10 min, the bottle was flushed with nitrogen to remove oxygen. Afterward the CPG was washed with Milli-Q water and then added to β-galactosidase in phosphate buffer (1500 units in 3−5 mL 0.1 M, pH 6). This was stored at 4 °C during at least 2.5 h and flushed with nitrogen every 10 min. Finally, the CPG was rinsed with cold phosphate buffer (pH 6) and stored at 4 °C in a Tris buffer solution (Tris buffer, pH 7.2, adjusted with HCl, 8 mM of $MgSO_4$ and 8 mM of DL-dithiothreitol from Fluka 43817). The immobilized enzyme was stored up to 2 yr at 4 °C without significant losses. Before measurements, an IMER was made out of a PTFE tube (1 cm length, 1.2 mm i.d.) filled with the enzyme-coated CPG. After measurements, the IMER was rinsed with the storage solution (see above) and stored at 4 °C. Every few days, the IMER was exchanged.

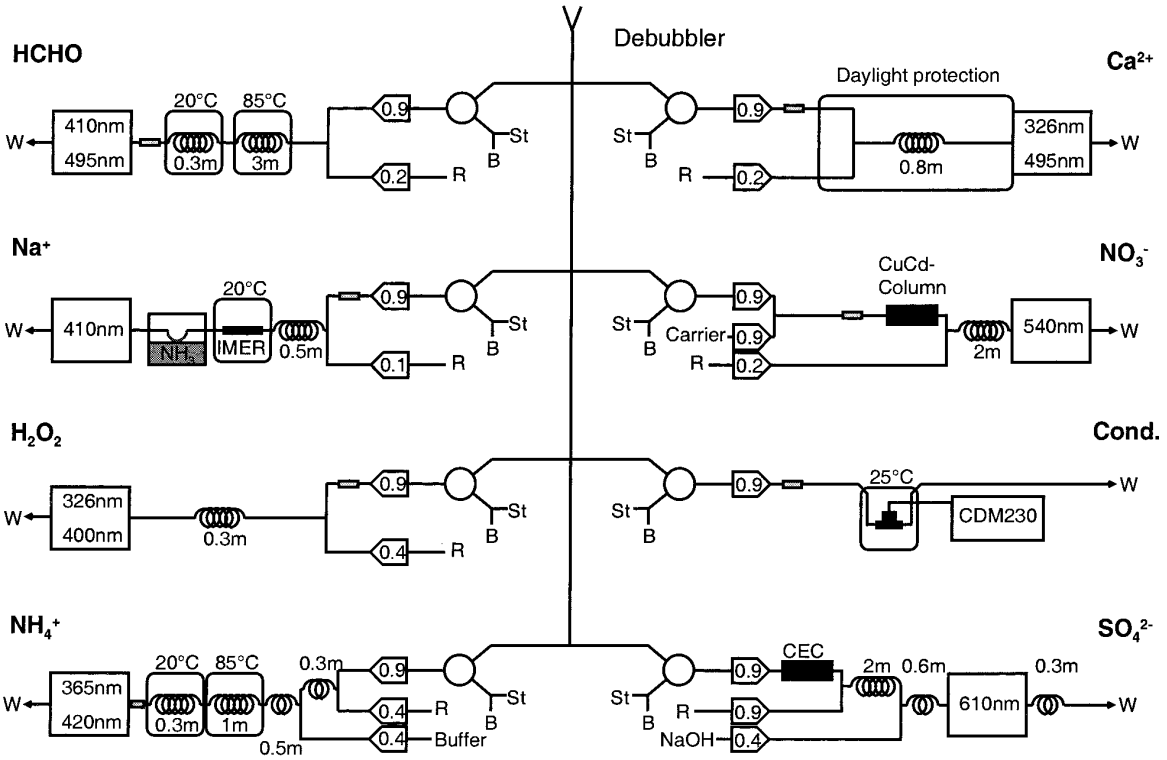

FIGURE 2. Flow chart of the CFA system. Water from the melter goes through a debubbler where air is removed from the liquid sample. The sample is then distributed to the eight components for analysis. Circles stand for the automatic valves, numbers in arrow boxes indicate flow rates in mL/min, and a gray tubing represents Accurel microporous membrane. B, blank; St, standard solution; R, reagent; W, waste; IMER, immobilized enzyme reactor; CEC, cation exchange column. See text for more explanation.

TABLE 1. Composition of Reagents[a]

substance name	concn
Ca^{2+} Reagent	
PIPES[b]	20 mM
NaOH[c]	35 mM
Quin-2[b]	0.01 mM
Na^{+} Reagent	
ONPG[d]	8 mM
DTT[b]	8 mM
$MgSO_4 \cdot 7H_2O$[c]	8 mM
Tris[c]	100 mM
HCl[c]	100 mM
pH Lifter	
NH_3[c]	25%
NO_3^- Carrier	
NH_4Cl[c]	190 mM
NO_3^- Reagent	
NED[d]	1 mM
Sulfanilamide[c]	75 mM
H_3PO_4[c]	1500 mM
SO_4^{2-} Reagent	
methylthymol blue[c]	0.09 mM
$BaCl_2 \cdot 2H_2O$[c]	0.09 mM
HCl[c]	6 mM
ethanol[c]	86%

[a] Abbreviations are explained in the text. The substances are from [b]Fluka, [c]Merck, and [d]Sigma.

TABLE 2. Detection Limit and Temporal Resolution (See Text) of the CFA Setup as Well as Concentration Ranges Encountered in the Dome C Ice Core during the Holocene Period[a]

	detection limit (ppb)	resolution (s)	Dome C concn range (ppb)
NH_4^+	0.1	15	0–5
H_2O_2	0.1	13	0–30
HCHO	0.1	13	0–10
Ca^{2+}	0.1	18	0–20
Na^+	0.5	16	0–100
NO_3^-	1.0	16	0–60
SO_4^{2-}	20	20	0–800

[a] The high values are usually only reached during short events.

NO_3^-. Nitrate is analyzed by a standard absorption technique (*6*). This method involves reduction to nitrite with copperized cadmium followed by diazotization with sulfanilamide and naphthylethylenediamine (NED) to form a pink–purple azo dye, thus the results indicate the total amount of nitrate and nitrite. However, nitrite occurs at extremely low levels in Antarctic ice and thus causes no significant interference (*7*). The detection takes place in a self-built absorption spectrometer provided with a cadmium lamp, an interference filter from Oriel (540 nm, 10 nm bandwidth), and a photosensor module from Hamamatsu (H5701-50). Depending on the desired concentration range, a flow cell with a path length between 20 and 40 mm (Hellma no. 178.010-QS) was used. The copperized cadmium (Aldrich, no. 41,489-1, 30–80 mesh) was filled in a self-made Plexiglas column (1 cm length, 4 mm i.d.). A new column was used every few days.

SO_4^{2-}. At present, we are developing a method for continuous sulfate measurements, based on a standard method using methylthymol blue (MTB) (*8*). The indirect determination of sulfate, based on competitive reaction of sulfate and MTB with barium in solution, can be accomplished by measurement of absorption of either un-

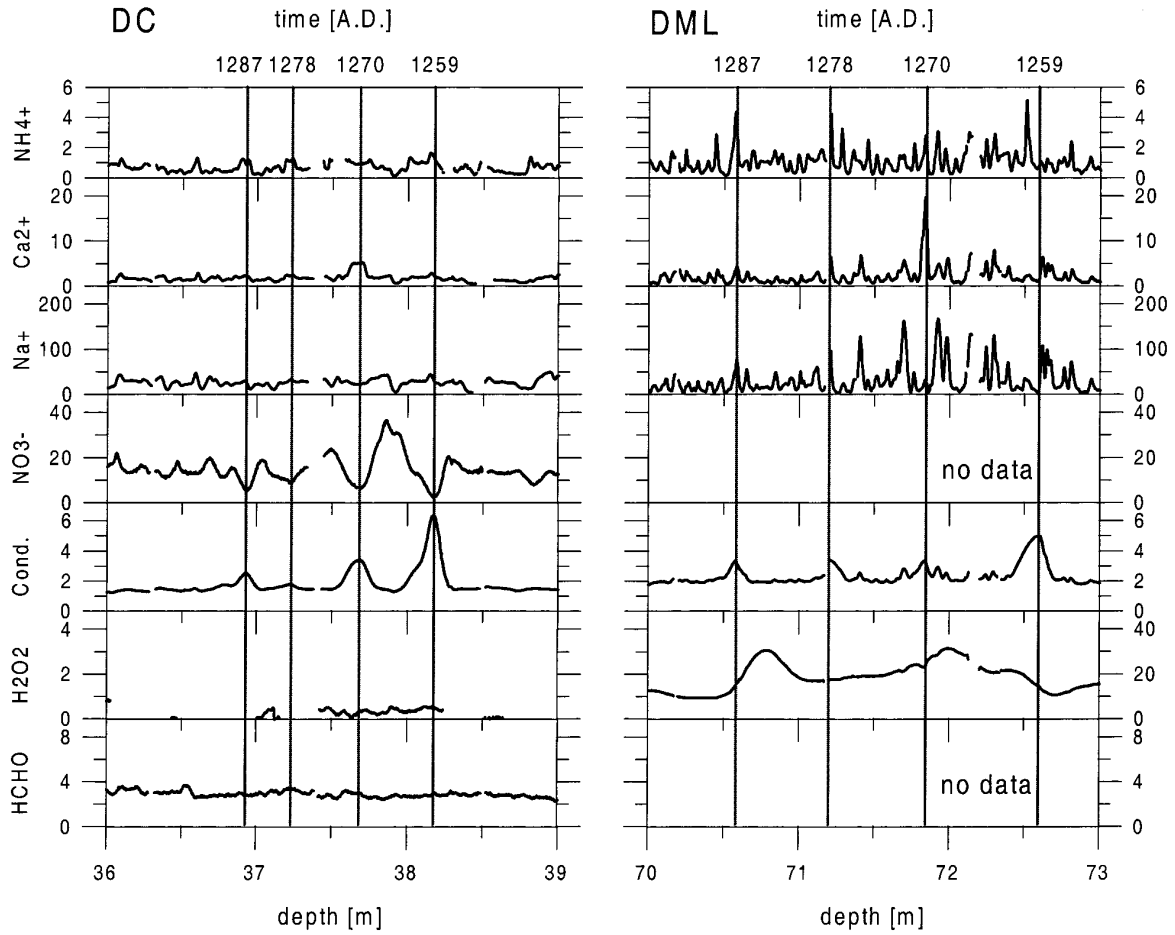

FIGURE 3. Data from Dome C (DC) and Dronning Maud Land (DML) firn cores. Vertical bars denote expected volcanic horizons. Concentrations are given in ppb; conductivity is given in μS/cm. Note the expansion of H_2O_2 in the DC panel relative to DML. Gaps in the data sets are caused by breaks in the ice core and concomitant contamination.

complexed MTB or the MTB−barium complexes. We chose the latter, where absorption at 608 nm decreases as sulfate concentration increases. Since the complexation of barium with MTB occurs only at high pH, a NaOH solution (0.066 M in ethanol 44% v/v) is added. To minimize degassing of the solvent, a narrow PTFE coil (0.3 m length, 0.4 mm i.d.) is inserted after the detector to create a higher back pressure in the manifold. Due to the high ethanol content of the reagents, Ismaprene pump tubing was used instead of Tygon. Interferences caused by multivalent cations (e.g., magnesium and calcium) are avoided by inserting a cation exchange column (CEC, 1 cm length, 3 mm i.d., Dowex 50WX4, Na^+ form, 100−200 mesh, Fluka) in the sample stream. The CEC has to be regenerated daily with a 20% NaCl solution.

The detector is equipped with a phosphor-coated mercury lamp (emission maximum at 615 nm), an interference filter from ORIEL (610 nm, 10 nm bandwidth), a flow cell from Hellma (150 μL, 20 mm light path, no. 178.010-QS), and a photosensor module from Hamamatsu (H5701−50). With this setup, a detection limit of 20 ppb can be achieved. However, during routine measurements, the detection limit was around 100 ppb. The detection limit is strongly affected by slight variance of the flow rates and the composition of the MTB reagent. Deviation of a 1:1 molar ratio of MTB and barium chloride leads to a smaller slope of the calibration curve for low sulfate concentrations. To estimate the purity of the MTB in order to calculate the optimum amount of barium chloride needed, we use a spectrophotometric procedure (*9*).

The method shows a linear behavior to at least 2000 ppb. So far, it has not yet been applied in the field, but at present, firn cores from North Greenland are analyzed at our laboratory for sulfate also.

Conductivity. Electrolytical conductivity was measured with a conductometer from Radiometer (CDM230) and a flow-through cell from Microelectrodes (volume 17 μL, cell constant 1.2 cm^{-1}). The cell was immersed in a thermostated water bath (25 ± 0.1 °C) and calibrated regularly with 0.5% NaCl solution.

Results and Discussion

In Figure 3, data from Dome C (75°06′ S, 123°24′ E) on the left and from Dronning Maud Land (75°0.14′ S, 0°0.42′ E) on the right are presented. The two intervals shown are of similar age but of a different depth due to different snow accumulation rates at the two sites. Due to logistic constraints, nitrate and HCHO were not measured in Dronning Maud Land. As mentioned above, the method for continuous sulfate measurements has not yet been applied in the field.

Electrolytical conductivity shows a few volcanic events that have been assigned in the Dronning Maud Land core to 1287, 1278, 1270, and 1259 A.D. (*10*). In the Dronning Maud Land core where the accumulation rate is estimated at 6.1 cm/yr (water equiv) (*11*), seasonal cycles of ammonium,

calcium, and sodium are clearly visible and can be used for layer counting. Due to the rather low accumulation rate, annual cycles of H_2O_2 have been smoothed out to a large extent by post-depositional processes.

At Dome C, the accumulation rate is only approximately 2.8 cm/yr (water equiv) (*12*) so that seasonal cycles are not preserved in the ice core. However, the volcanic events, most prominently the one at 1259 A.D., can be seen clearly. At locations with very low accumulation rates such as Dome C, snow may be redistributed after deposition. Therefore events which are affecting only a few annual layers may accidentally be missing, such as presumably the eruption of 1278 A.D.

Measurements of our CFA setup have been compared with ion chromatography, and the results are in very good agreement. To test the reproducibility, 1 m of ice has been analyzed in triplicate: twice melted top to bottom and once bottom to top. The uncertainty in assigning the depth to the concentration profile measured was approximately ±1 cm. The measured concentrations differed less than 10%, except for sulfate where the measured concentrations were below 100 ppb and the error was around 20 ppb.

It is shown that CFA allows us to quantify various relevant trace substances in ice cores at a typical depth resolution of 1 cm down to the ppb and sub-ppb range with 20 m of ice core routinely processed in 1 day.

Acknowledgments

This work is contribution No. 14 to the "European Project for Ice Coring in Antarctica" (EPICA), a joint ESF (European Science Foundation)/EC scientific program, funded by the European Commission under the Environment and Climate Program (1994−1998) Contract ENV4-CT95-0074 and by national contributions from Belgium, Denmark, France, Germany, Italy, The Netherlands, Norway, Sweden, Switzerland, and the United Kingdom. We thank René Nyffenegger for giving us advice on enzyme immobilization and Reto Knutti for computer support.

Literature Cited

(1) Legrand, M.; Mayewski, P. *Rev. Geophys.* **1997**, *35*, 219−243.
(2) Sigg, A.; Fuhrer, K.; Anklin, M.; Staffelbach, T.; Zurmühle, D. *Environ. Sci. Technol.* **1994**, *28*, 204−209.
(3) Fuhrer, K.; Neftel, A.; Anklin, M.; Maggi, V. *Atmos. Environ.* **1993**, *27A*, 1873−1880.
(4) Tsien, R. Y.; Pozzan, T.; Rink, T. J. *J. Cell Biol.* **1982**, *94*, 325−334.
(5) Quiles, R.; Fernandez-Romero, J. M.; Fernandez, E.; Luque de Castro, M. D.; Valcarel, M. *Clin. Chem.* **1993**, *39*, 500−503.
(6) McCormack, T.; David, A. R. J.; Worsfold, P. J.; Howland, R. *Anal. Proc.* **1994**, *31*, 81−83.
(7) Legrand, M.; Angelis, M. d. *J. Geophys. Res.* **1995**, *100*, 1445−1462.
(8) Madsen, B. C.; Murphy, R. J. *Anal. Chem.* **1981**, *53*, 1924−1926.
(9) Colovos, G.; Panesar, M. R.; Parry, E. P. *Anal. Chem.* **1976**, *48*, 1693−1696.
(10) Langway, C. C.; Osada, K.; Clausen, H. B.; Hammer, C. U.; Shoji, H. *J. Geophys. Res.* **1995**, *100*, 16241−16247.
(11) Oerter, H.; Wilhelms, F.; Jung-Rothenhäusler, F.; Götkas, F.; Miller, H.; Graf, W.; Sommer, S. *Ann. Glaciol.*, in press.
(12) Wolff, E.; Basile, I.; Petit, J.-R.; Schwander, J. *Ann. Glaciol.* In press.

Received for review June 28, 1999. Revised manuscript received October 20, 1999. Accepted October 27, 1999.

ES9907055

Kapitel 3

Experimentelle Arbeiten

Im ersten Unterkapitel (3.1) wird ein kurzer Überblick über das CFA-Messprinzip gegeben. In den darauffolgenden drei Kapiteln werden dann drei wesentliche Neuerungen vorgestellt und dokumentiert. Es handelt sich um den neuen Schmelzkopf und um Änderungen an der Schmelzanlage (Unterkapitel 3.2), um die Verbesserung des Sulfatnachweissystems (Unterkapitel 3.3) sowie um die Einführung des neuen Partikelmessgerätes Abakus (Unterkapitel 3.4).

3.1 Continuous Flow Analysis (CFA)

Mit dem Berner Continuous Flow Analysis (CFA) System können Spurenstoffmassenkonzentarionen in Eisbohrkernen kontinuierlich und in hoher Auflösung bestimmt werden [*Sigg et al.*, 1994; *Röthlisberger et al.*, 2000]. Unterdessen verfügt das System über die folgenden Komponenten: Kalzium Ca^{2+}, Natrium Na^{+}, Ammonium $NH_4{}^{+}$, Sulfat $SO_4{}^{2-}$ (Unterkapitel 3.3), Nitrat $NO_3{}^{-}$, Wasserstoffperoxid H_2O_2 und Formaldehyd HCHO. Weiter wird die elektrolytische Gesamtleitfähigkeit des Schmelzwassers und sowohl die Partikelgesamtkonzentration, wie auch deren Grössenverteilung (Unterkapitel 3.4) gemessen.

Einer der entscheidenden Vorteile des Berner Continuous Flow Analysis (CFA) Systems, welches für das effiziente Analysieren von grossen Probemengen ausgelegt ist, besteht in der Schmelzanlage. Um einen kontinuierlichen Probenfluss zu erhalten, wird ein Eiskernstück von typischerweise 110 cm oder 165 cm Länge und 3×3 cm^2 Querschnittfläche in kalter Umgebung bei typischerweise -20°C langsam auf einem Schmelzkopf geschmolzen. Dieser wird mittels einer Temperatursteuerung auf etwa 30°C beheizt. Üblicherweise wird eine Schmelzgeschwindigkeit von 3 bis 4 cm min^{-1} angestrebt. Um bei der Datenauswertung eine genaue Tiefenzuordnung zu erhalten, wird mit Hilfe eines Wegaufnehmers ein Weg-Zeit-Diagramm des Schmelzprozesses aufgezeichnet.

Das Schmelzwasser wird mittels einer Schlauchquetschpumpe kontinuierlich in das CFA-System, das sich in unmittelbarer Nähe in einem geheizten Labor befindet, eingespeist, entgast und auf die verschiedenen CFA-Nachweissysteme aufgeteilt. Da für viele Anwendungen eine gute Tiefenauflösung unerlässlich ist, werden alle Mischvolumen so klein wie möglich gehalten und so die Dispersion verkleinert. Die Tiefenauflösung beträgt typischerweise 1 cm.

Indem beim Schmelzen der Probe nur Wasser aus dem zentralen Bereich des Eiskernstückes für die Analyse verwendet wird und dieser kontinuierliche Probenstrom nicht mit der Umgebungsluft in Kontakt kommt, werden mögliche Kontaminationen minimiert. Das zeit- und arbeitsintensive Dekontaminieren von Einzelproben entfällt. Gerade aus diesem Grund ist der Einsatz einer Schmelzanlage nicht nur für unser CFA-System, sondern auch für viele andere kontinuierliche oder quasi-kontinuierliche Analysemethoden interessant. In den letzten Jahren wurde die Berner CFA-Schmelzanlage bei Messkampagenen häufig mitbenutzt, das heisst ein Teil des Probeflusses wurde jeweils abgezweigt und parallel zu den CFA-Messungen den beteiligten Gruppen zur Verfügung gestellt oder von Hand oder per Autosampler in kleine Gefässe abgefüllt. Diese Entwicklung war nur möglich, weil der Schmelzkopf so weiterentwickelt wurde, dass ein grösseres Volumen geschmolzen und aus dem inneren Bereich abgesaugt werden kann (Unterkapitel 3.2).

Dank der kompakten und modularen Messapparatur sind Messungen im Feld möglich. Dadurch werden mögliche Kontaminationen und Beschädigungen der Eis- und Firnproben während Transport und Lagerung verhindert. Weiter stehen erste Messresultate rasch zur Verfügung. Mit dem CFA-System können im optimalsten Fall bis 35 m Eis pro Tag hochaufgelöst analysiert werden, vorausgesetzt dass rund um die Uhr im Schichtbetrieb gemessen wird. Gerade bei Tiefbohrungen, die grosse Probenmengen ergeben, ist diese Kapazität wichtig, um innert nützlicher Frist und mit vertretbarem Aufwand lange Zeitreihen zu gewinnen. Es muss jedoch festgehalten werden, dass das entgültige Auswerten und Überarbeiten der Rohdaten mehr an Arbeitszeit in Anspruch nimmt, als das Messen selbst. Weiter ist der Aufwand zur Vorbereitung einer Messkampagne gross und zeitraubend.

Alle CFA-Nachweissysteme für Ionen basieren auf absorptions- oder fluoreszenzspektroskopischen Nachweismethoden. Die theoretische Basis dazu kann unter anderem in *Skoog und Leary* [1996] nachgelesen werden. Eine ausführliche Beschreibung der Absorptionsspektroskopie findet sich auch in *Bigler* [2000] im Kapitel 4. Je ein typischer Messablauf einer Absorptionskomponente ($NO_3{}^-$) und einer Fluoreszenzkomponente (Ca^{2+}) sind in der Figur 3.1 dargestellt. Vor und nach jeder Standard- und Probenmessung werden Blankintervalle aufgenommen. Um leichte Drifts zu eliminieren, wird zwischen diesen linear interpoliert. Im Folgenden wird kurz auf methodische Aspekte der Fluoreszenz- und Absorptionsspektroskopie eingegangen, eine CFA-spezifische Fehlerabschätzung durchgeführt und Kennzahlen definiert.

3.1.1 Fluoreszenzspektroskopie

Charakteristisch für die Fluoreszenzspektroskopie ist, bei nicht zu hoher Analytkonzentration, die Linearität zwischen Konzentration c (in ppbw) des mit einem fluoreszierenden Komplex markierten Analyten und dem Fluoreszenzsignal U (in V). Das Fluoreszenzsignal enthält auch ein Blanksignals U_{Blank} (in V), das unter anderem durch die Eigenfluoreszenz der Reagenzien verursacht wird (Gleichung 3.1).

$$U = \frac{c}{\alpha} + U_{Blank} \tag{3.1}$$

Traditionellerweise verwenden wir in Bern als Proportionalitätskonstante den Kalibrierungsfaktor der Fluoreszenzmessung α in der Einheit ppbw V^{-1}, der mittels Standardkali-

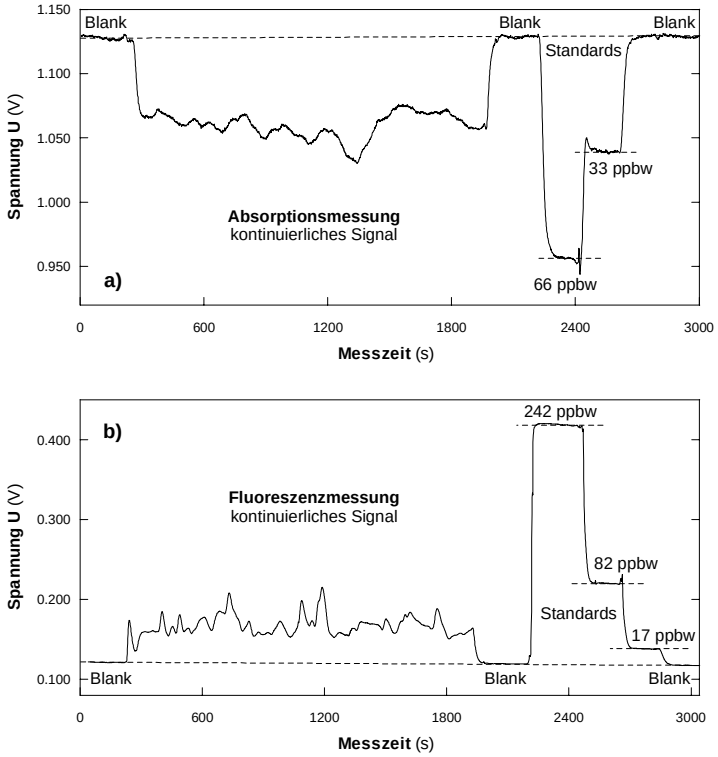

Abbildung 3.1: Typischer Messverlauf a) einer Absorptionsmessung, als Beispiel hier $NO_3{}^-$, und b) einer Fluoreszenzmessung, hier Ca^{2+}.

brierung gewonnen wird. Dazu werden in regelmässigen Abständen Substanzen mit bekannten Konzentrationen, sogenannte Standards, gemessen, um mögliche Änderungen der Messbedingungen zu berücksichtigen.

3.1.2 Absorptionsspektroskopie

Im wesentlichen basiert die Absorptionsspektroskopie auf dem Lambert-Beerschen Gesetz (Gleichung 3.2). Dieses besagt, dass die Extinktion A eines Lichtstrahls durch die Lösung (nach DIN auch spektrales dekadisch Absorptionsmass genannt) logarithmisch vom Verhältnis der Strahlungsintensitäten bei Blankmessungen I_{Blank} und bei Messungen an Standard oder Probe I (in $\mathrm{W\,m^{-2}}$) abhängt, respektive von den entsprechenden Spannungssignalen U_{Blank} und U des Photomultipliers (in V). Dieses Verhältnis wiederum ist proportional erstens zur Konzentration des mit einem absorbierenden Komplex markierten Analyten c (in ppbw), zweitens zur Küvettenlänge b (in cm) und drittens zum Extinktionskoeffizienten ε (in $\mathrm{ppbw^{-1}\,cm^{-1}}$). Üblicherweise fassen wir b und ε zusammen zum Kalibrierungsfaktor der Absortptionsmessung α mit der Einheit $\mathrm{ppbw^{-1}}$, der wie bei den Fluoreszenzmessungen mittels Standardkalibrierung gewonnen wird:

$$A = \log_{10} \frac{I_{Blank}}{I} = \log_{10} \frac{U_{Blank}}{U} = \varepsilon bc = \alpha c \tag{3.2}$$

3.1.3 Systematische und statistische Fehler

Prinzipiell ist jeder Messpunkt der kontinuierlich aufgenommenen Datenreihe eine Einzelmessung. Die klassische Fehlerrechnung ist daher nicht die geeignete Methode für eine Fehlerabschätzung. Ursache statistischer Fehler ist das chemische und instrumentelle Rauschen, das die Spannungsmessungen beeinflusst. Das Rauschen ist bei der Absorptionsmessung generell grösser. Weiter kann ein statistischer Fehler bei der schrittweisen Verdünnung der Standardlösungen entstehen. Um die statistischen Fehler abzuschätzen, kann das Signal-zu-Rausch-Verhältnis bei Standardmessungen betrachtet werden (Gleichung 3.3 bei Absorptionsspektroskopie, Gleichung 3.4 bei Fluoreszenzspektroskopie). Dieses ist häufig recht konstant, das heisst unabhängig von der Signalhöhe. Da es reziprok zur relativen Standardabweichung der Extinktion respektive des Fluoreszenzsignals ist, kann es als Mass für die Präzision oder Reproduzierbarkeit der Messung beigezogen werden.

$$\left(\frac{S}{N}\right)_{\text{abs}} \doteq \frac{\overline{A}_{\text{St}}}{s_{A_{\text{St}}}} \tag{3.3}$$

$$\left(\frac{S}{N}\right)_{\text{fl}} \doteq \frac{\overline{U}_{\text{St}}}{s_{U_{\text{St}}}} \tag{3.4}$$

Es muss jedoch klar festgehalten werden, dass meistens systematische Fehler dominieren, welche sehr schwer aufzudecken sind. Hierzu sind Vergleichsmessungen zwischen verschiedenen Labors hilfreich, um mit vernünftigem Aufwand solche Fehler zu quantifizieren, deren Ursachen sehr vielfältig sein können. Erwähnt seien hier falsche Konzentrationswerte von Standardstammlösungen (Absolutkalibrierung), Kontamination und systematische Fehler bei den Standardverdünnungsschritten (Dispensetten, Transferpetten), Kontamination des Blanks, Basislinienschwankungen, die mittels linearer Interpolation zwischen den Blankintervallen nicht erfasst werden können, verursacht beispielsweise durch Änderungen der Fliessraten (Pumpschläuche), Inhomogenitäten in den Reagenzlösungen, Luftblasen, schlechte Empfindlichkeit von Reaktionssäulen und Reagenzien, abrupte Temperaturänderungen im Labor und so weiter. Abschätzungen des Gesamtfehlers können sich somit naturgemäss nie auf einen ganzen Datensatz sondern ausschliesslich auf einzelne Abschnitte beziehen. Daher wurde der mittlere Fehler verschiedentlich auf 10% veranschlagt [*Röthlisberger et al.*, 2000; *Sommer*, 2000; *Bigler*, 2000]. Alternativ dazu bieten sich Parallelmessungen am gleichen Eisbohrkern an. Solche Messungen wurden mehrmals durchgeführt und haben recht gute Übereinstimmungen mit obigen Schätzungen gezeigt. Die Schwierigkeit bei Parallelmessungen besteht darin, dass eine genaue Tiefenzuordnung die gerade bei steilen Signalflanken wichtig ist, meistens nicht erreicht werden kann. Zudem können die Konzentrationsdifferenzen einzelner Spezies innerhalb kleiner Horizontalabstände im Eisbohrkern beträchtlich variieren. Weitere Parallelmessungen an grönländischen und antarktischen Eisbohrkernen finden sich in *Bigler* [2000].

3.1.4 Kennzahlen einer Nachweismethode

Neben der Abschätzung systematischer und statistischer Fehler der Nachweismethoden sind auch die Detektionslimite, der Arbeitsbereich, die Selektivität und die zeitliche Auflösung von Interesse. Detaillierte Definitionen dieser Kennzahlen findet man in *Bigler* [2000]. Zusammenfassend verstehen wir unter der Detektionslimite die mit Hilfe der Kalibrierungsfunktion auf ppbw umgerechnete dreifache Standardabweichung des Blanksignals (in V). Als untere Grenze des Arbeitsbereichs wird hingegen die zehnfache Standardabweichung verwendet; sie

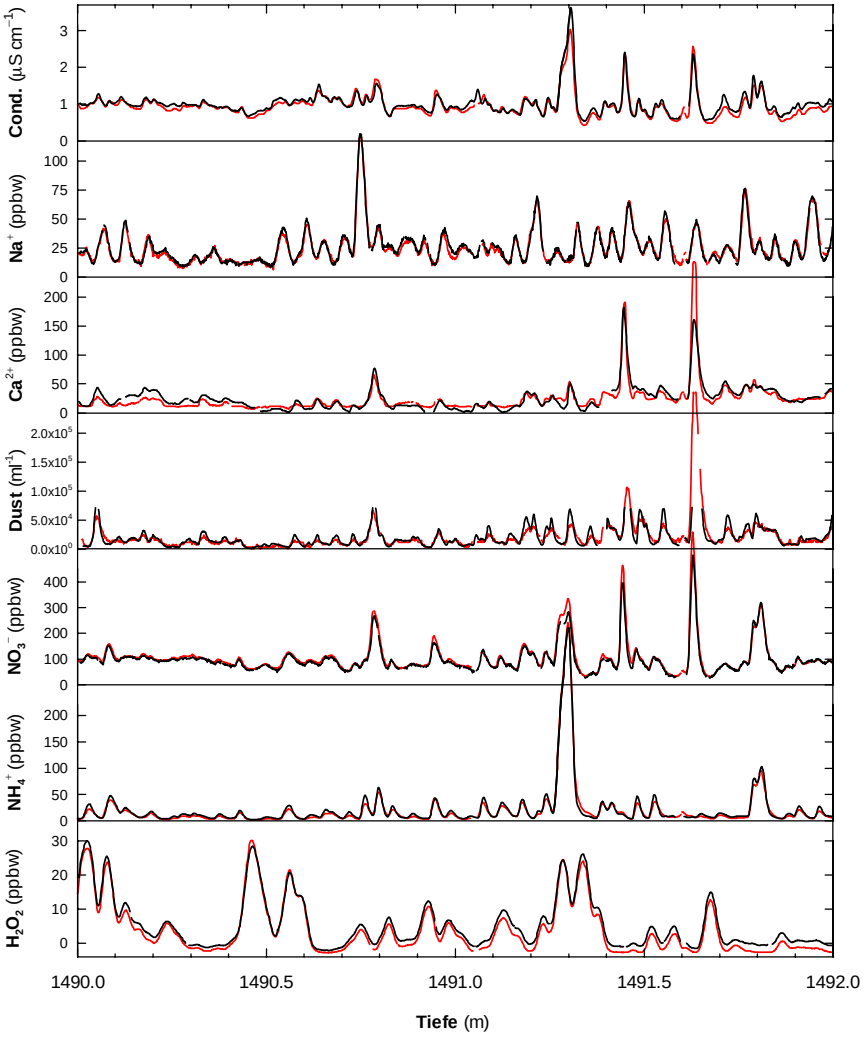

Abbildung 3.2: Zweimaliges Messen eines 2m-Tiefenabschnittes in NorthGRIP-Eis aus dem Holozän.

ist somit etwa um einen Faktor drei höher als die Detektionslimite. Die obere Grenze des Arbeitsbereiches wird bei linearen Kalibrierungsfunktionen durch Abweichungen von der Linearität erreicht, aber auch bei der Verwendung nicht-linearer Kalibrierungsfunktionen wächst die Ungenauigkeit sehr stark an, wenn die Kalibrierungsfunktion für hohe Konzentrationswerte abflacht. Im Gegensatz zur unteren Grenze, kann die obere Grenze häufig durch experimentelle Anpassungen an den auftretenden Konzentrationsbereich der zu messenden Spezies angepasst werden. Mittels Selektivitätskoeffizienten wird das relative Ansprechverhalten von interferierenden Spezies angegeben. Diese Koeffizienten sind im Idealfall Null oder aber ihre Konzentration im Probematerial ist vernachlässigbar. Die zeitliche Auflösung schliesslich erhalten wir aus der Messung von Standardlösungen, die direkt auf den Schmelzkopf gegeben wurden. Als Zeitkonstante definieren wir die Zeit, die das Standardsignal braucht, um 63% der entgültigen Signalhöhe zu erreichen, respektive um vom Plateau wieder bis auf 37% der vorherigen Signalhöhe abzufallen. Weil die Signaldispersion bei dieser Prozedur aus verschiedenen Gründen höher ist als bei einer normalen Messung, wird die Zeitkonstante daher eher

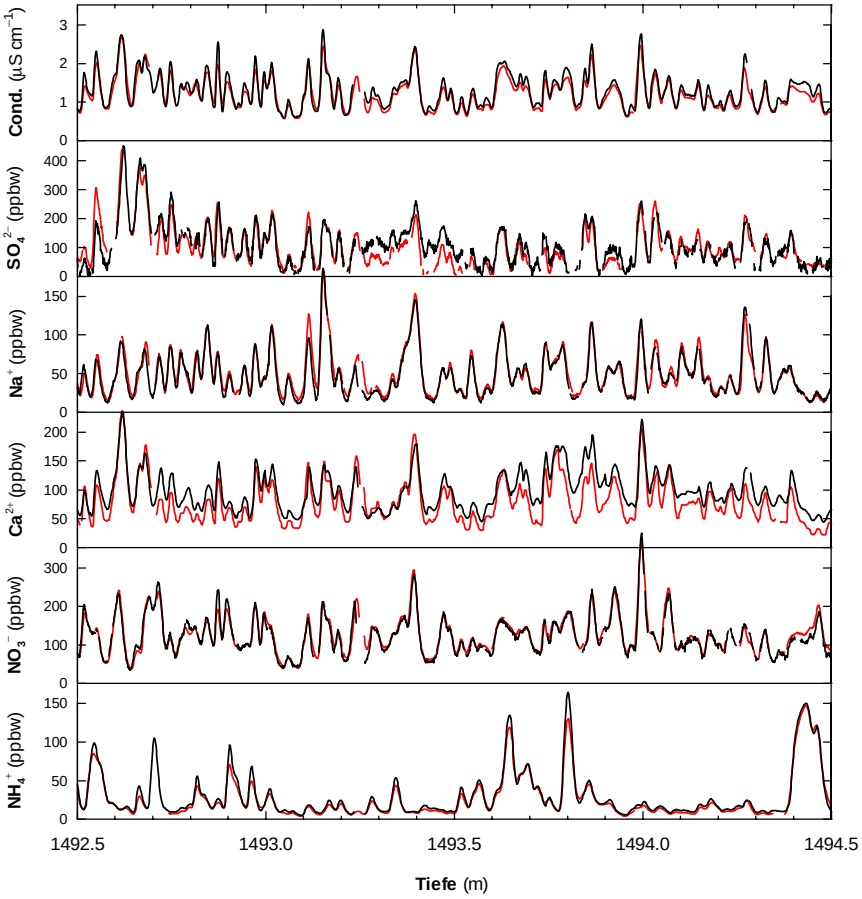

Abbildung 3.3: Zweimaliges Messen eines 2m-Tiefenabschnittes in NorthGRIP-Eis aus der Jüngeren Dryas.

überschätzt. Multipliziert man diese Zeitkonstante mit der Schmelzgeschwindigkeit erhält man eine konservative Abschätzung der Tiefenauflösung im Eis bei CFA-Messungen.

3.2 Schmelzsystem

In den letzten Jahren hat sich das kontinuierliche Schmelzen von Eiskernproben, anstelle der arbeitsintensiven, manuellen Dekontamination von Einzelproben im Kühlraum, für viele Analysemethoden durchgesetzt. Es werden nicht nur CFA-Systeme (im Einsatz unter anderem auch in Heidelberg, Tucson, Cambridge und Bremerhaven) und quasi-kontinuierliche Ionenchromatographie (FIC, in Florenz) zur Bestimmung von Ionen im Eis kontinuierlich mit kontaminationsfreiem Schmelzwasser versorgt, sondern zum Beispiel auch Massenspektrometer zur Bestimmung von Wasser- und Luftisotopen an Eisproben (an unserer Abteilung, *Huber et al.*, 2003; *Huber und Leuenberger*, 2003; *Huber und Leuenberger*, 2002) und ICP-Massenspektrometer zur Elementanalyse (am Departement für Chemie und Biochemie der Universität Bern, *Knüsel et al.*, 2003). Diese Schmelzsysteme stammen alle mehr oder weniger von der hier in Bern entwickelten Schmelzanlage ab.

Das scheinbar simple Problem Eisproben kontinuierlich zu schmelzen und das unkontaminierte Schmelzwasser nur vom zentralen Bereich abzupumpen, stellt sich als kniffliger heraus als angenommen, vor allem weil die benötigte Schmelzwassermenge in letzter Zeit zugenommen hat (mehr CFA-Komponenten, zusätzlich ans CFA-System gekoppeltes FIC, Autosampler, manuelle Probennahmen) und die Schmelzköpfe immer grösser gebaut werden mussten. Mit den bestehenden Schmelzköpfen ergaben sich verschiedentlich Probleme: Beispielsweise konnte manchmal die Schmelzgeschwindigkeit nicht genügend erhöht werden oder das Schmelzwasser wurde vom zentralen Bereich nach aussen verdrängt und konnte nicht in genügender Menge abgepumpt werden, dafür drang Luft ins System. Ein weiteres Problem war, dass das Schmelzen zum Teil nur ohne PTFE-Beschichtung im zentralen Bereich und mit Unterlegen von Unterlagsscheiben an den Rändern möglich war. Ausgehend von bestehenden Plänen und Überlegungen [*Sommer*, 2000], wurden daher neue, optimierte Schmelzköpfe konstruiert und gebaut. Die erste Neukonstruktion, die in NorthGRIP eingesetzt wurde, erfüllte die Erwartungen noch nicht, auch der in Bremerhaven eingesetzte zweiteilige Schmelzkopf befriedigte nicht. Erst für die Messkampagne 2001/2002 gelang es, einen zuverlässig funktionierenden Schmelzkopf zu bauen, der in der Folge noch etwas optimiert wurde. Die endgültige Konstruktion wird im folgenden Kapitel beschrieben. Der Vollständigkeit halber sei hier noch erwähnt, dass sich für Firnkerne ein spezieller Firnschmelzkopf (mit engen Schlitzen zum Ausgleichen der Kapillarkräfte im Firn), bewährt hat, der von Stefan Sommer, Dietmar Wagenbach und Hans-Georg Junghans entwickelt wurde [*Sommer*, 2000; *Röthlisberger et al.*, 2000].

3.2.1 Neukonstruktion des Schmelzkopfes

Der innere Bereich weist eine leicht konische Form auf, damit die Kontaktfläche vergrössert und der Wärmeübertrag verbessert wird. Das Gefälle hat keinen Einfluss auf das Fliessverhalten des Schmelzwassers, das ausschliesslich vom Stempeldruck des noch nicht geschmolzenen Eises und des aufgelegten Gewichtes beeinflusst wird. Die konische Form darf nicht zu ausgeprägt gewählt werden, weil sonst eine systematische Vermischung von Schmelzwasser aus verschiedenen Tiefenbereichen des Eises resultiert, was die Tiefenauflösung verschlechtert. Die Oberfläche muss sehr glatt ausgearbeitet sein, damit der Fluss des Schmelzwassers zu den Abpumpbohrungen erleichtert und hartnäckige Verschmutzungen vorgebeugt werden.

Weil Messungen ergaben, dass das Schmelzwasser durch den obengenannten Stempeldruck nach aussen gedrückt wird und damit nicht zur zentralen Abflussbohrung gelangt, sind neu sechs Abflussbohrungen radial angeordnet (Schnitt A in der Abbildung 3.4). Der Abstand der radialen Bohrungen zum Zentrum beträgt 8 mm, bei einem Durchmesser des Inneren Bereichs von 24 mm und sie liegen symmetrisch je 60° auseinander. Somit beträgt der maximale Abstand eines Punktes des inneren Bereiches von einer Abpumpbohrung etwa 6.5 mm, das entspricht fast einer Halbierung, verglichen zu Vorgängermodellen mit nur einer zentralen Bohrung. Aufgrund räumlicher Gegebenheiten mussten die Bohrungen erneut schräg mit einem Neigungswinkel von 45° aus dem Schmelzkopf geführt werden, was eine technische Herausforderung darstellt.

Als Grundmaterial wird reines Kupfer eingesetzt. Dieses weist eine sehr gute Wärmeleitfähigkeit bei relativ kleiner Wärmekapazität auf. Dadurch reagiert der Schmelzkopf viel weniger träge beim Beheizen und ist einfacher zu regeln. Ein Nachteil von Kupfer ist, dass es

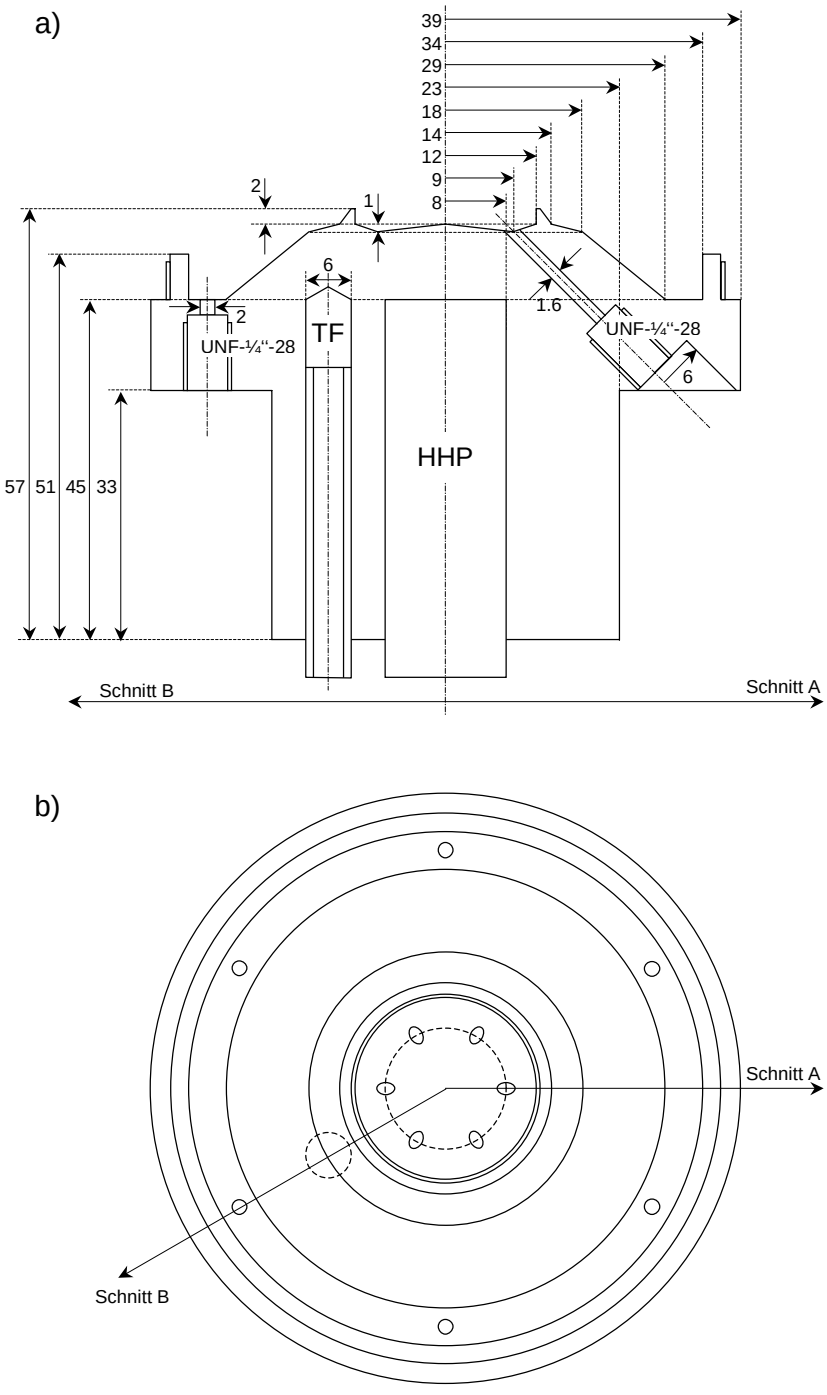

Abbildung 3.4: a) Schnittzeichnung und b) Grundriss des Schmelzkopfs für Dome C 2001/2002, mit Temperaturfühler (TF) und Hochleistungsheizpatrone(HHP).

sehr schwierig zu bearbeiten ist. Zum Beispiel reisst die Oberfläche beim Drehen sehr gerne auf oder Bohrer brechen ab, weil die Späne im Bohrloch stecken bleiben.

Die Oberfläche des Schmelzkopfes wird vergoldet. Das hat den Vorteil, dass sie chemisch inert ist und die Haftung von Schmutzpartikeln eingeschränkt wird. Im Gegensatz zu Teflonoberflächen (PTFE) wird eine sehr gute Wärmeleitfähigkeit erreicht. Weiter ist die mechanische Belastbarkeit hinreichend gut. Um eine optimale Beschichtung zu ermöglichen, sollte am Werkstück nur gedreht, gefräst oder gebohrt, nicht aber geschliffen oder poliert werden. Da ein chemisches Vergolden direkt auf Kupfer technisch nicht machbar ist, musste der Schmelzkopf zuerst mit etwa 5 μm chemisch Nickel, welches 7% Phosphor enthält, beschichtet werden. Darauf folgte eine Schicht von etwa 2 μm Glanzgold, welches etwa 2% Silber enthält. Diese Arbeiten wurden von der Firma Collini-Flühmann AG in Dübendorf ausgeführt.

Testmessungen beim Schmelzkopf für NorthGRIP haben ergeben, dass der Abfluss des Schmelzwassers aus dem inneren Bereich begünstigt wird, wenn nur im Zentrum des Schmelzkopfes geheizt wird. Dann bildet sich ein Temperaturgradient zwischen dem inneren und dem äusserem Bereich und die Schmelzgeschwindigkeit wird vor allem durch das Abschmelzen des äusseren Bereiches der Eisprobe definiert. Die Eisprobe liegt also vor allem aussen auf, so dass der innere Bereich besser abgedichtet und vor Kontamination geschützt ist. Innen ist eine höhere Energie zum Schmelzen vorhanden, dadurch entsteht ein weniger dünner Wasserfilm, so dass das Schmelzwasser einfacher zu den Abpumpbohrungen gelangen kann. Die Dichtheit des Kranzes zwischen dem inneren und dem äusseren Bereich wurde am GRIP-Schmelzkopf, welcher die gleiche Form aufweist (Höhe 2 mm, Dicke 2 mm, aussen konisch, innen senkrecht abfallend) im Zusammenhang mit Tests für kontinuierliche Isotopenmessungen an Eisproben nachgewiesen.

Geheizt wird der Schmelzkopf mit einer Hochleistungsheizpatrone (400 W von Electrolux Professional mit metrisch geschliffenem Edelstahlmantel). Im Gegensatz zu den bisher verwendeten Heizpatronen mit eingeschweisstem, nach innen gewölbtem Patronenboden weist die nun im Einsatz stehende Heizpatrone vorne einen flachen Kupferboden auf. Dadurch ist eine bessere Wärmeübertragung zum zentralen Bereich gewährleistet. Bedingt durch geometrische Gegebenheiten fiel die Wahl auf einen Patronendurchmesser von 16 mm. Um die nötige Leistung zu erreichen, muss die Patrone mindestens 50 mm lang sein, weil die Leistungsdichte an der Oberfläche höchstens 20 $\mathrm{W\,cm^{-2}}$ bei Passung nach H7 betragen darf. Damit ein allfälliger Ersatz der Heizpatrone möglich ist, wird sie jedoch nur 45 mm tief in den Schmelzkopf eingelassen, so dass sie mit einer Zange an den vorstehenden 5 mm (unbeheizte Zone) herausgezogen werden kann. Denn die Erfahrung hat gezeigt, dass sich Heizpatronen nach längerem Einsatz in der Bohrung festsetzen und nicht mehr an den einreduzierten Glasseidenlitzen herausgezogen werden können. Der Einsatz von Heizfolien und Flachheizelementen (Minco) wurde ebenfalls geprüft. Diese würden eine gleichmässige, flächige Energieverteilung im gesamten Schmelzkopf ermöglichen und könnten einfach mit einer Edelstahlplatte auf den Schmelzkopfkörper aufgeschraubt und angepresst werden. Die mit Heizfolien mögliche Leistungsdichte liegt jedoch weit unterhalb der erforderlichen, so dass der Einsatz von Heizfolien und Flachheizelementen nicht realisierbar ist.

Eigentlich würde sich der Einsatz von Hochleistungsheizpatronen mit eingebautem Temperatur-Widerstandsfühler aufdrängen, weil das Regelverhalten stabiler ist, wenn der Temperaturfühler möglichst nahe beim Heizkörper liegt (kurze Regelstrecke) und weil bei den sehr engen räumlichen Verhältnissen auf eine zusätzliche Bohrung für den Temperaturfühler verzichtet werden könnte. Eine Evaluation hat jedoch ergeben, dass die Heizpatrone mit eingebautem Fühler bei der gewünschten Leistung ungefähr 90 bis 100 mm lang ausgeführt werden müsste. Da jedoch die Heizleistung vor allem vorne erforderlich ist, und das weitere Vergrössern des Schmelzkopfes zu einer grösseren thermischen Trägheit führen würde, wurde auf den Einsatz solcher Patronen verzichtet und erneut eine spezielle Bohrung für einen Eigenbau-Temperaturfühler ausgeführt. Dieser besteht aus einem Temperatur-Widerstandsfühler Pt-100, der an ein Koaxialkabel gelötet und in einem kleinen zylinderförmigen Kupferstück fixiert ist. Dieses ist vorne kegelförmig abgedreht, so dass es optimal in die Bohrung passt und eine gute Wärmeübertragung möglich ist. Der Temperaturfühlerkopf wird nun auf ein Kupferröhrchen (6 mm AD, 4 mm ID) geschraubt, durch welches das Koaxialkabel geführt wird. Das Röhrchen und der Kopf wird mit Wärmeleitpaste bestrichen, in die Bohrung geschoben und mit Schraube und Unterlagsscheibe fixiert. Auch hier stehen 5 mm hervor, damit der Temperaturfühler leicht ausgebaut werden kann. Die Temperatursteuerung erfolgt über eine der mehrfach im CFA-System verwendeten Eigenbau-Temperatursteuerungen.

Damit alle Verbindungen dicht genug sind und nicht Luft eingesaugt werden kann, sind alle Anschlüsse mit UNF-$\frac{1}{4}$"-28-Fittingen versehen worden. Da die Oberflächenbeschichtung mit chemisch Nickel und Gold an den Innenwänden der Bohrung (Durchmesser 1.6 mm) aus verfahrenstechnischen Gründen nicht gewährleistet werden kann, werden die PTFE-Schläuche (1.6 mm AD, 0.5 mm ID) ohne Flansch durch die Bohrung bis fast zur Schmelzkopfoberfläche geführt. Die Fixierung geschieht durch ein etwa 2 mm langes Silikonschlauchstück (4.0 mm AD, 1.0 mm ID), das durch das Fitting zusammengedrückt wird und dadurch auch den PTFE-Schlauch festhält. Die Zusammenführung von je drei Leitungen aus dem inneren Bereich geschieht mittels eines X-Stückes mit vier UNF-$\frac{1}{4}$"-28-Anschlüssen.

Um das Ablaufen des Schmelzwassers vom äusseren Bereich zu unterstützen, wurde hier nicht auf eine Neigung verzichtet, denn das Wasser darf nicht rund um die schmelzende Eisprobe verbleiben. Bei einem möglichen Steckenbleiben der Probe würde dieses kontaminierte Wasser vom äusseren Bereich durch Kapillarkräfte und die Pumpe in den inneren Bereich gezogen. Sechs separate Wasteabflüsse mit separaten Pumpschläuchen vermindern zudem die Überlaufgefahr. Zur Illustration ist der Dome C 20001/2002 Schmelzkopf, der im wesentlichen der aktuellsten Version entspricht, auf Seite 12 abgebildet (Abbildung 1.8).

3.2.2 Wegaufnehmer, Probenhalterung und Probenvorbereitung

Neu wurde ein Wegaufnehmer (Inkrementeller-Wellen-Drehgeber BSM 16.05K500-F4-H) von Baumer Electric in Frauenfeld eingesetzt, mit 500 Impulsen pro Umdrehung, 5 V Ausgangssignal, einem sehr kleinen Drehmoment und einem Temperaturbereich von -20°C bis +85°C. Weil die maximale radiale Wellenbelastung 6 N nicht überschreiten darf, musste eine zusätzlich gelagerte Welle gebaut werden. Das Wegaufnehmerrad, über das ein dünner Stahldraht mit angehängtem Schmelz- und Gegengewicht führte, wurde durch ein Zahnrad ersetzt. Anstelle des Stahldrahtes hängen die Gewichte nun an einem dünnen Zahnriemen. Dadurch wird ein

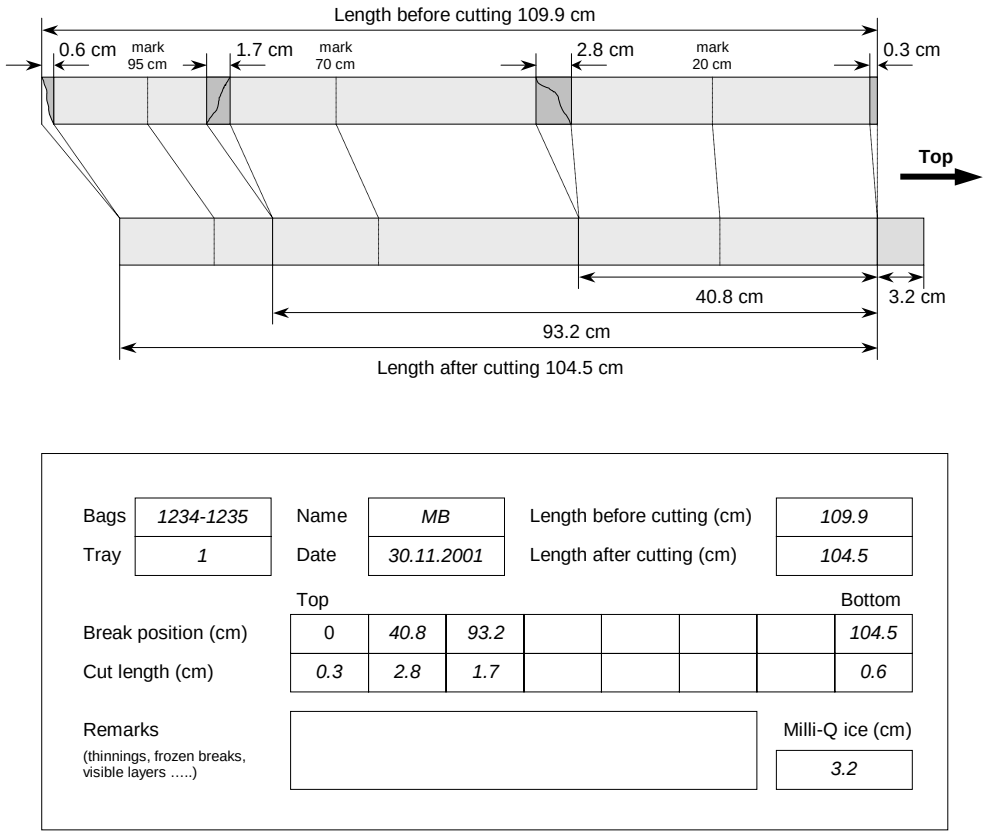

Abbildung 3.5: Eisprobenvorbereitung und Protokollblatt.

Rutschen und damit fehlerhaftes Aufzeichnen des Schmelzvorgang verhindert, wie es gelegentlich bei der Verwendung des Stahldrahts beobachtet wurde. Noch optimaler wäre eine berührungsfreie Distanzmessung anstelle eines Wegaufnehmers. Die evaluierten Modelle sind jedoch entweder sehr teuer, nicht genau genug oder nicht für Temperaturen unter dem Gefrierpunkt ausgelegt. Des weiteren wurde die bisherige Probenhalterung verbessert und neue, einfacher einzustellende Schmelzschienen hergestellt, deren Oberflächen wie bisher teflonisiert wurden. Dies führt zu besserem Gleiten und weniger Kontamination in der Schiene.

Neue Halterungen zur Probenvorbereitung ermöglichen ein schnelleres Arbeiten im Kaltlabor. Es hat sich bewährt, die beiden Enden der Eisproben und die Brüche nicht mehr mit der Bandsäge, sondern mit Microtome-Klingen senkrecht abzuschaben. Ein schräges Bearbeiten führt zu einem Verkeilen der Eisprobenstücke in der Schmelzschiene und zum Steckenbleiben der Probe während des Schmelzvorganges. Damit verbunden ist meistens das unliebsame Einbringen von Luft in die CFA-Nachweissysteme. Für die Bearbeitung der Schnitt- und Bruchflächen kamen Trimming-Klingen (80 mm, Feather, S35, F-80 von Stehelin AG in Basel) zum Einsatz. Die Probenvorbereitung gemäss dem in Abbildung 3.5 dargestellten Verfahren (samt Protokollblatt) hat sich bewährt. In dieser Notation werden die Masse der Eisproben und die Lage und Länge der Brüche in das Auswertungsprogramm übernommen und die Daten entsprechend korrigiert. Grosszügiges Zuschneiden aller irregulären Stellen an Eisproben

lohnt sich, da eine Datenlücke leichter zu verkraften ist, als ein Kontaminationspeak, der fälschlicherweise als Signal interpretiert werden könnte.

3.3 Verbesserungen bei der Sulfatnachweismethode

Die Sulfatnachweismethode ist ausführlich dokumentiert in der Diplomarbeit *Bigler* [2000] und kurz beschrieben in *Röthlisberger et al.* [2000] und *Bigler et al.* [2002]. Die im Hinblick auf die NorthGRIP-Messkampagne realisierten Verbesserungen werden in diesem Kapitel kurz beschrieben.

Das wesentliche Problem ist, dass die $SO_4{}^{2-}$-Absorptionsnachweismethode sehr empfindlich auf kleinste Flussänderungen reagiert, welche ein grosses chemisches Rauschen und Basislinieninstabilitäten verursachen. Die Situation wird verschärft, weil der Gegendruck im System sehr gross ist, wegen der notwendigen, grossen Kationentauschersäule und der Gegendruckschlaufe, die das Ausgasen des Probestroms verhindern. Die Ismaprene-Pumpschläuche, die wegen dem hohen Ethanolgehalt der Reagenzien verwendet werden müssen, weisen eine nicht besonders gute Pumpkonstanz auf. Eine wesentliche Verbesserung gelang daher durch das Entkoppeln der Flüsse nach der Kationentauschersäule mittels eines Pipettenspitzen-Debubblers. Die Abbildung 3.6 zeigt den neuen Systemaufbau, der etwas komplexer ist, als bei den anderen CFA-Komponenten.

Eine Verbesserung der Kalibration, vor allem bei tiefen Massenkonzentrationswerten, konnte durch das Anwenden einer nichtlinearen Kalibrationskurve erreicht werden. Fast bei jeder Kalibration zeigt sich nämlich, dass die hohen Werte auf einer Geraden mit negativem Ordinatenabschnitt liegen. Unterhalb einer bestimmten Schwelle knickt die Kalibrationskurve

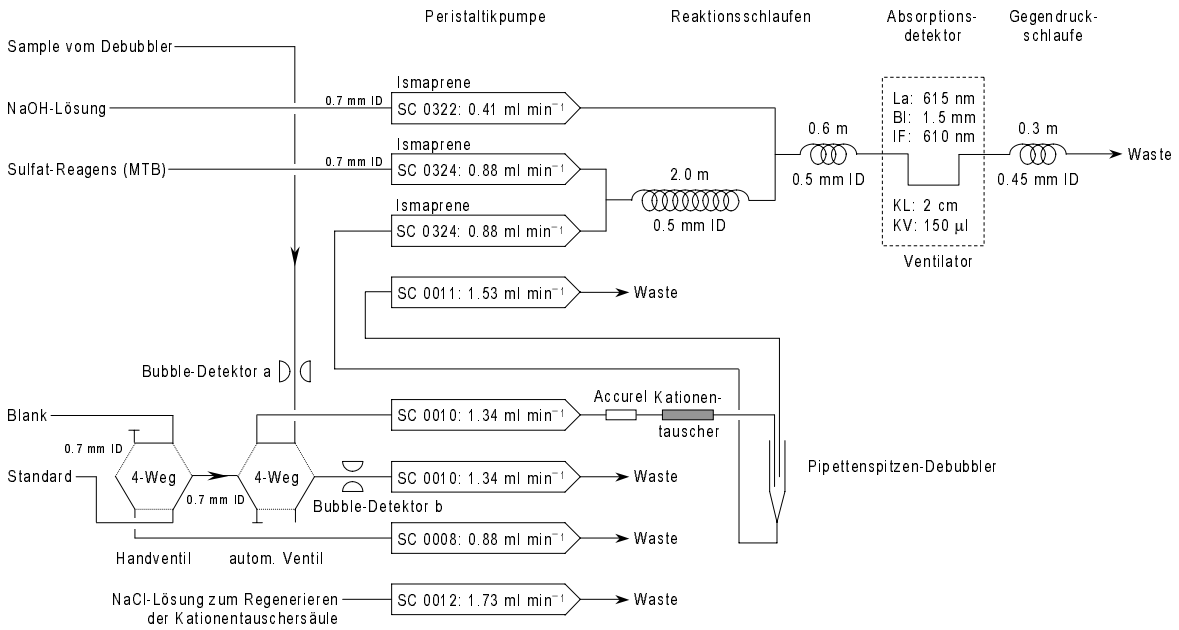

Abbildung 3.6: Der neue Systemaufbau des Sulfatnachweissystems.

ab und geht für kleine Konzentrationswerte proportional durch Null. Obwohl der Übergang bei der Schwelle fliessend ist, wird die Kalibration in zwei Abschnitte unterteilt, einen proportionalen Teil unterhalb der frei wählbaren Schwelle und einen linearen Teil oberhalb. Der Übergangspunkt wird visuell aufgrund der vier Standardmessungen ausgewählt, die bei jeder Kalibration durchgeführt werden. Die entsprechende Routine ist im Datenauswertungsprogramm eingebaut.

Aufgrund der fast Tausend Kalibrationsmessungen, die in NorthGRIP durchgeführt wurden, lässt sich die mittlere Detektionslimite zu 36 ppbw (Standardabweichung 31 ppbw) bestimmen. Dazu kommt eine, im Vergleich zu den anderen CFA-Komponenten, deutlich schlechtere Zeitauflösung. Obwohl sich mit der Nachweismethode brauchbare $SO_4{}^{2-}$-Datensätze erzeugen lassen, vor allem bei glazialen Konzentrationen oder bei Vulkanpeaks, wäre eine Verbesserung der Kenndaten wünschenswert, hin zu einer Detektionslimite von maximal 5 ppbw und einer besseren Zeitauflösung. Prüfenswert ist zum Beispiel die Barium-Dimethylsulfonazo-III-Methode [*Yang et al.*, 1997b; *Yang et al.*, 1997a], die jedoch vermutlich eine nicht wesentlich bessere Performance aufweist, als die eingesetzte Methylthymolblue-Methode. Unter Umständen wurden in den vergangenen fünf Jahren neue Nachweismethoden entwickelt, eventuell sogar Fluoreszenz-Nachweismethoden, die damals noch nicht verfügbar waren. Eine erneute Evaluation erscheint daher sinnvoll. Fest steht, dass das Potential des bestehenden Nachweissystems ausgeschöpft ist.

3.4 Messung der Partikelgesamtkonzentration und der Grössenverteilung

3.4.1 Überblick über den Partikelsensor und den Partikelzähler Abakus

Am Institut für Umweltphysik der Universität Heidelberg wurde in den letzten Jahren eine kontinuierliche, hochauflösende Messmethode zur Bestimmung der Gesamtkonzentration und Grössenverteilungen unlöslicher Mikropartikel im Schmelzwasser von Eisbohrkernen etabliert. Anwendungsgebiete des kommerziell erhältlichen Partikelsensors und Partikelzählers Abakus der Firma Klotz (Bad Liebenzell, Deutschland, www.fa-klotz.de) sind die Reinheitskontrolle von Wasser, pharmazeutischen Lösungen, Chemikalien, Getränken und die Korngrössenanalyse von technischen Suspensionen. Im Sommer 2001 wurde an der Abteilung für Klima- und Umweltphysik der Universität Bern ein ebensolches Gerät angeschafft, welches das bestehende CFA-System um eine weitere Messkomponente ergänzt. Damit konnte das unbefriedigend funktionierende Partikelmessgerät der Universität Kopenhagen ersetzt werden, das in den vorangegangenen Messkampagnen in Dome C eingesetzt wurde. Das Ziel dieses Kapitels ist es, das neue Gerät zu beschreiben sowie in dessen Handhabung einzuführen. Die folgenden Informationen stammen vorwiegend aus der Gerätebeschreibung des Partikelzählers Abakus (Ausgabe 09/2001), dem Datenblatt des Partikelsensors LDS 2187, den Arbeiten von Paul Saey und Urs Ruth [*Saey*, 1998; *Ruth*, 2002] und persönlichen Mitteilungen der beiden, sowie von Dietmar Wagenbach und von Mitarbeitern der Herstellerfirma.

Der Partikelsensor erfasst Mikropartikel in einem Probefluss mit Hilfe eines Diodenlasers, der eine Wellenlänge von 670 nm aufweist. Im Vergleich zur Messung an Einzelproben mittels der bewährten Coulter Counter Messmethode liefert das kontinuierliche Messen mit dem

Abakus in Verbindung mit einer Schmelzanlage eine höhere Auflösung und reduziert die Kontaminationsgefahr, insbesondere bei kleinen Partikeln. Vergleiche der beiden Messverfahren liefern gute Übereinstimmung für die Partikelgesamtkonzentration, jedoch systematische Abweichungen der Grössenverteilung. Zudem ist beim Abakus eine Partikelerfassung erst ab etwa einem Partikeldurchmesser von 1 μm möglich, statt ab 0.6 μm wie beim Coulter Counter. Der Partikeldurchmesser wird gemäss *Klotz* [1989] als Äquivalenzdurchmesser definiert, welcher ein kugelförmiges Partikel aufweist, das den gleichen Extinktionseffekt verursacht.

Als Partikelsensor wurde der Typ LDS 23/25 bs mit spezieller, linearer Verstärkung gewählt. Dieser weist einen Messbereich von 0.8 bis 50 μm auf. Bei kleinster Partikelgrösse wird ein Zählwirkungsgrad von mindestens 50% garantiert. Im kontinuierlichen Messbetrieb von Mineralstaub erweist sich eine untere Nachweisgrenze des Partikeldurchmessers von 1 μm als adäquater Wert. Die maximal erfassbare Konzentration liegt bei 150'000 Partikeln ml^{-1} bei einem Koinzidenzfehler von etwa 8%. Die untere Nachweisgrenze der Partikelgesamtkonzentration beträgt ungefähr 500 Partikeln ml^{-1}. Um Schlauchverbindungen mit UNF-$\frac{1}{4}$"-28-Fittings zu ermöglichen, wurden entsprechende Edelstahlübergangsstücke mitbestellt. Diese dürfen nur leicht festgezogen werden (Linksgewinde), so dass die Quarzglasküvette nicht unter Druck gesetzt wird.

Der Partikelzähler Abakus weist 32 frei definierbare Grössenklassen auf und ist mit einem Analogausgang bestückt. Auf unseren Wunsch hin, wurde durch Verwendung der Gerätesoftwareversion 'Korn 67 (2.91 01/09/11)' der Analogausgang speziell für einen kontinuierlichen Betrieb konfiguriert. Das heisst, dass eine einstellbare Partikelgesamtkonzentration von maximal 99'999 Partikeln pro Sekunde eine Ausgangsspannung von 10 V erzeugt. Standardmässig gibt dieser Ausgang lediglich die integrierte Partikelgesamtkonzentration einer Messung aus, wobei der errechnete Spannungswert bis zum Ende der nächsten Messung ausgegeben wird. Die Messergebnisse der Grössenverteilung können in kumulativer oder distributiver Form auf dem LCD-Display dargestellt werden. Der Messwertspeicher ist für 1400 Messungen ausgelegt; er kann über die serielle Schnittstelle (RS 232) mit Hilfe einer Auswertesoftware ausgelesen werden. Weitere Funktionen sind in der ausführlichen Betriebsanleitung zum Gerät und im Unterkapitel 3.4.4 beschrieben.

3.4.2 Inbetriebnahme, grundsätzliche Handhabung und Lagerung

Die grösste Gefahr ist, dass die Laserdiode des Partikelsensors bei Überlastung durchbrennt. Dies kann geschehen, wenn der Laserdiodenstrom maximiert wird, weil die Durchflusszelle des Partikelsensors luftgefüllt oder verstopft ist. Wird an einer der rückseitigen BNC-Buchsen des Partikelzählers ein Strom deutlich grösser als einige mV gemessen (maximal treten etwa 13 V an der einen beziehungsweise ungefähr 6.5 V an der anderen Buchse auf) muss das Gerät möglichst rasch am Netzschalter ausgeschaltet werden. Eine zunehmende Verschmutzung der Durchflusszelle des Partikelsensors äussert sich in einem langsamen Anstieg des Diodenstroms von einigen mV in den Bereich von 1 V. Auch in diesem Fall muss das Gerät ausgeschaltet und im ausgeschalteten Zustand gründlich gespült werden. Bei hartnäckiger Verschmutzung schafft Spülen mit 0.01M-HCl-Lösung, 50%-igem Ethanol oder kalklösender Spülmittellösung Abhilfe. Um einer zunehmenden Verschmutzung der Durchflusszelle des Partikelsensors vorzubeugen, sollte präventiv die Durchflussrichtung täglich gewechselt werden.

Das regelmässige Wechseln der Durchflussrichtung führt gleichzeitig zu einer verbesserten Datenqualität. Hierzu ist eine Halterung hilfreich, die eine 180°-Drehung des Sensors erlaubt, da die Durchflussküvette immer von unten nach oben durchflossen werden muss, damit Luftblasen nicht hängen bleiben. Weil die UNF-$\frac{1}{4}$"-28-Fittinge direkt am Partikelsensor mühsam mit Teflonband abgedichtet werden müssen (Metall-Kunststoff-Schraubverbindung), sollten bei der Änderung der Durchflussrichtung nicht diese Anschlüsse geöffnet werden, sondern eigens dafür vorgesehene Fittinge und Kupplungen (Kunststoff-Kunststoff-Schraubverbindung) einige Zentimeter von den heiklen Anschlüssen am Partikelsensor entfernt. Werden während einer Messkampagne für längere Zeit keine Daten aufgezeichnet und der Laserdiodenstrom nicht regelmässig überwacht, empfiehlt es sich, den Partikelzähler auszuschalten.

Es hat sich verschiedentlich gezeigt, dass der Fluss durch den Partikelzähler nicht zu klein gewählt werden darf. Ideal ist ein Wert zwischen 1.5 $\mathrm{ml\,min^{-1}}$ und 6 $\mathrm{ml\,min^{-1}}$. Ist vorauszusehen, dass die Partikelgesamtkonzentration Werte von 150'000 Partikeln $\mathrm{ml^{-1}}$ häufig übersteigen wird, wie zum Beispiel in grönländischem Eis aus dem letzten glazialen Maximum, ist ein Verdünnungsschritt der Probe vorzusehen. Dazu wird am einfachsten Milli-Q-Wasser mit einem T-Stück in einem gleichbleibenden Verhältnis der Probe beigemischt. Figur 3.7 zeigt den Systemaufbau der Partikelmessung während der Feldsaison 2001/02 auf Dome C, wo ein Verdünnungsschritt nicht notwendig war. Die Durchflussrate betrug etwas mehr als 1.7 $\mathrm{ml\,min^{-1}}$. Überall wurden möglichst kurze PTFE-Schläuche mit einem Innendurchmesser von 0.7 mm verwendet. Der Aufbau entspricht im wesentlichen dem üblichen Aufbau einer CFA-Komponente. Das automatische Ventil verhindert, dass vor und nach der geschmolzenen Eisprobe Luft in den Partikelsensor gelangen kann. Als Blank wird Milli-Q-Wasser verwendet, das bei ungenügender Qualität gefiltert werden sollte.

Bis zu einigen Tagen sollte die Messzelle des Partikelsensors nass gelagert werden, das heisst, es sollte beispielsweise durch Kurzschliessen der Anschlussschläuche sichergestellt werden, dass diese nicht austrocknen kann und keine Luftblase hinein gelangen kann. Vor längerer Lagerung sollte die Messzelle des Partikelsensors erst mit Wasser und dann kurz mit Ethanol gespült werden. Nach möglichst staubfreier Trocknung sollten die Anschlüsse durch Kurzschliessen der Anschlussschläuche oder durch Stopfen verschlossen werden. Bei drohenden Temperaturen unter dem Gefrierpunkt muss die Messzelle des Partikelsensors unbedingt getrocknet gelagert oder transportiert werden, weil sonst die Küvette beschädigt wird.

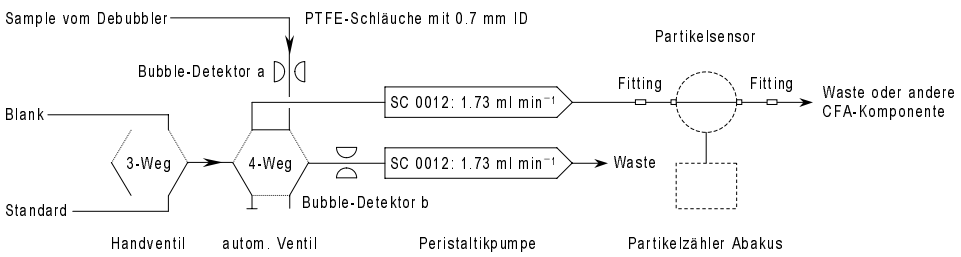

Abbildung 3.7: Systemaufbau zur Messung Partikelgesamtkonzentration und der Grössenverteilung.

3.4.3 Messung der Partikelgesamtkonzentration am Analogausgang

Der Analogausgang des Partikelzählers wird zur Angabe der Partikelgesamtkonzentration in Volt in hoher zeitlicher Auflösung verwendet. Diese Auflösung ist im Vergleich mit denjenigen der übrigen CFA-Komponenten sogar noch etwas besser. Der Analogausgang von 0 bis 10 V kann bei der 15-poligen Steckerbuchse (SUB-D) geräterückseitig an Pin 7 gegen Ground an Pin 14 oder 15 abgegriffen werden. Am besten benutzt man ein BNC-Kabel mit einem entsprechenden 15-poligen Stecker. Im Hauptmenü kann unter 'Einstellungen/Geräteeinstellungen/Analogausgang' die Partikelzählrate pro Sekunde eingestellt werden, die das maximale Ausgangssignal von 10 V erzeugt. Der grösstmögliche einstellbare Wert hängt von der verwendeten Gerätesoftware ab und beträgt bei unserem Gerät 99'999 Partikel $\mathrm{s}^{-1}\,(10\mathrm{V})^{-1}$ (Gerätesoftwareversion 'Korn 67 2.91 01/09/11'). Am einfachsten probiert man aus, welcher Wert den gegebenen Umständen am besten entspricht: Partikelpeaks sollten nicht oder wenigstens nicht zu häufig abgeschnitten werden, die Signale sollten jedoch auch nicht zu niedrig sein, da die Auflösung sonst zu schlecht wird und das Signal nur noch wenige diskrete Werte annimmt. Es ist ratsam, die Einstellung des Analogausganges bei sich ändernden Partikelgesamtkonzentrationen häufig anzupassen. Ein paar abgeschnittene Peaks, dann wenn die Partikelgesamtkonzentration plötzlich stark ansteigt, ist weniger gravierend als ständig zu kleine Ausgangssignale am Analogausgang. Die Einstellung des Analogausganges muss für die spätere Datenauswertung unbedingt im Messprotokoll festgehalten werden. Bei der Einstellung des Analogausganges darf ferner der Koinzidenzfehler nicht vergessen werden, der bei einer Durchflussrate von 1.5 $\mathrm{ml\,min}^{-1}$ und einer Einstellung des Analogausgangs von über 6000 Partikel pro Sekunde und 10 V Ausgangssignal bereits etwa 8% ausmacht. Der Start der Messung geschieht im Hauptmenü des Partikelzählers unter 'Messungen/Externer Start/Stop' durch Drücken von 'MES'. Wird die Pumpe ausgeschaltet oder wird längere Zeit Luft gepumpt, sollte der Abakus am Netzschalter ausgeschaltet werden.

Beim späteren Auswerten wird auch die genaue Durchflussrate benötigt, um die Partikelgesamtkonzentration in der Einheit Partikelanzahl (>1 μm) pro Milliliter anzugeben. Deshalb muss mindestens einmal täglich, auf jeden Fall aber bei jeder Änderung am System (auch vor und nach dem Spülen), die Durchflussrate in $\mathrm{ml\,min}^{-1}$ gemessen und festgehalten werden. Insbesondere empfiehlt sich die Messung der Durchflussrate knapp vor und nach dem Wechsel des Pumpschlauches. Zur Bestimmung der Flussrate genügt eine Stoppuhr sowie ein kleiner, präziser Messzylinder oder eine Waage. Der daraus folgende Kalibrierungsfaktor k, der bei der Auswertung mit dem Rohdatensignal (in V) multipliziert wird, hat die Einheit Partikelanzahl $\mathrm{ml}^{-1}\,\mathrm{V}^{-1}$ und berechnet sich aus der Durchflussrate f in in $\mathrm{ml\,min}^{-1}$ und der Einstellung a des Analogausgangs in Partikelanzahl $\mathrm{s}^{-1}\,(10\mathrm{V})^{-1}$ wie folgt:

$$k = \frac{a}{f} \cdot \frac{60\mathrm{s}}{\mathrm{min}} \tag{3.5}$$

3.4.4 Messung der Partikelgrössenverteilung

Für die Messung der Partikelgrössenverteilung ist es sinnvoll, alle zur Verfügung stehenden 32 Kanäle zu nutzen und die Kanäle logarithmisch auf den Grössenbereich von ca. 0.8 μm bis ungefähr 12 μm Durchmesser zu verteilen. Da für die Auswertung der Grössenverteilungen der Bereich zwischen 0.8 μm und 5 μm besonders wichtig ist, kann die Kanaldichte hier

n	d_n (μm)	Δ_n (μm)	n	d_n (μm)	Δ_n (μm)	n	d_n (μm)	Δ_n (μm)	n	d_n (μm)	Δ_n (μm)
1	0.8	0.8	9	1.8	0.2	17	3.9	0.4	25	8.6	0.8
2	0.9	0.1	10	2.0	0.2	18	4.3	0.4	26	9.5	0.9
3	1.0	0.1	11	2.2	0.2	19	4.8	0.5	27	10.5	1.0
4	1.1	0.1	12	2.4	0.2	20	5.3	0.5	28	11.6	1.1
5	1.2	0.1	13	2.6	0.2	21	5.8	0.5	29	12.8	1.2
6	1.3	0.1	14	2.9	0.3	22	6.4	0.6	30	14.1	1.3
7	1.4	0.1	15	3.2	0.3	23	7.1	0.7	31	15.6	1.5
8	1.6	0.2	16	3.5	0.3	24	7.8	0.7	32	∞	∞

Tabelle 3.1: Kanaleinteilung: Kanalnummer n, Intervallobergrenze d_n und Kanalbreite Δ_n.

höher gewählt werden. Für die Dome C Saison 2001/2002 wurden die Kanäle gemäss Tabelle 3.1 eingestellt. Sie weisen konstante logarithmische Grössenintervalle auf, welche alle 7 Kanäle verdoppelt werden: $d_{n+1}/d_n \approx \sqrt[7]{2}$. Vor der Messkampagne sollten die Speicherparameter des Partikelzählers unter 'Messwertspeicher/Organisation' wie folgt gesetzt werden: Datensätze auf '1', Messungen auf '1265'. Auch die Uhr muss eingestellt werden: 'Einstellungen/Geräteeinstellungen/Uhr stellen'. Die Messung wird wie gewohnt gestartet. Nach der Beendigung der Messung durch Drücken auf 'STOP', muss die Grössenverteilung in den Messwertspeicher geschrieben werden, dazu wird 'MEM' gedrückt. Achtung, nicht versehentlich 'BACK' wählen, dadurch würde die Grössenverteilung gelöscht, ohne in den Messwertspeicher geschrieben zu werden. Um ein möglichst kontinuierliches Signal der Partikelgesamtkonzentration über den Analogausgang zu erhalten, empfiehlt es sich die neue Messung schon während den Blank- und Standardmessungen der CFA-Komponenten sowie während dem Schmelzen des Milli-Q-Eises laufen zu lassen. Ist die Anzahl der gemessenen Partikel hoch, so wird die Grössenverteilung der anschliessenden Messung verfälscht. Deshalb sollte in diesem Fall die Messung beim Übergang von Milli-Q-Eis auf Probe kurz gestoppt und nach dem Löschen der bisher aufgenommenen Grössenverteilung sofort neu gestartet werden. Dies geschieht durch Drücken von 'STOP', 'BACK', 'MES'. Das Starten und Stoppen hat zur Folge, dass der Analogausgang kurz ausgeschaltet wird und je nach Softwareversion auf Null oder den maximalen Ausgangsspannungswert geht; diese falschen Messwerte können bei der Auswertung problemlos entfernt werden. Vorsicht ist geboten, da sich diese Tastenkombination von derjenigen des Speichervorgangs nur wenig unterscheidet und dort das Drücken auf 'BACK' einen Datenverlust zur Folge hat. Ein ähnliches Vorgehen empfiehlt sich beim Messende.

Mit Hilfe eines seriellen Kabels können die aufgezeichneten Grössenverteilungen regelmässig einmal ausgelesen werden. Dazu wird das Programm 'Log and Show 2.22m' gestartet, welches die Verbindung mit dem Partikelzähler Abakus aufnimmt. Im Menü 'Options' muss anschliessend 'Read measuring buffer' gewählt werden. Nun können die im Abakus gespeicherten Dateien ausgelesen und auf den Computer übertragen werden.

Latexpartikel Durchmesser (μm)	Signal (mV)
0.8	84
1	139
2	212
5	571
10	1288
15	2215
25	4066
40	6812
50	8720

Tabelle 3.2: Kennlinie des Partikelsensors vom 12. April 2001.

3.4.5 Kalibrierung

Der Code für den Zugriff auf das Kalibrierungsmenü des Partikelzählers lautet '4123'. Zum Beispiel kann hier die Rauschspannung, als Mass für die permanente elektrische Hintergrundstörung, eingestellt werden, welche erfahrungsgemäss zwischen etwa 60 mV und 200 mV liegt. Die Rauschspannung unseres Partikelsensors betrug gemäss Herstellerangaben bei der Auslieferung 58 mV. Die Rauschspannung muss so eingestellt werden, dass sie über dem Rauschen des angeschlossenen Partikelsensors liegt. Die Vorgabe der Rauschspannung erfolgt über einen D/A-Wandler, das heisst in Schritten von knapp 10 mV, so dass die tatsächlich eingestellte Spannung von der eingegebenen um einige Millivolt abweichen kann. Wenn die Rauschspannung des Sensors nicht bekannt ist, kann ein automatischer Abgleich erfolgen. Während dem automatischen Abgleich ist unbedingt sicherzustellen, dass sich keine Partikel im Partikelsensor befinden. Am besten stellt man einen Rauschspannungswert ein, der zwischen dem Mittelwert und dem Maximalwert einiger automatischer Abgleichsmessungen liegt. Die Kennlinie, welche mit Latexpartikeln ebenfalls vom Hersteller (12. April 2001) aufgenommen wurde, ist aus der Tabelle 3.2 und der Figur 3.8 ersichtlich. Diese Kennlinie sollte regelmässig neu aufgenommen werden.

Der Vergleich der Abakus-Messungen mit dem etablierten Coulter Counter Messverfahren liefert eine recht gute Übereinstimmung für die Partikelgesamtkonzentrationen, jedoch systematische Abweichungen der Grössenverteilung. Zudem hat Urs Ruth festgestellt, dass Feldmessungen andere Grössenspektren als die Kalibrierungsmessungen im Labor ergaben. Dies liegt vermutlich daran, dass die kontinuierlichen Partikelmessungen im Feld anders durchgeführt werden als die Einzelmessungen bei der Kalibrierung, was sich in einer unterschiedlich starken Koagulation der Partikel äussern könnte; bei der Feldmessung passiert die Probe zwischen dem Schmelzkopf und dem Partikelsensor diverse Schläuche, Pumpschläuche, Verbindungen, Ventile und Verteilerstücke. Die Koagulation von Mineralstaubproben ist ein grundsätzliches Problem, das die Herstellung eines zuverlässigen Standards sehr stark erschwert, wenn nicht gar verunmöglicht. Auf jeden Fall sollte nicht irgendeine Partikelsuspension zur Kalibrierung eingesetzt werden, da die atmosphärisch transportierten Partikel meistens viel kleiner sind und ein anderes Formenspektrum aufweisen. Aus dem gleichen Grund

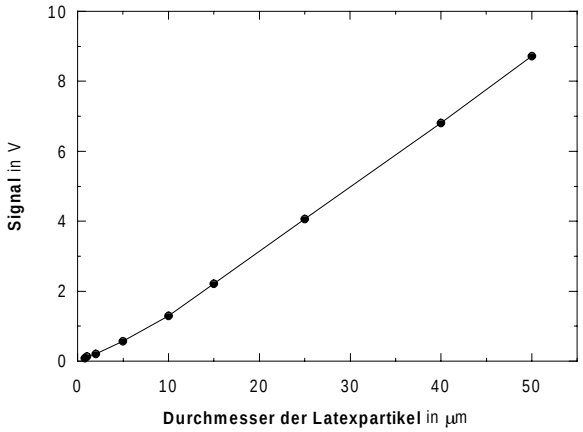

Abbildung 3.8: Kennlinie des Partikelsensors vom 12. April 2001.

hat sich auch die Kalibrierung mit Latexpartikeln als unzulänglich erwiesen, vor allem im Bereich der ganz kleinen Partikel. Daraus lässt sich schliessen, dass man für eine endgültige Grössenkalibrierung Referenzspektren gemessen an identischem Probenmaterial mit einem Coulter Counter heranziehen muss.

3.4.6 Weiterentwicklung der Partikelmessung

Eine erste grossangelegte Interkalibrierung wurde kürzlich an der Universität von Grenoble durchgeführt. Dort wurde mit allen innerhalb der EPICA Projekte (Dome C, DML) verwendeten Staubmessgeräten zahlreiche identische Proben von verschiedenen klimatischen Perioden gemessen. Die Auswertung dieser Interkalibration steht noch aus und wird im Rahmen der Dissertation von Fabrice Lambert weiterverfolgt. Ein erfolgreicher Abschluss dieser Interkalibrierung wird es möglich machen, die zahlreichen aufgenommenen Grössenverteilungen in Volumen- oder Massenverteilungen umzurechnen und zu interpretieren. Vorerst stehen somit nur hochaufgelöste Daten und Grössenspektren in der Einheit Partikelzahl pro Milliliter zur Verfügung. Methodisch ist es wünschenswert, zukünftig die gesamte Steuerung und Datenerfassung des Partikelzählers mittels ASCII-Befehlen vom CFA-Messprogramm aus zu übernehmen und die laufende Messung auf dem Bildschirm des CFA-Messcomputers darzustellen; dies wird den Messablauf vereinfachen und weniger fehleranfällig machen. Im weiteren wäre eine genaue, automatische und kontinuierliche Messung der Durchflussrate hilfreich. Die meisten dieser Arbeiten wurden im Rahmen der laufenden DML-Messkampagne von Urs Ruth in Angriff genommen. Der wichtigste Schritt um die hochaufgelöste, kontinuierliche Partikelmessung mit dem neuen Partikelmessgerät weiter zu etablieren, wird jedoch die Zurverfügungstellung von einfachen aber genauen Kalibrierungsroutinen sein.

Literaturverzeichnis

Adams, J. B., M. E. Mann, und C. M. Ammann, Proxy evidence for an El Niño-like response to volcanic forcing, *Nature, 426*, 274–278, 2003.

Anderson, T. L., R. J. Charlson, S. E. Schwartz, R. Knutti, O. Boucher, H. Rodhe, und J. Heintzenberg, Atmospheric science: Climate forcing by aerosol – a hazy picture, *Science, 300*, 1103–1104, 2003.

Bigler, M., 2000, Entwicklung und Anwendung einer neuen Methode zur kontinuierlichen, hochaufgelösten Messung der Sulfatkonzentration an alpinen und polaren Eisbohrkernen, Master's thesis, Physikalisches Institut der Universität Bern, Schweiz.

Bigler, M., R. Röthlisberger, F. Lambert, T. F. Stocker, G. C. Littot, E. W. Wolff, und D. Wagenbach, The continental contribution to the water-soluble aerosol deposited on the East Antarctic plateau (EPICA Dome C), *Journal of Geophysical Research, in preparation*, 2004.

Bigler, M., R. Röthlisberger, F. Lambert, T. F. Stocker, E. W. Wolff, E. Castellano, und R. Udisti, The Eemian interglacial represented in the chemical ice core record from Dome C, Antarctica, *Earth and Planetary Science Letters, in preparation*, 2004.

Bigler, M., D. Wagenbach, H. Fischer, J. Kipfstuhl, H. Miller, S. Sommer, und B. Stauffer, Sulphate record from a northeast Greenland ice core over the last 1200 years based on continuous flow analysis, *Annals of Glaciology, 35*, 250–256, 2002.

Curran, M. A. J., T. D. van Ommen, V. I. Morgan, K. L. Phillips, und A. S. Palmer, Ice core evidence for Antarctic sea ice decline since the 1950s, *Science, 302*, 1203–1206, 2003.

Delmonte, B., I. Basile-Doelsch, J.-R. Petit, V. Maggi, M. Revel-Rolland, A. Michard, E. Jagoutz, und F. Grousset, Comparing the EPICA and Vostok dust records during the last 220,000 years: Stratigraphical correlation and provenance in glacial periods, *Earth-Science Reviews, in press*, 2004.

Durand, G., J. Weiss, V. Lipenkov, B. Delmonte, G. Krinner, J. M. Barnola, R. Röthlisberger, und M. Bigler, Effect of impurities on grain growth in cold ice sheets: I Mechanisms and observations, *Journal of Geophysical Research, submitted*, 2004.

EPICA community members, Eight glacial cycles from an Antarctic ice core, *Nature, in press*, EPICA community members contributing to this paper are: L. Augustin, C. Barbante, P. Barnes, J.-M. Barnola, M. Bigler, E. Castellano, O. Cattani, J. Chappellaz, D. Dahl-Jensen, B. Delmonte, G. Dreyfus, G. Durand, S. Falourd, H. Fischer, J. Flückiger, M. Hansson,

P. Huybrechts, G. Jugie, S.J. Johnsen, J. Jouzel, J. Kipfstuhl, F. Lambert, G. Littot, R. Lorrain, V. Maggi, V. Masson-Delmotte, H. Miller, R. Mulvaney, H. Oerlemans, H. Oerter, G. Orombelli, F. Parrenin, D. Peel, J.-R. Petit, D. Raynaud, U. Ruth, J. Schwander, U. Siegenthaler, R. Souchez, B. Stauffer, J.P. Steffensen, B. Stenni, T.F. Stocker, R. Udisti, R. van de Wal, M. van den Broeke, J. Weiss, J.-G. Winther, E.W. Wolff, M. Zucchelli †, 2004.

EPICA Dome C 2001–02 science and drilling teams, Extending the ice core record beyond half a million years, *EOS, Transactions, American Geophysical Union, 83*(45), 509, The science team was E.W. Wolff, M. Bigler, E. Castellano, B. Delmonte, J. Flückiger, G. Krinner, F. Lambert, A. Landais, A. Marinoni, A. Migliori, M. Nyman, I. Schärmeli, M. Severi, and G. Teste. The drilling team was L. Augustin, M. Armeni, F. Frascati, N. Kjaer, A. Krasiliev, E. Lefebvre, A. Manouvrier, and S. Panichi, 2002.

Flückiger, J., 2003, *Nitrous oxide and methane variations covering the last 100,000 years: Insight into climatic and environmental processes*, Ph. D. thesis, Physikalisches Institut der Universität Bern, Schweiz.

Flückiger, J., und M. Bigler, Als Eisforscher in Dome C – ein Tagebuch, *Unipress – Forschung und Wissenschaft an der Universität Bern, 116*, 11–14, 2003.

Fuhrer, K., 1995, *Ammonium-, Calzium-, Wasserstoffperoxid- und Formaldehymessungen an einem grönländischen Tiefbohrkern: Diskussion der letzten 200,000 Jahre*, Ph. D. thesis, Physikalisches Institut der Universität Bern, Schweiz.

Huber, C., und M. Leuenberger, On-line determination of oxygen isotope ratios of water or ice by mass spectrometry, *Analytical Chemistry, 74*(18), 4611–4617, 2002.

Huber, C., und M. Leuenberger, Fast high-precision on-line determination of hydrogen isotope ratios of water or ice by continuous-flow isotope ratio mass spectrometry, *Rapid Communications in Mass Spectrometry, 17*, 1319–1325, 2003.

Huber, C., M. Leuenberger, und O. Zumbrunnen, Continuous extraction of trapped air from bubble ice or water for on-line determination of isotope ratios, *Analytical Chemistry, 75*(10), 2324–2332, 2003.

IPCC, Climate change 2001: The scientific basis. Contribution of working group I to the third assessment report of the intergovernmental panel on climate change. Cambridge University Press, Cambridge, United Kingdom and New York, NY, USA, 881 pp., 2001.

Klotz, M., 1989, Aufbau eines Lasergerätes zur Messung von Keimen und Partikeln in geringsten Konzentrationen, Master's thesis, Universität Ulm, Deutschland.

Knüsel, S., D. E. Piguet, M. Schwikowski, und G. H. W., Accuracy of continuous ice-core trace-element analysis by inductively coupled plasma sector field mass spectrometry, *Environmental Science and Technology, 37*(10), 2267–2273, 2003.

Krinner, G., und C. Genthon, Tropospheric transport of continental tracers towards Antarctica under varying climatic conditions, *Tellus, Series B, 55B*, 54–70, 2003.

Legrand, M., und P. Mayewski, Glaciochemistry of polar ice cores: A review, *Reviews of Geophysics, 35*, 219–243, 1997.

Lunt, D. J., und P. J. Valdes, Dust transport to Dome C, Antarctica at the Last Glacial Maximum and present day, *Geophysical Research Letters, 28*, 295–298, 2001.

Monnin, E., 2004, *Die natürliche Variabilität der atmosphärischen CO_2Konzentration seit der letzten Eiszeit anhand von Messungen an antarktischen Eisbohrkernen*, Ph. D. thesis, Physikalisches Institut der Universität Bern, Schweiz.

Mortensen, A. K., M. Bigler, K. Grönvold, J. P. Steffensen, und S. J. Johnsen, Ash layers from the last glacial termination in the NGRIP ice core, *Journal of Quaternary Science, submitted*, 2004.

North Greenland Ice-Core Project (NorthGRIP) Members, High resolution climate record of the northern hemisphere reaching into the last interglacial period, *Nature, submitted*, North Greenland Ice-Core Project (NorthGRIP) Members contributing to this paper are: K.K. Andersen, J.-M. Barnola, M. Bigler, P. Biscaye, N. Caillon, J. Chappellaz, H.B. Clausen, D. Dahl-Jensen, H. Fischer, J. Flückiger, Y. Fujii, K. Grønvold, N.S. Gundestrup †, M. Hansson, C. Huber, C.S. Hvidberg, S.J. Johnsen, U. Jonsell, J. Jouzel, S. Kipfstuhl, A. Landais, M. Leuenberger, R. Lorrain, V. Masson-Delmotte, H. Miller, T. Popp, D. Raynaud, R. Röthlisberger, U. Ruth, D. Samyn, J. Schwander, H. Shoji, M.-L. Siggard-Andersen, J.P. Steffensen, T.F. Stocker, A.E. Sveinbjörnsdóttir, A. Svensson, J.-L. Tison, T. Thorsteinsson, O. Watanabe, F. Wilhelms, J. White., 2004.

Petit, J. R., J. Jouzel, D. Raynaud, N. I. Barkov, J.-M. Barnola, I. Basile, M. Bender, J. Chappellaz, M. Davis, G. Delaygue, M. Delmotte, V. M. Kotlyakov, M. Legrand, V. Y. Lipenkov, C. Lorius, L. Pépin, C. Ritz, E. Saltzman, und M. Stievenard, Climate and atmospheric history of the past 420,000 years from the Vostok ice core, Antarctica, *Nature, 399*, 429–436, 1999.

Rankin, A. M., E. W. Wolff, und S. Martin, Frost flowers: Implications for tropospheric chemistry and ice core interpretation, *Journal of Geophysical Research, 107*(D23), 4683, 2002.

Röthlisberger, R., 2000, *Chemische Spuren in antarktischem Eis: Resultate des EPICA-Eisbohrkerns von Dom Concordia*, Ph. D. thesis, Physikalisches Institut der Universität Bern, Schweiz.

Röthlisberger, R., M. Bigler, M. A. Hutterli, S. Sommer, B. Stauffer, H. G. Junghans, und D. Wagenbach, Technique for continuous high-resolution analysis of trace substances in firn and ice cores, *Environmental Science and Technology, 2*(34), 338–342, 2000.

Röthlisberger, R., M. Bigler, E. W. Wolff, E. Monnin, F. Joos, und M. Hutterli, Ice core evidence for the extent of past atmospheric CO_2 change due to iron fertilisation, *Geophysical Research Letters, submitted*, 2004.

Röthlisberger, R., M. A. Hutterli, E. W. Wolff, R. Mulvaney, H. Fischer, M. Bigler, K. Goto-Azuma, M. E. Hansson, U. Ruth, M. L. Siggaard-Andersen, und J. P. Steffensen, Nitrate in Greenland and Antarctic ice cores: A detailed description of post-depositional processes, *Annals of Glaciology, 35*, 209–216, 2002.

Röthlisberger, R., R. Mulvaney, E. W. Wolff, M. A. Hutterli, M. Bigler, M. De Angelis, M. E. Hansson, J. P. Steffensen, und R. Udisti, Limited dechlorination of sea salt aerosols during the last glacial period – Evidence from the EPICA Dome C ice core, *Journal of Geophysical Research, 108*(D16), 4526, 2003.

Röthlisberger, R., R. Mulvaney, E. W. Wolff, M. A. Hutterli, M. Bigler, S. Sommer, und J. Jouzel, Dust and sea salt variability in central East Antarctica (Dome C) over the last 45 kyrs and its implications for southern high-latitude climate, *Geophysical Research Letters, 29*(20), 1963, 2002.

Ruth, U., 2002, *Concentration and size distribution of microparticles in the NGRIP ice core (Central Greenland) during the last glacial period*, Ph. D. thesis, Institut für Umweltphysik, Fakultät für Physik und Astronomie, Ruprecht-Karls-Universität Heidelberg, Deutschland.

Ruth, U., D. Wagenbach, M. Bigler, J. P. Steffensen, und R. Röthlisberger, High resolution microparticle profiles at NGRIP: Case studies of the calcium-dust relationship, *Annals of Glaciology, 35*, 237–242, 2002.

Ruth, U., D. Wagenbach, J. P. Steffensen, und M. Bigler, Continuous record of microparticle concentration and size distribution in the central Greenland NGRIP ice core during the last glacial period, *Journal of Geophysical Research, 108*(D3), 4098, 2003.

Saey, P., 1998, Konzentration und Grössenverteilung von Mikropartikeln in alpinen und polaren Eisbohrkernen: Einsatz eines neuen Detektors für kontinuierliche Messungen an einer Eiskernschmelzanlage, Master's thesis, Institut für Umweltphysik, Fakultät für Physik und Astronomie, Ruprecht-Karls-Universität Heidelberg, Deutschland.

Sigg, A., K. Fuhrer, M. Anklin, T. Staffelbach, und D. Zurmühle, A continuous analysis technique for trace species in ice cores, *Environmental Science and Technology, 28*(2), 204–209, 1994.

Skoog, D. A., und J. J. Leary, *Instrumentelle Analytik. Grundlagen – Geräte – Anwendungen*, Springer-Verlag, Heidelberg, Übersetzung von D. Brendel und S. Hoffstetter-Kuhn, 1996.

Sommer, S., 2000, *Klimainformationen von chemischen Spurenstoffkonzentrationen in polaren Eisbohrkernen*, Ph. D. thesis, Physikalisches Institut der Universität Bern, Schweiz.

Svensson, A., S. W. Nielsen, J. Kipfstuhl, S. J. Johnsen, M. Bigler, U. Ruth, und R. Röthlisberger, Visual stratigraphy of the NorthGRIP ice core during the last glacial period, *Journal of Geophysical Research, in preparation*, 2004.

Tschumi, J., 1999, *Zuverlässigkeit der Rekonstruktion der atmosphärischen CO_2-Konzentration mit polaren Eisbohrkernen*, Ph. D. thesis, Physikalisches Institut der Universität Bern, Schweiz.

Wagenbach, D., F. Ducroz, R. Mulvaney, L. Keck, A. Minikin, M. Legrand, J. S. Hall, und E. W. Wolff, Sea-salt aerosol in costal antarctic regions, *Journal of Geophysical Research, 103*(D9), 10,961–10,974, 1998.

Warneck, P., *Chemistry of the Natural Atmosphere* (2. ed.)., Academic Press, San Diego, 927 pp., 1999.

Wolff, E. W., A. M. Rankin, und R. Röthlisberger, An ice core indicator of antarctic sea ice production?, *Geophysical Research Letters, 30*(22), 2158, 2003.

Yang, Y., X.-X. Zhang, und T. Korenaga, Determination of passive-sampled sulphur dioxide in ambient air as sulphate ion by flow injection analysis with an in-line reaction column, *Talanta, 45*, 445–450, 1997a.

Yang, Y., X.-X. Zhang, und T. Korenaga, Determination of sulfur dioxide in Southeast Asia by flow injection rnalysis with on-line reaction column, *Analytical Sciences, 13*, 397–400, Supplement, 1997b.

Publikationsliste

1. Bigler, Matthias, Entwicklung und Anwendung einer neuen Methode zur kontinuierlichen, hochaufgelösten Messung der Sulfatkonzentration an alpinen und polaren Eisbohrkernen, Diplomarbeit, Physikalisches Institut der Universität Bern, 2000.

2. Bigler, M., R. Röthlisberger, F. Lambert, T.F. Stocker, G.C. Littot, E.W. Wolff, D. Wagenbach, The continental contribution to the water-soluble aerosol deposited on the East Antarctic plateau (EPICA Dome C), *Journal of Geophysical Research*, 2004, in preparation.

3. Bigler, M., R. Röthlisberger, F. Lambert, T.F. Stocker, E.W. Wolff, E. Castellano, R. Udisti, The Eemian interglacial represented in the chemical ice core record from Dome C, Antarctica, *Earth and Planetary Science Letters*, 2004, in preparation.

4. Bigler, M., D. Wagenbach, H. Fischer, J. Kipfstuhl, H. Miller, S. Sommer, B. Stauffer, Sulphate record from a northeast Greenland ice core over the last 1200 years based on continuous flow analysis, *Annals of Glaciology*, *35*, 250–256, 2002.

5. Durand, G., J. Weiss, V. Lipenkov, B. Delmonte, G. Krinner, J.M. Barnola, R. Röthlisberger, M. Bigler, Effect of impurities on grain growth in cold ice sheets: I. Mechanisms and observations, *Journal of Geophysical Research*, 2004, submitted.

6. EPICA community members, Eight glacial cycles from an Antarctic ice core, *Nature*, 2004, in press.
   L. Augustin, C. Barbante, P.R.F. Barnes, J.-M. Barnola, M. Bigler, E. Castellano, O. Cattani, J. Chappellaz, D. Dahl-Jensen, B. Delmonte, G. Dreyfus, G. Durand, S. Falourd, H. Fischer, J. Flückiger, M.E. Hansson, P. Huybrechts, G. Jugie, S.J. Johnsen, J. Jouzel, P. Kaufmann, J. Kipfstuhl, F. Lambert, V.Y. Lipenkov, G.C. Littot, A. Longinelli, R. Lorrain, V. Maggi, V. Masson-Delmotte, H. Miller, R. Mulvaney, J. Oerlemans, H. Oerter, G. Orombelli, F. Parrenin, D.A. Peel, J.-R. Petit, D. Raynaud, C. Ritz, U. Ruth, J. Schwander, U. Siegenthaler, R. Souchez, B. Stauffer, J.P. Steffensen, B. Stenni, T.F. Stocker, I.E. Tabacco, R. Udisti, R.S.W. van de Wal, M. van den Broeke, J. Weiss, F. Wilhelms, J.-G. Winther, E.W. Wolff, M. Zucchelli†.

7. Flückiger, J. und M. Bigler, Als Eisforscher in Dome C – ein Tagebuch, *Unipress – Forschung und Wissenschaft an der Universität Bern*, *116*, 11–14, 2003.

8. Mortensen, A.K., M. Bigler, K. Grønvold, J.P. Steffensen, S.J. Johnsen, Ash layers from the last glacial termination in the NGRIP ice core, *Journal of Quaternary Science*, 2004, submitted.

9. North Greenland Ice-Core Project (NorthGRIP) Members, High resolution climate record of the northern hemisphere reaching into the last interglacial period, *Nature*, 2004, submitted.
North Greenland Ice-Core Project (NorthGRIP) Members contributing to this paper are: K.K. Andersen, J.-M. Barnola, M. Bigler, P. Biscaye, N. Caillon, J. Chappellaz, H.B. Clausen, D. Dahl-Jensen, H. Fischer, J. Flückiger, Y. Fujii, K. Grønvold, N.S. Gundestrup†, M. Hansson, C. Huber, C.S. Hvidberg, S.J. Johnsen, U. Jonsell, J. Jouzel, S. Kipfstuhl, A. Landais, M. Leuenberger, R. Lorrain, V. Masson-Delmotte, H. Miller, T. Popp, D. Raynaud, R. Röthlisberger, U. Ruth, D. Samyn, J. Schwander, H. Shoji, M.-L. Siggard-Andersen, J.P. Steffensen, T.F. Stocker, A.E. Sveinbjörnsdóttir, A. Svensson, J.-L. Tison, T. Thorsteinsson, O. Watanabe, F. Wilhelms, J. White.

10. Röthlisberger, R., M. Bigler, M.A. Hutterli, S. Sommer, B. Stauffer, H.G. Junghans, D. Wagenbach, Technique for continuous high-resolution analysis of trace substances in firn and ice cores, *Environmental Science and Technology*, *2*(34), 338–342, 2000.

11. Röthlisberger, R., M. Bigler, E.W. Wolff, E. Monnin, F. Joos, M. Hutterli, Ice core evidence for the extent of past atmospheric CO_2 change due to iron fertilisation, *Geophysical Research Letters*, 2004, submitted.

12. Röthlisberger, R., M.A. Hutterli, E.W. Wolff, R. Mulvaney, H. Fischer, M. Bigler, K. Goto-Azuma, M.E. Hansson, U. Ruth, M.L. Siggaard-Andersen, J.P. Steffensen, Nitrate in Greenland and Antarctic ice cores: A detailed description of post-depositional processes, *Annals of Glaciology*, *35*, 209–216, 2002.

13. Röthlisberger, R., R. Mulvaney, E.W. Wolff, M.A. Hutterli, M. Bigler, M. De Angelis, M.E. Hansson, J.P. Steffensen, R. Udisti, Limited dechlorination of sea salt aerosols during the last glacial period – Evidence from the EPICA Dome C ice core, *Journal of Geophysical Research*, *108*(D16), 4526, 2003.

14. Röthlisberger, R., R. Mulvaney, E.W. Wolff, M.A. Hutterli, M. Bigler, S. Sommer, J. Jouzel, Dust and sea salt variability in central East Antarctica (Dome C) over the last 45 kyrs and its implications for southern high-latitude climate, *Geophysical Research Letters*, *29*(20), 1963, 2002.

15. Röthlisberger, R., R. Mulvaney, E.W. Wolff, M.A. Hutterli, M. Bigler, S. Sommer, J. Jouzel, Correction to "Dust and sea salt variability in central East Antarctica (Dome C) over the last 45 kyrs and its implications for southern high-latitude climate"by R. Röthlisberger et al., *Geophysical Research Letters*, *30*(5), 1216, 2003.

16. Ruth, U., D. Wagenbach, M. Bigler, J.P. Steffensen, R. Röthlisberger, High resolution microparticle profiles at NGRIP: Case studies of the calcium-dust relationship, *Annals of Glaciology*, *35*, 237–242, 2002.

17. Ruth, U., D. Wagenbach, J.P. Steffensen, M. Bigler, Continuous record of microparticle concentration and size distribution in the central Greenland NGRIP ice core during the last glacial period, *Journal of Geophysical Research*, *108*(D3), 4098, 2003.

18. Siggaard-Andersen, M.L., H. Fischer, M.E. Hansson, J.P. Steffensen, R. Röthlisberger, M. Bigler, K. Goto-Azuma, H. Miller, Characterization of ion composition in the North-

GRIP ice core. Implications for fraction of sea-salt and dust minerals during long-range atmospheric transport, *Journal of Geophysical Research*, 2004, in preparation.

19. Svensson, A., S.W. Nielsen, J. Kipfstuhl, S.J. Johnsen, M. Bigler, U. Ruth, R. Röthlisberger, Visual stratigraphy of the NorthGRIP ice core during the last glacial period, 2004, in preparation.

20. The EPICA Dome C 2001–02 science and drilling teams, Extending the ice core record beyond half a million years, *EOS, Transactions, American Geophysical Union*, *83*(45), 509, 2002.
The science team was E.W. Wolff, M. Bigler, E. Castellano, B. Delmonte, J. Flückiger, G. Krinner, F. Lambert, A. Landais, A. Marinoni, A. Migliori, M. Nyman, I. Schärmeli, M. Severi, and G. Teste. The drilling team was L. Augustin, M. Armeni, F. Frascati, N. Kjaer, A. Krasiliev, E. Lefebvre, A. Manouvrier, and S. Panichi.

Herzlichen Dank Euch allen ...

Die fast sechs Jahre, die ich an der Abteilung für Klima- und Umweltphysik am Physikalischen Institut der Universität Bern verbracht habe, waren geprägt durch interessante, spannende, lehrreiche, anregende, abwechslungsreiche, intensive, lebendige, faszinierende und fröhliche Momente. Es war insgesamt eine wunderbare Zeit, die mir in guter Erinnerung bleiben wird. Dazu haben viele Menschen beigetragen, hier in Bern, an anderen Institutionen, bei den Feldarbeiten in Grönland und in der Antarktis oder in meinem privaten Umfeld. Euch allen gilt mein grosser Dank:

Prof. Thomas Stocker und Prof. Bernhard Stauffer – Betreuer meiner Arbeit

Regine Röthlisberger, Manuel Hutterli, Stefan Sommer, Fabrice Lambert,
Patrick Kaufmann und Urs Ruth – Mitglieder des CFA-Teams

Dietmar Wagenbach und Eric Wolff – externe Betreuer

Eric Monnin, Urs Siegenthaler und Andreas Indermühle – Bürokollegen

Reto Knutti, Urs Beyerle und Stefan Zoller – Computerspezialisten

Doris Raetz, Hanspeter Moret, Ivan Schärmeli, Marc Keusen, Heiri Rufli,
Hans Riesen und Kurt Grossenbacher – Sekretariat, Elektronik und Werkstatt

Thomas Blunier, André Dällenbach, Marc Eyer, Grégoire Floch, Jacqueline Flückiger,
Stefan Gerber, Christof Huber, Fortunat Joos, Kenji Kawamura, Clemens Lang, Lukas Lanz,
Markus Leuenberger, Simon Müller, Kaper Plattner, Christoph Raible, Manuel Renold,
Jakob Schwander, Renato Spahni, Patrick Sturm, Karin Weiler und Oliver Zumbrunnen

Die Teams der NorthGRIP Feldsaison im Sommer 2000,
der Bremerhaven Messkampagne im Herbst 2000 und
der Dome C Feldsaison im Südsommer 2001/2002

Esther, Julian, Manuel, Simon und Elias Bigler,
Christian Bigler, Gertrud und Fritz Bigler,
Martha und Edy Hodel

Lebenslauf

Angaben zur Person

Name	Matthias Bigler
Adresse	Erlenauweg 7, 3110 Münsingen
Geburtsdatum	8. November 1969
Heimatort	Oberthal
Zivilstand	verheiratet mit Esther Bigler-Hodel
Kinder	Julian, Manuel, Simon, Elias

Ausbildung

17. Juni 2004	Doktorprüfung an der Universität Bern.
2000–2004	Doktorarbeit an der Abteilung für Klima- und Umweltphysik am Physikalischen Institut der Universität Bern unter der Leitung von Prof. Dr. Bernhard Stauffer und Prof. Dr. Thomas F. Stocker.
3. Februar 2000	Diplomprüfung an der Universität Bern.
1998–2000	Diplomarbeit an der Abteilung für Klima- und Umweltphysik (s.o.).
1991–1998	Grund- und Hauptstudium an der Universität Bern mit Hauptfach Physik, Zweitfach Mathematik und Ergänzungsfach Astronomie; mehrere Unterbrüche wegen Erwerbstätigkeit und Familienarbeit.
1989	Militärdienst als Radfahrersoldat.
27. Juni 1990	Patentierung zum Primarlehrer.
1985–1990	Staatliches Lehrerinnen- und Lehrerseminar in Langenthal.
1976–1985	Primar- und Sekundarschulen in Dürrenroth und Huttwil.

Polarexpeditionen

November–Februar 2001/2002	Dome Concordia, Antarktis: Messkampagne mit dem Berner Continuous Flow Analysis (CFA) System im Rahmen des European Project for Ice Coring in Antarctica (EPICA).
Mai–Juli 2000	NorthGRIP, Grönland: CFA-Messkampagne im Rahmen des North Greenland Ice Core Project.

Weitere Auslandaufenthalte

November 2003	Interkalibration von Staubmessgeräten, Universität Grenoble, Frankreich.
November 2002	NorthGRIP Datierungs-Workshop, Universität Kopenhagen, Dänemark.
Oktober 2000	CFA-Messkampagne am Dome C Eisbohrkern, Alfred-Wegener-Institut Bremerhaven, Deutschland.
Juni 1999	CFA-Messkampagne an alpinen Eisbohrkernen, Universität Heidelberg, Deutschland.
Dezember 1998	Zuschneiden des Nordgrönland-Traverse Eisbohrkerns B20, Alfred-Wegener-Institut Bremerhaven, Deutschland.

Konferenzen

April 2004	EGU General Assembly, Nizza, Frankreich.
Oktober 2003	NorthGRIP Meeting, Kopenhagen, Dänemark.
Oktober 2003	EPICA Science Subgroup Meeting, San Feliu, Spanien.
April 2003	EGS-AGU-EUG Joint Assembly, Nizza, Frankreich.
September 2002	EPICA Science Subgroup Meeting, Potsdam, Deutschland.
September 1999	EURESCO Polar Regions and Quaternary Climate, Giens, Frankreich.
September 1998	19. Internationale Polartagung, Bern, Schweiz.

Unterrichttätigkeit

Seit 1994	Teilpensum Physik, Mathematik u.a. an der Kantonalen Diplom-mittelschule und teilweise an der Höheren Mittelschule Marzili, Bern.
1993–1994	Teilpensum Mathematik am Staatlichen Seminar Langenthal.
1992–1993	Teilpensum Mathematik am Untergymnasium Bern-Neufeld.
1990–1992	Unterricht als Stellvertreter und Teilpenselehrkraft an verschieden Schulen im Kanton Bern.